Contribution to the study of friction phenomena : application to paper materials

Nicolas Fulleringer

UNIVERSITÉ DE GRENOBLE

THÈSE

Pour obtenir le grade de

DOCTEUR DE L'UNIVERSITÉ DE GRENOBLE

Spécialité : **Matériaux, Mécanique, Génie civil, Électrochimie**

Arrêté ministériel : 7 août 2006

Présentée par

Nicolas FULLERINGER

Thèse dirigée par **Jean-Francis BLOCH**

préparée au sein **Laboratoire de Génie des Procédés Papetiers**
et de **I-MEP2 (Ingénierie - Matériaux, Mécanique, Environnement, Energétique, Productique, Production)**

Contribution à l'étude des phénomènes de friction : application au matériau papier

Thèse soutenue publiquement le **11 décembre 2014**,
devant le jury composé de :

M. Carlos CANUDAS DE WIT
Directeur de recherche au CNRS, Président
Mme Marie-Ange BUENO
Professeur à l'ENSISA - Université de Haute Alsace, Rapporteur
M. Maxence BIGERELLE
Professeur à l'Université de Valenciennes et du Hainaut-Cambrésis, Rapporteur
M. Thomas MATHIA
Directeur de recherche à Centrale Lyon, Examinateur
M. Jean-Francis BLOCH
Maître de conférences à l'Institut Polytechnique de Grenoble, Directeur de thèse
M. Laurent FARLOTTI
Directeur Innovation et Brevets à Neopost Technologies, Invité

Acknowledgments

I would like to thank several people and organizations for they support and/or contribution to this thesis.

- My thanks to the Neopost company, to the Association Nationale de la Recherche et de la Technologie (ANRT), and to the Laboratory of Pulp, Paper, and Graphic Arts (LGP2) for their financial and administrative support. In particular, I would like to thank L. Farlotti and E. Mauret from Neopost and LGP2, respectively.
- My thanks to the members of the jury, for the time they spent on this memoir, but also for investigating ways to continue this work.
- My thanks to those who contributed to the content of this thesis. In particular, I would like to thank D. Curtil and D. Bernard for their help to address issues related to electronics and franking machines, respectively.
- My thanks to several friends, from Grenoble (Jérémy, Fred, Elsa, Nathalie, Raphaël, Florian, Pierre, Benoît, Bertrand, and others) and Paris (the 6th, 5th, and 1st floors, Olga, Athenaïs, and others), for their moral support.
- My thanks to my family for its lasting support.
- My thanks to J.-F. Bloch. Not only for its role as supervisor, but also for its valuable moral support during and after the thesis. I hope we will have new opportunities to work together.
- To finish with, my thanks and apologies to those I could have forgotten.

Contents

List of Figures

List of Tables

Notations

Notations for Parts I and II

Symbol	Meaning	Chapter
m	Mass of the sled	3.1.2
g	Standard gravity	3.1.2
α	Angle between the horizontal and the titled plane	3.1.1
α_{max}	Angle at which the sliding starts	3.1.1
F_N	Normal force applied on the contact	3.1.2
F_p	Pulling force applied on the sled	3.2.1
F_f	Force of friction	2.1
F_S	Break-away force	3.1.2
F_K	Force of kinetic friction	3.2.2.3
F_v	Force of viscous friction	3.2.2.4
μ_S	Coefficient of static friction	3.1.2
μ_K	Coefficient of kinetic friction	3.2.2.3
μ_v	Coefficient of viscous friction	3.2.2.4
A_r	Real area of contact	2.4
A_a	Apparent area of contact	2.4
v	Contact speed	3.2.2.4
v_S	Stribeck velocity	3.2.2.5
d_X	Local sliding distance of the sample X	9.1.2.2
N	Number of repeated slidings	9.1.2.2

Notations for Part III

Symbol	Meaning	Chapter
α	Angle of the envelopes to the horizontal	12.2
E_i	Envelope number i from the bottom of the stack	12.2
I_i	Interface above E_i	12.2
W_i	Weight of enveloppe E_i	12.2
m_i	Mass of the envelope E_i	12.2
F_i	Force applied by the envelope E_i on E_{i+1}	12.2
$F_{ext,i}$	Norm of the external forces applied on E_i	14.2.1
β_i	Orientation of the external forces applied on E_i	14.2.1
$\sum_i$	Balance of forces applied on E_i	12.2
$\mu_{S,i}$	Coefficient of static friction of I_i	13.3.2
$\mu_{K,i}$	Coefficient of kinetic friction of I_i	13.3.2
δ_i	Sign of the difference between the speeds of E_i and E_{i+1}	13.3.2
a_i	Acceleration of E_i	13.3.3
B	Common notation for a block of envelopes	13.3.3
E_a	Common bottommost envelope of a block	13.3.3
E_b	Common topmost envelope of a block	13.3.3
n	Number of envelopes in the stack	12.2
a_B	Acceleration of a block B	13.3.3
a_R	Acceleration of rollers	13.3.3
S_i	Split function of the interface I_i	14.1
$A(i)$	Critical acceleration, inducing a split of the interface I_i	14.2.2
$F_{c,e}(i)$	Critical external force applied on E_e inducing a split of I_i	14.2.3
$\alpha(i)$	Critical angle of the feeder inducing a split of I_i	14.2.4
F_p	Force applied by the selection pads on envelopes	15.6.1

Part I

Introduction

Chapter 1

Introduction

The postal network intensively uses automated systems to process mail, among which the franking machines. The goal of this study is to improve a fundamental section of those franking machines: the feeder. In this chapter, we introduce the franking machines and their feeders. We do a state of the art of the techniques involved and the failures typically encountered. We will conclude by introducing the goals and methods of this study.

1.1 The postal process

Market size In 2005, about 17 billion letters were sent in Germany and the same amount in France (approx. 270 letters per resident per year) [1] [2]. At this time, the mail market represented 10 billion euros of revenue in both Germany and France and employed 1.65 million people. However, due to the competition of emails and text messages, the volume of letters is expected to decrease at an average rate of 3 % per year. Several studies suggest that the mail market will stabilize at about 40 % of its actual size [1]. The mail market will therefore remain an important market in the long term and thus has to remain competitive.

Sender Private customers usually think that the mail service starts by the collecting of public mail boxes. However, 80 % of the total mail flow is directly delivered to post offices by senders. Those mails are usually sent by companies and organizations that intensively use mail, such as banks, insurances or governments. Their mailrooms can process tens of thousands of mail pieces per day. Thus, they often use highly automated mailroom equipment to (i) print the documents, (ii) insert them into envelopes, and (iii) frank the mail. Those operations are done by printers, folder inserters and franking machines, respectively.

Sorting and transportation The mail is picked up by the postal companies, or by so-called consolidators, and transferred to mail sorting centers. Those sorting centers organize the transportation of the mail worldwide, and can sort up to 1 million letters a day. In 2003, two third of this mail was processed by heavy-duty sorting machines [3]. Mail is then transported by road, train, or plane and delivered to new sorting centers that organize the delivery of the mail.

Recipient Carriers deliver the mail to the recipients. Because of the diversity of final destinations, the cost of this step represents about 50 % of the total cost [3]. Some recipients receive an important amount of mail. In this situation, the recipients use sorting systems to facilitate the distribution of mail within their organization. The recipient also sometime uses other mailroom equipment such as mail openers and scanners.

A challenging topic To increase the competitiveness of the mail market, the efficiency and reliability of automated mailroom equipment have to be improved. In this study, we consider the case of franking machines. The results of the study can however be extended to other equipment.

1.2 Franking mail

Parameters Franking mail permits the payment of the mail service, in particular collection (12 %), sortation (16 %), transportation (7 %), delivery (50 %), and fixed costs (15 %) [3]. The franking price thus depends on several parameters, among which the weight of the envelope, its size, and the destination. Several solutions permit the franking of mail.

Manual franking A well-known method consists in sticking a stamp on the envelope. Each stamp corresponds to a flat rate that itself corresponds to a maximum weight. Therefore, people usually overpay their mail by using stamps. Moreover, the sticking of stamps is not a viable technique for mailrooms.

Manual franking machines An intermediate solution consists in manual franking machines: envelopes are fed one by one into the machine by an operator. See for example the Neopost IJ 25 franking machine, represented on Figure 1.1a. No paper handling nor transporting system are required. However, their output is low and only suited to companies sending less than 100 letters per day.

Automatic franking machines Automatic franking machines are highly automated mailroom equipment. Their length ranges from 1 to 4 meters and they usually

(a) Neopost IJ 25 (b) Neopost Omega

Figure 1.1: Two examples of franking machines

require one operator per machine. Their functions are represented on Figure 1.1b and listed hereafter:

- **Feeder -** The operator places an envelope stack on the *feeder*. The feeder permits the feeding of the machine with a continuous flow of well-separated envelopes. Envelopes are optionally sealed in the feeder sealing liquid.
- **Dynamic scale -** The *dynamic scale* permits the weighting of envelopes while transported on a belt. In order to maintain the envelopes tackled on the belt, tongues are placed above the path taken by envelopes.
- **Franking -** The weight measurement permits the calculation of the postage. According to several parameters, an *imprint* (or *postal indicia*) is created. The imprint is printed on envelopes using an inkjet print head.
- **Stacking** Envelopes leaving the franking machine have to form a stack in order to be manipulated by an operator. It is the goal of the stacker, a simple module consisting in a large belt.

By facilitating the job of operators, automatic franking machines permit the treatment of thousands of envelopes per day.

1.3 Automatic franking machines

Automation Improving the efficiency and reliability of mailroom equipment is a great challenge. Franking machines are a good example of the differences between manual and automated solutions. The main differences are (i) the feeding, (ii) the transportation, and (iii) the stacking of the envelopes.

Feeding envelopes Feeding envelopes consists in delivering the envelopes one by one to the machine. Consequently, the core process consists in separating the documents from the stack. The feeding is ruled by the following specifications:

- **Capacity -** Increasing the capacity of feeders permits a reduction of the operating costs. However, heavy-duty franking machines are usually unable to process more than 3 kg of envelopes and/or 200 mm height.
- **Mix-mail -** The ability to process *mix-mail*, i.e. envelopes of different sizes, weights, paper qualities, or thickness.
- **Integrity -** The documents have to be undamaged at the end of the feeding.
- **Skew -** The *skew* of the imprint on the envelope has to remain low. The envelopes thus have to remain aligned with the machine.
- **Gap -** The distance between two successive envelopes, called *gap*, has to be low enough to guarantee the throughput (3 envelopes per second), and high enough to permit the processing of envelopes.

A particularity of franking machines feeders is that they are bottom feeders: envelopes are taken from the bottom of the stack. This process is called *First In First Out* (*FIFO*). The advantage of such a process is that the operator can place new stacks continuously. The drawback is that the selection is much more complex than for top feeders, because the whole stack applies a high load on the bottommost envelopes. The feeding step of franking machines is therefore a complex and difficult part of the franking machine automation.

Transporting envelopes The transportation of envelopes is a highly-reliable technology. Indeed, it mainly consists in rollers, belts, and tongues place above or below the *transport path* taken by documents. The challenge consists in ensuring that the transport path does not damage the envelope and avoids skewing. In particular, the designers of the machine have to ensure that there is no obstacle to the document along the path. Thanks to this transportation system, the inkjet printhead remains static, whereas it has to be mobile in manual franking machines.

Stacking envelopes The stacking of envelopes is also a reliable technology. The static stacking consists in placing the documents in a box at the exit of the machine, recreating the document stack. This solution is cheap and simple, but unadapted to high capacities and documents of varying sizes. Another solution consists in dynamic stackers which principle is summarized on Figure 1.2. Envelopes are moved on a motorized belt. Due to the inclined plate at the front end of the stacker, the front end of the envelopes is lifted. The stack is thus recreated.

Conclusion The automation of mailroom equipment, in particular franking machines, is a great challenge. We have shown that the feeding section is a complex and critical aspect of the automation of mailroom equipment. We thus propose to focus our study on this part.

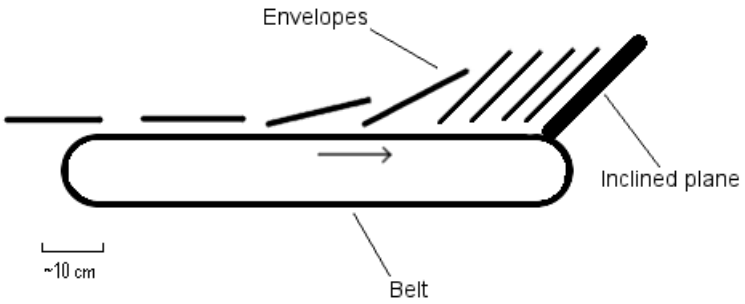

Figure 1.2: Principle of the dynamic stacking

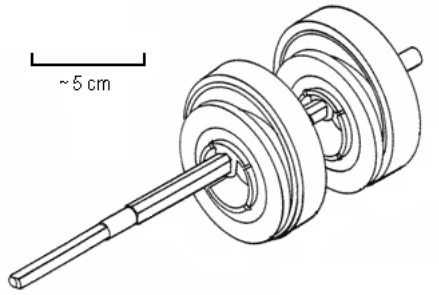

Figure 1.3: Eccentric rollers permitting the jog of the document stack [4]

1.4 Feeding envelopes: a state of the art

Introduction In the previous section, we introduced the feeding of envelopes in franking machines. We now propose an overview of the main techniques used to separate the envelopes. Some other techniques used for feeding paper materials are presented in annex A. These additional techniques may inspire new feeding mechanisms for envelopes in franking machines. A comparative study of several franking machines is also proposed in annex B.

Dynamics The acceleration applied on a document is supposed to be a major parameter of its separation from the stack. A well known experience involving this factor consists in removing the tablecloth of a table without removing plates and glasses: if the tablecloth is pulled very quickly, then plates and glasses do not move and remain on the table. It has thus been proposed to horizontally jog the documents stack with numerous accelerations in order to ease the separation.
On the other hand, eccentric rollers placed below a document stack permit its vertical jog, as represented on Figure 1.3. This process is supposed to permit an easier separation of the documents by (i) modifying the normal force applied between

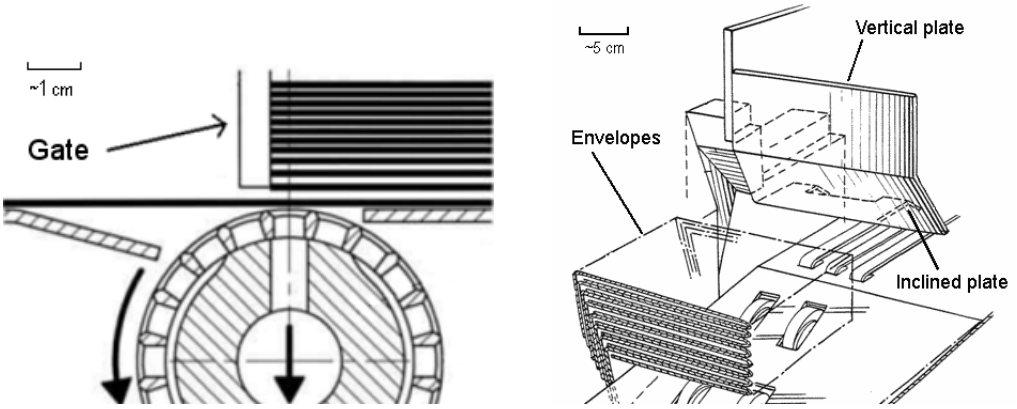

(a) Gate feeder with a suction roller [5] (b) Vertical plate in a franking machine [4]

Figure 1.4: Vertical plates favoring the separation of paper documents

envelopes and (i) introducing an air blanket between envelopes.

Geometry Modifying the machine geometry permits the development of reliable and cheap solutions for document separation. A common solution consists in placing a slot of various heights in front of the document stack: documents in front of the slot can move into the machine, whereas the plate avoids any movement of the rest of the stack. This solution is called *gap feeder*, *selection plate*, or *barrier plate*. When the thickness of documents is constant, the solution permits the selection of documents one by one, as represented on Figure 1.4a. This solution is very useful for thick documents of constant thickness. However, in the case of mix-mail and/or thin documents, the slot height does not fit with the selection of a single document. Consequently, franking machines use selection plate only to permit small stacks of envelopes (few centimeters) to be fed into the machine, easing the selection.
The vertical selection plate has often an inclined or bent plate at its bottom, as represented on Figure 1.4b. This solution is intended at (i) permitting a relative tangential displacement of documents to ease the selection process, (ii) increasing the pressure on the documents front to ease their transportation, and (iii) avoiding the damage of envelopes due to sharp edges.
Additionally, the stack support of franking machines is sometime tilted to the rear, a solution called *tilted hopper*. An example of a 5° tilted hopper is represented on Figure 1.5a. This solution permits (i) a backward tangential component of the weight that eases the document separation, and (ii) the reduction of normal forces between envelopes that reduces the friction force between them and eases the selection.

Friction The friction of belts and rollers on the bottommost envelopes permits the envelopes transportation. The challenge is then to avoid the displacement of

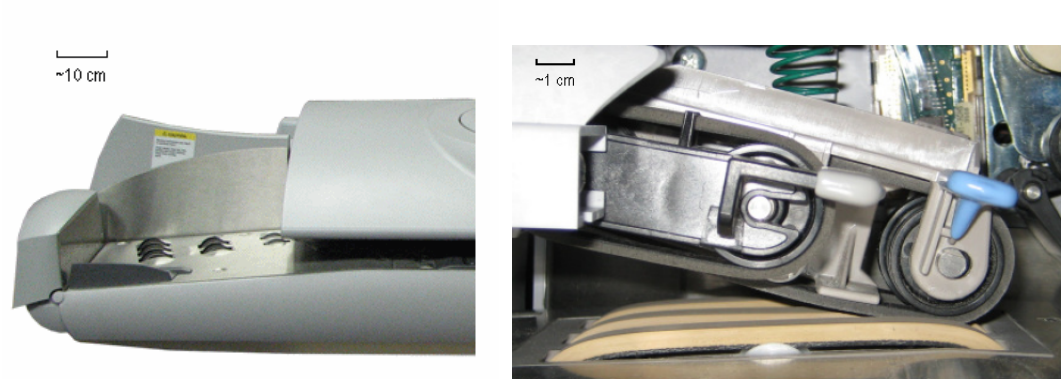

(a) 5° tilted hopper (b) Separation belts

Figure 1.5: Pitney Bowes DM1000 franking machine

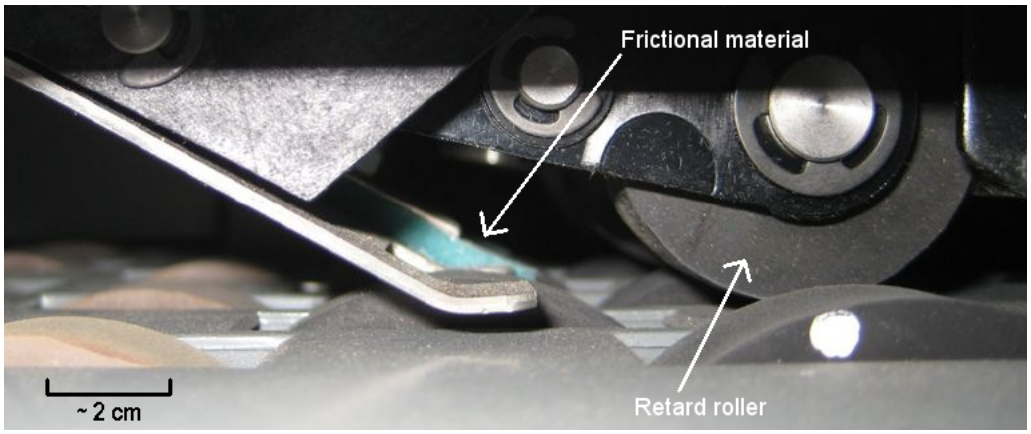

Figure 1.6: Selection system of a Neopost AFS IJ

other (upper) envelopes. A common technique consists in placing a frictional material in contact with the document stack. This material applies a force oriented backward that slows the envelopes. To permit the feeding of documents of various thicknesses, the frictional material is usually mounted on a system permitting its vertical displacement. In particular, frictional materials are often supported by a system permitting its vertical displacement or its rotation around an axis. The system usually includes springs that permit the pad to be vertically pressed on the document stack. Frictional solutions are widely used, because they are low-cost and flexible.
A common frictional material in franking machines is the polyurethane used in *friction pads*. Friction pads have a typical width of approximately 1 cm. An example is represented on Figure 1.6.

Friction pads can be replaced by *retard rollers*, also named *gate rollers* or *braking rollers*. These are fixed rollers that undergo small rotations after each feeding. This slight rotation avoids the abrasion of the roller and reduces the maintenance. The solution is however more expensive than friction pads. Such a system is represented on Figure 1.6. The retard rollers are sometime mounted on a gear torque. This system is more expensive but offers a more accurate control of the resisting force applied on the selected document.
Some franking machines also use *separation belts*, also called *friction belts*, and represented on Figure 1.5b. The rotation of such belts is opposed to this of the transportation mechanism. The belt is thus supposed to permit a better selection due to the backward movement applied on the stack. This solution is in particular used on Pitney Bowes machines.

1.5 Typical failures of the selection process

No-feed *No-feed*, also named *misfeed* or *extraction fault*, appear when envelopes are not carried into the machine. This failure corresponds to rollers and/or belts sliding on envelopes without displacing them. The consequences of this problem are (i) a reduction of the throughput of the machine, and (ii) a deterioration of the documents and rollers. The no-feed situation is typical when (i) the weight of the envelope stack is too small, (ii) lateral holds are too tight, and (iii) rollers are dusty.

Multi-feed *Multi-feed*, also named *double* or *triple*, appear when more than one envelope is fed into the machine at the same time, i.e. when the gap between envelopes is negative. It is particularly problematic because (i) only one envelope is franked instead of two, (ii) the weight and length are miscalculated, (iii) the machine may stop due to document jam, and (iv) operators have to control the printings continuously. The multi-feed situation is typical in the case of heavy envelope stacks. Machines present about 0.5 % of envelopes with multi-feeds.

Document deterioration A *document deterioration*, also named *document crash*, *wrinkling*, *tearing*, or *corner deterioration*, appears when some envelopes are harmed by the machine. The deterioration is problematic because envelopes may be rejected by the Postal Service or have a poor appearance for the recipient. It typically appears when (i) the friction of the selection pad is too important, (ii) the window, the flap, or the corners are hooked by different elements of the machine, and (iii) low load of envelopes, typically for thin envelopes with low stiffness.

Skew *Skew* appears when some envelopes have a bad orientation in the machine. This failure leads to a bad orientation of the imprint. The envelope may be rejected by the Postal Service. Skews appear when (i) the coefficients of friction, (ii) the front

tension applied on envelopes, and (iii) the normal loads applied by driving rollers are different along the envelope width [6, 7]. Lateral jog can reduce this defect.

1.6 Goal and method

Goal The two main failures associated to franking machine feeders are no-feeds and multi-feeds. Those failures decrease the machine throughput and require an operator to supervise the machine. Those failures generally constitute the main limit to the process automation of paper materials, as for example in copiers. Consequently, the goals of this study are to understand the mechanisms of no-feeds and multifeeds, and improve the feeders design.

Problem Simple mechanical considerations of the problem show that the main force involved in the envelopes feeding is the friction force. Indeed, considering an envelope being fed into the machine, it undergoes friction forces with rollers, belts, vertical plate, friction pads, and other envelopes. The friction of paper materials is however a complex topic, as paper friction forces have a high variability [8]. In particular, most of the literature focuses on the material properties, but the materials processed by the franking machine are unknown to the machine designer. The only parameters are the environmental and protocol factors of the paper friction.

Method The presentation of this work is divided in three parts:

- **Part I** – We introduce and adapt the existing test methods for the measurement of the paper friction.
- **Part II** – We study both the paper-on-paper friction and its friction on other materials. We focus on environmental and protocol parameters.
- **Part III** – Based on the acquired knowledge concerning paper friction, we study the mechanisms of no-feed and multi-feeds.

We conclude by several technical recommendations for both paper friction measurement and franking machine feeders design.

Summary and Conclusion of Chapter 1

Challenge Improving the reliability and efficiency of automated mailroom equipment constitutes a challenging topic. We consider the example of automated franking machines. Those machines are composed of four main sections: (i) the feeder feeds the envelopes one by one, (ii) the dynamic scale weights the envelopes, (iii) an inkjet print head prints the imprint, and (iv) the stacker recreates an envelope stack. The optimization of the feeders constitutes the major challenge in franking machines automation.

Franking machine feeders The feeders aim at feeding the franking machine with only the bottommost envelope of the envelope stack. This selection process is complex and relies on three types of techniques:

- **Dynamical solutions** (e.g., strong rollers accelerations or eccentric rollers),
- **Geometrical solutions** (e.g., vertical plates and tilted hoppers),
- **Frictional solutions** (e.g., friction pads/belts or retard rollers).

However, failures still often occur:

- **No-feeds or misfeeds** when envelopes are not carried into the machine,
- **Multi-feeds** when more than one envelope is simultaneously fed,
- **Deterioration** when the envelopes are damaged during the process,
- **Skews** when the envelopes have a bad orientation in the machine.

Goal and method The goals of this study are to understand the mechanisms of no-feeds and multi-feeds, and to improve the feeders design. A deep understanding of the friction between paper materials is thus required. We divide the study in three parts.

1. First, we introduce and adapt the methods for measuring the friction force between paper materials.
2. Then, we study the friction of paper materials, focusing on the environmental and protocol parameters.
3. We finally study the mechanisms of no-feeds and multi-feeds in franking machine feeders.

Part II

Friction and its characterization

Chapter 2

Defining friction

The optimization of franking machine feeders requires a deep understanding of the friction of paper materials. For clarity reasons, we introduce friction in this chapter. To do so, we successively propose a general, historical, and physical definition of this concept. We conclude by presenting two major properties of friction: its dependence on normal load and the apparition of stick-slip oscillations.

2.1 Definition

Tribology *Tribology* comes from the Greek *tribos* that means "friction". When two surfaces are in contact together, tribology occurs. Tribology is a domain of science that studies four phenomena:

- **Adhesion** – a tendency by which the surfaces tend to cling to each other. The adhesion can be divided into several types, among which the chemical, electrostatic, and mechanical adhesions.
- **Friction** – the phenomenon responsible for the force opposed to the relative sliding of the two surfaces in contact.
- **Wear** – the progressive damage, involving material loss, which occurs on a surface sliding on another surface.
- **Lubricants** – substances, such as grease or oil, that reduce friction and wear between two surfaces in contact.

Tribology is a complex subject involving numerous mechanisms, from macro to nano scales. In particular, discoveries show how strongly linked are the four phenomena previously described. This study focusing on the friction force, we will thus sometime refer to the three other phenomena, even implicitly.

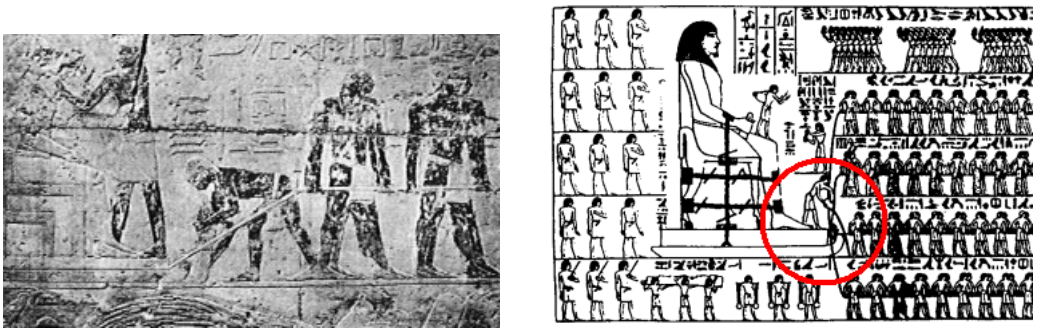

(a) Tomb of Saquara (2400 B.C) [9] (b) Tomb of Tehuti-Hetep (1880 B.C) [10]

Figure 2.1: Paintings from egyptian tombs. We can see "oilers" or "tribologists" pouring some lubricant onto the ground, in front of sleds used to move the statues.

Friction *Friction*, from the Latin word *fricare*, means "to rub". Friction is a phenomenon that opposes a resistive tangential force (the force of friction, noted F_f) to the relative sliding of two surfaces in contact. Friction develops between sliding surfaces and fulfills a dual role of (i) transmitting energy from one surface to another, and (ii) dissipating energy of relative motion. The friction force is present in our everyday life and fundamental in a wide range of mechanical studies at different scales, such as earthquakes, fuel consumption of engines, or atomic force microscopes (AFM).

2.2 Historical developments

Ancestors use of friction The use of friction dates from our ancestors and early civilizations. 400 000 years ago, they used friction to chip stone tools. 200 000 years ago, the Neanderthals used friction to produce fire. Later, Egyptian and Sumerian civilizations discovered and used lubricants to facilitate the transport of stone sleds, as represented on Figure 2.1. Instead of using rollers to reduce friction, they used lubricant that was poured from a jar onto the ground in front of the sleds.

First identification of the friction force Perhaps the first identification of the friction force by a scientist dates from Aristotle [11]. He analyzed the motion of bodies sliding on the ground. He observed that to maintain a uniform movement, a constant force must be applied on the sled.

First scientific study The first scientific study on the friction force dates from Leonardo da Vinci in about 1500 [12]. He pulled a sled on a plane along different sides and in different orientations, as represented on Figure 2.2. He then showed that the friction force does not depend on the apparent contact area, but is proportional

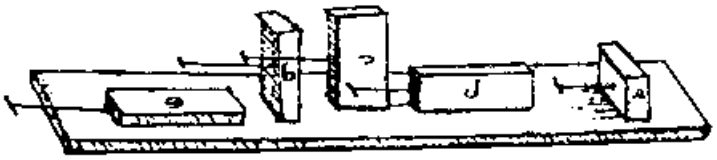

Figure 2.2: Extract from the journals of Leonardo da Vinci (1500 A.C). A sled was pulled on a plane along different sides and different orientations. The same force was measured.

to the weight of the sled. He moreover observed that different materials move with different ease. He supposed this phenomenon to be due to the roughness of the materials in contact.

Rediscovery of da Vinci's work In 1699, Amonton rediscovered the results of Leonardo da Vinci. To explain them, he imagined micro-asperities due to surface roughness. A mechanical work is required to (i) lift one surface over the roughness of the other, and (ii) to deform the other surface. He proposed that asperities can be assimilated to springs that absorb the work. Doing this, Amonton introduced a second mechanism of friction.

Role of adhesion In 1734, Desagulier observed that the smoother the surfaces are, the higher the friction is. This observation being in opposition to the roughness-dependency model of friction, he proposed surface adhesion to be a component of the friction force [12]. This concept completes the two previous mechanisms proposed by Leonardo da Vinci and Amonton and appeared later to be the most important one.

Coulomb's law In 1773, Coulomb proposed the first mathematical friction model [11]. During the late 18th century, Coulomb also observed that the force required to move a sled is higher than the force required to maintain the movement. He therefore proposed a two-state model of friction, the friction being either static (sticking) or kinetic (sliding). Coulomb laws of friction are still widely used.

An heat dissipative phenomenon In 1798, Thompson discovered that friction energy is transformed directly into heat. It was then proved by Joule in 1843 [12].

Velocity dependence At the beginning of the 20th century, Stribeck showed the dependence of the friction force on the sliding velocity. He observed a decrease in frictional force with low velocities, now called the *Stribeck curves* [11].

Explaining the laws of friction In 1950, F. Philip Bowden and David Tabor gave a physical explanation of the laws of friction. They showed how the real area of contact is much less important than the apparent contact area. Indeed, the real area of contact is created by surface asperities from both materials that are in contact. They showed that the higher the normal load is, the more the asperities are compressed and the higher the real area of contact is. Consequently, the adhesion (that is proportional to the real area of contact) is demonstrated as being the major component of the friction force.

Current trends Nowadays, the study of friction is mainly concentrated on the study of friction at atomic scales. The development of Atomic Force Microscopes (AFM) permits the study of low scale friction mechanisms. Scientists expect those study to permit the development of improved friction models and/or to permit the development of micro/nano-systems [13].

Further information For further information concerning the history of friction, the reader is invited to refer to the book *History of Tribology* by D. Dowson [9].

2.3 Friction and energy conservation

Energy conservation The energy conservation requires the mechanical energy dissipated by friction to be transformed into other forms of energy, which are:

- **Heat** – It was shown by Thomson and Joule that the major part of the energy dissipated by friction is transformed into heat [12]. This phenomenon was used by the Neanderthals 200 000 years ago to produce fire.
- **Surface energy** – The change in surface energy can be due to tribocharging, tribochemical reactions, or the triboemission effect (among others). This phenomenon is well-known in our everyday life, as for example the electric charging of cars in summer.
- **Mechanical energy** – The energy also dissipates into mechanical energy. For example, the oscillations created in the materials sometime lead to a sound, e.g. the brakes of a train or the sound of a violin. In the case of plastic deformations the material structure also evolves (e.g. abrasion).

The transformation of energy is linked to the following main processes [14], summarized on Figure 2.3:

- **Adhesion** – When two surfaces are put in contact together, bonds are created between the surfaces. Different adhesions may appear, among which (i) the dispersive adhesion due to forces (e.g., van der Waals forces), (ii) the chemical adhesion (e.g., hydrogen bonds), (iii) mechanical adhesion (interlacing of

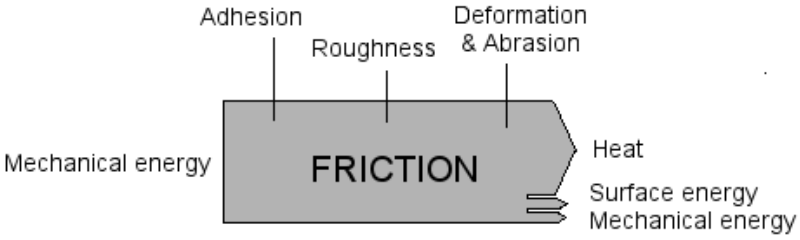

Figure 2.3: Main transformations of the energy due to friction

surface elements), (iv) electrostatic adhesion (due to a difference in electrical charges), and (v) diffusive adhesion (migration of molecules from a surface to the other). The energy required to break those bonds contributes to the friction force.

- **Roughness** – The surfaces in contact are not perfectly flat. The asperities of the surfaces create ascending or descending slopes that contribute to the dissipation of the mechanical energy.
- **Deformations and abrasion** – The deformation of materials and chocs dissipate a part of the friction force. If the stiffness of the materials is very different, then abrasion may even appear. The disruption of the material structure also dissipates energy.

2.4 Real area of contact

A fundamental aspect of friction Tribology pioneer F.P. Bowden is reported to have said that "putting two solids together is rather like turning Switzerland upside down and standing it on Austria – the area of intimate contact will be small" (Bowden, 1950) [15]. As shown in the previous section, the friction force mainly appears on contacting zones between the two surfaces. Several studies thus pointed out the linear dependence of the friction force to the so-called *real area of contact*, noted A_r [16]. However, this real area of contact is difficult to measure because it is much smaller than the *apparent area of contact*, A_a, as represented on Figure 2.4a. According to Kawashima et al. [17], there is even no evaluation method for the real area of contact for the paper-on-paper contact.

Paper-on-glass contact Estimations of the real area of contact are available by measuring the contact between paper and a plane smooth surface [18] using four methods: (i) an electrical contact resistance method, (ii) an optical method, (iii) an ultrasonic method, and (iv) an ink transcription method [19] [20]. For paper

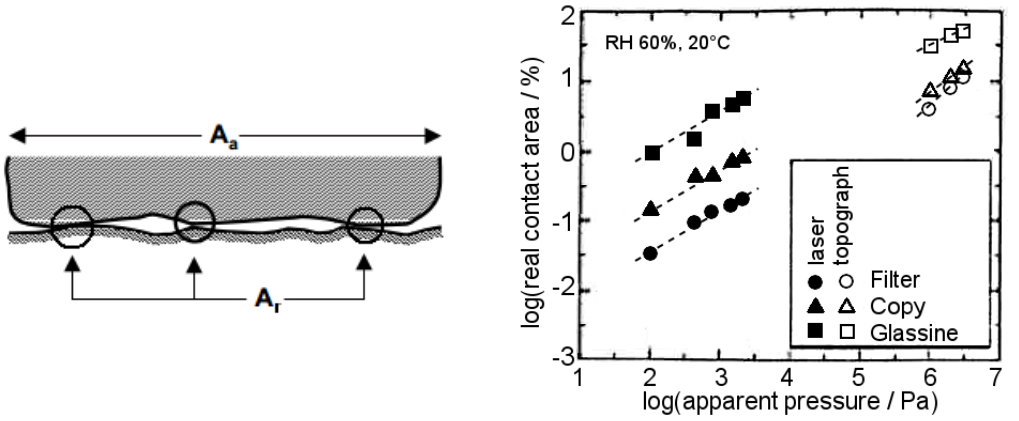

(a) Comparison between A_r and A_a

(b) Real area of contact vs. apparent pressure for different types of papers [17]

Figure 2.4: The real area of contact, A_r, is compared to the apparent area of contact, A_a (left). As the apparent pressure applied on the samples increases, the asperities are deformed and the real area of contact increases (right).

materials, the optical method permitted estimations of the real contact area ratio (A_r/A_a) between 0.1 and 1 % for pressures of about 2.3 kPa [17][1].

Dependence of real area of contact on normal load It was shown that the real contact area linearly increases with the normal load, as represented on Figure 2.4b. This result was predicted by the Bowden and Tabor theory [16]: the deformation of the asperities in contact is proportional to the normal load. In other words, the more those asperities are pressed, the more they dilate and the higher the real area of contact becomes. We finally observe that the friction force between two surfaces is proportional to the normal load, supporting the idea that the friction force is proportional to the real area of contact.

Independance of real area of contact on apparent contact area Similarly, the real area of contact is constant when modifying the apparent contact area, the normal load remaining equal. Indeed, the real contact area remains the same because the deformation of asperities is inversely proportional to the apparent contact area. In this situation, the friction force remains unchanged. The friction force can thus be considered as proportional to the normal load and independent from apparent contact area. This non-obvious result will be detailed in the following section.

[1]Literature sometime suggested much lower ratios for paper-based wet friction materials: from 0.1 % [21] to 0.005 % [20]. However, those results were obtained for much higher pressures (0.1-5 MPa) and for materials with less than 30 % of paper, the rest being mainly resins and elastomers

2.5 Stick-slip phenomenon

Introduction An interesting consequence of friction is the apparition of the stick-slip oscillations. A shearing stress applied on two materials in contact creates a force of static friction at their interface. The surfaces stick to each other if the stress is low enough. Due to the elasticity of the materials or systems in contact, a potential elastic energy is stored. As the sliding starts, this energy is released and contributes to the relative displacement of the two surfaces. If this displacement is high enough, it overcomes the stress applied on materials. The materials then stick again, and the process is repeated. From a macroscopic view, this phenomenon is reflected by a discontinuous sliding, with fast oscillations between sticking and slipping.

Model A model of stick-slip is proposed in annex C. This model permits the determination of the amplitude and period of the stick-slip oscillations. The model shows that stick-slip is favored by (i) a high force during sticking compared to sliding, (ii) a low stiffness of the system, and (iii) a low average velocity of the motion. This model represents well the experiment. It was however observed that below a critical period of oscillation, stick-slip disappears and the movement becomes continuous [22] [23].

Examples and consequences A well-known example of stick-slip oscillations consists in earthquakes [11]. Due to the displacement of Earth's litosphere, high mechanical stresses are created on faults. When the stress reaches a critical level, the seismic faults start to slip. The mechanical energy stored is released a creates long-range oscillations. Another example is the sound created by friction: chalk on a blackboard, bowed instruments, or train brakes for example [11]. Stick-slip can also have critical consequences on mechanical systems. For example, the stick-slip oscillations that sometime appear when drilling oil wells can destroy the machine and the well. Stick-slip oscillations change the behavior of friction and its consequences can be critical. Understanding and controlling this phenomenon is therefore a challenging topic.

Summary and Conclusion of Chapter 2

Friction Friction is part of tribology, a domain of science that studies the contact between surfaces. Friction is the phenomenon responsible for the force opposed to the relative sliding of the two surfaces in contact.

Historical development Friction appears in our everyday life at different scales and was used for thousands of years. The scientific study of friction however dates from Leonardo da Vinci in about 1500, rediscovered by Amontons in 1699. Friction is still studied nowadays, in particular at atomic scale.

Energy transformation We consider two surfaces in contact and sliding on each other. Interactions take place between the surfaces due to (i) the adhesion, (ii) the roughness, and (ii) the deformation/abrasion of the surfaces in contact. In this situation, friction:

- **transmits** the mechanical energy from a surface to the other, and
- **transforms** the mechanical energy into heat, but also noise, modifications of the surface structures, or modifications in surface energies.

Real area of contact Friction is due to the interactions between the surfaces in contact. However, at a microscopic scale, the real area of contact is much smaller than the apparent area of contact at a macroscopic scale (ratio between 0.1 and 1 % for the paper-on-glass contact). We observe that the real area of contact is (i) proportional to the normal load between the surfaces, and (ii) independent of the apparent contact area. Consequently, this fundamental observation explains the linear relation between the friction force and the normal load.

Stick-slip oscillations Due to the relative elasticity of the materials in contact, friction sometime creates stick-slip oscillations. Stick-slip consists in a sequential build-up and release of stored energy in elastic components. The result is a cyclical acceleration and deceleration of the relative displacement. The next chapters will heavily rely on the different mechanisms we introduced here.

Chapter 3

Standard methods for measuring the friction force

Numerous test methods permit the measurement of the friction force between two materials. However, their domains of application are often limited to specific materials, constraints, or movements. In this chapter, we propose an overview of the methods used for the paper-on-paper friction force measurement. For each method, we will study successively the experimental setup, the associated models, and finally the advantages and drawbacks.

3.1 Inclined plane

3.1.1 Experiment

Perhaps the most famous and simpler method for measuring the friction force is the *inclined plane*. To characterize the friction force between two samples, one is fixed on a plane and the other is fixed on a weighted sled. The method then consists in tilting the plane from the initial horizontal position ($\alpha = 0$) to an angle, α_{max}, at which the sled starts sliding, as represented on Figure 3.1a. The apparatus we used is represented on Figure 3.1b. For paper materials, this method is described by the TAPPI T 815, T 548, T 541, and NF Q 03-083 standards [24, 25, 26, 27].

3.1.2 Model

Break-away force We consider the sled, of mass m, in the Galilean referential. The sled undergoes two forces, represented on Figure 3.1a: (i) its weight that can be divided into a tangential and normal components, and (ii) the force of friction F_f that is opposed to the tangential component of the weight.
Before the sliding, the sled is immobile on the plan. The balance of forces gives:

$$F_f = mg.\sin\alpha \tag{3.1}$$

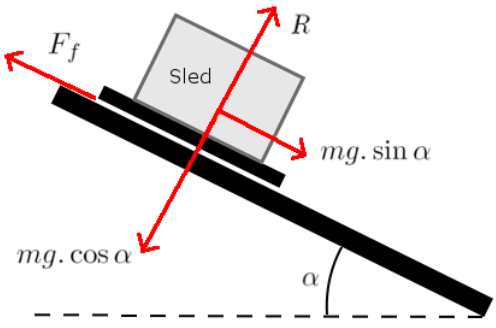

(a) Forces underwent by the sled

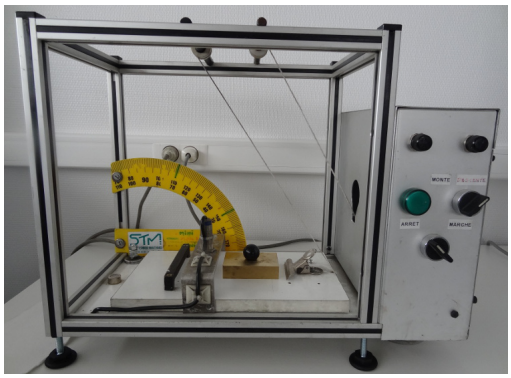

(b) Apparatus (LGP2 Laboratory)

Figure 3.1: Inclined plane test method

Where F_f and g are the force of *static friction* and the standard gravity (g = 9.81 m.s^{-2}), respectively. The force or static friction (also sometime abbreviated *stiction*) is oriented backward to the slope. The force avoids any relative movement between the surfaces.
As sliding starts, the angle and the force of static friction are maximal. This force is called the *break-away force* or *maximal force of static friction*. However many authors call it *force of static friction*. For commodity reasons, it is often noted F_S.

$$F_S = mg.\sin\alpha_{max} \tag{3.2}$$

Coefficient of static friction As it was introduced in the previous chapter, experiments show that the break-away force is highly dependent on the normal force. We thus introduce the *coefficient of static friction*, μ_S, defined by:

$$F_S = \mu_S.F_N \Leftrightarrow \mu_S = \tan\alpha_{max} \tag{3.3}$$

Where F_N represents the normal component of the weight. In most cases, the coefficient of static friction is constant under various test conditions (e.g., normal load, direction of the displacement, or contact time). The coefficient is thus usually considered as a characteristic of the surfaces in contact.

3.1.3 Advantages and drawbacks

Advantages The method is cheap, intuitive, and easy to run. In particular, the model is also very simple to use. The coefficient of static friction obtained characterizes the force of static friction in a wide range of conditions.

Drawbacks The method suffers however from several drawbacks listed hereafter:

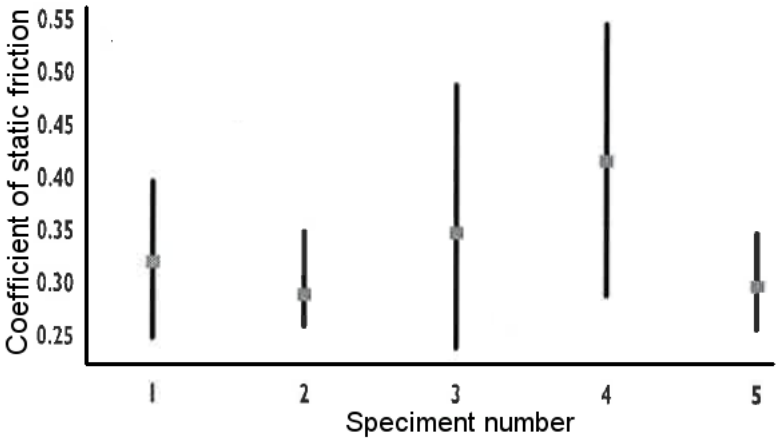

Figure 3.2: Measurements delivered by five inclined plane apparatus respecting TAPPI T 815 standards [8]. Measurements on five specimens of linerboards. Vertical bars show the range of friction readings for each of the specimens.

i. Different coefficients of static friction cannot be compared as they are measured for different applied loads. Indeed, in the case of polymer for example, it was shown that the coefficients of static friction evolve with the normal load [28, 29].

ii. The repeatability of the measurement is poor (precision of $\pm$ 4 %) due to the difficulty to observe the beginning of the sliding. As we observed in our experiments, it is in particular the case for contacts involving rubber due to a large difference of stiffness of the materials [30].

iii. As the sliding is not controlled, this method cannot be used to study the effect of successive tests on a single couple of samples. It is a major drawback if the coefficient of static friction evolves with repeated slidings, as for example in the case of paper-on-paper contacts [31].

iv. The method is useful to study only simple models of friction. In particular, the method does not allow the measurement of the force of kinetic friction, i.e. the force of friction during sliding. It is also impossible to measure the presliding displacements.

Those drawbacks contribute to the variations observed from an equipment to another, as represented on Figure 3.2.

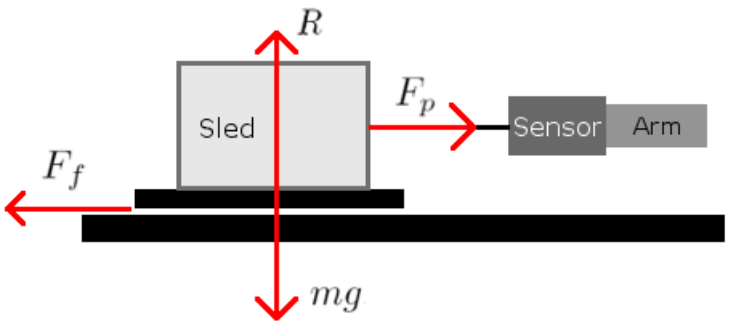

Figure 3.3: Horizontal plane test method. F_p, R, and F_f represent the pulling force, the reaction of the plane to the sled weight, and the force of friction, respectively.

3.2 Horizontal plane

3.2.1 Experiment

The plane, the sled, and the samples are placed similarly to the inclined plane test method, but the plane remains horizontal. A pulling force is applied on the sled by an arm moving at constant speed. A force sensor measures the pulling force, noted F_p. An example of measurement is proposed on Figure 3.4. We note that the ISO 15359 standard requires a slightly increasing pulling force at the beginning of the sliding [32]. For the standards TAPPI T549, TAPPI T816, and NF Q03-082, on the other hand, the displacement can be due to a shock between the force sensor and the sled [33, 34, 35]. As a consequence, the acceleration of the sled can be high and the peak (2) of Figure 3.4 very sharp.

3.2.2 Models

3.2.2.1 Conventions

We consider that the sled undergoes only four forces in the Galilean referential: (i) its weight, (ii) the reaction of the plane to the weight, (ii) the pulling force applied by the sensor on the sled, and (iii) the force of friction in the opposite direction than the pulling force. Those forces are represented on Figure 3.3.

3.2.2.2 Static friction

Between points (1) and (2) of Figure 3.4, the sled is immobile on the plane. Similarly to the inclined plane, the force opposed to the displacement is the force of static friction. When reaching the point number (2), the force of static friction is maximal: the break-away force is reached. The break-away force, F_S, is thus considered as the maximal pulling force measured. The previously described concept of coefficient

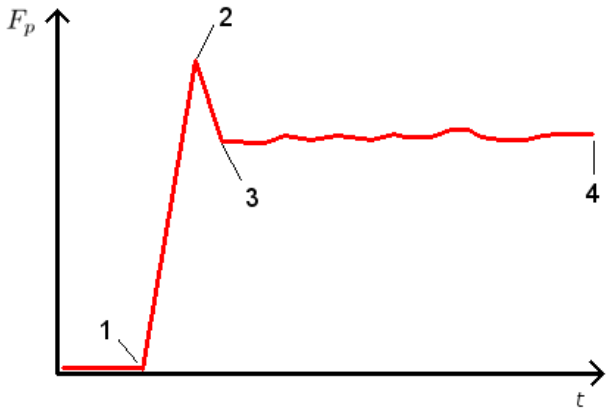

Figure 3.4: Typical measurement obtained with the horizontal plane. The pulling force, F_p, is represented as a function of the time. The different phases are (1) the sensor starts applying a force on the sled, (2) the sled starts to slide, (3) the sled reaches the desired velocity, and (4) end of the measurement.

of static friction remains valid ($\mu_S = F_S/mg$). A representation of the model is proposed on Figure 3.5a.

3.2.2.3 The Coulomb's model

The Coulomb's model is a first approach to the characterization of the friction force during this kinetic regime. Between the points (3) and (4), the sled has roughly a constant velocity. The balance of forces is thus approximately zero. The force of kinetic friction, F_K, is thus equal but opposed to the pulling force, F_p. Similarly to the static friction, the force of kinetic friction appears to be proportional to the normal load. We thus introduce the *coefficient of kinetic friction*, μ_K, defined by:

$$\mu_K = \frac{F_K}{mg} \tag{3.4}$$

The coefficient of kinetic friction is usually constant under various test conditions (e.g. normal load or sliding direction). The coefficient is thus considered as a characteristic of the surfaces in contact. The model is represented on Figure 3.5b.

3.2.2.4 High velocities - Viscous model

The theory of hydrodynamics developed in the 19th century led to an expression of the influence of sled velocity on the friction force [11]. This influence is called viscous friction and often summed to the Coulomb friction:

$$F_K = F_C + F_v \tag{3.5}$$

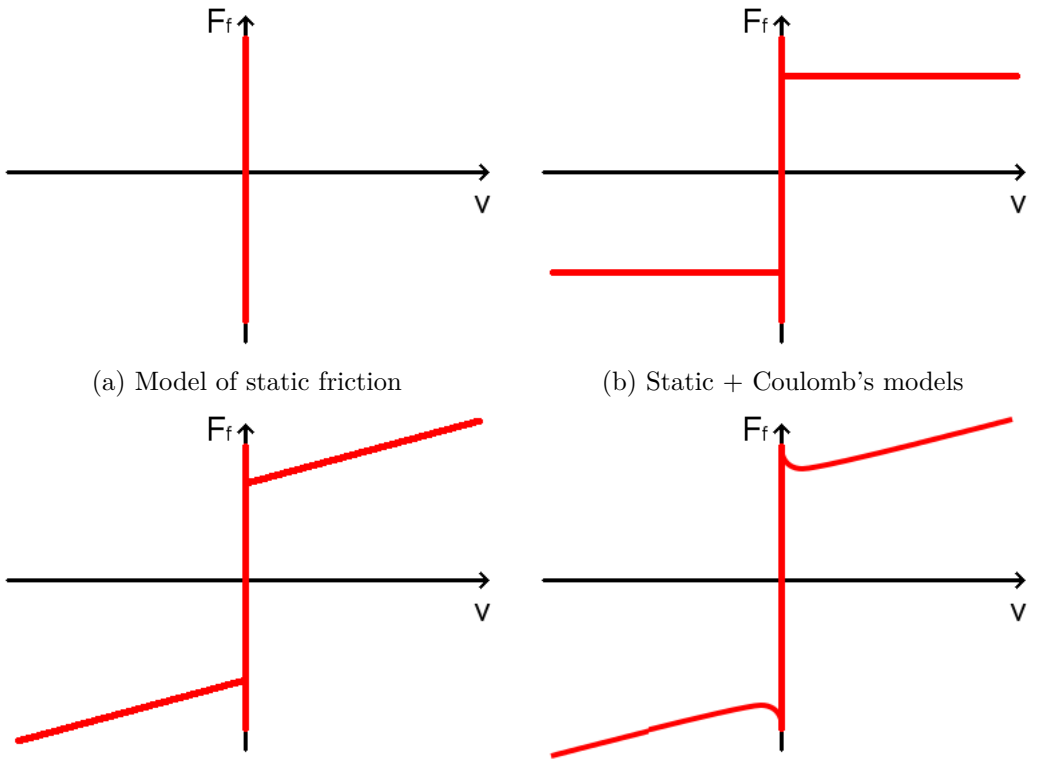

(a) Model of static friction

(b) Static + Coulomb's models

(c) Static + Coulomb's + viscous models

(d) Stribeck curves

Figure 3.5: Different *static* models of friction force, F_f, as functions of the relative velocity, v, of the surfaces in contact. The models are called "static" because they depend only on the relative velocity between the two bodies in contact.

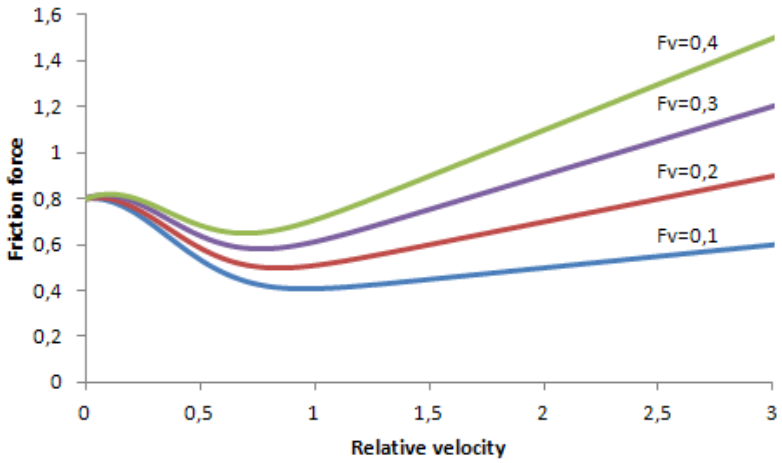

Figure 3.6: Stribeck curves for $F_C = 0.3$, $F_S = 0.8$, $v_S = 0.5$, and $\delta_S = 2$

Where F_C and F_v represent the Coulomb and viscous frictions, respectively. The simplest model for this correction is a linear dependency to the velocity, v, as represented on Figure 3.5c:

$$F_v = \mu_v.v \tag{3.6}$$

Where μ_v represents the coefficient of viscosity. To measure the viscous friction, F_v, with the horizontal plane setup, the force of kinetic friction, F_K, has to be determined for several sled velocities. However, the range of speeds required to observe this phenomenon is often too large for common apparatus. It was indeed the case for the paper-on-paper contact using the apparatus available at LGP2.

3.2.2.5 Low velocities - Stribeck curves

The previously described models have a major drawback: the transition from static to kinetic friction is non-linear. In many mechanical problems, this non-linearity of the friction models becomes problematic. In 1902, R. Stribeck proposed curves describing the transition between the forces of static and kinetic friction. Stribeck proposed a model of kinetic friction force that is function of the sled velocity [36]:

$$F_K(v) = F_C + F_v + (F_S - F_C).e^{-|v/v_S|^{\delta_S}}.sgn(v) \tag{3.7}$$

Where v_S, $sgn(v)$, and δ_S are the Stribeck velocity, the sign of the relative velocity, and a shape factor that is fixed to 1 in the Tustin exponential model, respectively. Examples of Stribeck curves are given on Figure 3.6. The Stribeck parameters are theoretically identifiable by using the horizontal plane method at different low speeds. However, the range of velocities permitted by the apparatus may be not sufficient for this measurement.

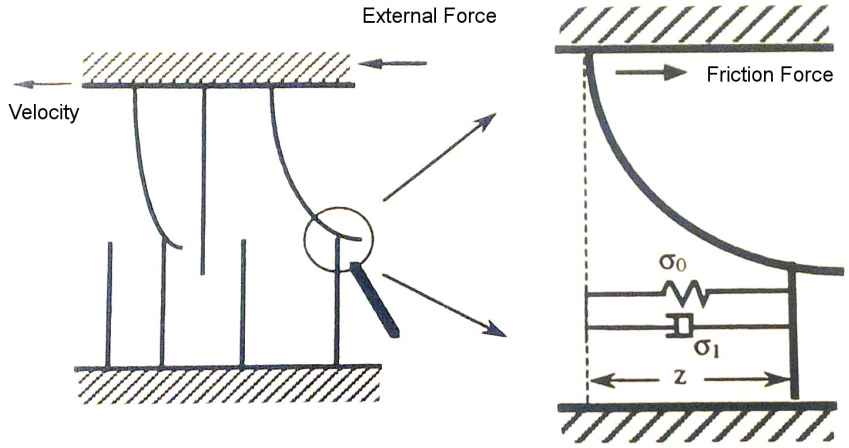

Figure 3.7: Principle of the LuGre model. On the left, the considered bristle deflections. On the right, a detail of the model. (Adapted from [37].)

3.2.2.6 Dynamic friction models

Dynamic models The previous models are called *static friction models* because they consider constant velocities. However, the need for precision servomotors required much more deeper analyzes of the friction force. Scientists thus developed *dynamic friction models*. Such models consider the friction before the macro-displacement or during changes in sliding direction, for example. The dependence of friction on the relative velocity between the two bodies in contact is modeled using a differential equation [11].

Bristle model The first dynamic model developed was the Dahl's model. Latter, *bristle model* considers the asperities in contact between the two surfaces as bristles: as a shearing stress appears between the surfaces, asperities deflect, creating a force opposed to the displacement. When the shearing becomes too high, the contact between bristles breaks: the break-away force was overcome and the sliding starts.

The LuGre model Based on the bristle model, the LuGre model[1] is based on the average deflection of the bristles, z, represented on Figure 3.7. An expression is given by:

$$\begin{cases} \dot{z} = \dot{q} - \sigma_0 \frac{|\dot{q}|}{g(\dot{q})} z \\ g(\dot{q}) = \alpha_0 + \alpha_1 e^{-\left(\frac{\dot{q}}{v_S}\right)^2} \\ F_f = \sigma_0 z + \sigma_1 \dot{z} + \alpha_2 \dot{q} \end{cases} \tag{3.8}$$

[1] LuGre stands for Lund (Sweden) and Grenoble (France)

With $\dot{z}$, $\dot{q}$, and F_f representing the derivative of the bristles deflection, the velocity of the displacement and the friction force, respectively. In particular, α_0, α_1, and α_2 represent the Coulomb's friction, the difference between the break-away force and the Coulomb's friction, and the viscous friction, respectively.

Test on horizontal plan The model permits an in-depth study of the friction force behavior, in particular the pre-displacement mechanisms and the Stribeck curves. However, the horizontal plane test method has no position sensor, so that pre-displacements cannot be studied. Similarly, to determine the Stribeck velocity (v_S), low velocities are required but are usually not available on the horizontal plan. Consequently, dynamic models permit a deeper analysis of friction force, but are beyond the possibilities of the horizontal plan method.

3.2.3 Advantages and drawbacks

Advantages The method is often used for measuring both the static and kinetic friction forces of a wide range of materials. Indeed, the method is intuitive, maintains the normal load constant, and is adapted to the study of successive slidings.

Drawbacks The method suffers however from several drawbacks listed hereafter:

i. The maximum pulling force does not necessarily correspond to the beginning of the sliding. We exemplified this problem in the rubber-on-steel case, as it will explain in the next chapter.

ii. The acceleration of the sled is often neglected in the calculation of the friction force. Moreover, the determination of the maximal pulling force is based on a low number of measured points that decreases with the acceleration of the arm (from points 1 to 2). As a consequence, the errors due to the acceleration of the sled increase with the acceleration.

iii. Stick-slip consists in a sequential build-up and release of stored energy in elastic components, resulting in cyclical acceleration and deceleration of the sled. The horizontal plane method does not allow the separation of the force components due to static friction, kinetic friction, and mass-acceleration [38], as noticed by IS0 15359 [32]. Avoiding stick-slip by increasing the stiffness of the sensor and/or the velocity of the displacement [22] would increase the sled acceleration and therefore the errors described in (ii).

iv. The test conditions may be far from technological applications. In particular, the method is usually restricted to slow motions (up to 5 mm.s^{-1}) and does not study complex movements such as jerky movements.

v. The method does not allow the measurement of micro-displacements. These measurements are required for dynamic models of friction [37].

Method/ material	Size of the apparent contact area of the sled	Surface pressure, kPa/ backing	Sliding distance, mm	Pulling rate, mm/s	Number of slidings/ static or kinetic
ASTM 3247/ corrugated or solid fibreboard	2000mm^2 or 62,5mm x 62,5mm	3,44/ hard	62,5	2,54	Three. Only the third static value is evaluated.
ASTM ANSI/ASTM D 1894-78/ plastic film and sheeting	63,5mm x 63,5mm	0,49/ soft	130	2,5	One Static and kinetic
DIN 6729/ punched tapes	15mm x 75mm	6,54 / soft	0	0,04	One static
DIN 53375/ plastic film	4000mm^2 or 63mm x 63mm	0,49/ soft	60	1,67	One. Static and kinetic (no stick-slip allowed)
ISO 8295/ Plastic film	4000mm^2 or 63mm x 63mm	0,49/ soft	60	1,67	One. Static and kinetic
T 816 om-92/ corrugated and solid fibreboard	2000mm^2 or 63,5mm x 63,5mm	3,5/ hard	63,5	2,5	Three. Only the third static value is evaluated.
T 549 pm-90/ writing and printing papers	63,5 mm x 63,5mm	0,48/ optional, soft	130	2,5	One. Static and kinetic

Table 3.8: Comparison of different standard methods based on the horizontal plane [38]

vi. There are different possibilities of test conditions as defined by standards (contact area, normal load, velocity, or sliding distance), as represented on Table 3.8. The methods also do not provide justifications for the measurement conditions [39].

3.3 Strip-on-drum

3.3.1 Experiment

The *strip-on-drum test method*, also called *cabestan test method*, consists in placing a paper sample around a cylinder. Another paper sample lays on it, with a mass at the one end and a dynamometer at the other end, as represented on Figure 3.9. The

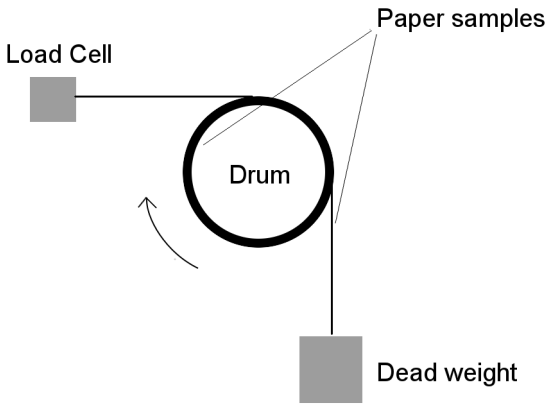

Figure 3.9: Principle of the strip-on-drum test method. A paper sample is placed around a rotating cylinder. Another paper sample lays on it, with a mass at the one end and a dynamometer at the other end.

two paper materials are thus in contact over an arc of 90°. By making the cylinder rotate, a kinetic friction force is created between both samples and measured by the dynamometer. In particular, the rotation speed can be high (over 1 $m.s^{-1}$).
The method has been widely used for testing textiles, rubber webs, and magnetic tape in strip forms for example [40]. However, the method is not considered as a standard for testing paper materials in the frame of TAPPI or ISO. Thus, we will just make an overview of this solution. Details can be found in the works of de Silveira and Hutchings [40] [41].

3.3.2 Model

Independence of the kinetic friction to the normal load The force of kinetic friction of the paper-on-paper contact is supposed to be independent from the normal load. The relation between the applied normal load, T_1, and the measured load, T_2, was first studied by Euler in 1762 [9]. We obtain an expression of the coefficient of kinetic friction:

$$\mu_K = \frac{1}{\theta_0} \ln\left(\frac{T_2}{T_1}\right) \tag{3.9}$$

Where θ_0, T_1, and T_2 represent the contact angle ($\pi/2$ in this study), the applied load by the dead weight, and the measured load, respectively [40].

Dependence of the kinetic friction to the normal load Polymeric or fibrous materials often do not obey the Amonton's first law of friction. The friction force then depends on the nominal contact pressure. In this situation, a common expres-

sion of the force of friction is [40]:

$$F_f = \alpha \left(\frac{P}{P_0} \right)^{\nu} A \tag{3.10}$$

Where P, P_0, ν, and A represent the nominal contact pressure, a reference pressure, a coefficient that is different from 1, and the apparent contact area, respectively. Both ν and α coefficients have to be identified, requiring several measurements with different normal loads. However, the nominal pressure evolves along the drum. The expression of the force of kinetic friction is therefore not obvious. Details of the method and theoretical aspects can be found in the work of Sato et al. [40].

3.3.3 Advantages and drawbacks

Advantages The strip-on-drum test method is useful to study high speeds and/or long runs. Indeed, the method is not limited by the plane length.

Drawbacks The method suffers however from several drawbacks listed hereafter:

1. The strip sample is in lateral tension, possibly modifying the fibrous structure. This drawback limits the dead weight to 300 g [40].
2. The method supposes the bending of the materials. The method therefore does not allows the testing of envelopes and boards.
3. The bending may also induce an asymmetric deformation of the surfaces in contact. Indeed, the surface of the strip sample is compressed when the drum one is stretched.
4. At high rotation speeds, air may be aspirated between the drum and the strip, reducing the normal load [42, 7]. On the other side of the drum, paper dust created by abrasion is ejected, avoiding the paper abrasion characterization and the comparison with plane methods.
5. Similarly to the plane methods, the two samples involved do not undergo the same mechanical stress. In particular, a point of the strip is always in contact with the drum, whereas a point of the drum alternates between contact and no-contact with the strip.
6. The literature concerning paper-on-paper friction using the strip-on-drum method is very poor. In particular, results often highlight unexplained differences with the results obtained using the plane methods [41].

These drawbacks (the last one in particular) justify our decision not to consider the strip-on-drum test method in this study.

Summary and Conclusion of Chapter 3

Inclined plane test method The inclined plane test method (TAPPI 815/816) consists in placing the studied samples between a sled and a plane. The plane is then tilted until the sled starts sliding. The tilt reached characterizes the maximal force of static friction reached between the samples.

Horizontal plane test method The horizontal plane test method (TAPPI 549/816, ISO 15359) is similar to the inclined plane test method. However, the plane remains horizontal. The sliding of the sled is permitted by a moving arm. The force of friction is then measured by a force sensor placed on the arm. The forces of static and kinetic frictions can be determined using this method.

Strip-on-drum test method The strip on drum method consists in placing a sample around a rotating cylinder. Another sample lays on it, with a mass at the one end and a dynamometer at the other end. The dyanomometer thus measures the force transmitted by friction between both samples.

Models for friction force The Coulomb's model of friction considers two regimes:

- **Samples stick to each other -** The force of static friction is sufficient to avoid any relative displacement between the surfaces. The maximal force of static friction, called *break-away force*, is equal to the normal load multiplied by the coefficient of static friction, μ_S.
- **Samples slide on each other -** The force of kinetic friction is equal to the normal load multiplied by the coefficient of kinetic friction, μ_K.

This model is clear and simple. More accurate models are available (e.g., Stribeck or dynamic models). However, the determination of their parameters using the inclined or horizontal plane test methods is nearly impossible for the paper-on-paper contact.

Chapter 4

The oscillating sled method

The optimization of franking machine feeders requires a deep understanding of the friction between paper materials. We showed that the standard methods for measuring the friction forces have several drawbacks. Thus, we built a new experimental setup. We compare its measurements to those acquired using standard methods. Advantages of the proposed setup and possible improvements are finally discussed.

4.1 Materials and methods

Proposed setup The proposed setup, called *oscillating setup*, is based on the horizontal plane method in accordance with the standards (NF Q 03-082 [35] and TAPPI 549 [33]). We place a spring between the force sensor and the sled. The sled-spring-sensor system has a constant spring stiffness, k (390 N.m^{-1}). The spring induces a stick-slip phenomenon at roughly 2 Hz. We plug an analog filter to decrease the noise delivered by the force sensor, as it was initially up to 10 % of the measurement. A Linear Variable Differential Transformer (LVDT) position sensor (Sensorex 12F5 under Schaevitz license, accuracy ±0.01 mm) is placed between the sled and the arm, parallel to the spring, as represented on Figure 4.1a. The sled weights 837 g. The velocity of the arm is set to 5 mm.s^{-1}. The frequency of acquisition is 400 Hz. The measurements are processed using a Labview program we developed, which interface is represented on Figure 4.1c. The apparatus actually developed is represented on Figure 4.1b.

Proposed method The LVDT sensor measures the spring elongation, $u(x)$, defined as: $u(x) = x_a - x - l_0$, where x_a, x, and l_0 represent the position of the arm, the position of the sled, and the spring elongation at rest, respectively. The fundamental principle of dynamics applied to the sled can be included in the expression

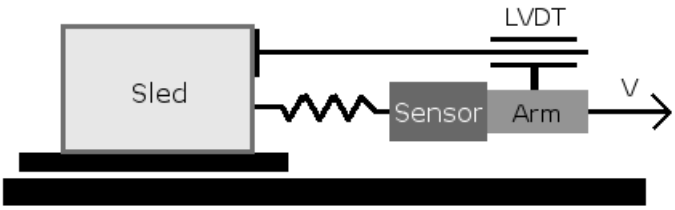

(a) Schematic view

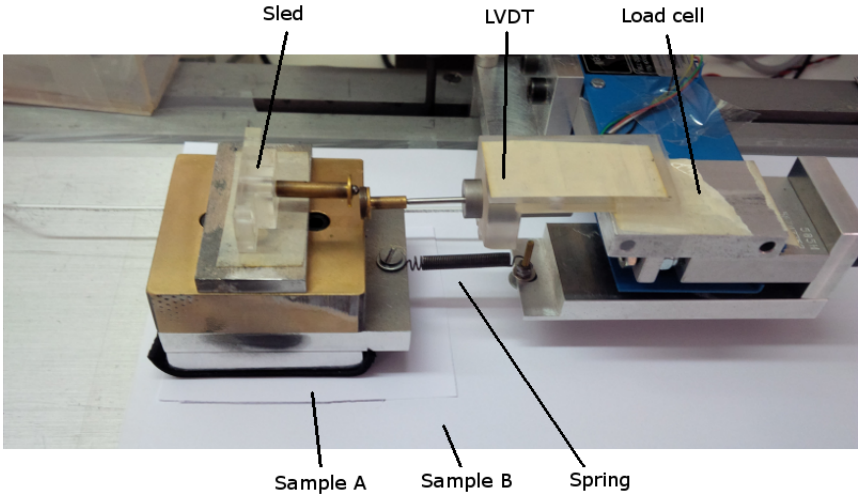

(b) The setup actually developed

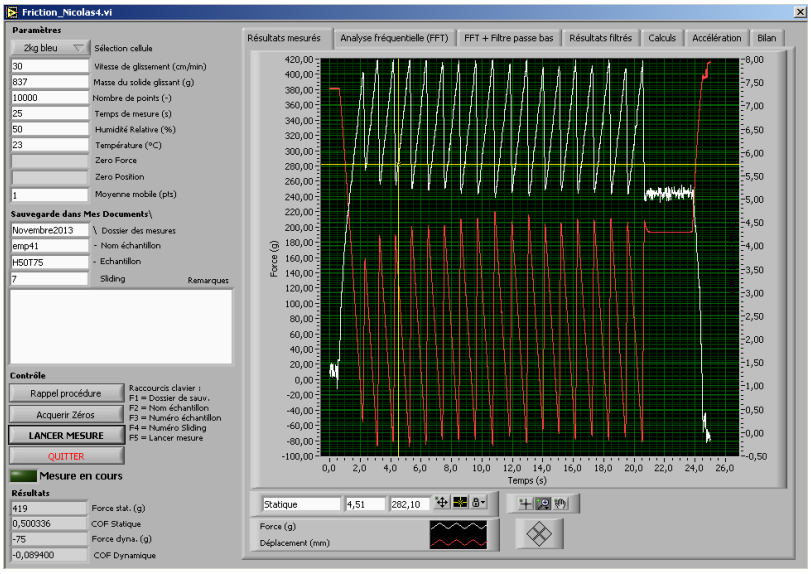

(c) Interface of the Labview programm developed for the measurements acquisition

Figure 4.1: The oscillating sled setup

of the coefficient of friction:

$$\mu = \frac{F_f}{F_N} = \frac{1}{m.g}\left(F_p - m.\frac{\mathrm{d}^2x}{\mathrm{d}t^2}\right) = \frac{k.u}{m.g} - \frac{1}{g}\left(\frac{\mathrm{d}^2x_a}{\mathrm{d}t^2} - \frac{\mathrm{d}^2u}{\mathrm{d}t^2}\right) \tag{4.1}$$

Where F_f, F_p, m, g, and k represent the friction force, the pulling force applied by the arm on the sled, the mass of the sample-sled system, the standard gravity ($g = 9.81$ m.s^{-2}), and the spring stiffness of the spring, respectively. The second derivative of the elongation is noisy. Therefore, we estimate this elongation by identifying a sixth order polynomial interpolation of the elongation measurement, $u(x)$. For each spring elongation, we compute a polynomial interpolation based on the $N/2$ previous and $N/2$ next measurements. The result of the interpolation is noted $w(x)$. The difference between $w(x)$ and $u(x)$ is found to be lower than 0.1 % which allows us replacing u by its estimation w. The arm moving at a constant speed, its acceleration is therefore zero. We thus obtain from equation 4.1:

$$\mu = \frac{k.w}{m.g} + \frac{1}{g} \cdot \frac{\mathrm{d}^2w}{\mathrm{d}t^2} \tag{4.2}$$

In conclusion, the proposed method permits (i) the measurement of the pulling force applied by the arm on the sled, (ii) the calculation of the velocity of the sled, (iii) the calculation of the coefficients of friction, and (iv) the measurement of the acceleration of the sled.

Influence of stick-slip oscillations on the friction measured The movement of the sled is different in the oscillating and horizontal plane setups. Consequently, the friction forces measured on both setups may be different, as reported in the literature [15]. The two main reported observations are (i) a change in time spent in static friction (also called *dwell time*), and (ii) a time delay between a change in velocity and the corresponding change in friction (also called *frictional lag*) [15, 43]. On the one hand, the decrease in dwell time with stick-slip oscillations is known to reduce the coefficient of static friction. On the other hand, the frictional memory does not allow the proper characterization of the friction force during stick-slip oscillations, as the relative speed evolves quickly. These mechanisms are usually observed for low velocities and high spring stiffness [22].
However, these conditions are far from those involved in our experiment. Literature suggests that in the conditions considered in the oscillating setup, the two previously listed observations are not met for the paper-on-paper contact [22, 38]. Consequently, the friction force can be properly characterized by the viscous model of friction [22]. This model consists in a linear increase in friction force with relative speed. This behavior can be characterized by our oscillating setup, as the relative velocity and the friction force are simultaneously measured.

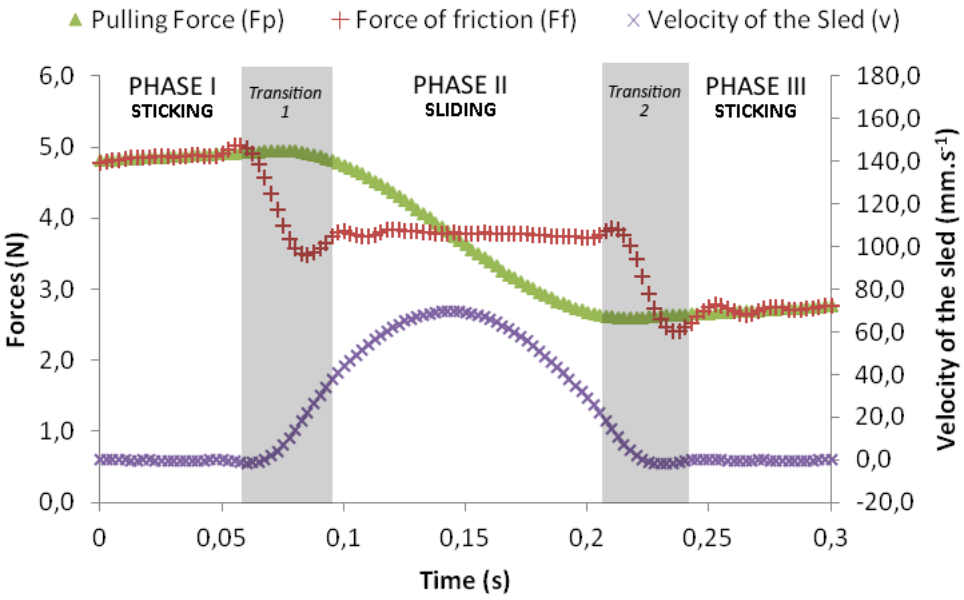

Figure 4.2: Typical records obtained with the oscillating setup. The force of friction is calculated using equation (4.2).

Experiments We study the friction of 80 g.m^{-2} writing papers. The experiments are carried out on a length of ten centimeters. For each experiment, ten pairs of samples are tested and the sliding is repeated five times. The results obtained from the oscillating setup are compared to results of the inclined and horizontal planes setup. We also study separately the influence of three experimental parameters on the measurements: (i) the rubber of the sled is set directly on the horizontal metalic plane, (ii) the spring constant is decreased to 315 N.m^{-1}, and (iii) the arm velocity is decreased to 2.5 mm.s^{-1}.

4.2 Results and discussion

4.2.1 An evolution of forces in three phases

Typical records for the paper-on-paper friction during the fifth repeated sliding are shown in Figure 4.2. We choose to consider the fifth repeated sliding as it is more stable than the previous slidings. Indeed, the force of friction of the paper-on-paper contact is known to decrease by up to -50 % between the first and third repeated slidings [44, 45]. Three phases (I, II, and III) and therefore two transitions (1 and 2) may be observed.

- **Phase I and III -** The first and last phases consist in the sticking between

the two samples. The arm moves at a constant velocity, inducing a linear elongation of the spring and a linear increase of the force of static friction. The phase ends when the break-away force is reached and the sliding begins.

- **Phase II -** The second phase consists in the sliding between the two samples. During this phase, the ratio between the sled and arm velocities ranges from 1 to 10. This difference of velocity leads to a shortening of the spring and therefore a continuous decrease of the pulling force, F_p. On the other hand, the calculated friction force is nearly constant. Assimilating the pulling force to the force of friction is consequently not accurate in the sliding zone. The importance of the acceleration of the sled is underlined as we estimate the inertial parameter, $m.\frac{\mathrm{d}^2x}{\mathrm{d}t^2}$, to be up to 25% of the friction force.

- **Transitions 1 and 2 -** The transitions are situated between the sticking and sliding phases. The force of friction thus evolves between the break-away force and the force of kinetic friction. We observe that the duration of the phase evolves with the number of measurement points used to calculate the interpolations of u, as described in the supplementary information. The calculated force of friction is therefore mainly governed by the mathematical errors created by the calculation of interpolations. Additionally, the transition is also influenced by complex physical phenomena such as the so-called Stribeck effect [36] or the frictional lag [15].

In conclusion, our oscillating setup allows the measurement of both the break-away force and the force of kinetic friction. In addition, the method characterizes the sled position, velocity, and acceleration

4.2.2 Mathematical errors induced by the interpolation

To show the influence of the parameter N on the friction force calculation, we make the parameter vary from 10 to 50 points on Figure 4.3. We clearly observe that a low N value is associated to (i) a high dispersion in friction forces (represented by A_N) and (ii) a low duration of the transient phases (represented by B_N), and *vice versa*. In other words, reducing the N value gives a better accuracy of the moment at which the sliding begins (see B_{10}). Conversely, increasing the N value gives a better accuracy of the friction force (see A_{50}).
In our experiment, using $N = 30$ points appears to be a good compromise. Indeed, we want the duration of the transient phases to be as low as possible, the break-away force remaining more accurately measured than with the horizontal plane.

4.2.3 Influence of experimental conditions

We modify successively the materials, the velocity of the arm, and the stiffness of the spring to study their influence on the measurement.

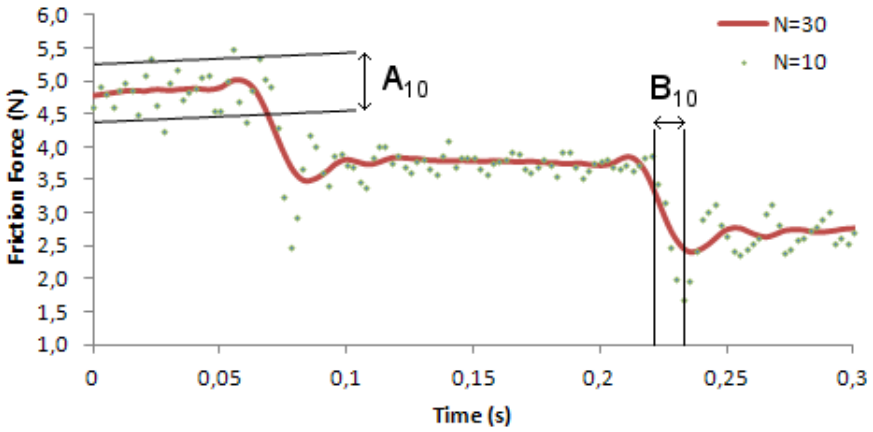

(a) N =50 points

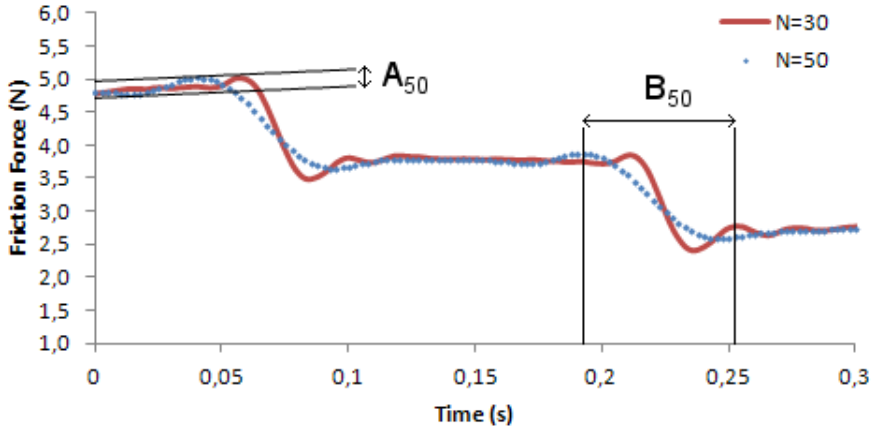

(b) N =10 points

Figure 4.3: Influence on the friction force calculation of the number of points, N, used in the 6th order polynomial interpolation of the spring elongation. We also represent the case $N = 30$ points used in our experiment. A_N and B_N represent the dispersion in friction force and the duration of the transient phases, respectively.

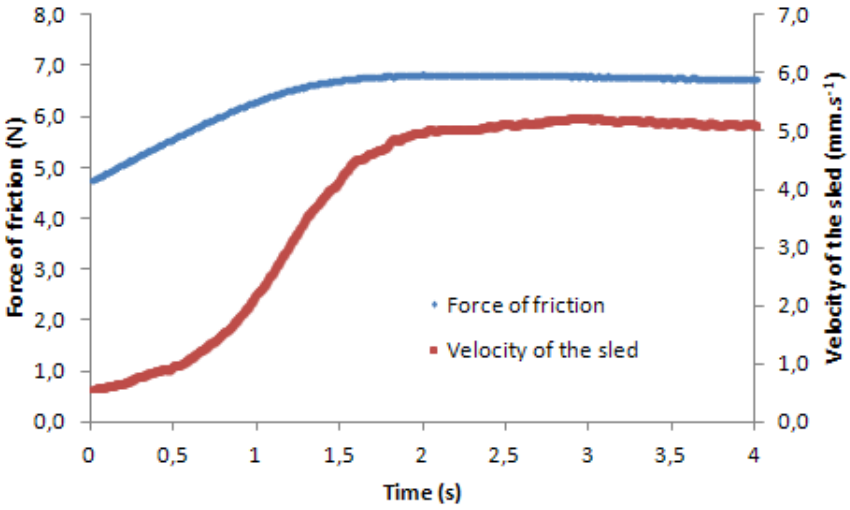

Figure 4.4: Typical records of the rubber-on-steel friction measured with the oscillating sled test method. The force of friction (top curve) and the velocity of the sled (bottom curve) are represented.

The rubber of the sled is set on the horizontal metalic plane. We observe a 2 seconds transient phase (Fig. 4.4). During this transient phase, the velocity of the sled and the force of friction increase. This observation shows that the maximal force of friction does not necessarily correspond to the begining of the sliding of the sled, as assumed by standard methods. The proposed method permits however a clear distinction between the static and kinetic regimes.
We also change the velocity of the arm and the spring stiffness, successively. The modified velocity of the arm is 2.5 mm.s^{-1}. The modified spring stiffness is 315 N.m^{-1}. The durations of the movement are 60 s and 30 s, respectively, to obtain similar distances of sliding. We do not observe any clear difference between the results (see Table 4.1). We conclude that our proposed method is robust in the explored domains of experimental parameters.

4.2.4 Comparison of the different methods

We compare the measurements obtained for the paper-on-paper friction with the inclined plane, the horizontal plane, and our oscillating setup. The results are summarized in Table 4.2. We make the following observations:

- The oscillating setup and the inclined plane methods give similar mean values and dispersions of the coefficient of static friction (differences and standard deviations up to 4 % and 2 %, respectively).

- The coefficient of static friction measured with the horizontal plane is different

		Reduced Velocity 390 N.m^{-1} - 2.5 mm.s^{-1}			Proposed Conditions 390 N.m^{-1} - 5 mm.s^{-1}			Reduced Stiffness 315 N.m^{-1} - 5 mm.s^{-1}		
	Sliding	Average	c_v	Δref	Average	c_v	Δref	Average	c_v	Δref
μ_S	1	0.70	2.1 %	-1.4 %	0.71	0.3 %	(ref)	0.71	1.0 %	-0.0 %
	2	0.67	1.0 %	-0.1 %	0.67	1.1 %	(ref)	0.68	1.2 %	-1.6 %
	3	0.65	1.1 %	0.4 %	0.65	1.1 %	(ref)	0.65	1.2 %	-1.0 %
	4	0.63	1.6 %	0.6 %	0.63	1.5 %	(ref)	0.64	1.4 %	-2.0 %
	5	0.62	1.2 %	0.3 %	0.62	1.5 %	(ref)	0.63	1.4 %	-2.6 %
μ_K	1	0.60	0.7 %	1.3 %	0.59	1.2 %	(ref)	0.60	0.8 %	1.7 %
	2	0.54	0.5 %	0.5 %	0.54	0.9 %	(ref)	0.55	0.9 %	1.7 %
	3	0.51	0.7 %	0.2 %	0.51	0.9 %	(ref)	0.52	0.7 %	2.3 %
	4	0.50	0.7 %	-0.2 %	0.50	0.8 %	(ref)	0.51	0.7 %	1.6 %
	5	0.48	0.8 %	-0.7 %	0.49	0.9 %	(ref)	0.50	0.8 %	1.6 %

Table 4.1: Comparison of the coefficients of static and kinetic friction obtained with the proposed setup in varying experimental conditions of spring stiffness and applied velocities. c_v represents the coefficient of variation of the measurement. Δref represents the gap between the reference, indicated by (ref), and the measurement.

from the one measured with the other methods (difference up to 9 %), but also more dispersed (standard deviations up to 5 %). This result can be explained by the low frequency and noisy signal of the force sensor, as it is not totally removed by the analog filter. Increasing the filter level would however alter the peak measured at the beginning of the sliding and therefore is not implemented.

- The coefficient of kinetic friction is much more dispersed using the horizontal method than using the oscillating setup (standard deviations up to 5 % and 1 %, respectively). This horizontal plane defect is due to the apparition of stick-slip oscillations. Indeed, those oscillations are of the order of magnitude of the characteristic time of the analog filter, leading to a distorted signal.

The limits of the horizontal plane method are confirmed: the method delivers poor estimations of the coefficient of static friction and should not be used in case of macroscopic stick-slip movements. This macroscopic movement can be spotted when the standard deviation in pulling force measurements is greater than the standard deviation in friction force measured with the oscillating sled (roughly 1.5 %). On the other hand, the oscillating setup appears to be adapted to the measurement of the coefficients of both static and kinetic friction.

		Inclined plane			Horizontal plane			Oscillating setup		
	Sliding	Average	c_v	Δref	Average	c_v	Δref	Average	c_v	Δref
μ_S	1	0.72	1.5 %	(ref)	0.75	1.5 %	3.5 %	0.71	0.3 %	-2.2 %
	2	0.67	1.8 %	(ref)	0.68	2.6 %	1.4 %	0.67	1.1 %	-0.5 %
	3	0.66	2.0 %	(ref)	0.64	3.7 %	-3.9 %	0.65	1.1 %	-2.5 %
	4	0.66	1.8 %	(ref)	0.62	3.6 %	-6.1 %	0.63	1.5 %	-4.5 %
	5	0.64	1.6 %	(ref)	0.59	5.3 %	-9.1 %	0.62	1.5 %	-4.5 %
μ_K	1	-	-	-	0.58	3.5 %	(ref)	0.59	1.2 %	3.0 %
	2	-	-	-	0.53	3.7 %	(ref)	0.54	0.9 %	1.4 %
	3	-	-	-	0.51	3.1 %	(ref)	0.51	0.9 %	-0.2 %
	4	-	-	-	0.50	3.4 %	(ref)	0.50	0.8 %	0.0 %
	5	-	-	-	0.49	4.7 %	(ref)	0.49	0.9 %	0.2 %

Table 4.2: Comparison of the coefficients of static (μ_S) and kinetic (μ_K) frictions obtained with different experimental setups. c_v represents the coefficient of variation of the measurement. Δref represents the gap between the reference, indicated by (ref), and the measurement. 10 experiments are carried out for each experiment.

4.2.5 On the validity of averaging the friction force

During the phase II, see Figure 4.2, the force of kinetic friction is constant. In the studied conditions, the paper-on-paper kinetic friction can thus be described by the Coulomb's law of friction. In this situation, the sled oscillates around an equilibrium position, which evolves with the arm displacement. Consequently, the average acceleration of the sled is zero during the sliding. We therefore obtain an approximation of the coefficient of kinetic friction:

$$\mu_K = \frac{F_f}{F_N} \approx \frac{\overline{F_f}}{F_N} = \frac{k.\overline{u}}{m.g} + \frac{1}{g}\frac{\mathrm{d}^2\overline{u}}{\mathrm{d}t^2} \approx \frac{k.\overline{u}}{m.g} = \frac{\overline{F_p}}{m.g} \tag{4.3}$$

Where $\overline{*}$ represents the mean value of the quantity $*$. Moreover, the average pulling force during the sticking phases is equal to the force of kinetic friction, as the sled oscillates around an equilibrium position. The equation 4.3 can thus be extended to the whole stick-slip oscillations. Equations 4.3 and 4.2 lead to similar results (differ by less than 1 %). The approximation proposed in equation 4.3 is however much easier to use, as it consists in averaging the pulling force measured.
Conversely, the approximation gives poor results with the horizontal plane, as indicated on Table 4.2. According to Johansson *et al.*, the high force components associated to accelerations, decelerations, and static friction are supposed to be responsible for this low accuracy [38]. But equation 4.3 shows that these components are canceled when averaging the pulling force. Thus, we rather suggest high-frequency stick-slip oscillations to be associated with a limited definition of the

force measurement. For example, the stick-slip frequency observed on the horizontal plane is of the order of magnitude of the characteristic time of the analog filter we use. In this situation, the measured pulling force becomes inaccurate (in particular its extremes) and so would be the approximation proposed in equation 4.3.
In conclusion, we suggest the measurements obtained with the horizontal plane to be rejected in the case of stick-slip oscillations with periods that are similar to the sampling rate of the sensor. In the case of oscillations of lower frequency, the force of kinetic friction may be approximated by averaging the pulling force.

4.3 Conclusion and perspectives

The two studied standard methods for the measurement of the friction forces (the inclined and horizontal plane methods) are limited and suffer from severe drawbacks. We have shown that the horizontal plane method can be improved to get an oscillating setup, by (i) placing a spring between the arm and the sled and (ii) using a position sensor measuring the spring elongation. Such a modification induces a controlled stick-slip movement. The proposed method gives lower dispersions and better accuracies for both the coefficients of static and kinetic friction. Although the velocity of the sled is no more constant, it follows a well-defined evolution up to 70 $mm.s^{-1}$ (compared to 5 $mm.s^{-1}$ for the horizontal plane method).
Several improvements should be investigated in future works: (i) a position sensor permitting the study of micro-displacements would allow the use of more complete models of friction, (ii) the varying velocities of the sled during the stick-slip movement allow the study of their influence on friction, and (iii) the transient phases between the static and kinetic friction should be reduced by either replacing the LVDT by a velocity sensor, or by improving the mathematical calculation of the sled acceleration.

Summary and Conclusion of Chapter 4

Principle of the method The two standard methods for the measurement of the friction forces are limited and suffer from several drawbacks. We therefore proposed a new experimental setup, called *oscillating sled*. The setup consists in a modified horizontal plane: (i) a spring is placed between the force sensor and the sled, and (ii) a position sensor is placed between the sled and the moving arm, as represented on Figure 4.1a. Such modifications induce a controled and measured stick-slip movement.

Advantages and drawbacks The oscillating sled test method gives lower dispersions and better accuracies for both the coefficients of static and kinetic friction. Although the velocity of the sled is no more constant, it is controled and measured on a range that is 10 times wider than with horizontal planes. The normal load is the same for different coefficients of friction. Finally, the study of the velocity and acceleration dependences of the friction force is also made possible.

Perspectives The micro-displacements of the position sensor could allow the study of dynamic models of friction. Moreover, the transient phases between the static and kinetic frictions should be reduced by replacing the displacement sensor (LVDT) by a velocity sensor and/or by improving the mathematical calculation of the sled's acceleration.

Chapter 5

The ring-on-plane method

The optimization of the franking machine feeders requires a deep understanding of paper friction. In franking machine feeders, the velocity of the relative displacements between paper materials is approximately 1.2 $m.s^{-1}$. However, the standard methods for measuring the friction force between paper materials are limited to low speeds (up to 5 $mm.s^{-1}$). Moreover, the friction between paper materials at high speeds is only poorly documented. We therefore developed a tribometer involving speeds above 1 $m.s^{-1}$.

5.1 Materials and methods

Apparatus We develop a tribometer, called *ring-on-plane method*, and based on a rotating ring in contact with a plane, as represented on Figure 5.1. This method is often used in the frame of abrasion measurements, as it allows long runs. The nominal properties of the DC motor (G30.1 of the Dunkermotoren compan) are 24 V, 3400 rpm, and 0,45 A. The characteristic diagram of the motor is represented on Figure 5.2. The motor is connected to a planetary gearbox (PLG30H of the Dunkermotoren company) with a reduction ratio of 11.5/1 and an efficiency of 0.9. Finally, the gearbox is connected to an aluminium ring with an external radius of $r_{ext} = 27$ mm and an internal radius $r_{int} = 7$ mm radius, as represented on Figure 5.3a. The motor is fixed on a vertical slide strongly fixed to the frame. The vertical slide allows only vertical translations of the motor. The mobile and its slides weight 670 g. They are placed so that the ring is parallel to the bottom part of the frame. A soft rubber is fixed to the frame, below the ring. The rubber permits a homogeneous pressure on the ring. We apply electric tensions from U =12 to 35 V. A multimeter measures the electric intensity I.

Materials We test two writing papers (80 $g.m^{-2}$). The paper samples are placed between the ring and the rubber of the frame. The samples are placed in order to

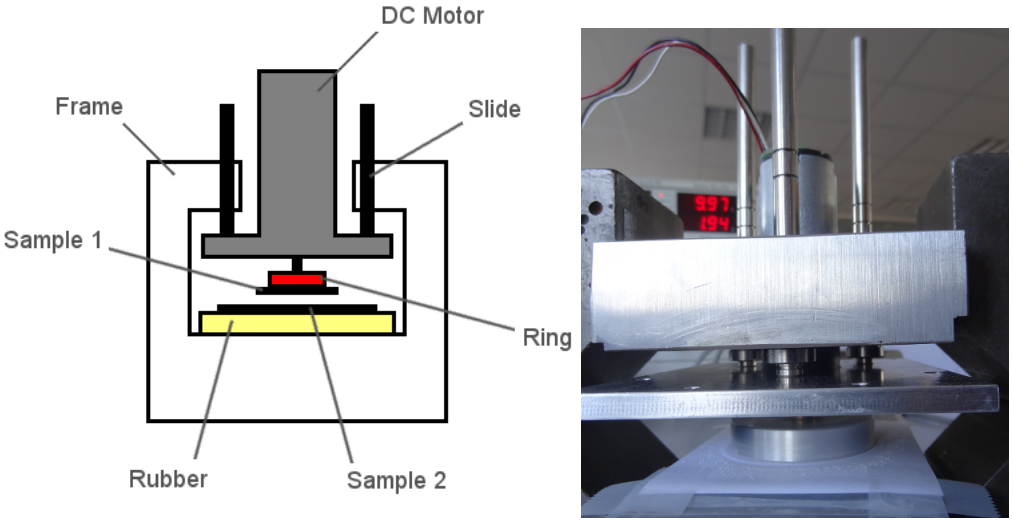

(a) Principle of method (b) Picture of the apparatus

Figure 5.1: The ring-on-plane test method

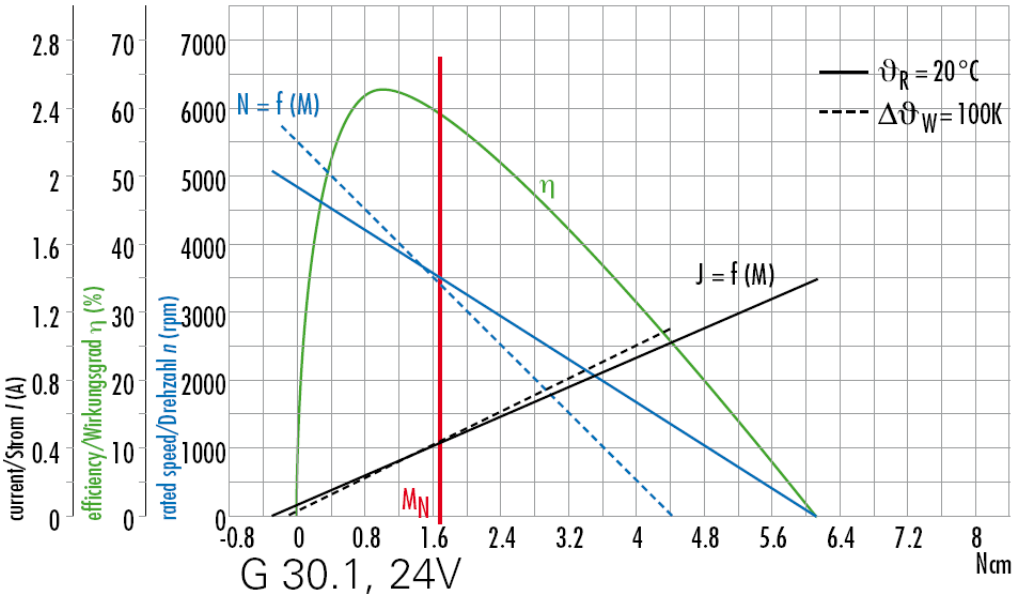

Figure 5.2: Characteristic diagram of the motor used [46]

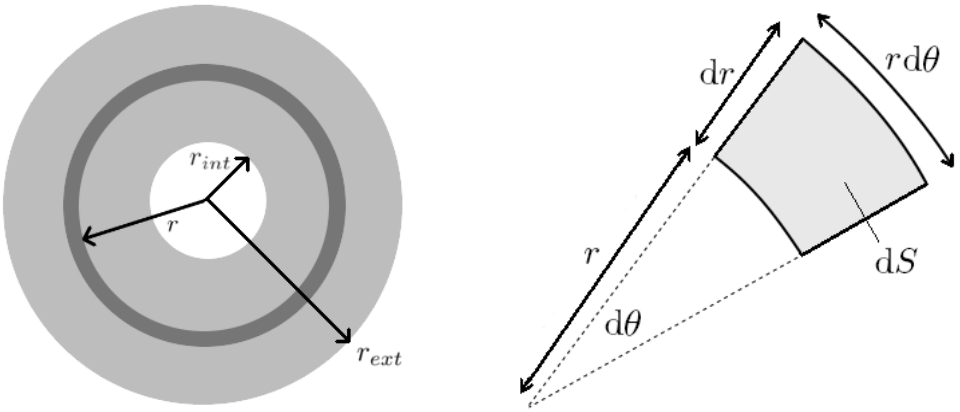

(a) Geometry of the ring

(b) Elementar surface on the ring.

Figure 5.3: Geometry of the ring-on-plane contact. The distance of considered infinitesimal surface to the center of the ring is r. The apparent angle of the surface is $\mathrm{d}\theta$. We obtain an expression of the infinitesimal surface: $\mathrm{d}S = r\mathrm{d}r\mathrm{d}\theta$.

ensure the contact between the same sides of the materials.

Friction force We consider an infinitesimal surface on the ring, called $\mathrm{d}S$. The distance of the infinitesimal surface to the center of the ring is called r, as represented on Figure 5.3b. The elementar surface can be expressed:

$$\mathrm{d}S = r\mathrm{d}r\mathrm{d}\theta \tag{5.1}$$

Where θ represents the apparent angle of the infinitesimal surface. The force of friction applied on the infinitesimal surface is given by:

$$\mathrm{d}F_f = \mu_K F_y \frac{\mathrm{d}S}{S} \tag{5.2}$$

Where F_f, μ_K, F_y, and S represent the force of friction, the coefficient of kinetic friction, the normal load applied by the ring on the plane, and the area of the ring, respectively. The coefficient of kinetic friction is described by the viscous model of friction as a linear function of the relative speed:

$$\mu_K = \alpha v + \beta = \alpha r\omega + \beta \tag{5.3}$$

Where v, α, and β represent the relative velocity, and two parameters of the model we aim at determining, respectively. The surface of the ring is given by:

$$S = \pi(r_{max}^2 - r_{min}^2) \tag{5.4}$$

Finally, the normal load applied on the ring is given by:

$$F_y = mg \tag{5.5}$$

The force of friction applied on the infinitesimal surface becomes:

$$\mathrm{d}F_f = \frac{mg(\alpha\omega r^2 + \beta r)}{\pi(r_{max}^2 - r_{min}^2)}\mathrm{d}r\mathrm{d}\theta \tag{5.6}$$

The elementar moment $\mathrm{d}M$ of the force of friction $\mathrm{d}F_f$ is expressed as:

$$\mathrm{d}M = r\mathrm{d}F_f = \frac{mg(\alpha\omega r^3 + \beta r^2)}{\pi(r_{max}^2 - r_{min}^2)}\mathrm{d}r\mathrm{d}\theta \tag{5.7}$$

Finally, we obtain an expression of the moment of the force of friction:

$$\begin{aligned} M &= \int_{r_{min}}^{r_{max}} \int_0^{2\pi} \frac{mg(\alpha\omega r^3 + \beta r^2)}{\pi(r_{min}^2 - r_{max}^2)}\,\mathrm{d}\theta\mathrm{d}r \\ &= \int_{r_{min}}^{r_{max}} \frac{2mg(\alpha\omega r^3 + \beta r^2)}{(r_{min}^2 - r_{max}^2)}\,\mathrm{d}r \\ &= \frac{\alpha\omega mg}{2}\frac{r_{max}^4 - r_{min}^4}{r_{max}^2 - r_{min}^2} + \frac{2\beta mg}{3}\frac{r_{max}^3 - r_{min}^3}{r_{max}^2 - r_{min}^2} \end{aligned} \tag{5.8}$$

The moment of the force of friction is calculated using the intensity measurement and the characteristic curve of the motor (Figure 5.2). The rotation speed of the motor is calculated using the electric tension and/or by measurement.
We propose the determination of the moment of friction for different rotation speeds. Equation 5.8 then permits the identification of the α and β parameter of the viscous friction model.

Experiments A first experiment consists in measuring the motor rotation speed as a function of the electric tension. We place paper samples between the ring and the plane. The motor speed is measured using an optical tachometer. The experiment is repeated 10 times for tensions from 12 to 35 V. The paper samples are changed after each experiment.
Because of the high speed, the samples undergo runs of hundreds of meters in few minutes. A second experiment therefore consists in characterizing the evolution of the friction force between paper materials during long runs. We measure the friction force for times up to 5 min at 24 V (i.e up to 300 m). After 5 minutes, we lift the ring and blow it to evacuate dusts. We then measure the evolution of the coefficient of kinetic friction during one minute. We repeat this operation 7 times.

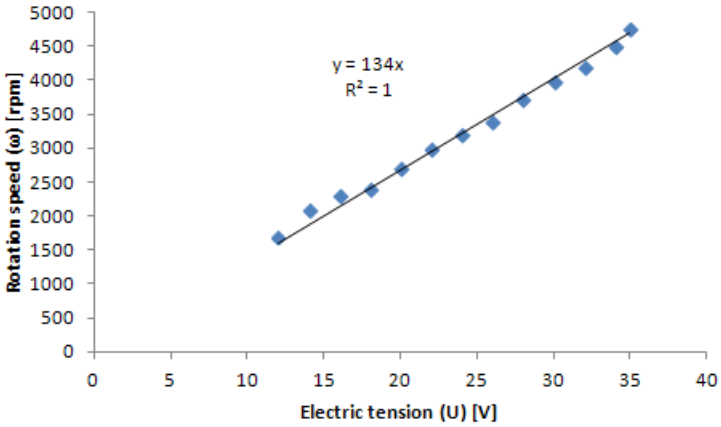

Figure 5.4: Measured rotation speed of the motor, ω, as a function of the electric tension, U. Paper samples were placed between the ring and the plane. The torque applied on the motor is thereofre equal to the torque applied in paper-on-paper friction experiments.

5.2 Results and discussion

5.2.1 Characterization of the rotation speed

From 12 to 35 V, the motor rotation speed is proportional to the electric tension, as represented on Figure 5.4. This result is supported by the theory on DC motors. The maximal velocity is measured at a distance r_{max} of the center of the ring and for 35 V tension. In this situation, the maximal velocity measured is $v_{max} = 1.2$ m.s^{-1}.

5.2.2 Evolution of the friction force in three phases

An example of result for a long run experiment is represented on Figure 5.5a. We decided not to average the measurements on 10 experiments, as the different phases represented have highly variable durations. We observe four phases:

Phase I The friction force is constant. The regime corresponds to the regime usually measured using the horizontal plane test method, but the speed is much higher.

Phase II The friction force linearly decreases with sliding distance. This decrease is associated to (i) an increase in noise (acoustic), (ii) the creation of paper dust, and (iii) a change in surface aspect, as represented on Figure 5.5b. The creation of dust suggests that this phase involves paper abrasion.

Phase III The friction is constant again but much reduced compared to Phase I (approx. -50 %). The dust particles created during Phase II remained between

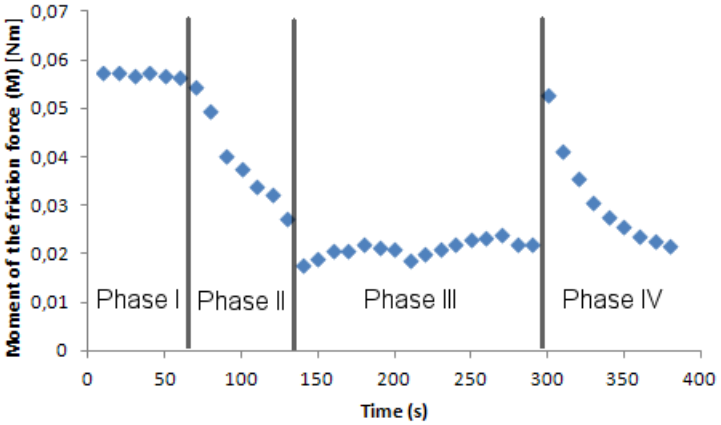

(a) Evolution of the moment of friction force. This moment is much different from the moment of the motor, due to the gerbox. Phase IV is averaged on 7 successive experiments with the same samples.

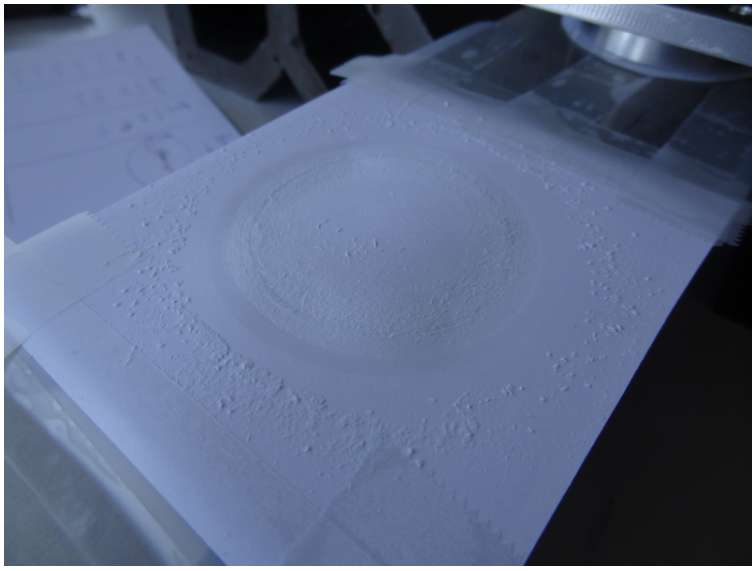

(b) Apparition of dust and change in surface aspect after a 5 minutes sliding

Figure 5.5: Typical results obtained for the long run experiment

the ring and the plane. We suppose that the particles roll, avoiding a direct sliding between the ring and the plain: it is called *rolling effect* or *rolling friction*.

Phase IV At the beginning of Phase IV, dusts were blown. We observe an initial increase of the friction force that can reflect the reduction of rolling effect. Then, after one minute, we observe a new stabilization to the level reached at Phase III (see Figure 5.5a). This reduction of the friction force reflects the contribution of a new rolling effect.

This method therefore permits the characterization of the force of kinetic friction, the abrasion of paper materials, and the rolling friction.

5.2.3 Abrasion of paper materials

The study of the abrasion phenomena of paper materials is beyond the scope of this study. However, we have to ensure that abrasion occurs far after the force of kinetic was measured.

5.2.4 Proposed measurement methods

Friction force We propose the following procedure for measuring the friction force between paper samples at various relative speeds:

1. The paper samples are placed between the ring and the plane. The paper samples undergo a normal load of approximately 6.7 N.
2. The electric tension applied to the motor is set to 12 V. During the 10 first seconds, the intensity delivered to the motor is averaged. Using the characteristic curves of the motor, the moment of the friction force is determined.
3. The samples are changed and the measurements repeated 10 times.
4. The experiment is repeated for electric tensions of 24 and 35 V.
5. Using equation 5.8 and the characteristic curves of the motor, the α and β parameters of the viscous friction model are identified.

Abrasion We also propose a procedure for characterizing the abrasion between paper samples during long runs. The paper samples are placed between the ring and the plane. The electric tension applied to the motor remains at 24 V during 5 minutes. The paper abrasion is then characterized by (i) the duration of Phase I and (ii) the friction force level during Phase III. Those parameters represent the sliding length before abrasion appears and the friction force during rolling friction, respectively. However, the study of abrasion phenomena is beyond the scope of this study.

Summary and Conclusion of Chapter 5

Apparatus The *ring-on-plane test method* is intended at measuring the force of kinetic friction between paper materials for relative velocities up to 1.2 $m.s^{-1}$. The setup consists in a rotating ring mounted on vertical slides. The ring thus applies a normal load and a rotation to the samples.

Measurement of the friction force The electric intensity delivered to the motor is measured and allows the determination of the moment of the friction force. This moment is measured for different rotation speeds. The measurement finally allows the identification of the parameters of the viscous friction model (see equation 5.3).

Characterization of the abrasion The measurement of the friction force during long runs permits the characterization of the abrasion of paper materials. In particular, we consider (i) the sliding length before abrasion appears, and (ii) the friction force during rolling friction.

Advantages The ring-on-plane test method permits the measurement of the friction force at high velocities (far beyond the velocities usually involved in standard methods). Moreover, the method involves mechanical stresses that are similar to those involved in the horizontal plane test method. In particular, (i) the load is homogeneous, (ii) the normal load is constant, and (iii) the materials are not bent. To finish with, the apparatus is low-cost, easy-to-use, and easy to adapt.

Possible improvements The ring-on-plane test method is highly sensible to the measurement of the electric intensity. The DC motor we used was oversized and the intensity was acquired using a multimeter. The measurement therefore has a low accuracy and should be improved. Moreover, we involve a relative rotation of the samples, rather than a linear displacement. This difference may influence the friction force measured, and thus has to be considered.

Perspectives The ring-on-plane test method appears to have great potentials. The method will be used in chapter 9.2 to study the paper-on-paper friction.

Chapter 6

Studying contacts of paper with other materials

The optimization of the franking machine feeders requires a deep understanding of the friction of envelopes. In franking machine feeders, envelopes are in contact with other envelopes, friction pads, and driving rollers. The standard test methods introduced previously are however not adapted to the measurement of such friction forces. In this chapter, we adapt the horizontal plane test method to the study of those contacts. The measurements obtained will be presented in chapter 11.

6.1 Envelope-on-envelope contact

We developed the sled represented on Figure 6.1a used in accordance with the horizontal plane test method. A 260x135 mm^2 plate applies a homogeneous pressure on the surface of envelopes. On the frond end of the sled, we placed a tip pushed by the moving arm, so that the contact is punctual. The system, called *tip-on-plane*, is represented on Figure 6.1b. The long tail at the back end of the sled reduces the orientation errors commited when installing the sled. The weight of the sled is 745 g, but can be easily modified. The sled was adapted to envelopes of different thicknesses. Finally, the sled was made of a 1 cm thick aluminium plates with a high stiffness that reduces stick-slips oscillations.

6.2 Pads-on-paper contact

We developed a sled for the measurement of the pads-on-paper friction force. The sled is represented on Figure 6.2. It is intended at being used in accordance with the horizontal plane test method. For stability reasons, the sled consists of 3 pads. The pads have an orientation of -16 degrees to the horizontal, equivalent to the angle measured on Omega franking machines. This angle can however be modified. The

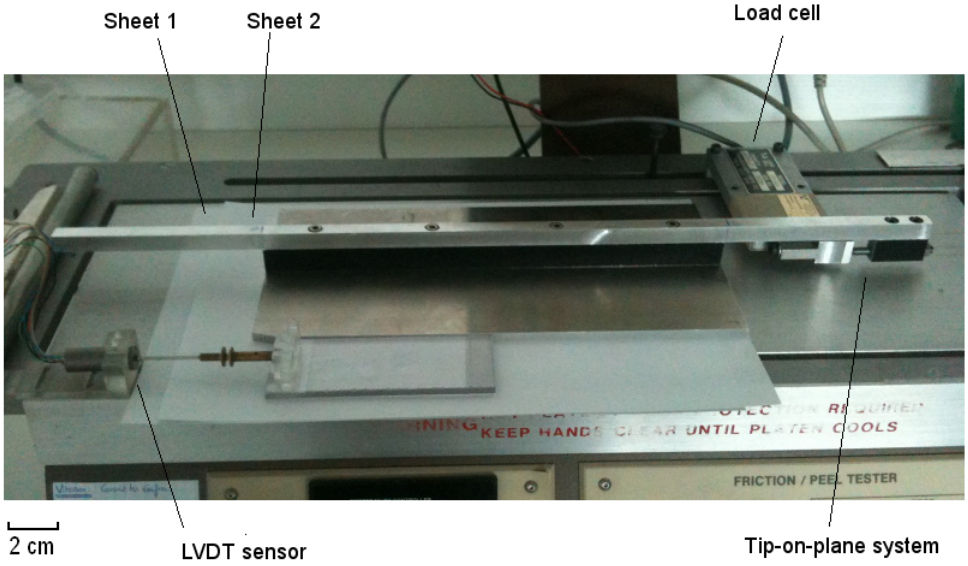

(a) Sled used to measure the envelope-on-envelope friction force. For clarity reasons, the envelopes are replaced by paper sheets. A position sensor (LVDT) is also placed on the mobile sample for development reasons.

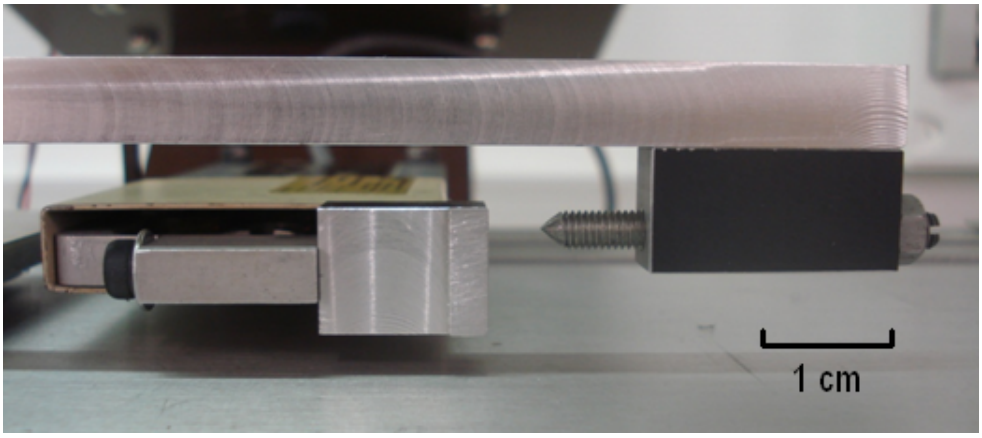

(b) Tip-on-plane system

Figure 6.1: Setup used to measure the envelope-on-envelope friction force

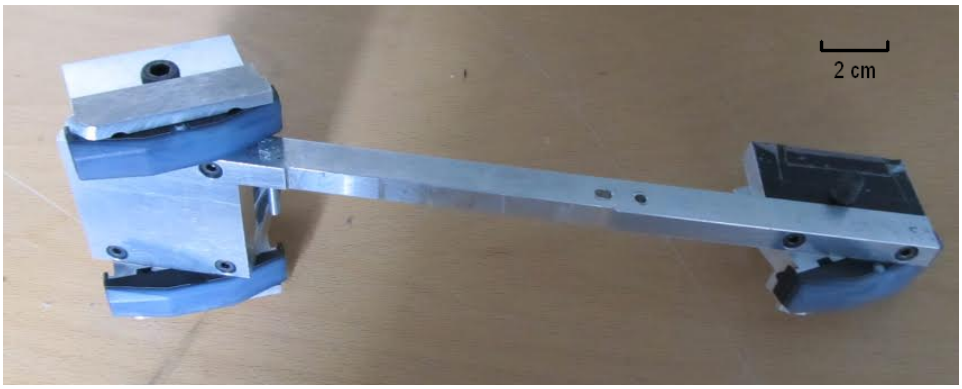

Figure 6.2: The sled used to measure the pads-on-paper friction forces. The sled is pushed by its front-end using the point-on-plane system.

sled is pushed by its front-end using the tip-on-plane system presented on Figure 6.1b. Made of aluminium, the sled weights 787 g. This weight can be modified. Each pad undergoes the same normal force and the tip-on-plane system is aligned with the center of gravity of the sled. The LVDT can be fixed to the rear of the sled in order to study the micro-displacements.

6.3 Rollers-on-paper contact

Low-speed On the previous sled, the pads can be replaced by rollers, as represented on Figure 6.3. In this situation, the sled weights only 500 g. The position of the rollers was calculated so that the normal force applied by each roller on the paper is the same. Due to the low stiffness of rollers (compared to pads), the use of an LVDT at the rear of the sled is of particular interest (Figure 6.3).

High-speed When franking machine rollers start to slide on the bottommost envelope, the relative velocities are much higher than those measured using the horizontal plane (up to 1.5 $m.s^{-1}$). Similarly, the stack weight ranges from 3 kg to tens of grams. The standard horizontal plane does not permit the study of (i) normal loads below 500 g, and (ii) speeds above 5 $mm.s^{-1}$. We thus proposed to measure the roller-on-envelope friction force directly on the machine using the method presented on Figure 6.4. Envelope stacks of various weights (from 100 g to 3 kg for example) were placed on the bottommost envelope. The bottommost envelope was in contact with 6 rollers of the franking machine. The bottommost envelope was fixed to a force sensor, itself fixed to the machine. When rollers start rotating, the bottommost envelope remains static. A kinetic friction force thus appears between rollers and the bottommost envelope. This force is measured by the force sensor.

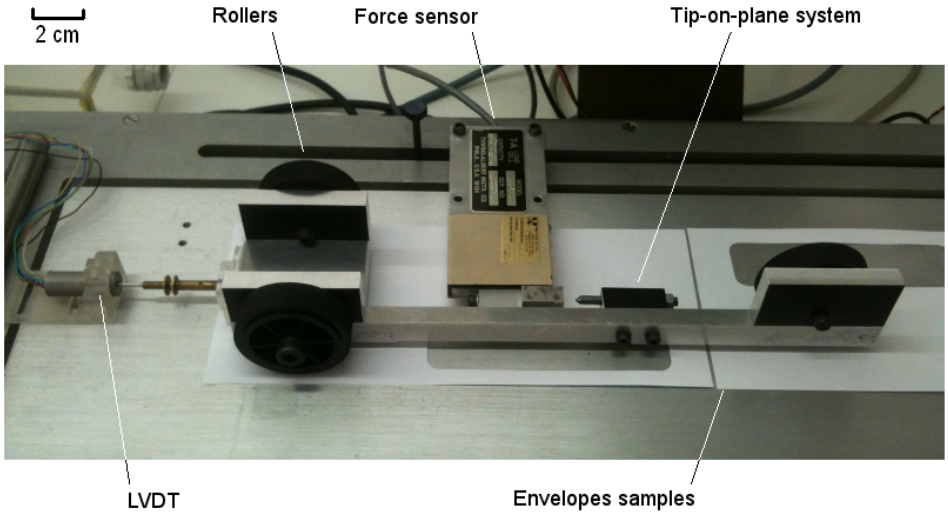

Figure 6.3: The sled used to measure the rollers-on-paper friction forces. The sled is pushed by its front-end using the point-on-plane system.

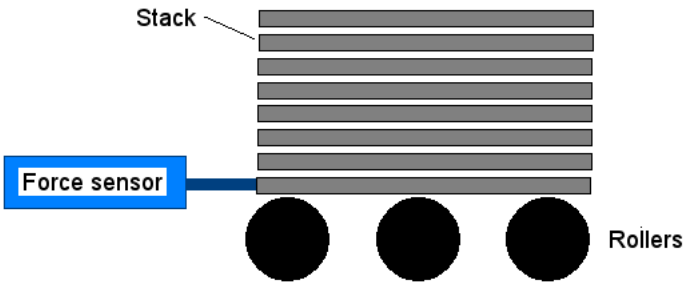

Figure 6.4: Method for measuring the force of kinetic friction between rollers and envelopes, for high speeds and/or small stacks.

Summary and Conclusion of Chapter 6

Situation The standard test methods do not allow the study of the friction force on some specific contacts. We thus developed methods adapted to the study of (i) the envelope-on-envelope contact, (ii) the pad-on-paper contact, and (iii) the rollers-on-paper one. Those methods will be used in chapter 11.

Envelope-on-envelope contact We first conceived a new sled to adapt the horizontal plane test method to the envelope-on-envelope contact.

- The size of the sled permits a homogeneous load on the envelope.
- The weight of the sled fits with the horizontal plane test method.
- The high rigidity of the sled avoids stick-slip oscillations.
- The tip-on-plane system allows a punctual contact with the moving arm.
- The tail of the sled permits an accurate positioning of the sled on the plane.

Pads-on-envelope contact We conceived a new sled to adapt the horizontal plane test method to the pads-on-envelope contact. The sled is composed of 3 friction pads. Each pad applies the same normal load on the envelope. The pads have an orientation of -16°, equivalent to the orientation measured on franking machines. The sled is pushed using the tip-on-plane system.

Rollers-on-envelope contact at low speed On the previous sled, we replaced the pads by driving rollers of a franking machine. The rollers are fixed.

Rollers-on-envelope contact at high speed To measure the influence of high speed roller-on-envelope slidings, we placed an envelope stack on a franking machine feeder. The bottommost envelope is fixed to a force sensor. Consequently, rollers slide on the envelope and the envelope does not move into the machine. The force measured is the force of kinetic friction of the rollers-on-envelope contact at a velocity of 1.2 $m.s^{-1}$.

Part III

Paper friction

Chapter 7

Basics of paper friction

Most people think that paper is an unsophisticated and outdated material with weak properties. It is supposed to disappear in everyday-life due to the competition with computers and because its fabrication requires trees to be cut. Those assertions are basically wrong. In this chapter, we show why studying paper materials and their friction is both important and complex. First, the relations between paper and society will show the current and future importance of this material in our everyday-life. Secondly, some basics concerning paper science will be presented, including the composition, structure, and properties of paper. In a third and last part, we will introduce some basics concerning paper friction.

7.1 Paper and society

7.1.1 One definition and five dates

Paper is usually defined as a material produced by pressing moist fibers. Invented in China 2200 years ago, the paper fabrication spread worldwide after the defeat of the Chinese against the Arabs during the Battle of Taslas in 751. In 1450, the rediscovery of printing presses by Johannes Gutemberg widespread the use of paper. The production of paper skyrocketed with the invention of Fourdrinier machines in 1799 by Louis-Nicolas Robert. Nowadays, the global turnover of the paper industry is higher than the one of aeronautics [47].

7.1.2 Uses and grades

Paper materials are present in everyday life: as support of the information, as packaging material, and for hygiene products for example. Papers are commonly organized into grades, based on their properties or uses. A common example of classification is listed hereafter [48]:

- **Newsprint** Lightweight papers (basis weight between 40 and 57 g.m^{-2}), mainly made from mechanical pulp. The paper is bright and opaque. This paper is typically used for newspapers.

- **Printing and writing** Mediumweight paper (around 80 g.m^{-2}), typically made from chemical pulp. This paper has a high whiteness, opacity, and stiffness. The material is suitable for writing or printing with inks and thus used for envelopes, magazines, books, mail, copy paper, or catalogs.

- **Board** Highweight paper (over 150 g.m^{-2}) used essentially for packaging. The material is usually made of mechanical pulp without bleaching.

- **Tissue and towel** Lightweight paper (below 40 g.m^{-2}) used for consumer sanitary products such as toilet tissue paper or kitchen towel.

- **Specialty papers** Different types with various properties. For example: thin papers for electric insulation or cigarettes, abrasive papers, banknote papers, adhesive papers, filter papers, barrier papers, carbon paper, flame resistant and so on.

Envelopes being made of printing and writing papers, we will focus on this grade.

7.1.3 Strengths

A reason for the paper importance in our everyday-life is that it is a cheap material, permitting strong cost reductions. For example, medical tests can be 40 times cheaper than the current ones [49], and microscopes can cost only 0.50 dollars [50]. Beyond this economical interest, the mechanical properties of the material are good, specifically considering the weight of the material. Other specific properties of the paper are often involved, such as thermal and electrical insulation. In particular, paper is a biodegradable material that is highly recycled: in France, the recycling rate of paper and boards was 92 % in 2012 [51].

7.1.4 Trends

Due to the increasing use of computers, the use of newsprint and printing and writing papers decreases in developed countries. However, the use of boards and tissues increase sharply due to the increase in international trades and world population, respectively. Specialty papers continue to evolve.
In the future, paper is often considered as an alternative to plastic-based materials. New techniques, based or using paper, will also permit its development, such as printing electronics, active packaging or nanocellulosis. It is thus expected that paper will pursue its diversification and increase its presence in our society.

Fiber source	Length (mm)	Width (μm)	Length/Width
Scots pine (summer wood)	2.1	30	70
Western hemlock	2.4	31	77
Douglas fir	2.8	34	82
Cotton	18	20	900
Hemp	15	22	700

Table 7.1: Typical dimensions of paper fibers ([53] and [52])

7.2 Paper science

7.2.1 Composition

Porosity The main component of paper in volume is *void*. For writing papers, void represents about 50 % of the total paper volume. This level vary with grades: it is very low for tracing paper or very high for filter papers. Void has major consequences on paper properties, in particular on its thickness and compressibility.

Fibers The second main component of paper are *fibers*. Fibers represent from 100 % of the paper weight for filter papers to less than 30 % for the paper-based frictional materials used in wet clutches. For common writing papers, there are about 80 % of fibers. The most common source of fibers is wood, like Douglas fir, scots pines, and eucalyptus. Other sources are sometime used for specific applications, in particular cotton and hemp fibers [52] or synthetic fibers. Typical dimensions of fibers used in the papermaking processes are listed on Table 7.1.

Fillers The third main component of paper are mineral *fillers*. Fillers are often used to reduce costs and improve optical paper properties. For example, clay or precipitated calcium carbonate (PCC) are often used to make the paper more opaque. Fillers often represent up to 20 % of the mass of common writing papers.

Coating and additives Coating consists in adding chemicals on the paper surface. This process permits the improvement of specific paper properties such as optical or barrier properties. Additives can also be added to the material during its fabrication. For example, colloids and polymeric additives can contribute to the retention of fine particles within the paper web. The properties and compositions of those chemicals are very wide. If their contribution in terms of weight is usually low, they can however have a major influence on the paper properties.

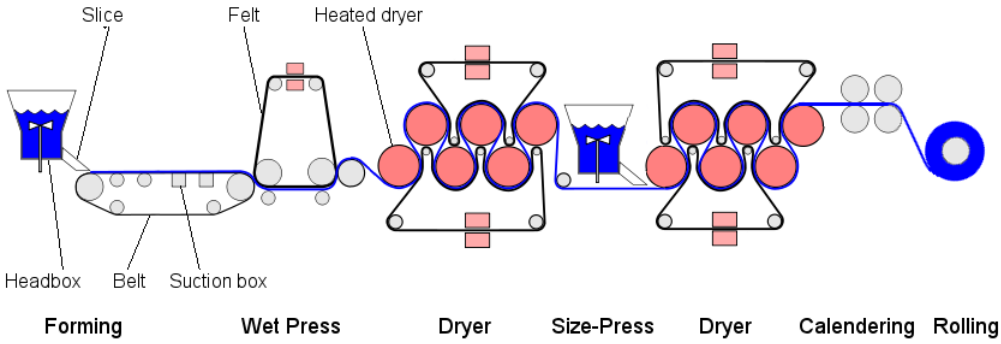

Figure 7.1: Overview of a paper machine based on the Fourdrinier Machine. The different sections are represented. Adapted from [54]

7.2.2 Fabrication process

Basic principle The paper fabrication is based on wet pulp. The pulp is homogeneously dispersed on a wire, filtered and then dried by different means. The paper filtration permits the creation of the fibrous web, as fibers interlace together. Then, the drying step creates hydrogen bonds between the fibers: hydrogen bonds are the basis of paper properties.

The Fourdrinier Machine The most common process for paper fabrication is based on the Foudrinier Machine. The process usually consists in seven sections, represented on Figure 7.1:

- **The pulp preparation -** The pulp is wetted and processed until reaching a homogeneous repartition of fibers. For this purpose, the wet pulp often contains up to 98 % of water. Chemicals are also added in order to improve paper mass-properties and process efficiency.

- **The forming section -** Also called *wet end*, the *forming section* consists in the dispersion of the pulp on a moving wire. The challenge consists in obtaining an homogeneous and targeted repartition of fibers. The pulp is then filtered, permitting the creation of the fibrous web.

- **The press section -** The wet fiber web passes under a press. This section is of particular interest, because squeezing about 80 % of the web water while consuming only 20 % of the total energy.

- **Drying -** The remaining water contained in the web has to be removed. Therefore, the drying section consists in the heating of the fiber web by the mean of steam heated drying cylinders.

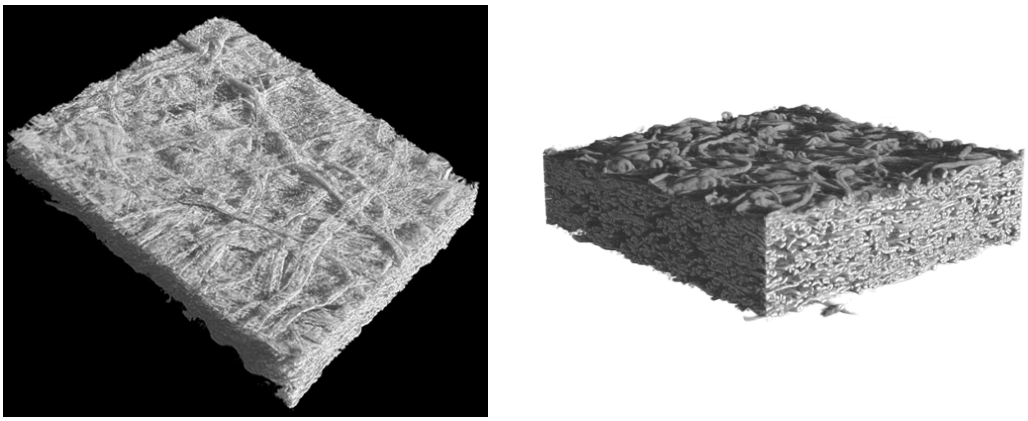

Figure 7.2: A sheet of paper observed under tomography. Reproduced with permission from Jean-Francis Bloch, Grenoble INP - Pagora (see also [55]).

- **Coating -** In order to change the surface properties of paper the coating section is placed at the middle of the drying section. This coating section permits the addition of chemicals on the paper surface. For printing and writing papers, this section often consists in the paper sizing, i.e in the addition of chemicals that modify the water penetration in the final product.
- **Calendering -** To improve the surface properties of paper, such as gloss and smoothness, the paper often passes through a calendering section. This section consists in the heating and pressing of the paper by the mean of rolls, permitting the flattening of the paper surface.
- **Rolling** The paper is finally rolled on a reel for further processing, such as printing, cutting, or packing.

Main drawbacks The wet state is necessary for the creation of the chemical linkages (hydrogen bonds). However, this process involves important quantities of water. Moreover, the drying step is very energy-consuming.

7.2.3 Structure of paper

General structure From a qualitative point of view, paper is a web structure constituted by interlacing fibers that are linked by hydrogen bonds (see Figure 7.2). Printing and writing papers usually have a thickness of about 100 μm and a basis weight of 80 g.m^{-2}. Consequently, 10 fiber layers can be observed in the thickness direction and 100-200 fibers in a square millimeter.

Heterogeneity of the fiber repartition on a sheet The stochastic nature of the fabrication process leads to heterogeneities in the position and orientation of the

fibers and other constitutive elements [53]. This heterogeneity appears at different scales: at the fiber scale (micrometers), at the flocculation scale (centimeters), or at the machine scale (meters to kilometers).

Anisotropy of fiber orientation A difference of velocities between the pulp and the wire increases the orientation of fibers in *machine direction* (MD) as represented on Figure 7.2. The fibers will be therefore less oriented in the *cross direction* (CD), that is orthogonal to the machine direction.

Heterogeneity in the thickness Heterogeneities also appear in the thickness direction. Indeed, the process consists in removing water by the wire side only or on both sides. Consequently, fines tend to move within the fibrous web and may even be ejected from the structure. This process creates an asymmetry between the two sides and a heterogeneity within the material thickness. In addition to this phenomenon, surface properties may be different from mass properties, in particular due to calendering and coating. Calendering compresses the surface layers while coating changes both the structure and the composition of the paper, for example by filling the pores.

7.3 Paper friction: an introduction

Importance of paper friction According to Gunderson [8], the friction of paper is of particular interest in the situations listed hereafter:

- Roll winding and rewind problems,
- Crepe wrinkles within the roll (see [45]),
- Roll telescoping during transit,
- Web tracking and print registration,
- No feed or multiple feed during sheet feeding,
- Registration errors in die cutting or converting,
- Corrugator runnability problems of several kinds,
- Sliding on conveyer when product should not and vice versa,
- Stack and pallet instability whether cartons, sheets, sacks, or printed materials.

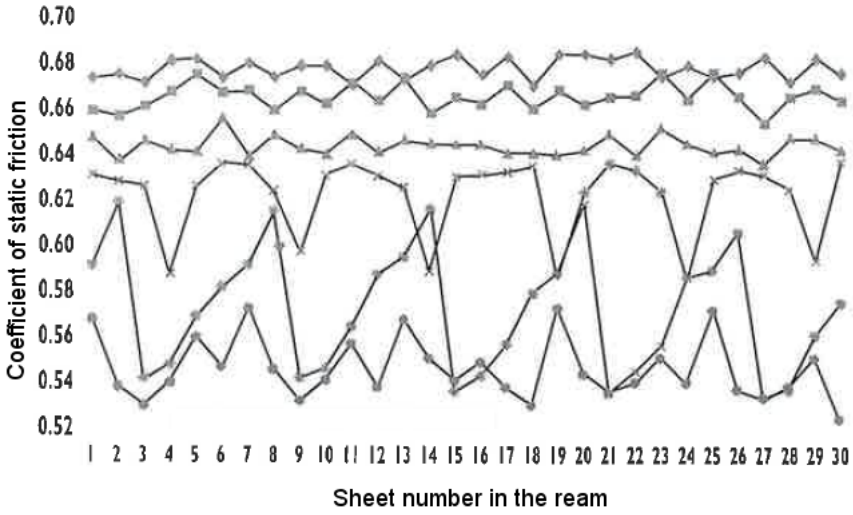

Figure 7.3: Evolution of the coefficient of static friction for the first 30 sheets of paper in each of six reams of copier paper [8]

Research and literature Paper friction remains however relatively poorly studied and documented. In 1952, Broughton and Gregg [56] reviewed the literature. They found only one article concerning the coefficient of friction of paper. Since this date, the paper friction was studied by the team of C. Fellers and several japan copiers companies such as Hitachi for example.

High variability in measurements However, the comparison of lab results remains difficult, not to say impossible, because of the high variability of paper friction and measurement methods. For example, we showed in chapter 3 that the protocols or conditions greatly evolve from a standard to the other. For a given standard, the measurements also greatly vary from a lab to the other, as represented on Figure 3.2. In particular, this figure shows that the variations in coefficients of static friction represent up to 50 % of their average value. We also observe strong variations in measurements on a single apparatus. For example, the evolution of the coefficient of static friction of common writing paper sheets was studied by Gunderson [8]. The author showed that this coefficient greatly evolves in a ream and from a production to another, as represented on Figure 7.3. The variations in coefficients of static friction in a ream represent up to 15 % of their average value. In particular, the cyclical pattern observed is likely to be due to the fact that a ream is composed by multiple rolls produced at different moments. In conclusion, lab results published in the literature are hardly comparable.

A complex topic There are two main causes to this variability. On the one hand, tribology is a complex and difficult topic particularly due to the wide range of phenomena occurring at microscales or nanoscales. All the parameters of paper friction are thus neither measured nor controlled. On the other hand, paper has also its own variability up to macroscopic scales. Consequently, the representative volume of the material has to be macroscopic. Characterizing the material thus consists in considering its properties from the nano scale to macro scale. The study of paper-on-paper friction therefore becomes complex.

Goal and method We showed that the study of the paper friction is a complex topic. This study is however fundamental for the optimization of franking machine feeders and other machines involving paper materials. In the following chapters, we therefore study successively (i) the structural factors, (ii) protocolar factors, and (iii) the environmental factors of the paper-on-paper friction. The study of structural factors will be mainly bibliographic, as this factor cannot be influenced by franking machine feeders. Finally, we will study (i) the envelope-on-envelope, (ii) the pads-on-paper, and (iii) the rollers-on-paper contacts, as they are also involved in franking machine feeders.

Summary and Conclusion of Chapter 7

Paper and society Paper is a cheap and biodegradable material, with good physical properties (specifically considering its weight). Thus, paper materials are present in our everyday life, as support of the information, for packaging, for hygiene products, or as specialty papers. New technologies based on paper materials will also be introduced in our everyday life.

Paper science Printing and writing papers are typically made of 80 % of interlacing cellulosic fibers, with 50 % of porosity. The stochastic nature of the fabrication process leads to heterogeneities in the position and orientation of the fibers. In particular, fibers are often mainly oriented in the machine direction (MD) and slightly oriented in the cross direction (CD). Mineral fillers are also added to the paper and represent about 20 % of the printing and writing papers. Finally, coatings and additives are widely used to improve specific material properties.

Paper friction The study of paper friction is fundamental for the optimization of franking machine feeders. It is also of particular interest for (i) roll winding and rewind problems, (ii) slidings on conveyors when products should not and vice versa, or (iii) stack and pallets instabilities, for example. However, paper friction was relatively poorly studied and documented. Moreover, the comparison of lab results is difficult due to the high variability of paper friction and measurements methods. In conclusion, the study of paper friction is complex but fundamental to optimize the franking machine feeders.

Chapter 8

Structural factors

The optimization of franking machine feeders requires a deep understanding of the paper friction. The paper friction strongly depends on structural factors. However, the machine designers and the customer have no control on the papers that are fed into the machine. Consequently, having a deep understanding on the influence of structural factors on the paper friction is not included in our study. In this chapter, we thus limit this analysis to a literature review. We study separately the influence of fibrous structure, fillers, and chemicals on paper friction. Then, the influence of calendering and paper sides on friction will complete the analysis.

8.1 Fibrous structure

Roughness Early friction models suggested a strong influence of roughness on friction. However, roughness is a complex notion that can vary at different scales: from few millimeters to few nanometers [57]. In other words, the influence on friction of macro-roughness may be different from that of micro-roughness.
Inoue *et al.* produced papers which sides had different rugosities: one side was smoother than the other side [58]. They showed that the contact between two rough paper surfaces has a lower friction (-25 %) than the contact between two smooth surfaces. This result suggests that the interlocking of surface asperities is not a factor of the paper-no-paper friction. However, this difference may be also due to the anisotropy in the paper thickness.
Kawashima *et al.* studied the influence of pression on the kinetic friction of papers [17]. They pressed a filter paper between two metal plates at 350 kPa (without heat). This experiment is similar to the Inoue *et al.* one, but the distribution of particles within the thickness remains the same. The increase in smoothness led to a sharp increase in real contact area but a negligible increase in coefficient of kinetic friction. Similar results were obtained by Garoff *et al.* [59]. This result corresponds to the conclusions of Delcroix in 1947 [60] suggesting that the fiber structure (e.g. orientation and roughness) has a little influence on friction. The experiment also

shows that in the studied conditions, the real area of contact is not a crucial factor of paper friction.

Fibrous direction Two directions are possible for the machine direction (MD): in the direction of the rolling section (MD+) or in direction of the headbox (MD-) (see Figure 7.1). Broughton and Silveira *et al.* observed no differences between the MD+ and MD- directions on the coefficients of friction [56, 41].

Fibrous orientation Fibers are usually highly oriented in the machine direction (MD) and slightly in the cross direction (CD). Consequently, we may suggest that the force of friction in the MD/MD directions is lower than in the CD/CD ones.
However, Fellers *et al.* did not observe any difference between MD/MD and CD/CD frictions [39]. Similarly, Broughton showed a negligible increase in coefficient of friction for CD/CD runs compared to MD/MD runs (about +4%) [56].
On the other hand, Silveira *et al.* measured coefficients of static and kinetic friction increased by +10 % and +15 %, respectively, for the CD/CD contact compared to the MD/MD one. However, those result were obtained using the strip-on-drum test method. As seen in chapter 3, this method can hardly be compared to the horizontal plane method. Back showed that the decrease in coefficients of friction can be as high as 25 % [31][1].
Finally, we did not find any information concerning the influence of anisotropy on paper-on-paper friction. In conclusion, the influence of the fibrous orientation appears to be low or negligible.

Microfibrils At a lower scale, we may observe at the surface of fibers many small fibers called *microfibrils*, as represented on Figure 8.1a. When microfibrils get out of the fibers surface (*outer microfibrillation*), they increase the specific surface of fibers. In this situation, they increase the interactions between paper surfaces, as represented on Figure 8.1b. This situation is created by the beating of the pulp (a unit operation of the pulp preparation consisting in frictioning the fibers). Literature showed that pulp beating does not significantly affect friction [56, 63].

Conclusion In conclusion, the fibrous structure has a controversial influence on paper friction. The roughness of the fibrous structure is claimed nowadays to have a negligible influence on paper friction. This conclusion is opposed to the early friction models. For future works on the influence of fibrous structure on paper-on-paper friction, we support (i) the systematic analysis of the fibrous orientation and/or a multi-scale topography of the samples in different directions, and (ii) the use of linear nozzles rather than circular nozzles in the air leak systems.

[1] The Back's results are however poorly documented. The author neither indicates which coefficient was measured, nor in which direction the minimum was observed.

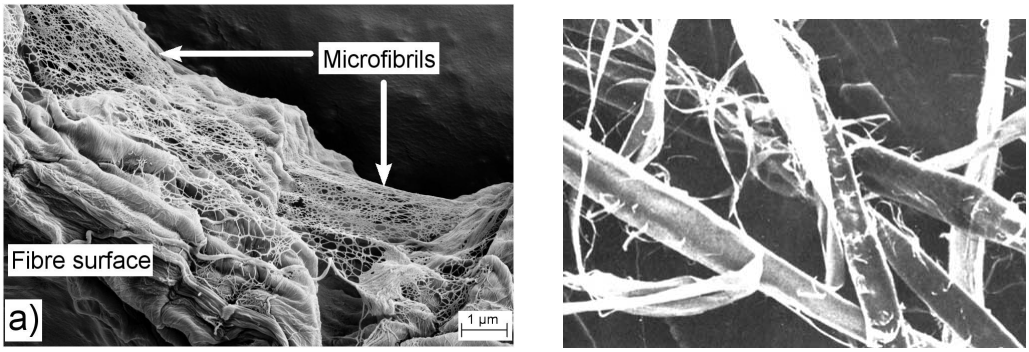

(a) Microfibrils covering fibers surface [61] (b) Outer microfibrillation [62]

Figure 8.1: Microfibrils in wood pulp

8.2 Chemistry

Surface energy Surface energy originates from intermolecular interactions, such as the van der Waals interactions, or acid-base forces [39]. Surface energy is influenced by wood extractives, surface contamination, or moisture content [58]. Those interactions are responsible for adhesion phenomena between two surfaces. It is therefore reasonable considering surface energy as a major parameter of friction.
Inoue *et al.* tried to evaluate the influence of surface energy on friction by studying 13 different commercial linerboards of similar surface roughnesses [58]. They observed that the coefficient of static friction increases with the surface energy. No correlation was observed in other experiments [39, 64]. The results of Fellers *et al.* suggest that the influence of surface energy on paper friction can be observed only in particular conditions (e.g. humidity, extraction agents, or contaminants) [39]. The method used in both experiments is however questionable: by studying different samples, other parameters may evolve (e.g. type of fibers, fibrous orientation, thickness, or coatings). In particular, Rättö *et al.* [65] showed that in the case of coated papers, the surface energy could have a negligible influence on friction compared to fillers.
In this situation, the use of corona treatment is useful. The treatment consists in an oxidation of the chemical compounds at the surface of fibers. The treatment therefore modifies the surface energy without modifying the other paper properties. Measurements show that this treatment increases the friction force [31, 66], supporting the results of Inoue *et al.* [58]. The same results can be obtained by flame treatment and nitric acid treatment [31]. Back also observed that after few days, the friction force decreased, an evolution he supposed to be due to the redistribution of lipophilic compounds from the interior to the surface of paper [31].
Surface energy thus appears to be a major parameter of the friction force.

Chemicals reducing friction The chemistry of the paper surfaces is complex. In the absence of coating, surface chemistry usually consists in *wood extractives*. Among those wood extractives, aliphatic molecules (fatty acids) [31] and oleophilic materials (such as low-molecular-mass lipophilic compounds (LLC)) [31, 10] reduce friction. Several authors showed that the reduction in friction force due to these chemicals is up to 50 % [56, 31, 41, 64]. Broughton *et al.* in particular showed that the highest decrease in force of kinetic friction (-50 %) was associated with the longest fatty acid chain (above 18) [56]. Similarly, Gurnagul *et al.* showed an increase in coefficient of friction with oxygen/carbon ratio [66]. Finally, Back showed that the lipophilic compounds also slightly contribute to the variations of the force of static friction (about + 3%) [31].
We interpret those different results as the creation of a thin film of natural lubricants. This creation is due to the mutual action of two types of chemicals:

- **Lubricants** - Fatty acids[2] and fatty alcohols[3]. Fatty acids act as lubricant and ease the sliding. A sharp decrease in friction force is observed for chains of 14 carbon atoms or more. Vertically oriented lubricant molecules are also expected to reduce the surface energy and finally the friction force between the surfaces [67].

- **Oleophilic materials** (e.g. LLC) - Those chemicals ease the fixing of lubricants that are naturally present in the paper (see the previous group) or that come from contaminations. A common example of contamination consists in touching the paper with the thumb/hand five times: we observe a decrease in friction for of 15 % and 30 %, respectively [38].

Considering the amount of lubricants measured in papers, the thickness of the lubricant film is expected to be close from a monomolecular film on each surface [59]. This situation is called boundary lubrication.
An interesting consequence was found by Fellers *et al.* They showed that the friction between papers from chemical pulps is twice that of papers from mechanical pulp [39]. Indeed, the process of chemical pulping extracts an important part of the lipophilic compounds, increasing friction. Similarly, it was found by Bäckström *et al.* that hardwood pulp has a high amount of wood extractives compared to softwood pulp (1.16 % and 0.1 % respectively) [64]. Consequently, wood extractives highly reduced the friction between paper materials made of hardwood pulp (roughly -50 %), contrary to those made of softwood pulp. These observations suggest interesting technical applications to modify the friction of papers.

[2]Composed of long-chain saturated fatty acids (e.g. palmitic acid, stearic acid), short-chain saturated fatty acids (e.g. dodecanoic acid, tetradecanoic acid), and unsaturated fatty acids (e.g. oleic acid, linoleic acid) [59].
[3]In particular octadecanol, icosanol, and docosanol [59]

Chemicals increasing friction Wood extractives also contain chemicals that increase the friction between paper surfaces. In particular, resin acids with their aromatic molecular structure tend to increase the coefficient of friction of paper-on-paper contacts [31]. This effect is known for thousand years: for example, it was applied to violin bow when Arabs introduced this instrument in Europe. Nowadays, it is also well-known by climbers.
The chemicals can also come from the coating and/or from contamination. For example, the addition of anti-skid agents significantly increases the coefficient of friction [58]. They are from two kinds: (i) polymeric, and (ii) colloidal silica or alumina [8]. Colloidal silica, in particular, creates interlockings at the micro-level between the contacting surfaces, increasing friction [68].

Conclusion In conclusion, surface energy appears to be a major parameter of paper-on-paper friction. The chemistry of paper surfaces strongly influences paper friction. Four types of chemicals were listed:

- Some wood extractives act like natural lubricants, in particular fatty acids.
- Oleophilic materials are also naturally present in the paper and fix the natural lubricants on the paper surface.
- Other wood extractives increase the friction between paper surfaces, in particular resin acids.
- To finish with, contaminants can increase or decrease the friction force between paper materials.

8.3 Fillers

Shape and size of particles The effect of fillers on friction was first studied by Delcroix in 1947 [60], then by Broughton [56], Withiam [69], and Rättö *et al.* [65]. Authors usually consider that this influence depends on the shape of the filler particles that can be divided into two categories:

- **Sharp-edged particles -** Clay (in particular calcined kaolin and synthetic precipitated silica [56, 45, 69]), calcium sulphate [60], and precipitate calcium carbonate (PCC) [70] tend to increase the friction force. Broughton and Gregg observed, for example, an increase of +87 % of the coefficient of kinetic friction for a clay filling increasing from 0 to 15 % [56].
- **Lamelar particles -** Hydrous kaolin [69], talc [60] and ground calcium carbonate (GCC) [70] for example, tend to decrease the friction force.

It was suggested that the size of filler particles has no significant effect on the friction properties, in particular in the case of clay [65].

Causes To explain the dependency of the friction force on the particles shape, Withiam [69], and latter Rättö *et al.* [65], suggested that the fillers change the micro-roughness at a scale below the one observed with common air leak instruments. To observe such changes, Atomic Force Microscopes (AFM) are required to replace air leak systems. The authors suggested that those changes in micro-roughness could modify the friction force.

Long runs The studies presented in this section were made on short distance slides. However, after a high number of slides, abrasion occurs and filler particles move on the paper. De Silveira and Hutchings [41] observed a redistribution and grinding of the filler particles on the surface of the top fiber layer. These changes lead to (i) a *rolling friction* that tends to decrease the friction and (ii) a *ploughing effect* that tends to increase it [40]. The ploughing effect consists in the damage of the fibers surface, and was in particular observed with calcium carbonate particles.

Conclusion Fillers have various influences on paper friction. These influences mainly depend on the particles shapes and may be considered in the frame of a study on the micro-roughness influence on paper friction. On long sliding distances, their influence is more complex due to abrasion (apparition of both rolling friction and ploughing effect).

8.4 Case of the calendering process

The process Calendering is an important step of the fabrication process of printing and writing papers, aiming at obtaining a paper surface that is smoother. The process consists in pressing the paper material under heated smooth rolls. Heating the paper surface permits to exceed the glass transition temperature of the material, softening its surface and easing its structural modification. The process is supposed to strongly modify the friction force of the produced paper, because modifying the surface smoothness. We propose to investigate this assertion.

Influence on friction The influence of calendering on paper-on-paper friction is subject to controversy:

- Broughton *et al.* [56], latter Back [31], and Fellers *et al.* [39], showed that calendering of paper leads to lower coefficients of friction (about -17%). Furthermore, Broughton *et al.* observed that after a few calendering steps, the coefficient of friction increased from about 6%.
- On the other hand, Whitiam [69], Back [31], and Jones and Peel [71] observed no influence on the coefficient of friction.

The influence of calendering on paper friction is not clear, as different factors are involved. For example, pressing and heating may have different influences.

Role of fibrous structure Back distinguished papers with and without oleophilic materials. In the case of papers that underwent a chemical extraction, he observed that the PPS-surface roughness was reduced from 7 to about 1.5 μm during this process. Back however observed no variations in friction. Roughness, at this scale, has thus a low influence on the coefficient of friction [31]. Kawashima *et al.* obtained the same results in the case of paper pressing [17].

Role of chemicals In the case of papers that did not underwent chemical extractions, Back observed a decrease of friction force with calendering. He deduced from this observation that the presence of oleophilic material leads to a reduction of the coefficient of friction with calendering. This result suggests that fatty acids may migrate into the web at elevated temperatures.

Lack of information Those results cannot be compared to the results obtained by Broughton *et al.*, Fellers, Withiam, and Jones and Peel. Indeed, those authors did not indicate in their articles if they heated their rollers. Other information are also lacking, such as the rolls pressure.

Conclusion At first glance, we may suggest that calendering modifies the roughness of papers and thus the coefficient of friction. However, the Back and Kawashima *et al.* experiments showed that the situation is much different. On the one hand, the load applied on paper materials modifies their structure with a negligible influence on paper friction. On the other hand, heating the paper modifis its chemistry and thus greatly influences the paper friction. In conclusion, these results tend to support the relative influence of fibers and chemicals on the paper friction.

8.5 Case of paper sides

Problem Because of the filtration during the fabrication process of the paper, differences between the two paper sides exist. In particular, it is common considering that there are much less thin fibers, fillers, or chemicals on one surface than on the other. Additionally, the roughness of both sides may be different. Considering the previous sections of this chapter, the two paper sides thus should have different frictional properties.

Measurements For clarity reasons, we note WS and FS the wire and felt sides, respectively. Broughton made its measurement by ensuring that the same paper sides were in contact [56]. He measured a negligible increase in coefficient of friction

on the WS-WS compared to FS-FS runs (about +3%). De Silveira and Hutchings [41] compared WS/FS, WS/WS, and FS/FS. They observed an influence on the coefficient of friction only for the 100% non recycled pulp linerboard. But contrary to the other samples tested, a pronounced topographic texture was observed on this sample.

Conclusion The difference between the two sides of paper appears to have a little (not to say negligible) influence on paper friction. This difference mainly depends on the process parameters. It is therefore reasonable considering that a particular fabrication process can produce papers with a strong side effect on friction.

Summary and Conclusion of Chapter 8

Summary A summary on the paper structure's influence on paper-on-paper friction is proposed on Table 8.1.

	Influence	Friction increase	Friction decrease	Consensus
Chemicals	Up to 50 %	Resin acids	Fatty acids	Strong
		Some coatings	Oleophilic materials	
		Some contaminants	Some coatings	
			Some contaminants	
Fillers	Up to 90 %	Sharp-edge particles	Lamellar particles	Strong
Fibers	Up to 15 %	CD/CD slides	MD/MD slides	Low
		High anisotropy	Isotropy	
		Smooth surfaces	Rough surfaces	

Table 8.1: Influence of chemicals, fillers, and fibers on the paper-on-paper friction

Conclusion Chemicals and fillers have much stronger influences on friction than the paper structure. In the following chapters, we will study the influence of protocolar (e.g. relative velocity or normal load) and environmental factors (e.g. relative humidity or temperature) on the friction of paper materials. We will sometime have to refer to the structural factors studied in this chapter, as they are strongly linked.

Chapter 9

Protocolar factors

The optimization of the franking machine feeders requires a deep understanding of the friction between paper materials. In the previous chapter, we studied how the structure and composition of the paper can influence its friction. We now study the protocolar factors, i.e. the factors associated to the contact itselfE. We will study successively the sliding directions, the sliding dynamics, and the normal stress.

9.1 Sliding direction

9.1.1 Literature

9.1.1.1 Proposed formalism

Definition *Repeated slidings* between paper materials are defined as repeated slidings the same direction, from the same starting position, and on the same distance. *Reversed slidings* are defined as slidings in alternate directions: after one sliding, the sliding starts in the opposite direction on the same distance. Reversed slidings occur, for example, during the separations and stackings in franking machines.

Formalism We propose a formalism for those slidings, represented on Figure 9.1. The starting position of the forward sliding is taken as a reference. The forward sliding consists in a sliding (i) in the forward direction, (ii) on a distance D, and (iii) from the reference position. The backward sliding consists in a sliding (i) in the backward direction, (ii) on a distance D_b, and (iii) from a distance D_f to the reference position in the forward direction. Repeated slidings thus consist in repeated forward slidings. Reversed slidings consist in alternatively forward and backward slidings. This formalism is fundamental, because literature often considered reversed slidings from different (or non-specified) starting positions. Comparing the results of the literature is therefore difficult (not to say impossible).

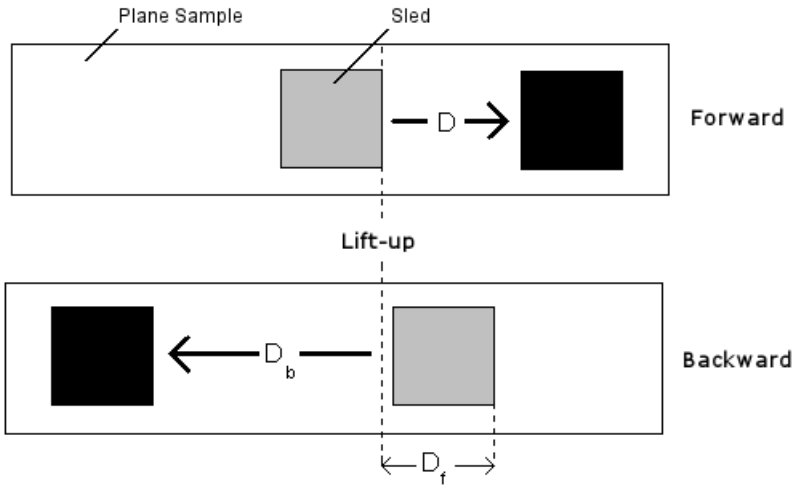

Figure 9.1: Formalism used to describe repeated and reversed slidings. Repeated slidings consist in repeated forward slidings. Reversed slidings consist in alternatively forward and backward slidings.

Friction hysteresis Garoff *et al.* proposed to call *friction hysteresis*, FH, the ratio between the difference in force of friction between the reversed and repeated slidings on the one hand, and the friction force observed in the reversed sliding on the other hand:

$$FH(\%) = 100\frac{\overline{F_{\text{reversed}}} - \overline{F_{\text{repeated}}}}{\overline{F_{\text{reversed}}}} \tag{9.1}$$

Where $\overline{F_{\text{reversed}}}$ and $\overline{F_{\text{repeated}}}$ represent the average friction forces measured during reversed and repeated slidings, respectively. We consider forces of static and kinetic frictions and note their friction hysteresis FH_S and FH_K, respectively.

9.1.1.2 Repeated slidings

Influence on paper friction The friction force between two paper samples decreases with repeated slidings. The decrease has a logarithmic shape and no asymptotic value appears to be approached [56]. For a given couple of papers, the difference of friction before and after those slidings can be as high as 50 % [44]. This phenomenon was first observed by Broughton *et al.* [56, 31, 44] and is nowadays well accepted. In fact, only one experiment reported a slight increase in friction force with repeated slidings [72]. Interestingly, such an evolution has not been reported for other materials [31].

Possible causes Sato *et al.* [40] and de Silveira and Hutchings [41] used a Scanning Electron Microscope (SEM) to examine specimens that underwent several repeated slidings. They observed a progressive disruption in surface fibers layers: fiber

debonding, breakage of fibrils bridging fibers, and surface debris. Mineral particles even induced a ploughing effect [40]. Sato *et al.* therefore suggested that the decrease in coefficient of friction with repeated sliding largely results from a reduction in surface strength associated with surface damage. However, another study could collect no surface debris after repeated slidings [31].
Another hypothesis consists in considering that the roughness of the paper is modified with repeated slidings. However, Fellers *et al.* observed no modification of paper roughness with repeated slidings [39]. Other works suggested the decrease in friction force with repeated slidings to be due to the flattening of protruding parts of the filler particles [70].
Back suspected that the work of friction leads to heat that reduces the moisture content in the surface layer. However, a reconditioning time of 10 minutes between each repeated sliding did not modify the evolution of friction with slidings [31].
Finally, Back showed that the decrease was reduced when the lipophilic compounds are removed from the paper [31].

Consequences on the characterization of the friction force The higher decrease occurs between the first and third repeated slidings. Current standards therefore support the measurement of the force of static and kinetic frictions at the first and third slidings. For some authors, the first sliding should be chosen whenever possible, because of the shorter testing time needed [42]. Other suggest that the third sliding should be chosen when comparing materials that have different histories [39]. From a more general point of view, we recommend the choice to be based on the property we want to highlight and on the history of the samples.

9.1.1.3 Reversed slidings

The paper-on-paper contact The force of friction between papers was reported to sharply increase with reversed slidings compared to repeated slidings (up to +50 %) [31, 72, 44]. This behavior is also not observed for other materials [31].

Observations Garoff *et al.* intensively studied this phenomenon for $D_f = 0$ and $D_b = D$ [44]. They showed that:

- The friction hysteresis was very high for filter paper and very low for backing and coated papers.
- Lubricants reduce the coefficient of friction but do not change the friction hysteresis.
- The friction hysteresis is independent from the sliding direction (MD/CD).
- The friction hysteresis sharply increases for contact pressures from 0 to 0.5 kPa for a given surface. Above 0.5 kPa, the rate of increase leveled out.

- The static and kinetic friction hysteresis have the same trends.
- The paper-on-glass contact did not present any friction hysteresis, suggesting that this behavior is specific to the interactions between paper surfaces or rough surfaces.

A possible mechanism Johansson *et al.* proposed the friction hysteresis to be due to the reorientation of *'structural elements'* in the direction of the sliding. To figure out this mechanism, we consider the micro-barbs at the surface of wheat awns [73]. These asperities increase the friction force when sliding against the micro-barbs, favoring the displacement of the ears in the opposite direction. However, if the stiffness of surfaces and strucural elements is low enough, the surface structures may reorient themselves, especially in the direction of the sliding. Such reorientations are involved in numerous biological systems, such as snake scales [73, 74], shark skins, ants forelegs [74], insect pads [75], or gecko toes [76]. Indeed, the reorientation of surface structures can improve the friction asymmetry of the materials [77, 74]. The mechanism is also observed in several non-biological systems, such as toothbrushes during brushing, climbing skins for ski touring, or textiles with a "cat fur" effect [78, 79, 80]. However, contrary to these mechanisms, the paper materials highlight a non-elastic reorientation of structural elements. Indeed, a memory effect is observed, as the phenomenon remains unaffected after several hours without contact. We thus propose to compare the mechanism to hairs during combing: hairs get reoriented in the direction of the combing. But as the combing ends, the hairs are supposed to remain aligned in the samed direction. Such a mechanism is also observed on long textile fibers or lamellae on polymers [81, 82].
The nature of the structural elements remains however unknown. Garoff *et al.* observed the presence of fibers at the surface of paper that are not linked to the fibrous web structure and called them *raised fibers* [44]. Microscopy showed that the raised fibers get reoriented in the direction of the sliding, as represented on Figures 9.2a and 9.2b. They suggested that the friction hysteresis may be due to the reorientation of raised fibers, as represented on Figures 9.2c and 9.2d. This hypothesis is based on the hypothesis formulated by Johansson *et al.* To support their hypothesis, Garoff *et al.* measured the total area of the raised fibers per unit width of the test piece. The principle of the measurement method is represented on Figure 9.3a. They found a good correlation with the friction hysteresis of paper, as represented on Figure 9.3b. In particular, they suppose that the increase with pressure is due to the number of fibers that have to be reoriented.

Critics The literature concerning the effect of reversed slidings on the friction force between papers is incomplete.
First of all, for $D_f = 0$ and $D_b = D$, both forward and backward slidings start from the same position. Consequently, the backward sliding and the forward sliding

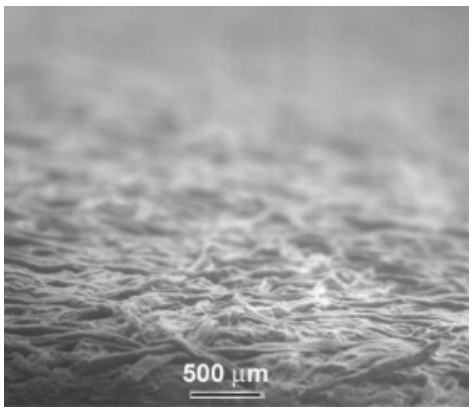

(a) ESEM image (before sliding)

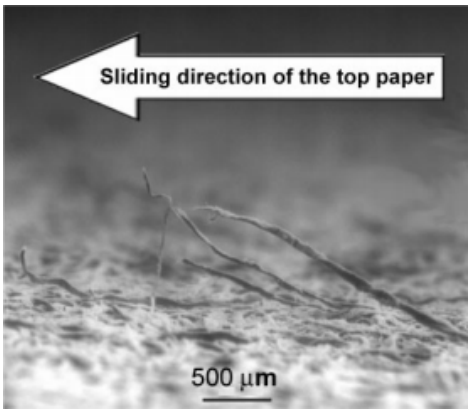

(b) ESEM image (after 10 slidings)

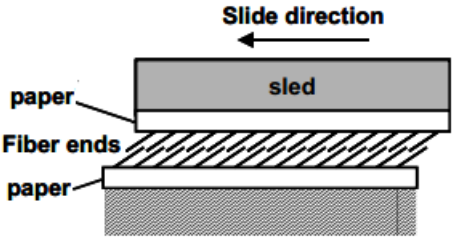

(c) Proposed model (before sliding)

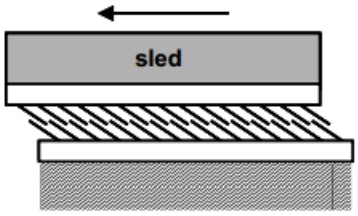

(d) Proposed model (after sliding)

Figure 9.2: ESEM image of a filter paper before/after 10 repeated slidings and proposed model of raised fibers reorientation [44]

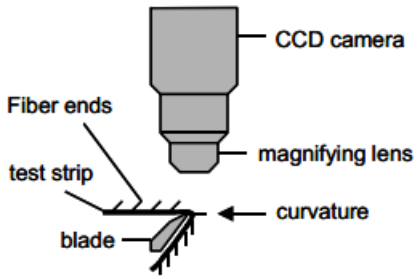

(a) Principle of the method

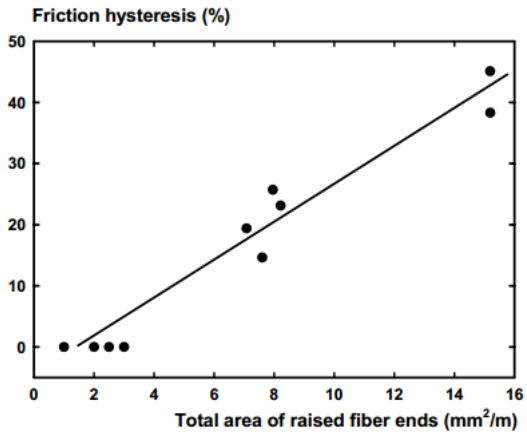

(b) Measurements

Figure 9.3: Friction hysteresis of paper against the total area of raised fibers per unit width of the test piece. Measurements before 10 repeated slidings [44].

partly occur on different areas of the plane sample. The mechanisms involved are thus difficult to characterize.
Johansson *et al.* also studied backward displacements at increasing distances in the direction of the sliding (increasing D_f with $D_b = D_f$). The samples area involved in the backward sliding is thus also involved in the forward sliding. However, they only studied displacements from 0.1 mm to 0.5 mm between *"fresh samples"* that never underwent any repeated sliding.
Beyond those issues, the authors did not compare the decrease in friction force with repeated slidings to the evolution with reversed slidings. Such a study should however permit a better understanding of both mechanisms.

9.1.2 A model of friction force

9.1.2.1 Problem and goal

The literature shows that the decrease in friction force with repeated slidings is very important: up to 50 % of the initial value. This decrease may be a problem for processes involving papers because the number of repeated slidings the material underwent is not always mastered. However the evolution of paper friction with repeated slidings has been poorly characterized, in particular the trends, the parameters, and the causes. In this chapter, we propose to characterize mathematically the decrease in friction force with repeated slidings. We will also observe their consequences on the fibrous structure. We will finish by giving hypothesis to the cause of such a decrease.

9.1.2.2 A dimensional model for friction

We develop a model that links the force of friction to dimensional parameters – in particular the sliding distance and the samples sizes. We consider a *mobile* sample sliding on a *plane* sample. The surface of both samples has surface structures that get reoriented in the direction of the sliding. The size of these structures is infinitesimal compared to the size of the samples. We call $f_{f,0}$ the force of friction in a point of the contact where the surface structures are fully-reoriented in the direction of the sliding (e.g., after a few repeated slidings). When the mobile and plane structures are not fully-reoriented in the direction of the sliding, the force of friction increases. The increases are noted $f_{f,mobile}$ and $f_{f,plane}$, respectively. Thus, the force of friction, F_f, is calculated as the sum of those different contributions on the whole apparent contact surface, S:

$$F_f = \int_S (f_{f,0} + f_{f,mobile} + f_{f,plane}) \, \mathrm{d}S \tag{9.2}$$

We consider that the mobile and plane surfaces are made from the same material. Their surface structures are therefore of the same nature. Thus, the contribution of

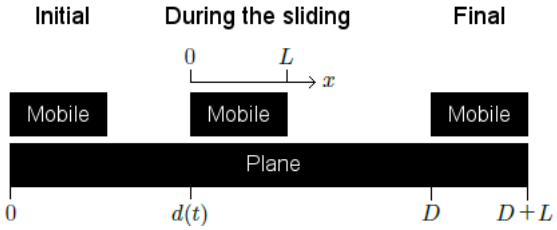

Figure 9.4: Mobile (top) of length L sliding on a plane (bottom). The rear of the mobile slides from 0 to D. At a time t during the sliding, the position of the mobile rear is $d(t)$. The position on the contact is called x.

these structures to the friction force ($f_{f,mobile}$ and $f_{f,plane}$) can be described by the same f_f function. Literature suggests that the sliding modifies the force of friction. Therefore, we propose that the f_f function depends on the total sliding distances underwent by the surface structures, called *Local Sliding Distances*:

$$\begin{cases} f_{f,mobile} = f_f(d_{mobile}) \\ f_{f,plane} = f_f(d_{plane}) \end{cases} \tag{9.3}$$

Where d_{mobile} and d_{plane} represent the local sliding distances of the mobile and plane surface structures, respectively. We consider a mobile of length L moving on a plane. At a time t of the sliding number N, the mobile moved from a distance $d(t)$, as represented on Figure 9.4. At a position x of the contact, the local sliding distances are given by:

$$d_{mobile}(x,t) = d(t) + D.(N-1) \tag{9.4}$$

$$d_{plane}(x,t) = \begin{cases} (N-1).x + N.d(t) & \text{if } x + d(t) < L \\ N.L - x & \text{if } L < x + d(t) < D \\ N.(L-x) + (N-1)(D-d) & \text{if } D < x + d(t) \end{cases} \tag{9.5}$$

We exemplified these evolutions on Figure 9.5. In particular, the local sliding distances are constant along the samples width, W. Thus, equation 9.2 becomes:

$$F_f = W \int_0^L \left(f_{f,0}(x) + f_f(d_{mobile}(x)) + f_f(d_{plane}(x))\right) \mathrm{d}x \tag{9.6}$$

The functions $f_{f,0}$ and f_f have to be identified to determine F_f. To identify the f_f function, the local sliding distances of both the mobile (d_{mobile}) and the plane (d_{plane}) have to vary separately. In the next section, we will therefore propose a method to achieve this identification. Then we will validate experimentally the model.

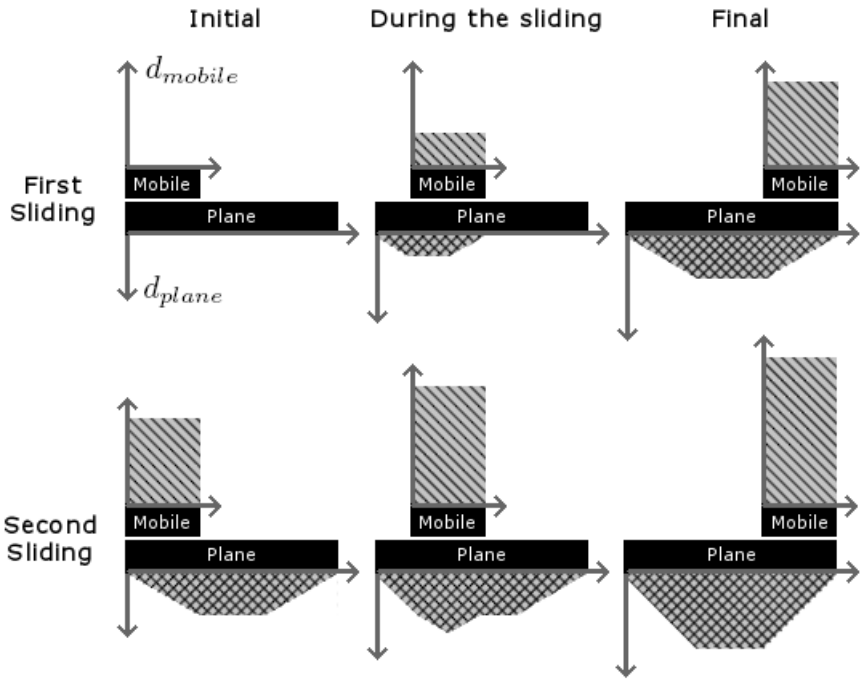

Figure 9.5: Evolution of the local sliding distances of a plane (d_{plane}, double-hashed areas) and a mobile (d_{mobile}, simple hashed areas) during two repeated slidings.

9.1.2.3 Materials and method

Methods We measure the force of friction using the oscillating sled test method. We call hereafter *fresh* and *old* materials that underwent no sliding and ten repeated slidings, respectively. We carried out three different experiments involving ten repeated slidings (from $N = 1$ to 10):

i *PlaneChange* (PC_N) – After each repeated sliding,(i) the plane sample is changed by a fresh one, and (ii) the mobile is lifted and placed at its initial position.

ii *MobileChange* (MC_N) – After each repeated sliding, the mobile sample is changed by a fresh one, and placed at its initial position.

iii *NoChange* (NC_N) – After each sliding, the mobile is lifted and placed at its initial position without changing any sample. The experiment corresponds to the standard conditions.

Each experiment is carried on ten different pairs of samples, and the results are averaged. The local sliding distances of the materials at the beginning of the second repeated sliding of each experiment are represented on Figure 9.6.

To identify the model, we measure the friction force at the beginning of each PC_N experiment, i.e., when the mobile starts sliding. At the beginning of the PC_N

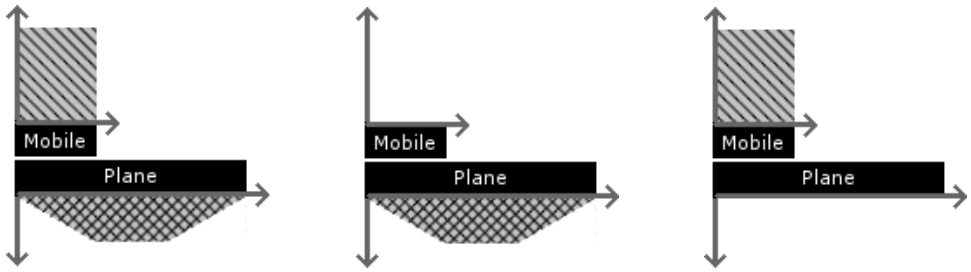

(a) *NoChange* (b) *MobileChange* (c) *PlaneChange*

Figure 9.6: Local sliding distances of the plane (d_{plane}, double-hashed areas) and the mobile (d_{mobile}, simple hashed areas) at the start of the second repeated sliding.

experiments, the plane is a fresh sample. Thus, the contribution of its surface structures to the friction force remains constant: $f_f(d_{plane}) = f_f(0)$. On the other hand, the local sliding distance of the mobile is homogeneous along the mobile length and increases linearly with the sliding number, N, as represented on Figure 9.6c. The contribution of the plane's surface structures to the friction force becomes: $f_f(d_{mobile}) = f_f(D(N-1))$, with D the total sliding distance of the sled, see equation 9.4. This method allows the identification of the $f_f(d)$ function, and finally the identification of the whole model.

To validate the model, we calculate the evolution of the friction force during the whole *MobileChange*, *PlaneChange*, and *NoChange* experiments. The theoretical results are compared to the results of the measurements.

Materials We use writing papers (basis weight 80 g.m^{-2}). The papers were stored 48 hours at 24^{o}C and 50 % RH. For each experiment, ten couples of materials are tested. As paper is anisotropic, the sliding is undergone in the direction of the main fiber orientation (called machine direction). Furthermore, we place the same paper sides in contact. This can be achieved by using the same sheet of paper for the two samples.

9.1.2.4 Identification of the model parameters

We now present the results of the identification of the proposed model. The friction forces measured at the beginnings of the PC_N experiments are represented on Figure 9.7.

The forces is the sum of a logarithmic-shape and a linear decreases in friction force with the local sliding distance of the mobile. We describe the logarithmic-shape decrease, $F_1(d_{mobile})$, by a sixth-order polynomial decrease:

$$F_1(d_{mobile}) = \sum_{i=0}^{6} \alpha_i {d_{mobile}}^i \tag{9.7}$$

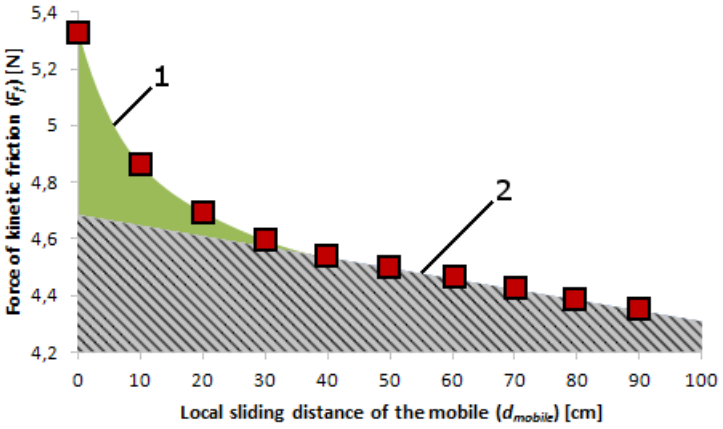

Figure 9.7: Friction force at the start of each repeated sliding of the *PlaneChange* experiments (squares). The friction force is represented as a function of the local sliding distance of the mobile: for example, the start of the third repeated sliding corresponds to a local sliding distance of the mobile of $2 \times 10 = 20$ cm. The proposed model consists in the sum of a logarithmic-shape decrease (1) and a linear decrease (2).

Where α_i represent the parameters of the model. Numerical values for those parameters are presented on Table 9.1. The logarithmic-shape decrease is observed up to the fourth repeated sliding (corresponding to $d_{mobile} = 4x10 = 40$ cm). We propose to explain this decrease by the reorientation of mobile surface structures, described by the f_f function. The function f_f may be written as:

$$f_f(d(x)) = \frac{F_1(d(x))}{LW} = \frac{1}{LW} \sum_{i=0}^{6} \alpha_i d(x)^i \tag{9.8}$$

Where $d(x)$ represents either $d_{mobile}(x)$, or $d_{plane}(x)$.

On the other hand, the linear decrease, $F_2(d_{mobile})$, can be described by the following expression:

$$F_2(d_{mobile}) = \beta_0 + \beta_1 . d_{mobile} \tag{9.9}$$

Where β_0 and β_1 are the two parameters. Numerical values for those two parameters are presented on Table 9.1. The linear decrease in friction force with mobile's local sliding distance is measured above the tenth repeated sliding ($d_{mobile} = 100$ cm). Thus, we explain this decrease as the materials with fully-reoriented surface structures, $f_{f,0}$, plus the eventual contribution of plane asperities remaining fresh, $f_f(0)$. In this situation, we propose this linear decrease in contribution to the friction force to be proportional to the larger local sliding distance of both materials (d_{mobile} and d_{plane}). An expression of $f_{f,0}$ may be proposed:

$$f_{f,0}(x) = \frac{1}{LW}(\beta_0 - \alpha_0) - \frac{1}{LW}\beta_1 . \max(d_{mobile}(x), d_{plane}(x)) \tag{9.10}$$

Equation	Parameter	Estimation	R^2
$F_1(d_{mobile}) = \sum_{i=0}^{6} \alpha_i {d_{mobile}}^i$	α_0	0.66 N	1.0
	α_1	-7.6×10^{-2} N.m^{-1}	
	α_2	4.7×10^{-3} N.m^{-2}	
	α_3	-1.7×10^{-4} N.m^{-3}	
	α_4	3.6×10^{-6} N.m^{-4}	
	α_5	-3.7×10^{-8} N.m^{-5}	
	α_6	1.5×10^{-10} N.m^{-6}	
$F_2(d_{mobile}) = \beta_0 + \beta_1.d_{mobile}$	β_0	4.7 N	0.98
	β_1	-3.8×10^{-3} N.m^{-1}	

Table 9.1: Parameters of the model describing the friction force evolution during the *PlaneChange* experiment: $f_f = F_1 + F_2$. The estimation of the parameters is based on the average results obtained on ten different pairs of materials.

Finally, the expression of the friction force becomes:

$$\begin{aligned} F_f &= \beta_0 - \alpha_0 + \frac{1}{L}\int_0^L \beta_1.\max(d_{mobile}(x), d_{plane}(x))\,\mathrm{d}x \\ &\quad + \frac{1}{L}\int_0^L \sum_{i=0}^{6} \alpha_i \left[d_{mobile}(x)^i + d_{plane}(x)^i \right] \mathrm{d}x \end{aligned} \tag{9.11}$$

Where $d_{mobile}(x)$ and $d_{plane}(x)$ are described by equations 9.4 and 9.5, respectively.

9.1.2.5 Validation of the model

We identified the two functions of the proposed model of friction, $f_{f,0}$ and f_f, see equation 9.6. To validate the model, we calculate the friction force for the *PlaneChange*, *MobileChange*, and *NoChange* experiments. The results are represented on Figure 9.8, 9.8, and 9.8.

The model is in good agreement with the experimental results:

i. The coefficients of correlation, R^2, between theoretical and experimental results for the three experiments (*PlaneChange*, *MobileChange*, and *NoChange*) are higher than 0.99 in the three cases.

ii. The model highlights the differences in friction forces between the three experiments.

iii. The model shows that the friction force measured at the end of a *NoChange* sliding is equal to the friction force at the start of the next sliding.

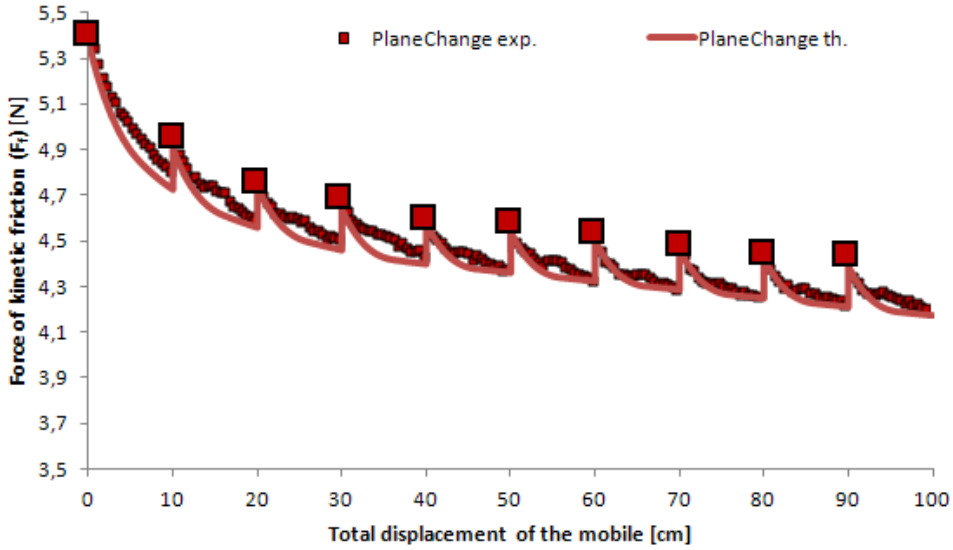

Figure 9.8: Friction forces during the *MobileChange* experiment. The measurements (dots) and calculations (lines) are represented. The big squares represent the data used to identify the model and represented on of Figure 9.7. Coefficient of correlation $R^2 > 0.99$.

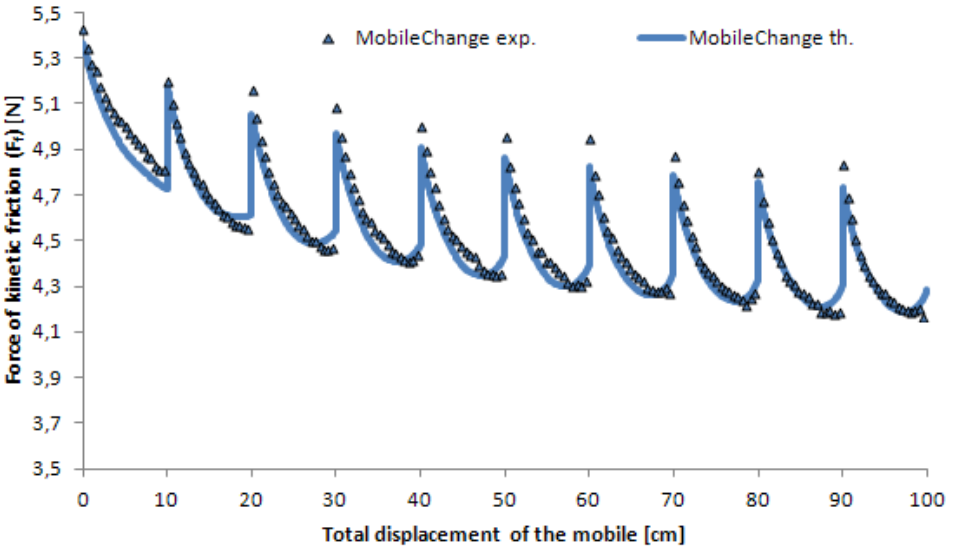

Figure 9.9: Friction forces during the *PlaneChange* experiment. The measurements (dots) and calculations (lines) are represented. Coefficient of correlation $R^2 > 0.99$.

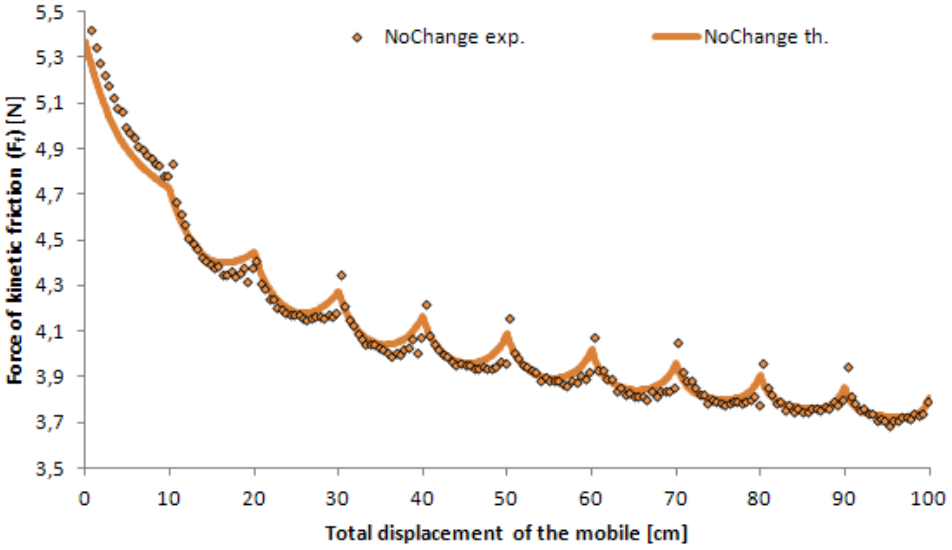

Figure 9.10: Friction forces during the *NoChange* experiment. The measurements (dots) and calculations (lines) are represented. Coefficient of correlation $R^2 > 0.99$.

9.1.2.6 Conclusion and perspectives

- The force of friction between paper materials decreases with the sliding distance, and variations can be as high as 50 %.
- We proposed a model of friction force which is able to characterize the decrease of friction with the sliding distance.
- Theoretical results are in good agreement with the experimental measurements.

The model depends on the samples sizes and sliding distance, allowing changes in sliding scales. In particular, this allows the investigation of the friction force at an infinitesimal scale. Such a study could be related to microscopy measurements to study the mechanisms involved.

The method and model could be extended as follows:

- Complex movements could be studied, e.g., circular slidings or slidings in alternate directions.
- Other materials undergoing reorientations of surface structures could be studied. These reorientations may induce either decreases (e.g., textile fibers [80] or lamellae on polymers [81, 82]) or increases of the force of friction (e.g., textiles with a "cat fur" effect [78, 79, 80]). In particular, these changes in friction force could be non-persistent (e.g., reorientation of micro-hairs on biological surfaces [76, 74]).

- Finally, the influence on friction force of irreversible modifications could be studied, such as abrasion mechanisms.

9.1.3 Surface micro-structure

9.1.3.1 Problem and goal

In the previous section, we observed that the complex decrease of friction force with repeated slidings can be assimilated to a decrease in friction potential of both the plane and mobile samples. We clarified the behavior of the decrease in friction force, but its causes remain unclear. For some authors, the decrease is due to the disruptions in surface fiber layers, so that the fibrous structure is expected to evolve. However, this hypothesis is usually based on Scanning Electron Microscopy (SEM) measurements at the fibers scale rather than at the fibrous structure scale. Moreover, microscopic observations are made at different locations of the paper before and after sliding, so that the comparison is difficult. In this section, we propose the observation of a single location of the paper samples before and after several slidings, focusing on the evolution of the fibrous structure.

9.1.3.2 Materials and methods

Materials We used a 80 $g.m^{-2}$ writing paper. The paper material being highly anisotropic, the samples were placed so that the same side of the paper is in contact, undergoing a sliding in the direction of the main fiber orientation. This method ensured that the properties of the paper involved during the sliding are the same for the mobile and plane samples.

Method We used the oscillating sled test method to produce 3 repeated slidings. Before and after each repeated sliding, we made a microscopic observation of the paper surface at the same position of the mobile sample. To do so, we used an InfiniteFocus Standard microscope (Alicona) permitting the observation of the paper surface at a microscopic scale and the measurement of the surface topography.

9.1.3.3 Results

Qualitative characterization Results clearly show that fibers do not move after repeated slidings, as represented on Figure 9.11. We also observe that after several repeated slidings, the paper samples appear glossier. Using the microscope, we observe that the fibers tend to reflect more light, as represented on Figure 9.11g for example.

Quantitative characterization The topography measurements show that the peaks at the samples surface tend to disappear, as indicated on Table 9.2.

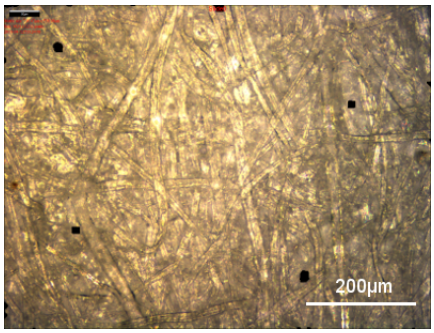

(a) Before the first sliding (real colors)

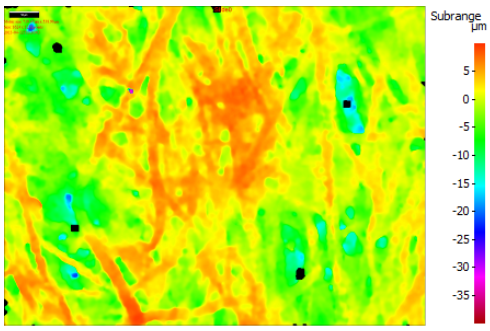

(b) Before the first sliding (colorized)

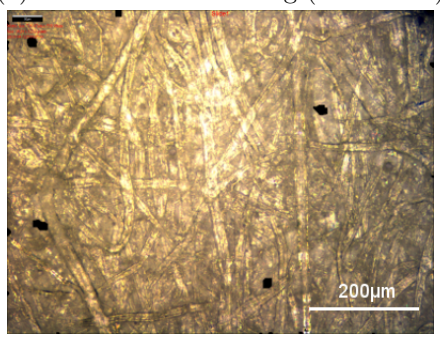

(c) After the first sliding (real colors)

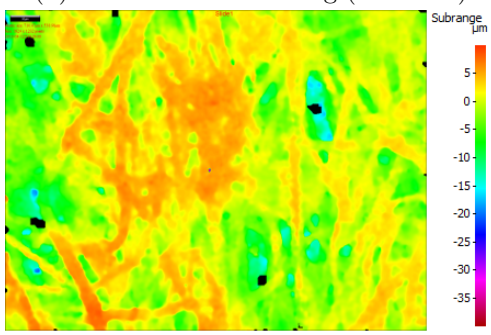

(d) After the first sliding (colorized)

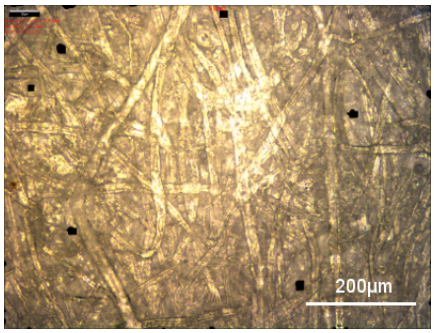

(e) After the second sliding (real colors)

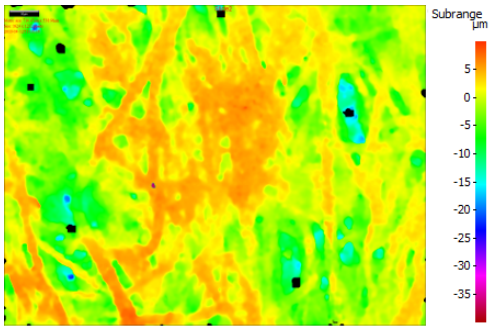

(f) After the second sliding (colorized)

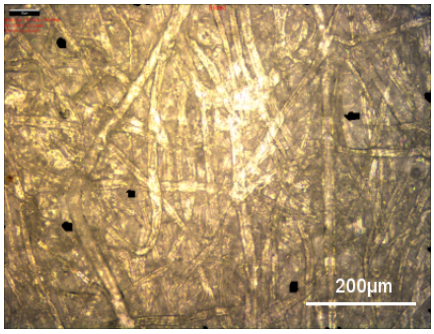

(g) After the third sliding (real colors)

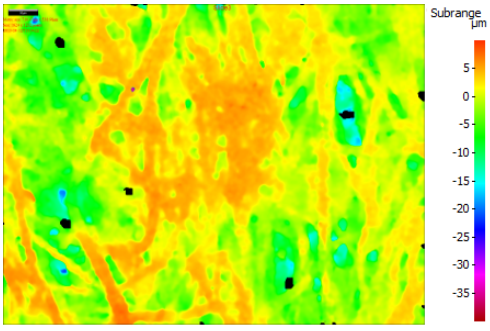

(h) After the third sliding (colorized)

Figure 9.11: Topographies of the mobile sample before/after repeated slidings

Param.	Description	Initial	Slide 1	Slide 2	Slide 3
Sa	Average Roughness	2.78	2.65	2.62	2.56
Sq	Root Mean Square Roughness	3.61	3.46	3.40	3.36
Sp	Max Peak Height	7.11	6.91	6.20	5.95

Table 9.2: Evolution of the height (amplitude) parameters before/after repeated slidings. The values refer to the mobile sample represented on Figure 9.11. All the values are expressed in micrometers (μm). More details concerning the calculation of those parameters are available in [57]

Those results reflect the disappearance of local *asperities* at the paper surface, i.e. peaks where friction takes place.

9.1.3.4 Discussion

The fibers do not move after several repeated slidings. We thus suggest that the fibers displacements have a negligible contribution to the decrease in friction force. The glossy aspect on fibers surface may be due to (i) a flattening of the fibers (more horizontal), and (ii) a decrease in fibers' surface optical roughness. The fibers and their surface are therefore flattened. This may be due to (i) a deformation of the fibers, (ii) a reorganization of the microfibrils web structure (see Figure 8.1a), or (iii) a reorganisation of wood extractives and contaminants at the surface of fibers. These observations are not sufficient to conclude on the mechanism responsible for the decrease in friction force with repeated slidings. To complete this study, we will consider the reversed slidings in the next section.

9.1.4 Cold calendering

9.1.4.1 Problem and goal

We showed that repeated slidings are associated with (i) a decrease in friction force, (ii) a glossy aspect on fibers, and (iii) a disappearance of surface asperities at the scale of the fibrous structure. The paper roughness (at a fibrous scale) can be reduced by cold pressing [83]. The influence of pressing on paper friction has already been studied by Kawashima *et al.* The authors observed a negligible increase in force of kinetic friction [17]. However, they studied neither the static friction force, neither the evolution with repeated slidings. We now propose to carry out such measurements.

9.1.4.2 Materials and methods

We studied a printing paper (80 g.m^{-2}). Ten couples of samples were tested and placed so that the same paper sides and directions are in contact. The samples were pressed (without heat) 10 times under a 50 kN.cm^{-1} linear load. We clearly observed

an electrostatic charging of the paper samples due to the repeated contacts with the calendering rolls. We thus discharged the static electricity of the paper samples by placing them on an aluminum fold connected to the electric ground. We stored the samples during 48 hours at 50 % RH and 24°C. We then measured the evolution of the forces of static and kinetic frictions during ten repeated slidings using the oscillating sled test method.

9.1.4.3 Results

The pressed material appears glossier. The coefficients of friction measured are represented on Figure 9.12a and 9.12b. We observe that the pressing reduces the coefficient of friction. However, pressing the paper samples does not modify the friction force they reach after numerous repeated slidings.

9.1.4.4 Discussion

Cold calendering has a similar influence on paper materials than repeated slidings: the paper becomes glossier, the roughness is reduced, and the paper friction is decreased. We observed that the "potential of friction" gets reduced due to cold pressing. These results are however opposed to the results of Kawahsima *et al.* and should therefore be considered with prudence.

9.1.5 Reversed slidings

9.1.5.1 Materials and methods

We study the same printing and writing paper as previously (basis weight 80 g.m^{-2}). Contrary to Garoff *et al.*, we study the case $D_f = D_b$, the sled being displaced by hand in the backward direction. The sled is not lifted between the backward and forward movements. Our method consists in two phases. First, we make 10 repeated slidings in the forward direction from the same starting point. Then, the backward displacement is set from D_f =1 mm to D. The measurement of the force of friction is made during the forward displacement only. This experiment is different from the Johansson *et al.* one in the sense that (i) it involves much longer reversed slidings (up to $D_f = D$), and (ii) initial repeated slidings permit a comparison between both mechanisms.

9.1.5.2 Results

The results are represented on Figure 9.13. We observe three phases:

Phase I Before the tenth sliding, we performed repeated slidings ($D_f = D_b = 0$). As explained in the previous section, the static and kinetic friction forces both decreased of 10 % and 30 %, respectively.

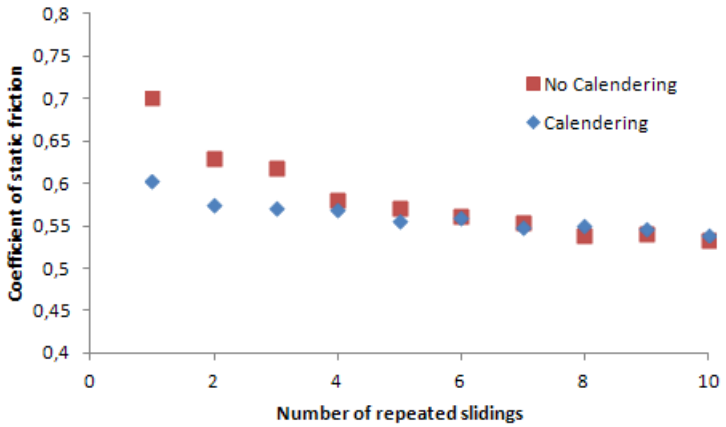

(a) Coefficient of static friction

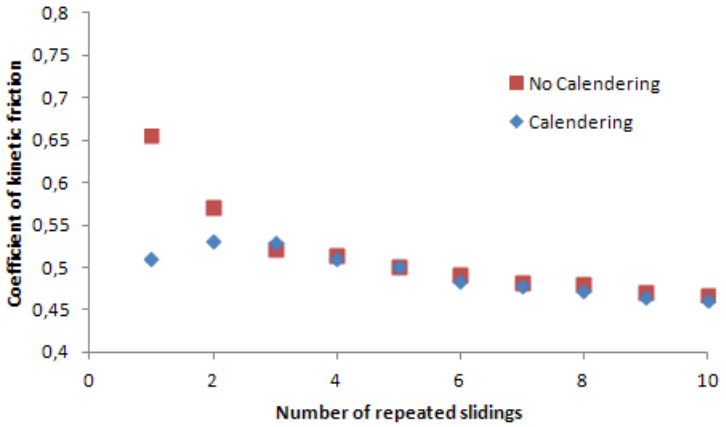

(b) Coefficient of kinetic friction

Figure 9.12: Evolution of the coefficients of static and kinetic friction with repeated slidings. Comparison of calendered and non-calendered papers.

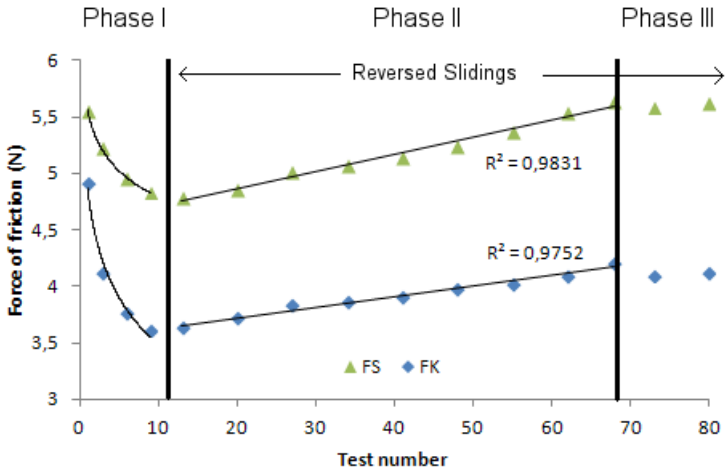

Figure 9.13: Force of friction as a function of the test number. The ten first slidings are standard repeated slidings (forward slidings from the same starting point). Reversed slidings are then carried out (forward and backward slidings, as described in Figure 9.1). The forces of static friction, F_S, and kinetic friction, F_K, are represented.

Phase II In the second part we performed reversed slidings. We clearly observe a linear increase in friction force with the number of reversed slidings. The backward sliding distance ($D_f = D_b$) had no influence on this increase.

Phase III In the last phase, we observe that the forces of static and kinetic friction remain constant. The force of static friction is similar to the measurement at the first repeated sliding. The force of kinetic friction is slightly lower (about -20 %), approximately equal to the level at the second repeated sliding. In this situation, the static and kinetic friction hysteresis are equal to 15 %.

9.1.5.3 Discussion

Our results suggest that the decrease in friction force with repeated slidings is a reversible mechanism: the samples can (at least partly) recover their initial properties by the mean of reversed slidings. This recovering is proportional to the number of reversed slidings.
The results support the hypothesis proposed by Johansson *et al.*: the decrease in friction force with repeated sliding would be due to the reorientation of surface elements in the direction of the sliding. The *'raised fibers'* hypothesis proposed by Garoff *et al.* complies with this observation but appeared incomplete: (i) we were unable to observe any raised fiber in our experiment (whereas the friction hysteresis was strong), and (ii) the hypothesis does not explain the glossy aspect of fibers.

9.1.6 Summary and conclusion

Summary The paper-on-paper contact has a very specific behavior with repeated slidings: its friction force decreases by up to -50 % after about 3 repeated slidings of 10 cm each. This behavior was previously little characterized and authors mainly suggested that it was due to the disruption of inter-fibers bonds.
In a first step, we studied the complexity introduced by the difference in samples size. The complex decrease in friction force observed reflects a simple decrease in potential stored in the different locations of the materials. In a second step, we observed that the fibers do not move in the paper plane, contrarily to the hypothesis usually admitted. However, the topmost fibers are flattened and they appear glossier. In other words, the paper surface is flattened at different scales. In a third step, we observed that cold calendering has the same consequences on the paper material. In particular, the friction potential seems to be be sharply reduced. Finally, we showed that the decrease in friction force with repeated slidings is a reversible mechanism.

Conclusion Our results show that the decrease in friction force with repeated slidings is not due to paper damages. The results rather strongly support the hypothesis proposed by Johansson *et al.*. We therefore consider that the decrease in friction force with repeated sliding is mainly due to the reorientation of surface elements in the direction of the sliding. However, contrarily to Garoff *et al.*, we did observe no raised fibers at the surface of the paper. Similarly, the raised fibers theory does not explain the gloss aspect of fibers. We therefore rather propose the decrease in friction force with repeated slidings to be due to the alignment of much smaller surface elements. For example, microfibrils and/or surface chemicals may get reoriented in the sliding direction.

Perspectives Further works on friction may benefit from a validation of the proposed model of friction and an extension to static friction forces. Moreover, a deep investigation on the evolution, with friction, of the fibers surface at a nanoscopic scale should be carried out. This investigation may permit a better understanding on the evolution of the paper friction with sliding directions. Beyond the scientific interest, technological applications of this phenomenon may be proposed. For example, the development of surfaces with highly anisotropic frictional properties may be of particular interest.

9.2 Sliding dynamics

9.2.1 Literature

Time at rest We call *time at rest* the time of contact between samples before the movement starts. The increase in force of static friction with the time at rest

was observed for various materials (e.g. rock [23]). In particular, a logarithmic increase in force of static friction with the time at rest was often observed. Several causes were proposed, among which (i) the formation of capillary bridges in a humid atmosphere, (ii) an increase in contact area due to time dependent plastic flow, (iii) a chain interdiffusion for polymers or solids covered by grafted monolayer films, or (iv) a shear stress relaxation at the interface [84].
Such results were also observed for paper-on-stainless steel contacts, for resting times between 0 and 30 seconds [31, 42]. The authors supposed this increase to be due to the disappearance of the air layer between the samples.
The case of the paper-on-paper contact was studied by Johansson *et al.* They experimented time at rest from 1 to 20 seconds and did not observe any influence on the coefficient of static friction [72].

Ramp time Johansson *et al.* also experimented the *ramp time*, they define as the time required to reach the break-away force [72]. Considering the oscillating sled test method for example, the ramp time is the duration of the spring elongation before the sled starts sliding. For ramp times from 1 to 3 seconds, the authors did not observe any influence on the coefficient of friction.

Velocity Literature only slightly studied the influence of velocity on the paper friction. Such a lack is very important, considering the wide range of velocities underwent by paper materials when processed. Umano and Yamaura showed that the coefficient of kinetic friction of the paper-on-glass contact increases by +50 % from 0 to 1 $m.s^{-1}$ [85]. From 1 to 10 $m.s^{-1}$, the coefficient of kinetic friction decreases from roughly -15 %. Heslot *et al.* studied the paper-on-paper contact. They made accurate measurements on Bristol papers after numerous repeated slidings and in the absence of stick-slip [23]. They observed a logarithmic decrease in force of kinetic friction up to 1 $mm.s^{-1}$ (minimum coefficient of kinetic friction 0.3). For higher velocities, they observed a linear increase in coefficient of kinetic friction with a rate of 3.4 $s.m^{-1}$ up to 50 $mm.s^{-1}$. Similarly to the paper-on-glass contact, we suggest that this linear increase in coefficient of kinetic friction with velocity is limited. Indeed, considering a velocity of 30 $m.s^{-1}$ (e.g. during papermaking processes), the coefficient of friction would be approximately 100.

Acceleration To finish with, the paper materials often undergo high accelerations during their sliding. However, we did not find any literature considering the influence of acceleration on friction. We suspect this to be caused by the lack of sensors to evaluate the acceleration.

9.2.2 Materials and methods

Materials We used the same printing and writing paper as in the previous chapters (basis weight 80 g.m^{-2}). The samples were placed so that the same sides and directions are involved.

Time at rest Johansson *et al.* made measurements on paper samples with resting times from 1 to 20 seconds. We propose to extend this duration. To do so, we used the oscillating sled test method but waited 10 seconds, 1 minute or 5 minutes before making the movement starts.

Ramp time At the beginning of the oscillating sled test method, the spring length increases and so does the pulling force. To make the ramp time vary, we stopped the arm displacement during this phase from 0 second to 1 minute.

Velocity We measured the force of kinetic friction between papers for low speeds (between 0.5 and 70 mm.s^{-1}) and high speeds (from 0.1 to 1.2 m.s^{-1}). Three different experiments were carried out:

- **Between 0.5 mm.s^{-1} and 5 mm.s^{-1}**, we used the standard horizontal plane test method after 10 repeated slidings.
- **Between 5 mm.s^{-1} and 70 mm.s^{-1}**, we used the oscillating sled test methods. Indeed, during an oscillation, the sled accelerates from zero to 70 mm.s^{-1}. We also studied the samples after ten repeated sliding.
- **Between 0.1 m.s^{-1} and 1.2 m.s^{-1}**, we used the ring-on-plane test method. We used electric tensions of 12, 24, and 35 V to determine the parameters of the viscous model of paper-on-paper friction.

It is important being aware that those measurements involve different movements. Their comparison may thus be questionable. In particular, the ring-on-plane test method involves long runs that are not measured with horizontal plane test methods. In every case, we studied 10 different pairs of samples.

Acceleration To measure the influence of sliding acceleration on the paper friction, we analyzed the results obtained with the oscillating sled test method. Indeed, during an oscillation, the sled accelerates and then decelerates so that the velocities from 5 mm.s^{-1} to 70 mm.s^{-1} are reached twice with opposed accelerations. We are thus able to study the influence of sliding acceleration on paper friction. We studied the tenth repeated sliding and studied ten different pairs of samples. Studying the tenth repeated sliding only avoids the influence of the decrease in friction force with repeated slidings.

9.2.3 Results and discussion

Time at rest and ramp time We observe no influence of the time at rest and ramp time on the friction force. This result confirms the Johansson *et al.* result, suggesting that the increase can be observed only for materials of different natures. Singleton and Allan suggested the increase in friction force with the time at rest to be due to the disappearance of the air layer between the paper and the steel surface. We rather suggest that the difference in electronegativity of the materials creates an electrostatic force between them, increasing the friction force. For example, a paper sheet sliding on a polyvinyl chloride (PVC) plane creates strong electrostatic forces in few centimeters.

Velocity We observed no evolution of the force of kinetic friction with sled velocity in the range 0.5 to 70 $mm.s^{-1}$. Interestingly, this result shows that it is impossible to use the horizontal plane methods to describe the Stribeck curves in the case of paper-on-paper contacts. We thus appear to be unable to develop complex friction models such as the LuGre one.
For velocities in the range 0.1 to 1.2 $m.s^{-1}$ however, we found the following expression of the viscous model of friction:

$$\mu_K = 0.1\frac{v}{v_0} + 0.4 \tag{9.12}$$

Where v and v_0 represents the relative velocity of the contact (expressed in $m.s^{-1}$) and a reference velocity ($v_0 = 1.0$ $m.s^{-1}$), respectively. The coefficient of variation was low (2 %). According to this model, the coefficient of kinetic friction for low velocities is equal to 0.4. This value seems lower than the coefficients of kinetic friction usually measured. However, the rotational speed of the ring being high, the samples undergo sliding distances above 1 m. This sliding distance would be reached in more than 10 repeated slidings on the horizontal plane. This viscous model of friction thus refers to the asymptotic value of the coefficient of kinetic friction with repeated slidings.
The observed increase in coefficient of kinetic friction (0.4 $s.m^{-1}$) is lower than the increase observed by Heslot *et al.* [23]. The value however appears much more realistic for the printing and writing papers. For example, the coefficient of kinetic friction reached in the papermaking process (approx. 30 $m.s^{-1}$) would be approximately 1.6. In franking machine feeders, the driving rollers velocity is approximately 1.2 $m.s^{-1}$. Consequently, the coefficient of kinetic friction would be equal to 0.52.

Acceleration We observed no clear evolution of the friction force with the oscillating sled test method. The results thus suggest that the sled acceleration has also no influence on the friction force. This result is of particular interest when considering franking machines, because of the high accelerations observed.

However, the method involves speeds ranging from 0.5 to 70 $mm.s^{-1}$ and accelerations ranging from -1.5 to 1.5 $m.s^{-2}$. The studied conditions are therefore far from the ones found in franking machines (accelerations up to 100 $m.s^{-2}$).
In conclusion, this experiment gives new and interesting data concerning paper friction, but should be extended to high acceleration ranges.

9.2.4 Conclusion

In conclusion, we observed that the paper-on-paper friction is relatively stable with sliding dynamics. In particular, the friction force was not influenced by the time at rest, the ramp time, the low velocities, and the acceleration. For high velocities however, we observed an increase in force of kinetic friction with increasing velocities. In franking machine feeders, this increase counterbalances the decrease in friction force with sliding distance. However, we highlighted that the precision of this viscous model of friction is low. Similarly, envelopes often undergo accelerations up to 100 $m.s^{-2}$, far above the accelerations we tested. We thus think that future works should extend the domain of validity of our study.

9.3 Normal stress

9.3.1 Literature

Deposit of the sled The mean of sled deposit on the horizontal plane is expected to influence the paper friction [31]. Indeed, we can suspect the impact between the sled and the horizontal plane to damage the samples. Standards thus require the horizontal planes to be equipped with elevator systems permitting a standard lay down of the sled (see ISO 15359 or DIN 6723 for example). However, we were unable to find any data concerning this supposed influence of sled deposit on paper friction. Johansson *et al.* suggested that the elevator system should be integrated into the ISO 15359 standard, but only in order to avoid displacement or orientation defects. The influence of the sled deposit on the paper-on-paper friction is thus questionable.

Backing Johansson *et al.* intensively studied the influence of backings on the paper-on-paper coefficient of friction [72]. The studied backings were successively (i) a 2mm thick soft foam-rubber sheet, (ii) a 2mm thick hard rubber sheet, (iii) a pad of 30 sheets of copy papers, and (iv) the metal of the horizontal plane apparatus. The backing was placed indifferently on the horizontal plane only, the sled only, or on the sled and the horizontal plane. They obtained up to +30 % in variations of coefficient of static friction. In particular, a pad of copy papers had a force of static friction increased by about 8 % compared to the one measured with hard rubbers. They showed that wherever the backing was placed, the harder the backing was, the higher the coefficient of static friction was. They also observed that the scatter in

coefficient of friction was higher for higher hardness of the backing. In particular, they showed that the paper sensitivity to the backing decreases with paper thickness.

Apparent pressure Kawashima *et al.* observed that the real area of contact increased with a shape of the type [17]:

$$A_r = k.\left(\frac{P}{P_0}\right)^{2/3} \tag{9.13}$$

Where A_r, k, P, P_0 are the real area of contact, a constant, the apparent pressure and a standard pressure for homogeneity, respectively. This behavior corresponds to the elastic contact model, also named Hertz contact, and supposes that the coefficient of kinetic friction decreases by one-third power of the pressure. Such a relation was however not observed, suggesting that the contact area is not a decisive factor of paper friction. The paper materials thus appeared to respect the Amonton's law of friction: the coefficient of friction is independent from apparent surface pressure. Johansson *et al.* [72] also verified this law for different paper grades and under apparent surface pressures ranging from 0.5 kPa to 6 kPa. Back [31] also noticed that the coefficient of friction remains constant above 5 kPa.
On the other hand, Back indicates that the coefficient of friction was reported to increase with apparent surface pressures decreasing below 5 kPa [31]. Sato *et al.* [40] observed a relation between the paper-on-paper coefficient of friction and the pressure verifying equation 9.13. However, Sato *et al.* used a strip-on-drum test method, so that the results are hardly comparable to those obtained by other authors. In particular, increasing the tension on the strip sample deforms the material, and finally modifies the topography of the material.

9.3.2 Materials and methods

Problems The influence of the impact between the sled and the horizontal plane during the sled deposit was never studied. The requirement of an elevator system is thus questionable.
Johansson *et al.* studied the influence of backing on the coefficient of static friction, but not on the coefficient of kinetic friction. Moreover, the variability of measurements carried on the horizontal plane is high and potentially explains the scattering in coefficients of friction they measured.
Finally, the influence of the apparent pressure on the paper-on-paper friction force is controversial.

Materials and method For each experiment, we used 10 different pairs of printing and writing papers (basis weight 80 $g.m^{-2}$). For each experiment, we used the oscillating sled test method and measured both the static and kinetic friction force. In a first experiment, we used the oscillating sled test method but the sled deposit

was replaced by a drop from 0 to 1 cm. The impact is thus much higher when the sled drops from 1 cm compared to when it is layed slowly. This experiment is intended at studying the influence of sled deposit on the friction force.
In a second experiment, we used a 810 g sled on a 60x60 cm^2 area as follows:

- *0 layers*: the standard method, consisting in hard rubber on metal.
- *3 layers*: 3 sheets of paper are placed on the metal plane. The hard rubber is kept on the sled.
- *10 layers*: 10 sheets of paper are placed on the metal plane. The hard rubber is kept on the sled.
- *soft/soft*: a foam rubber is placed on the metal plane while the hard rubber is kept on the sled.
- *hard/hard*: nothing is placed on the metal plane and the hard rubber of the sled is removed.

In a third experiment, we studied a 2790 g sled with the same 60x60 cm area.

9.3.3 Results and discussion

Influence of sled deposit We observe no influence of the sled drop on the paper-on-paper friction force. We suppose this result to be due to the hard rubber placed on the sled. This rubber may reduce the damages of the samples and finally the increase in friction force.

Influence of backing The measurements of the coefficients of static and kinetic frictions are represented on Figure 9.14a. We observe a higher friction force for the hard/hard backing than for the standard backings made of paper sheets (+5 %). The number of sheets used as backing (0, 3, or 10) had no clear influence on the force of friction we measured. This result suggests that measuring the friction between two paper samples is representative of the friction between paper materials in a stack. To finish with, the soft/soft backing showed a reduction of friction of 2 %. Those results confirm the influence of the backing rigidity on the coefficient of friction of the paper-on-paper contact. In particular, the results confirm that the harder the backings are, the stronger the damages are during the sled deposit, and finally the higher the friction forces are. We also observe that the Johansson *et al.* results appear to be extendable to the force of kinetic friction.
However, those results are based on the first oscillation of the first sliding (on approximately 20). When studying the second oscillation, then the results are much more constant, as represented on Figure 9.14b. Identical results are obtained for the following oscillations, as represented on Figure 9.14c. In particular, the increase in scatter with hardness appears to be hardly observable (see Figure 9.14b). This

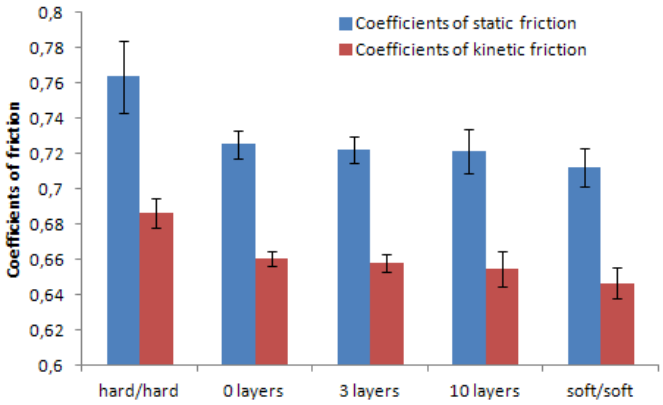

(a) First oscillation of the first repeated sliding

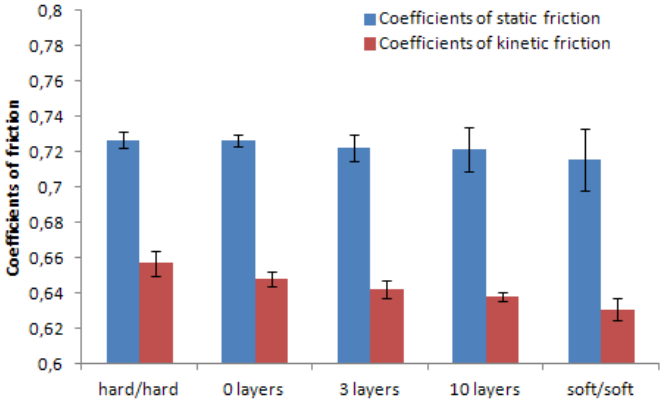

(b) Second oscillation of the first repeated sliding

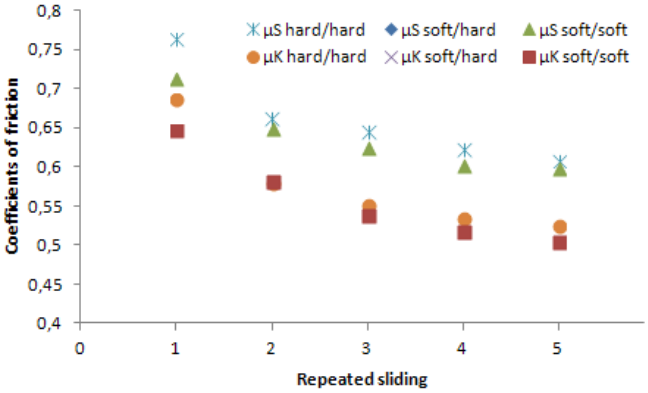

(c) Repeated slidings

Figure 9.14: Influence of different hardnesses of sled/plane on the coefficients of friction. The dispersion in coefficients of friction is reduced after the first oscillation of the first repeated sliding.

(a) Before the first oscillation (b) After the first oscillation

Figure 9.15: Influence of the samples damaging on the friction force. The circle shows the perfect fit between the plane damage and the mobile sample.

observation supports the hypothesis that the increase in friction force with backing hardness is related to the deposit of the sled. The influence disappears during the sliding.

Influence of sled weight From 810 to 2790 g, we observed no influence of the sled weight on the coefficients of static and kinetic friction. Those measurements confirm the results usually observed in the literature and the Amonton's law for paper friction. We thus strongly believe that the pressure-dependency of the friction force observed by Sato *et al.* is due to the method used. In particular, the modification of the pressure applied in the strip-on-drum test method is expected to modify the surface properties of the samples and consequently the friction properties observed.

9.3.4 Conclusion

We observed that the harder the backings are, the higher the coefficients of friction of the first oscillation are. We suppose that this phenomenon is due to the damages applied to the samples by the sled deposit. A possible mechanism for this influence is represented on Figure 9.15. In the case of hard/hard backings, the paper materials are more strongly damaged by the sled deposit. Before the first oscillation, the shape of the mobile sample and the damages to the plane sample are therefore highly interlaced. Consequently, the displacement of the mobile sample is more difficult, as represented by a circle on Figure 9.15a. The friction force increases. On the other hand, after the first oscillation, the mobile sample does not fit with the plane damage anymore. The damage thus has no more influence on the friction force.
Those results are of particular interest because they show that the use of foam under the sled avoids damages, validating the oscillating sled test method. Moreover, the study of a single sheet of paper is representative of the behavior of paper materials within a paper stack. The elevator system appears to be required only to avoid orientation and displacement defects. Our oscillating sled test method uses an alternative: we placed a long stem behind the sled that permits a much more accurate positioning of the sled compared to common manual positioning. Moreover, the moving arm was farther from the center of gravity of the sled, reducing the influence of a bad positioning on the measurement. We thus consider that our oscillating sled

test method does not require an automated elevator system.

Summary and Conclusion of Chapter 9

Sliding direction The force of paper-on-paper friction decreases with few repeated slidings in the same direction and from the same starting position (up to -50 %). We linked this decrease to a "potential of friction" stored in each sample, that dissipates with sliding distance. We showed that the mechanism is reversible and linked to a decrease in roughness of the fibers surface.
Our results support the reorientation of surface elements as the major mechanism responsible for the decrease in friction force with repeated slidings. The friction potential highlighted by our model would therefore be linked to the disorder of those surface elements. In particular, we suggested that microfibrils or lubricants may get oriented in the sliding direction. Additionally, by flattening those surface elements, cold pressing reduces the influence of their disorder on friction force.

Sliding dynamics We observed no influence on the friction force of the time at rest, ramp time, low acceleration ($<$1.5 m.s^{-2}), and low velocities ($<$70 mm.s^{-1}). However, we found an increase of the coefficient of kinetic friction of approximately 25 % per m.s^{-1} for high velocities. In franking machine feeders, this increase partly compensates the decrease associated to long runs in the same direction. Further works should study higher accelerations and improve the accuracy of the viscous model of friction.

Normal stress Normal load appeared to have no influence on the coefficient of friction, supporting the Amonton's law of friction. The foam fixed under the sled seemed to be sufficient to avoid the samples damages created by the sled deposit.

Conclusion We recommend future works to (i) study the interactions between frictional histories, (ii) study the evolution with repeated slidings of fibers structure at a nanoscopic scale, and (iii) improve the precision of the viscous model friction.
We studied the influence of structural and protocolar factors. In the next chapter, we will study the environmental factors.

Chapter 10

Environmental factors

The optimization of the franking machine feeders requires a deep understanding of the friction between paper materials. In the previous chapters, we studied how the structural and protocolar factors influence the paper-on-paper friction. We now study the role of environment. We study successively the static electricity, the humidity, and the temperature.

10.1 Literature

10.1.1 Static electricity

Tribocharging The *triboelectric effect*, also called *triboelectric charging* or *tribocharging*, is the phenomenon by which a pair of different materials in rubbing exchange charges (in particular electrons) [86]. Tribocharging is common in our everyday life, because of short static discharges experienced when touching a car in summer or when removing a pullover in the dark, for example. Although the charging is usually associated to a sliding between the materials, only a brief contact is sufficient to electrically charge them (usually called *contact charging*).

Influence on friction The static electricity has been shown to be a major parameter of the friction force. A proposed mechanism consists in the increase in normal load due to the Coulomb force created by static electricity [87]. However, if the contribution of static electricity to friction of electric conductors is well-documented, the contribution of triboelectricity to friction of dielectrics is yet poorly understood and documented. In particular, no sufficient data permit the development of quantitative models for friction dependence on surface potential due to tribocharges. The use of systems permitting the discharging of the materials remains however advisable [87].

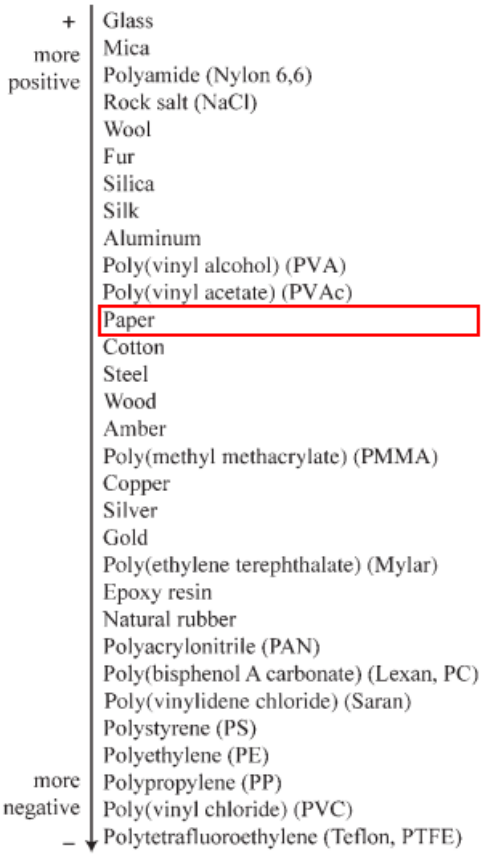

Figure 10.1: An example of triboelectric series [86]. Paper is indicated at the center of the serie.

The case of paper materials Static electricity is expected to be a parameter of the separation defects in machines involving paper materials [14, 88, 89]. It was however only barely studied. Paper is a dielectric usually placed at the middle of the triboelectric series[1], as represented on Figure 10.1. It thus may produce tribocharging when in contact with PVC or polyethylene. The static electricity of paper is favored by (i) improper grounding, (ii) low humidity, (iii) contact pressure, (iv) temperature, and (v) the contact with materials that are apart in the triboelectric series [88]. The resistivity of paper was shown to be lower in the main direction of the fibers [89] and to decrease with moisture content ratio [90]. This result explains why most issues created by electrostatic electricity are associated with dry environments. Most pigments and starches contained in commercial papers have a negative charge, as represented on Figure 10.2. The ink of printing process can also influence the

[1]Empirically organized list of materials based on their tendency to charge either positively or negatively

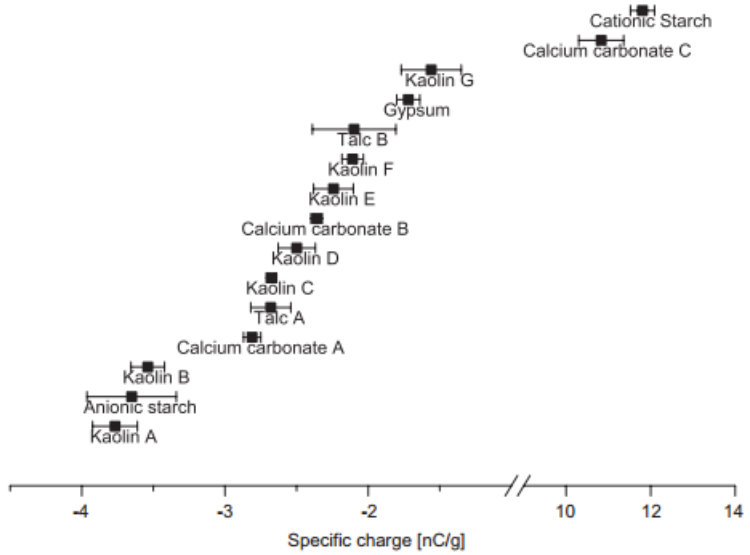

Figure 10.2: Specific electrostatic charge of different pigments and starches when sliding through a stainless steel pipe [89]

surface potential of the paper, from about 2 kV [89].

10.1.2 Humidity

Observations On the other hand, the influence of humidity on paper-on-paper friction was extensively studied. Literature suggests that the forces of static and kinetic frictions between papers increase with the relative humidity [39, 56], as represented on Figure 10.3. This increase is high for relative humidities above 60 % RH (+100 % between 50 and 90 % RH). Fellers et al. also found a linear relationship between the force of static and kinetic friction and the moisture ratio, defined as the ratio of moisture to dry matter in the sheet [39]. Additionally, Kawashima et al. showed that the real contact area between paper and a smooth surface increases from about 0.35 % to 0.55 % with the relative humidity evolving from 10 % to 95 % [17]. They interpreted this evolution as the expansion and the increase in plasticity of fiber wall. However, the friction force less increased than supposed by the increase in contact area, suggesting that another phenomenon decreases the friction force (e.g. lubrification).

Causes Several hypotheses were proposed to explain the increase of the friction force with the relative humidity, but none were able to quantify the friction force evolution:

- The capillary condensation [67, 10].

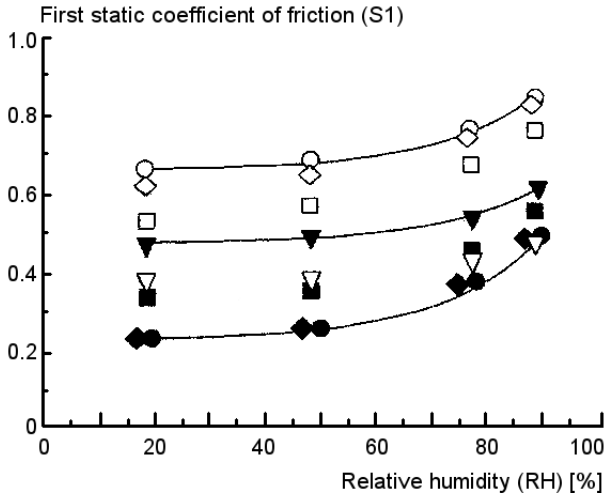

Figure 10.3: Influence of the relative humidity on the force of static friction of the paper-on-paper contact at the first sliding for several commercial papers [39].

- The swelling of fibers with the relative humidity [56, 17].
- The fiber softening [58, 31, 17].
- The modification of surface energies [58, 31], and in particular the variations in hydrogen bondings [31, 91].
- The increase in segmental diffusion of hemicelluloses chains due to a reduction in the glass transition temperature [58].

The capillary condensation hypothesis is of particular interest. Water condensation forms a thick lubricating layer of water that reduces friction with increasing relative humidities, as observed on steel contacts for example. However, water meniscus are formed around the asperities in contact. Such meniscus induce a Laplace pressure that increases the normal load and consequently the friction force [67]. We finally observe an increase in friction force with increasing relative humidity for granular media and paper surfaces [10].

10.1.3 Temperature

Paper-on-paper Contrary to humidity, only a little has been done concerning the influence of temperature on the paper-on-paper friction. The only literature concerned the hot calendering experiments. However, other mechanical phenomena are involved (such as pressing), so that the results are not representative. An increase in temperature was suspected to reduce the moisture content of samples, reducing the friction force [31].

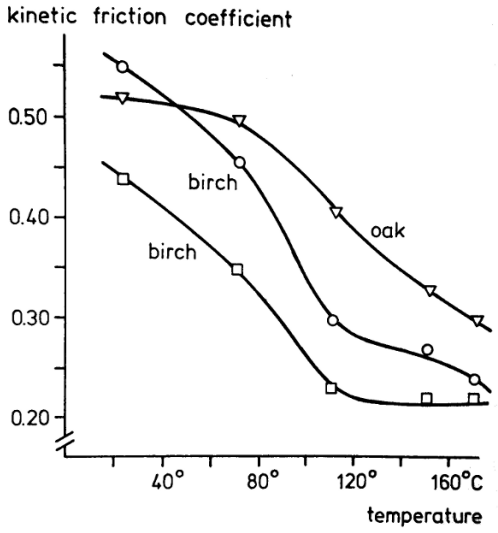

Figure 10.4: Influence of the temperature on the coefficient of kinetic friction between corrugators medium and a metal surface [31].

Paper-on-metal The paper-on-metal friction evolution with temperature was studied by Back [31]. He showed that the force of kinetic friction decreases from about 50 % from 25°C to 160°C, as represented on Figure 10.4.

10.1.4 Problem

There is an important lack of knowledge concerning the influence of the temperature and static electricity on the paper-on-paper friction. Moreover, the samples moisture ratio appeared to give an interesting view of the influence of humidity on paper-on-paper friction. It was however only poorly studied. To finish with, humidity and temperature on the one hand and humidity and static electricity on the other hand are expected to be strongly linked. For example, temperatures and humidity modify the water condensation on paper samples, whereas dry materials are expected to increase the tribocharging effect. We thus propose to measure the influence of the material humidity, temperature, and static electricity together on the paper-on-paper contact.

10.2 Materials and methods

Static electricity The paper samples being similar, there is no distance on the triboelectric series. The tribocharging between similar papers is thus expected to be negligible. However, it was reported that the same materials can sometime produce tribocharging [92]. In particular, the diversity in paper components (fibers, fillers,

and coating in particular) may produce tribocharging at a microscopic scale. The static electricity of samples would thus increase with repeated slidings, then modifying the friction force measured after repeated slidings. We propose to characterize to what extent the static electricity influences the force of friction between papers, measured after repeated slidings. Hence, we first made 5 repeated slidings using the oscillating sled test method. We then put the samples in contact with an aluminium fold connected to the electric ground, so that we expected the samples to be electrostatically discharged. We then made new repeated slidings and compared the friction forces before and after the electric discharge. This experiment would thus give a qualitative overview of the influence of tribocharging on friction.

Temperature The temperature was modified from 24°C to 85°C by using the heating system included in the plate of the tribometer we used (Model 225-1 by the Thwing-Albert Company). The samples were stored during 60 seconds on the heated plate: it was experimentally confirmed that this time was sufficient to maintain the samples at the temperature of the plate. To permit a quite constant temperature, we heated the plate at a very high temperature, and then let it decrease slowly. To measure the temperature of the paper material, we used different techniques: (i) the plate temperature sensor, (ii) an infrared sensor, and (iii) a Peltier sensor.

Humidity In order to modify the humidity of the paper samples, we used a humidity generator (Humidity Generator by the TechPap SAS Company). The generator is designed to provide air with controlled humidities at 10, 50, and 90 % RH (<2 % error). We first stored the samples in a box conditioned at the desired humidity and at 24°C during 4 hours. The samples were then placed on the horizontal plane, in a box permitting to keep the air humidity quite similar, as represented on Figure 10.5. However, we observed that the humidity tended to 50 % RH (the room humidity). The corrected humidities were (25, 50, and 67 % RH) for (10, 50, and 80 % RH), respectively. Our measurements thus have to be considered as qualitative.

Moisture ratio The measurement of the relative humidity is here only qualitative. Moreover, the moisture ratio appeared to give a good overview of the influence of humidity on friction. We thus measured the moisture ratio of the samples to obtain a quantitative characterization of the humidity actually absorbed by the samples for varying relative humidities and temperature. We made the samples temperature vary from 24°C to 76°C and the relative humidity from 25 % RH to 67 % RH using the methods previously described. We then measured the weight of the samples, called m_H. We stored the samples during 24 hours in an oven at 105°C. The humidity of the paper is supposed to be totally removed. We measured the weight of the samples, called m_0. The moisture ratio of the samples is then given by $mr = \frac{m_H - m_0}{m_0}$. For each couple of temperature and humidity, we tested ten samples of approximately 5 grams.

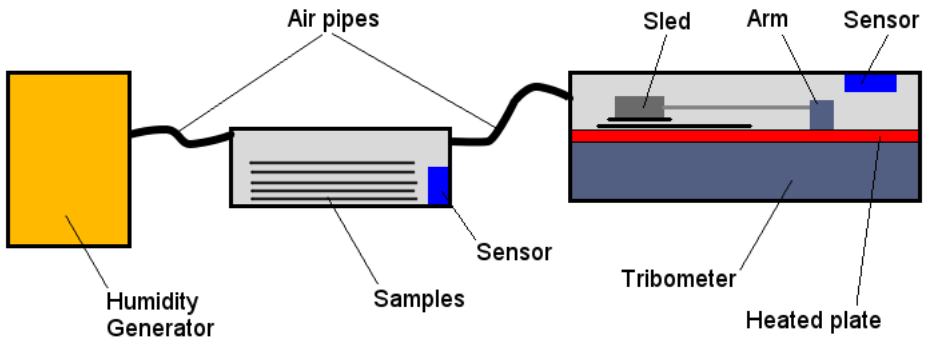

(a) Schema of the experiment

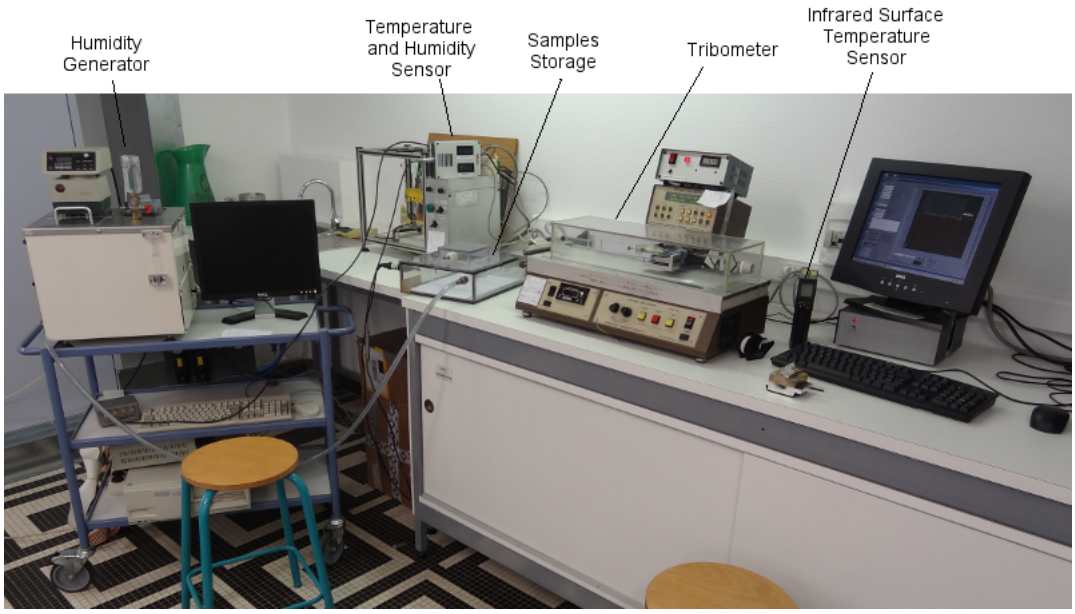

(b) Picture of the experiment

Figure 10.5: Experiment permitting the modification of the humidity and temperature of the samples

Materials We measured the friction force between printing and writing papers (basis weight 80 $g.m^{-2}$). Due to variations in temperature and humidity, the plane sample tended to curl (i.e. to deform outside of the material plan). We thus decided to stick the plane sample on the horizontal plane. We considered that the consequences of the material structure modifications on paper-on-paper friction would have a lower influence than the consequences of macroscopic deformations of the material.

Experiments All the experiments were carried on ten different pairs of samples, using the oscillating sled test method. We carried out three different experiments:

1. We studied the influence of tribocharging on the paper-on-paper friction for different humdities (25, 50, and 67 % RH, respectively) using the method previously described.

2. We studied the influence of temperature and humidity on paper-on-paper friction by making 5 repeated slidings at different temperatures (from 24 to 85°C) and relative humidities (25, 50, and 67 % RH).

3. We used samples that underwent 5 slidings at 50 % RH and different temperatures. We stored them at 50 % RH and 24°C during 24 hours. Then we made two friction force measurements. This experiment permits to determine whether the material modifications leading to the temperature-dependency of the friction is a reversible process or not.

10.3 Results and discussion

10.3.1 Static electricity

The discharging of paper samples after 5 repeated slidings did not change the friction force. In particular, this result was obtained for 25, 50, and 67 % RH. In the studied situation, tibocharging thus does not modify the friction force measured after repeated slidings. This result tends to confirm that the paper samples having the same position on the triboelectric series, their tribocharging is negligible in the studied conditions. The tribocharging sometime observed on franking machines has thus be associated to the contact with other materials (PVC for example). Due to the diversity in materials in contact and test conditions, the contact between paper and other materials is however difficult to study. We can only recommend the use of discharging systems.

10.3.2 Moisture ratio

Relative humidity and temperature strongly influence the moisture ratio of the samples, as represented on Figure 10.6. This result is obvious, considering that the

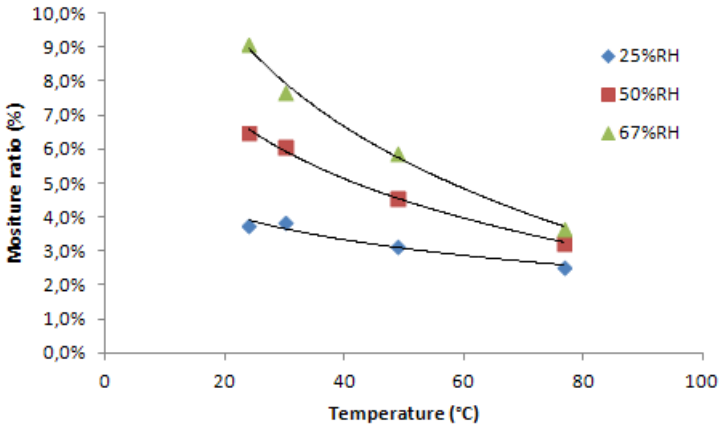

Figure 10.6: Influence of temperature and relative humidity on the moisture ratio of the paper samples

condensation of the ambient humidity into the paper samples is favored by low temperatures and high relative humidities. This result will be used in the following sections in order to study the influence of water adsorption on paper-on-paper friction. However, the use of this physical quantity, rather than the relative humidity, may be subject to controversy. Indeed, the moisture ratio represents the quantity of water adsorbed by the whole paper sample (even inside the material and inside the fibers). It does not necessary represent the quantity of water actually observed at the surface of the sample. On the other hand, the relative humidity represents the quantity of water available in the surrounding gaz. Relative humidity may be associated to the quantity of water actually observed at the surface of the material, but the link appears to be complex. In the following sections, we thus propose to use both the relative humidity and moisture ratio quantities to characterize the influence of humidity on friction.

10.3.3 Temperature and humidity

10.3.3.1 First repeated sliding

The friction force between two papers is known to sharply decrease during the first sliding. This decrease remains ununderstood, even if several mechanisms have been suggested [40, 41, 63, 31, 44]. Due to these variations in friction force, the measurements represented on Figure 10.7 are characterized by a high variability and have to be considered as qualitative. In the studied range of temperatures and humidities, we observe that the forces of kinetic friction (i) are roughly constant up to 60°C (point 2 on Figure 10.7), (ii) linearly decrease above 60°C, and (iii) are roughly independent from the relative humidity. On the other hand, the force of static friction at 50 and 67 % RH (i) linearly decreases with temperature and (ii) increases with

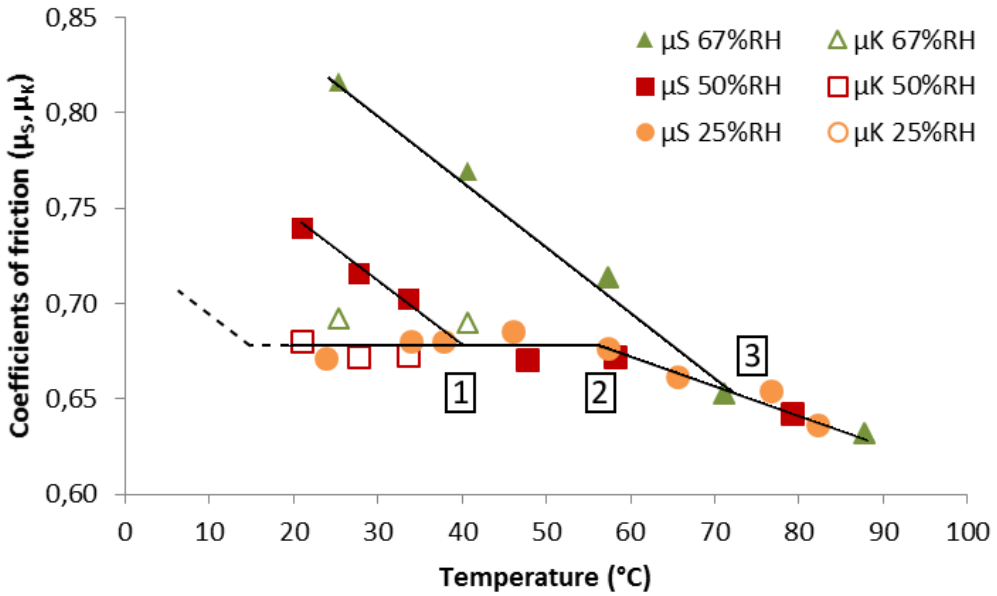

Figure 10.7: Coefficients of static and kinetic friction at the first sliding, for various temperatures and humidities. Black lines represent master curves. The dashed line represents a possible evolution of the force of static friction at 25 % RH.

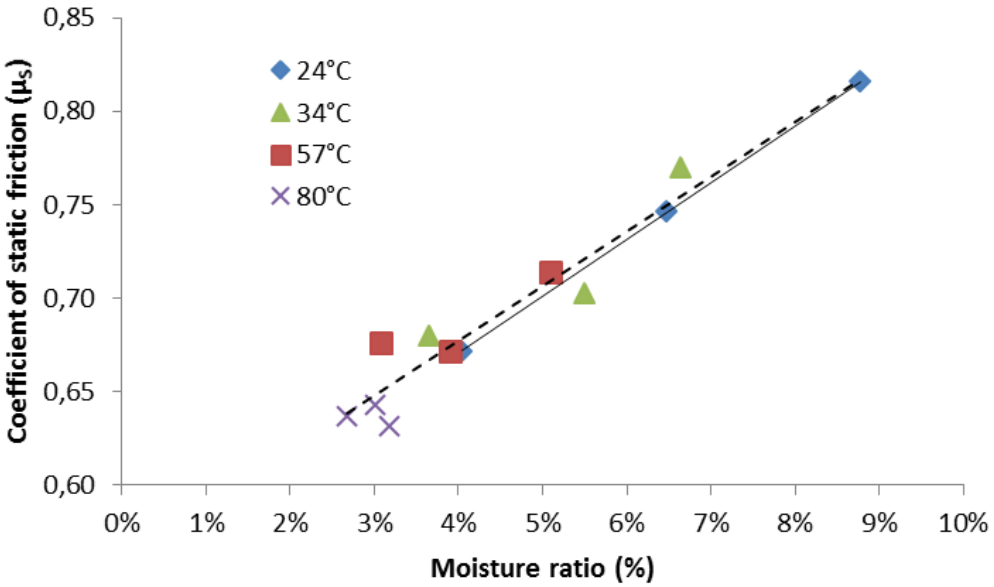

Figure 10.8: Coefficients of static friction measured during the first sliding for different relative humidities (25, 50, and 67 % RH) and temperatures (24, 34, 57, and 80°C). The full line represents the linear correlation ($R^2 = 1.0$) obtained at 24°C only. The dashed line represents the linear correlation ($R^2 = 0.94$) obtained with all the temperatures.

relative humidity. The forces of static and kinetic friction become equal above a critical temperature, T_c, equal to 40 and 75°C for relative humidites of 50 and 67 %, respectively (points 1 and 2 on Figure 10.7). In this situation, the stick-slip oscillations disappear. To finish with, the force of static friction at 25 % RH is equal to the force of kinetic friction in the range of studied temperatures. Thus, no stick-slip oscillation could be observed. We suggest that the critical temperature at 25 % RH is lower than 24°C. A possible evolution of the force of static friction below 24°C is represented by a dashed line on Figure 10.7. Finally, the proportionality between the force of static friction and the moisture ratio is verified at 24°C, as represented on Figure 10.8. Beyond 24°C, the same proportionality is respected but becomes difficult to determine as the coefficients of static friction converge.

10.3.3.2 Third and fifth repeated slidings

During the third repeated sliding, as the force of friction stabilized, measurements can be considered in a much more quantitative way. The influence of temperature and relative humidity on the coefficients of static and kinetic friction at the third and fifth repeated sliding are represented on Figure 10.9a. For clarity reasons,

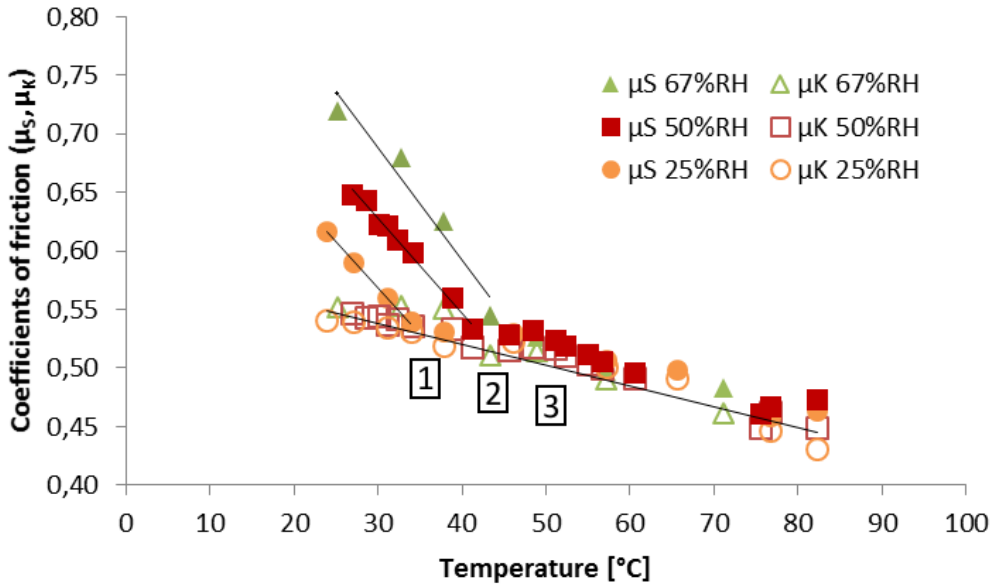

(a) Third repeated sliding

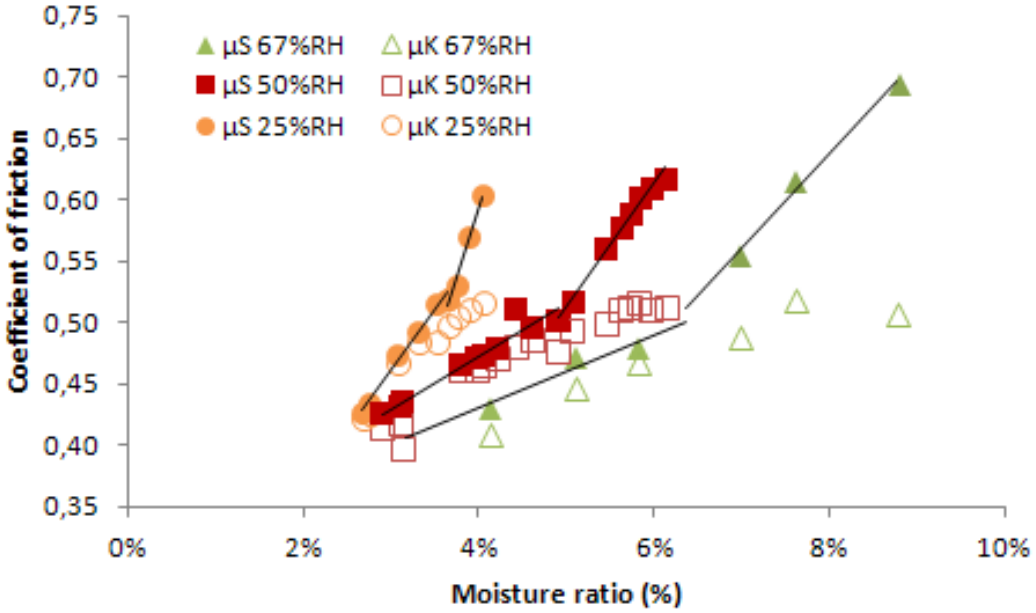

(b) Fifth repeated sliding

Figure 10.9: Coefficients of static and kinetic friction at the third and fifth repeated slidings, for various temperatures and humidities. Black lines represent master curves. The points (1), (2), and (3) indicate the threshold temperature, T_c, for which the coefficients of static and kinetic friction become equal at 25, 50, and 67 % RH, respectively.

the coefficients of static and kinetic friction can also be represented on a humidity/temperature graph, see 10.10. We observe that the coefficient of kinetic friction (i) linearly decreases with temperature (about -0.3 %/°C) and (ii) is roughly independent from the relative humidity. Moreover, the coefficients of static friction (i) linearly decrease with temperature (about -1.4 %/°C) and (ii) increase with relative humidities (+25 % from 25 to 67 % RH), identical to the value found during the first sliding. We also observe threshold temperatures above which stick-slip oscillations disappear. The threshold temperatures we measured are 35, 40, and 45°C for relative humidities of 25, 50, and 67 %, respectively. In conclusion, we observed similar behaviors of the force of friction at the first, third, and fifth repeated slidings.

10.3.3.3 Reversibility of the mechanism

After a reconditioning of 24 hours at 24°C/50 % RH, all the samples gave the same friction force, see Figure 10.11. In other words, whatever were the environmental conditions during the 5 first repeated slidings, the samples have similar frictional properties after reconditioning in a given environment. Thus, varying humidities and temperatures do not induce lasting modifications of the surfaces in contact. This experiment proves that the influence of humidity and temperature on the friction force is a reversible mechanism.

10.3.3.4 Proposed mechanism

We observed that a decrease in temperature or an increase in humidity both increase the friction force between paper materials. This result suggests that the swelling and softening of fibers is not the main mechanism responsible for the influence of environment on friction force between papers. Indeed, this swelling and softening of fibers is increased by increases in both relative humidity and temperature.
Moreover, the mechanism involved was shown to be reversible. This reversibility suggests that the diffusion of chemicals inside the paper has a negligible influence on frictio, as it is an irreversible mechanism.
In conclusion, we suggest that in the studied conditions, the dependence of the friction force between paper materials to the environment is mainly due to the creation of water bridges and changes in surface energy. In particular, we propose that capillary bridges are formed between contacting surfaces before the sliding starts. As the sliding starts, these bridges break and are not significatively recreated during the sliding. This mechanism explains why the force of kinetic friction is little influenced by the temperature and humidity, contrary to the force of static friction. To finish with, we propose that the differences between the first and third/fifth slidings is caused by changes in surface structures, e.g., a flattening of the samples surface.

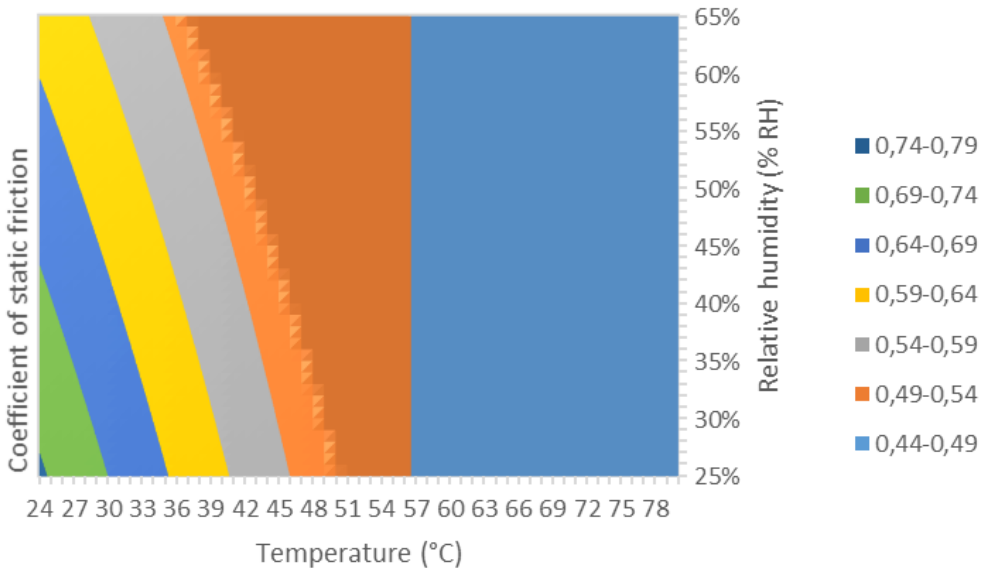

(a) Coefficient of static friction

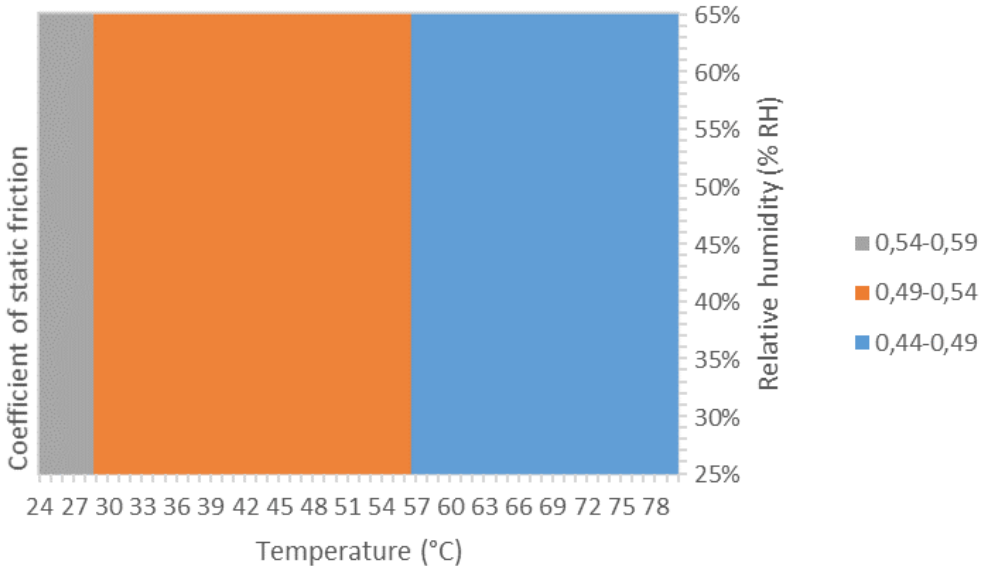

(b) Coefficient of kinetic friction

Figure 10.10: Coefficients of static and kinetic friction at the third repeated sliding, for various temperatures and relative humidities.

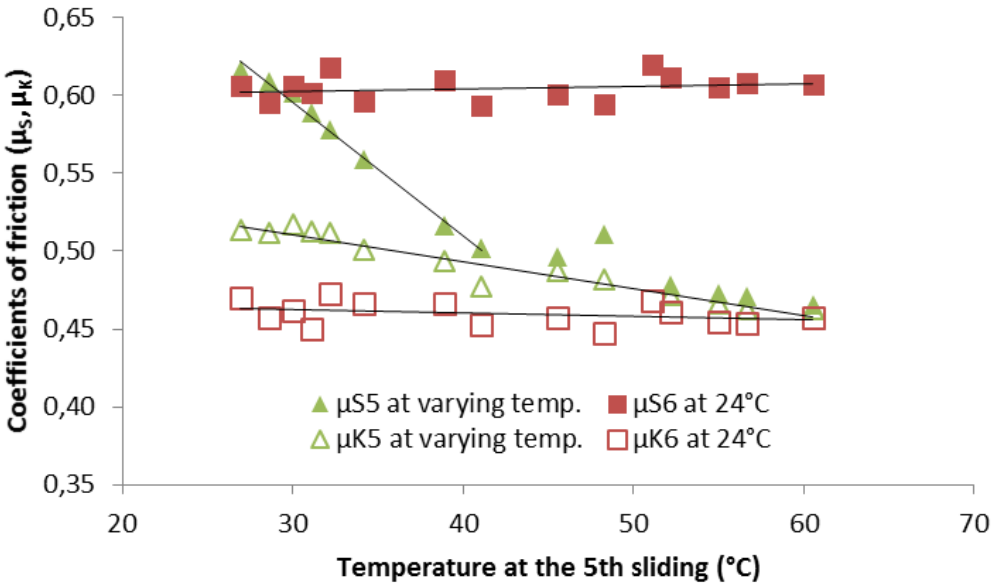

Figure 10.11: Comparison of the coefficients of static and kinetic friction between (i) the fifth sliding at varying temperature, and (ii) the sixth sliding at 24°C. Both experiment carried out at 50 % RH and stored during 24 hours. Each dot corresponds represents 1 to 3 experiments.

10.3.3.5 Proposed characterization

Interface-volume equivalence Complex models for water bridges can be found in the litterature (see in particular [93, 94]). However, those models mainly rely on a microscale characterization of the water bridges, with parameters we cannot measure. We thus propose an analysis based on parameters that are measurable at a macroscopic scale.
We make the hypothesis that the condensation of water at the interface between two similar papers is equivalent to the condensation inside the materials. Indeed, the chemistry and structure is roughly equivalent at the interface or inside the materials. In other words, studying paper volume properties (e.g. moisture ratio) is equivalent to studying the properties of the paper-on-paper interface.

Characterization of the bridge strength We want to characterize the contribution of the capillary bridges to the paper-on-paper friction force. We make the hypothesis that this contribution is proportional to the capacity of the interface to create water bridges with the available water in the surrounding humid air. Indeed, if an interface condensates a high volume of water in a dry air, then it means that the bonds between the water molecules and the structure are strong. Consequently, the water bridge is strong and contributes to the friction force at the interface.
We therefore introduce the concept of adsorption ratio, A_r. The adsorption ratio is defined as the ratio between (i) the concentration in water in the inter-fibers void and (ii) the relative humidity. An expression of the adsorption ratio is:

$$A_r = \frac{m_w}{m_{w,s}} \frac{m_{v,s}}{m_v} \tag{10.1}$$

Where m_w, $m_{w,s}$, $m_{v,s}$, and m_v represent the mass of water in the inter-fibers void, the maximal possible mass of water in the inter-fibers void, the mass of water in a given volume of saturated humid air, and the mass of water in actually in the same volume of humid air, respectively. We represented the principle of the adsorption ratio concept on Figure 10.12a. We also gave examples of structures with high and low adsorption ratios on Figures 10.12b and 10.12c.

Measuring the adsorption capacity To test this hypothesis, parameters that are measureable at a macroscopic scale are required.
First, the relative humidity, RH, can be expressed as:

$$RH = \frac{m_v}{m_{v,s}} \tag{10.2}$$

Secondly, considering that the porosity of the material is approximately 0.5, we have the approximation:

$$m_p = m_{w,s} \frac{\rho_w}{\rho_c} \tag{10.3}$$

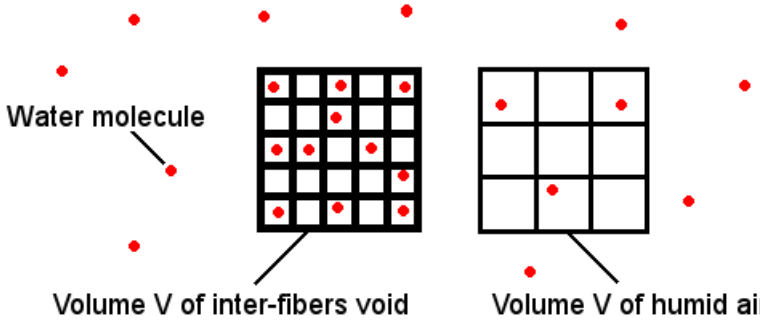

(a) Principle of the adsorption ratio. For an equal volume V, the mass of water in the inter-fibers void is higher than in the surrounding humid air. On this example, the fibrous structure stores 11 water molecules on a maximum of 25. At the same time, the humid air stores 3 molecules on a maximum of 9. Thus, the adsorption ratio is: $A_r = \frac{11}{25}\frac{9}{3} = 1.32$.

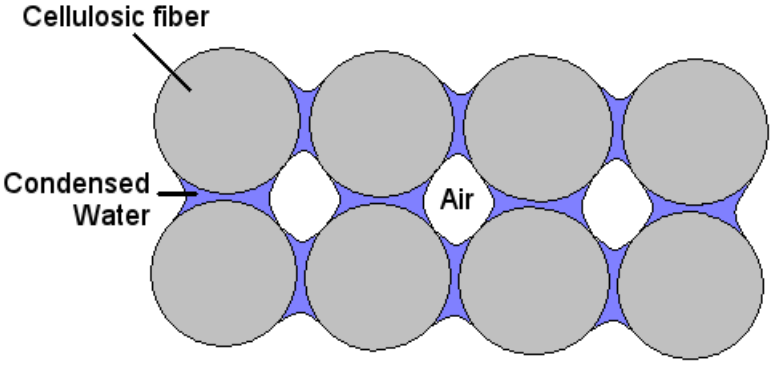

(b) Example of low adsorption ratio. Due to its structure and chemistry, this interface requires highly saturated air in the environment to be saturated. Consequently, the strength of its water bridges is low.

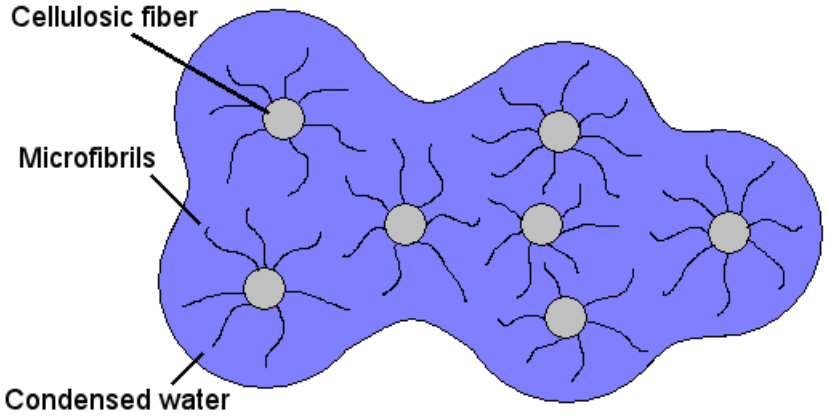

(c) Example of high adsorption ratio. Due to its structure and chemistry, this interface is saturated by water even in the case of dry air. Consequently, the strength of its water bridges is high.

Figure 10.12: Principle and examples of adsorption ratios

Where m_p, ρ_w, and ρ_c represent the paper mass and the densities of water and cellulose, respectively. The equation of the adsorption ratio, A_r, becomes:

$$A_r = \frac{m_w}{m_{w,s}} \frac{m_{v,s}}{m_v} = \frac{m_w}{m_p} \frac{1}{RH} \frac{\rho_c}{\rho_w} = \frac{mr_{ext}}{RH} \frac{\rho_c}{\rho_w} \tag{10.4}$$

Where mr_{ext} represents the moisture ratio associated to water out of the fibers.

Determination of the intra-fiber moisture ratio When measuring the moisture ratio, mr, we measure the amount of water contained both inside and outside the fibers, and called mr_{int} and mr_{ext}, respectively. Another equation of the adsorption ratio is therefore:

$$A_r = \frac{mr - mr_{int}}{RH} \frac{\rho_c}{\rho_w} \tag{10.5}$$

The evolution of the coefficients of friction with moisture ratio are represented on Figure 10.13. We observe that below a moisture ratio of $mr_0 \approx 2.3$ %, the water has no influence on the coefficient of friction. We thus suggest that the water is absorbed inside the fibers, so that is has no influence on the interface. In a first approximation, we suggest that above this moisture ratio, the fibers are saturated. The water is then adsorbed by the surface of fibers. Consequently, the moisture inside the fibers, mr_{int}, is equal to the mr_0 ratio. We finally obtain an expression of the adsorption ratio relying only on macroscopically measurable parameters:

$$A_r = \frac{mr - mr_0}{RH} \frac{\rho_c}{\rho_w} \tag{10.6}$$

Interestingly, we observe on Figure 10.13 that no clear correlation between the coefficient of friction and the moisture ratio can be found.

Results For each experiment, we calculated the adsorption ratio using equation 10.6. We represented the evolution of the coefficients of friction with the adsorption ratio on Figure 10.14. We observe that all the curves are very close together. In other words, the coefficients of static/kinetic frictions under varying environmental conditions are well represented by the adsorption ratio. We also observe three different regimes:

- During the regime 1, the coefficients of static and kinetic frictions are equal. Those coefficients increase in an increasing adsorption ratio.
- During the regime 2, the coefficients of static and kinetic frictions are still equal. But they remain constant with an increasing adsorption ratio.
- During the regime 3, the coefficient of kinetic friction still remain constant with an increasing adsorption ratio. However, the coefficient of static friction again increases with increasing adsorption ratio.

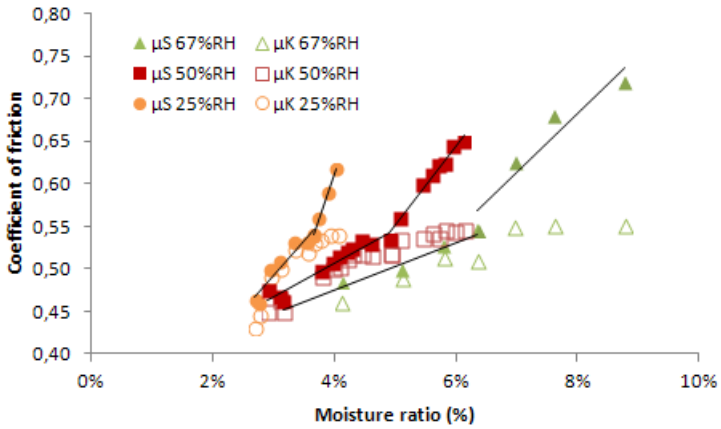

(a) Third repeated sliding

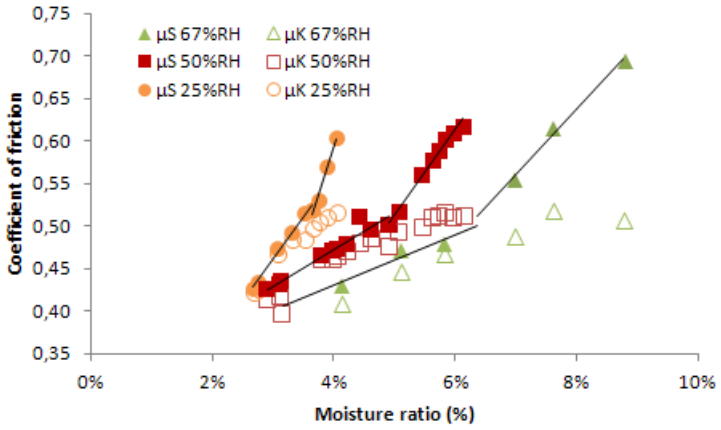

(b) Fifth repeated sliding

Figure 10.13: Relation between moisture ratio and coefficients of static and kinetic friction at different relative humidities and temperatures

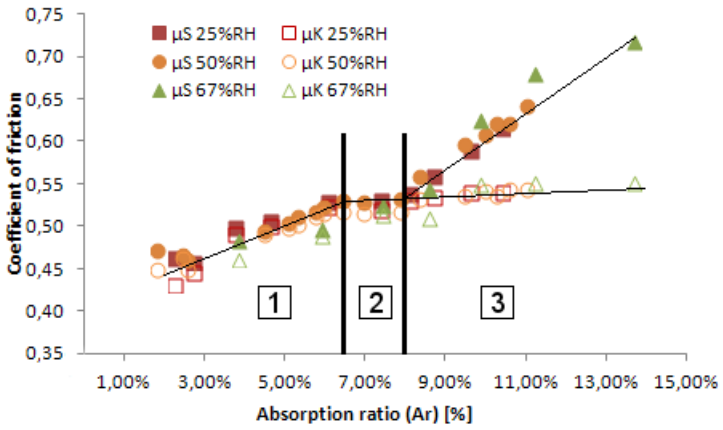

(a) At the third repeated sliding

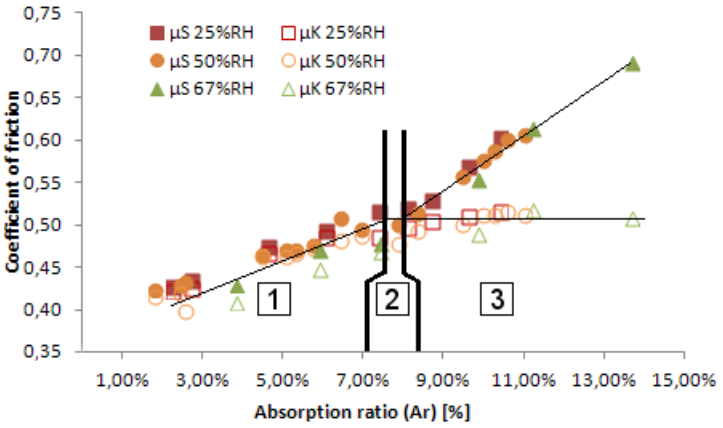

(b) At the fifth repeated sliding

Figure 10.14: Coefficients of friction vs. adsorption ratio (A_r). Master curves are represented by black lines. Three different regimes and noted 1, 2, and 3.

All the increases with adsorption ratio appear linear.

A possible mechanism We propose the following mechanism:

- During the regime 1, an increase in adsorption ratio represents an increasing capacity to condensate water. But the condensation remains low and mainly occurs on the surface of fibers. Thus, the surface properties of the fibers change linearly with the water condensation. The coefficients of static and kinetic friction therefore follow the same trend.

- During regime 3, an increase in adsorption ratio still represents an increasing capacity to condensate water. In this situation however, the water also condensates between the fibers, creating water bridges between the surface asperities. The higher the adsorption ratio is, the higher the strength of the water bridges is, and the higher the coefficient of static friction is. However, as the sliding starts, the water bridges are broken. The only influence of water condensation on friction is then due to the water at the surface of fibers. The coefficient of kinetic friction is then equal to the one reached at the end of the regime 1.

This mechanism is intended at explaining the results observed on Figure 10.14. However, further studies based on the litterature, on other materials, or on varying air pressures/chemistry may give a more accurate understanding on the mechanisms involved.

10.3.3.6 Influence of friction dissipation on friction force

The problem It was shown in chapter 2.3 that the major part of the friction force dissipates into heat. Heat is thus created on the contact asperities and then dissipates into the materials, as represented on Figure 10.15. The temperature at the contact point, called *flash temperature* and noted T_f, thus increases. We observed that the material temperature has an influence on the friction force. The dissipation of friction into heat is thus expected to change the friction force. In this section, we propose to give an order of magnitude of the influence of friction dissipation on the friction force.

Energy created by friction An expression of the energy dissipated by friction, E, is given by:

$$E_f = \int F_f \mathrm{d}x \tag{10.7}$$

Where E_f and x represent the mechanical energy dissipated by friction and the relative displacement of the surfaces in contact, respectively. We make the hypothesis

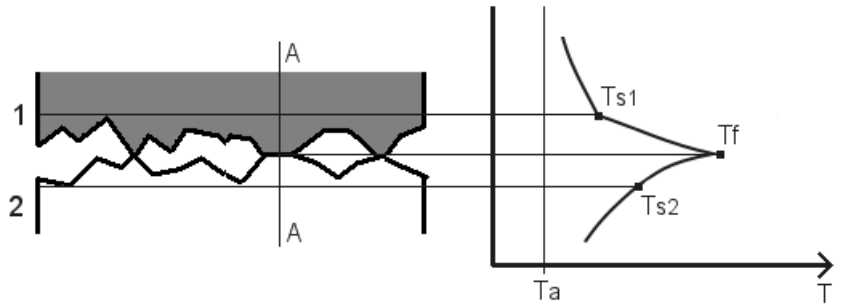

Figure 10.15: Temperature profile of the surfaces in contact. Adapted from [95]. T_a and T_f represent the average temperature of both materials and the flash temperature (temperature at the contact point), respectively.

that all this energy is dissipated into heat. The materials being similar, we consider this dissipation as symmetric. The thermal energy dissipated in each material during a sliding, E_{th}, is thus given by:

$$E_{th} = \frac{1}{2} \int F_f \mathrm{d}x \tag{10.8}$$

Assuming that the force of kinetic friction is constant during a sliding, we obtain for the mobile sample:

$$E_{th} = \frac{1}{2} \int_0^D \mu_K mg \mathrm{d}x = \frac{\mu_K mgD}{2} \tag{10.9}$$

Where x, D, μ_K, m, and g represent the displacement, the total sliding distance, the coefficient of kinetic friction, the sled mass, and the standard gravity, respectively. In our standard experiments, we have $D = 10$ cm, $\mu_K = 0.6$, $m = 0.857$ g, and g $= 9.81$ m.s^{-2}, leading to a thermal energy of $E_{th} = 0.25$ J.

Thermal power This energy is dissipated in a time $T = \frac{D}{v}$, where v is the mean sled velocity. The friction force being constant, the thermal power created by friction, P_{th}, is given by:

$$P_{th} = \frac{\mu_K mgD}{2} \frac{v}{D} = \frac{\mu_K mgv}{2} \tag{10.10}$$

In our experiment, the mean velocity is equal to $v = 5\ 10^{-3}$ m.s^{-1}. We calculated a thermal power $P_{th} = 1.26\ 10^{-2}$ W.

Local flux density The thermal power is created on the real area of contact A_r. Consequently, the local heat flux density, ϕ, is given by:

$$\phi = \frac{P_{th}}{A_r} = \frac{\mu_K mgv}{2A_r} \tag{10.11}$$

The apparent contact area is considered as $A_a = 3.6\ 10^{-3}$ m^2. In the chapter 2.4, the literature suggested that the real contact area is comprised between 1 % and 0.1 % of the apparent contact area for the studied pressure. We thus obtain a real contact area comprised between $3.6\ 10^{-5}$ m^2 and $3.6\ 10^{-4}$ m^2. Our experiment thus produces a local flux density comprised between 350 W.m^{-2} and 3.5 kW.m^{-2}.

Flash temperature We make the hypothesis that the paper is constituted by 100 % of cellulose. We consider the following thermodynamic properties of cellulose: a thermal conductivity $\lambda = 0.23$ W.(m.K)$^{-1}$, a massic heat capacity $C_p = 1549$ J.(kg.K)$^{-1}$ and a density $\rho = 1500$ kg.m^{-3} Considering the local flux density produced by friction, an expression of the flash temperature is [95]:

$$T_f = T_0 + \frac{2.\sqrt{t}}{\sqrt{\pi\lambda\rho C_p}}\phi \tag{10.12}$$

With T_f, T_0, t, λ, ρ, and C_p representing the flash temperature, initial temperature, time of contact, thermal conductivity coefficient, the density of the material, and its massic heat capacity, respectively.
The numerical application gives a flash temperature comprised between $T_f = 26$°C and 48°C for $T_0 = 24$°C.

Influence of friction dissipation on friction force We observed in the previous section that an increase in temperature leads to a decrease in force of kinetic friction. Based on the calculated flash temperature, we represented the expected decrease in friction force with sliding time on Figure 10.16. At the end of the first sliding, the decrease in friction force is comprised between 0.7 and 7 %.

Discussion We observed that the heat dissipation with sliding induces a decrease in friction force up to 7 %. This result strongly depends on the real area of contact that is itself difficult to measure. However, this decrease may partly explain the 15 % decrease observed during standard experiments. In conclusion, further investigations on the role of friction dissipation on the friction force are required.
Further studies should be carried out:

- The real area of contact should be measured more precisely.
- The model of paper surface was simplified and should be improved. For example, the model does not consider the cooling of the mobile sample in contact with fresh parts of the plane sample. Similarly, we considered the material as pure cellulose.
- The paper material has a much lower stiffness than metals. Deformations of the web structure may thus appear inside the paper material. Consequently,

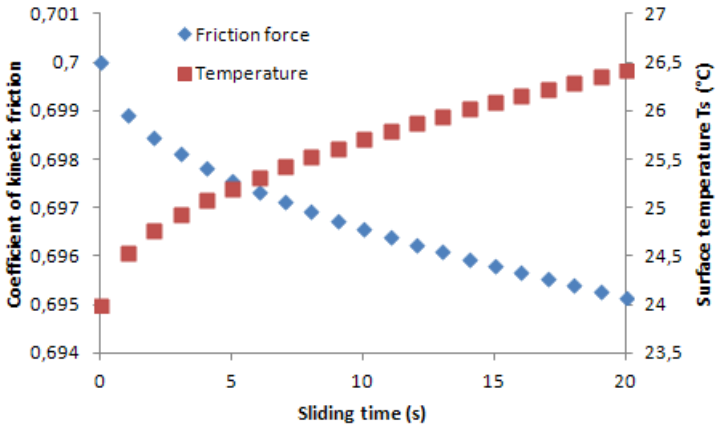

(a) High real contact area ($A_r/A_a = 1$ %)

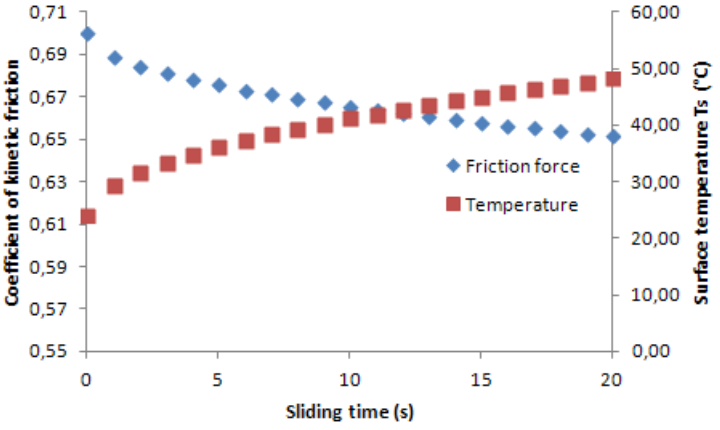

(b) Low real contact area ($A_r/A_a = 0.1$ %)

Figure 10.16: Models of decrease in friction force due to temperature increase, itself due to friction dissipation. We considered a velocity $v = 5\ 10^{-3}$ m.s^{-1}.

the frictional forces may be absorbed inside the material and this phenomenon should be taken into account [96].

- To clarify the observed phenomenon, an experimental measurement of the temperature of the asperities should be carried out. This measurement is however complex.

Summary and Conclusion of Chapter 10

Static electricity We observed no influence of the tribocharging on the friction force between two similar papers. The tribocharging produced by the separation of envelopes is thus expected to have a negligible influence on the friction between envelopes. However, the contact with other materials can create strong tribocharging effects, but this study is beyond the frame of this chapter.

Relative humidity At 24°C, the coefficient of static friction increases with relative humidity (+25 % from 25 to 67 % RH), even after repeated slidings. On the other hand, relative humidity has a negligible influence on the coefficient of kinetic friction, especially after repeated slidings. We suggested that the moisture creates water bridges between the surfaces in contact. Those water bridges contribute to the break-away force. They break as the sliding starts, so that humidity has no influence on the kinetic friction.

Temperature During the first sliding, the temperature has a low influence on the coefficient of friction between papers. After the first sliding however, the coefficient of kinetic friction decreases linearly with the temperature (about -0.3 %/°C). The coefficient of static friction sharply decreases (-1.4 %/°C) until reaching the coefficient of kinetic friction at about 40°C. Humidity modifies this critical temperature, but does not modify the rate of the static friction decrease. For higher temperatures, the coefficients of static and kinetic friction are equivalent. The stick-slip oscillations thus disappear. We showed that the influence of temperature on friction is a reversible phenomenon. We suggested that temperature modifies the creation of water bridges between papers. We also showed that the temperature induced by friction dissipation can modify the friction force itself (up to -7 %).

Conclusion and perspectives The friction between paper materials seems to be severely influenced by environmental factors. A deeper study on the influence of those factors on friction may permit (i) a better understanding of the kinetic and static friction mechanisms, (ii) a better control of stick-slip phenomena, (iii) the control of the coefficients of friction, and (iv) the control of machine design as a function of environmental conditions. In particular, further works should study the tribocharging effects between papers and the influence of static electricity on paper-on-paper contact. Further works should also extend the study to temperatures below 24°C and/or different gasses to highlight and study the mechanisms involved.
The previous chapters studied the structural, protocolar, and environmental factors of the paper-on-paper friction. In the next chapter, we now study the envelope-on-envelope, pads-on-envelope, and rollers-on-envelopes contacts.

Chapter 11

Friction between paper and other materials

The optimization of franking machine feeders requires a deep understanding of the paper friction. We previously studied the paper-on-paper friction. However, the franking machine feeders involve envelope-on-envelope, pads-on-paper, and rollers-on-paper contacts, as represented on Figure 11.1. The friction properties of those contacts are however poorly documented. For example, we found no information concerning the envelope-on-envelope or pads-on-envelope frictions. Thus, we propose to study the main frictional properties of the contacts previously listed.

11.1 Envelope-on-envelope

11.1.1 Materials and methods

Envelopes An envelope structure is represented on Figure 11.2. Envelopes are made of a single sheet of paper. Consequently, the external surfaces of the front and back flap of an envelope are made of same paper side. The back flap is usually glued over the slide flaps. A window may also be glued inside the envelope, made of plastic or transparent paper. Finally, glue permits the sealing of the envelope. The glue being mainly composed of water, the humidity of the flap becomes high during the sealing, and the paper material may wrinkle. The envelope is usually fed with one to three paper sheets. All those elements together make the envelope's thickness evolves along its length, as represented on Figure 11.3. For this study, we considered a range of widely used envelopes from different countries worldwide (Columbia #10, C4 US 30394, C4 FR 12957, Printmaster 03975, Printmaster 450973, Printmaster 3957, Printmaster 27561, Curtis 1000 524-11, and CO375 envelopes).

Envelope-on-envelope contact Franking machines always involve contacts between the front and back of envelopes. As previously explained, the same sides of the

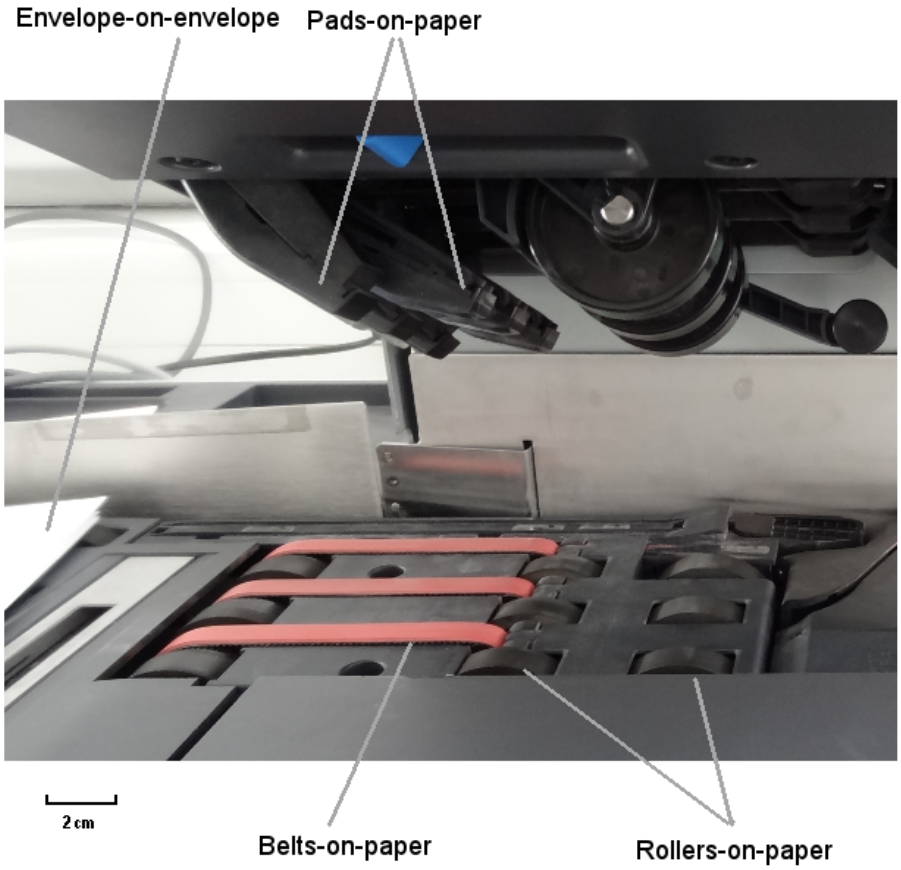

Figure 11.1: The different contacts underwent by envelopes in a feeder. The belt-on-paper contact can be assimilated to the rollers-on-paper contact.

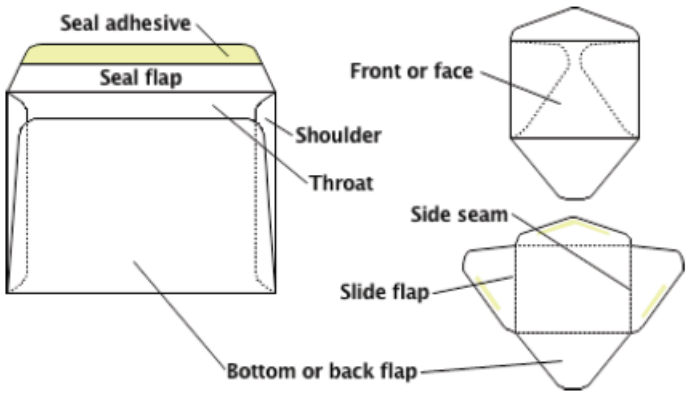

Figure 11.2: An example of envelope's structure

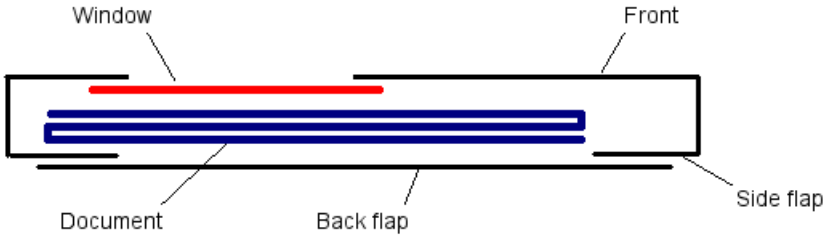

Figure 11.3: Cross section of an envelope fed with one sheet of paper. The seal flap and the seal adhesive are not represented.

paper materials are therefore in contact. In our friction experiments, we therefore ensured that the same paper sides are in contact. The inkjet printhead being placed above the paper path, the envelopes are always placed with the front face oriented topward. The contact usually occurs on the whole envelope surface.

Paper materials In a first experiment, we characterized the paper materials used in the studied range of envelopes. We cut them to obtain paper samples made of a single layer. We then determined their mechanical anisotropy by comparing their stiffness in both main directions. We also measured their coefficients of static and kinetic friction using the horizontal plane test method. We chose this test method to permit the comparison of our results to those that may be obtained in the future and/or in other labs. For each envelope, we made 7 measurements.

Envelope properties In a second experiment, we used the standard horizontal plane test method to measure the coefficients of friction of the envelope-on-envelope contact. We thus used the sled introduced in chapter 6.1 and made 10 measurements for each envelope. We studied the range of envelopes previously introduced, but also equivalent envelopes with/without window. We thus could study the influence of the windows on the friction force between envelopes. To finish with, we studied the influence of the sealing.

11.1.2 Results and discussion

Fibrous orientation Contrarily to paper sheets used in our everyday life, we observed that the mechanical anisotropy varies from an envelope type to the other. For example, a higher stiffness is observed in the side direction of CO125 or 50012 envelopes. This result suggests that fibers are mainly oriented in this direction. On the other hand, a lower stiffness is observed in the side direction for 30394 or 13997 envelopes. This result suggests that fibers are mainly oriented in the opening direction. The other envelopes present a mechanical isotropy, as for example either CO175 or 26316 envelopes.

Paper material Measurements of the coefficients of static and kinetic friction between envelopes are represented on Table 11.1.

	$\mu_{S,1}$ (c.v.)	$\mu_{S,3}$ (c.v.)	$\mu_{K,1}$ (c.v.)	$\mu_{K,3}$ (c.v.)
Columbia #10	0.69 (1.7 %)	0.66 (3.0 %)	0.58 (1.9 %)	0.55 (1.6 %)
C4 US 30394	0.66 (2.3 %)	0.65 (2.4 %)	0.55 (2.2 %)	0.52 (0.9 %)
C4 FR 12957	0.54 (4.2 %)	0.50 (3.3 %)	0.43 (8.4 %)	0.40 (5.6 %)
Printmaster 03975	0.59 (4.5 %)	0.55 (6.5 %)	0.47 (5.3 %)	0.43 (3.3 %)
Printmaster 450973	0.68 (2.9 %)	0.66 (4.7 %)	0.57 (2.6 %)	0.54 (2.1 %)
Printmaster 3957	0.64 (1.8 %)	0.60 (1.6 %)	0.53 (1.6 %)	0.47 (1.6 %)
Printmaster 27561	0.58 (2.2 %)	0.49 (3.2 %)	0.47 (2.7 %)	0.40 (2.8 %)
Curtis 1000 524-11	0.63 (4.0 %)	0.58 (2.6 %)	0.50 (2.5 %)	0.46 (1.3 %)
CO375	0.56 (3.9 %)	0.51 (5.0 %)	0.47 (1.4 %)	0.42 (0.9 %)
Average	0.61	0.57	0.50	0.45
Std. Dev.	0.06	0.07	0.06	0.06

Table 11.1: Coefficients of static and kinetic friction of the paper-on-paper contact for the studied range of envelopes. The values in brackets represent the coefficient of variation (c.v.) of the measurements.

The measurements are close from those measured on the printing and writing paper. Table 11.1 shows that a mix-mail stack would have a dispersion in coefficients of friction of approximately 10 %. The three first envelopes of Table 11.1 are often referred to as the most problematic envelopes for the selection process. Interestingly, we observe that their coefficients of static and kinetic friction correspond to extrema[1]. Very high or very low coefficients of friction may thus create feeding defects.

Design We observed a negligible difference (<5 %) between the coefficients of friction of envelopes, and the ones of their paper material alone. This result suggests that the design of the envelopes had no effect on the friction between envelopes. The result validates our method consisting in studying the paper-on-paper friction rather than the envelope-on-envelope one.
However, some envelopes have specific designs. For example, we studied the case of an irish envelope, called *Autofast*, which side flaps were glued above the back flap. This structure creates asperities that interact with the window on the envelope face. In practice, those envelopes appeared to be highly problematic on franking machine feeders (up to 3 % of failures observed, compared to the 0.1 to 0.5 % usually observed). We thus consider that the envelope-on-envelope friction is equivalent to the paper-on-paper one, out of some particular cases.

[1]The Printmaster 450973 envelope has also very high coefficients of friction, but this envelope is rarely used in franking machine tests.

Envelopes windows Envelopes windows have no influence on the coefficients of static and kinetic friction. We suggest this result to be due the low normal load between the windows and the other envelopes. Indeed, the window is glued inside the envelope.

Sealing liquid Based on the industrial experience, we expected the sealing liquid to increase the friction force between envelopes. This phenomenon would be due to (i) the increase in humidity, and (ii) the wrinkling observed on the flap. However, we measured no influence of the sealing on the envelope-on-envelope friction. A possible reason for this difference is that we sealed the envelopes long time before the experience (>3 days). Consequently, their humidity was reduced to 50 %. The selection process may occur few minutes after the envelope was sealed by an inserter. Employees consider however that humidity is not responsible for this defect, as the problem occurs even when the envelopes were sealed days before. We thus suspect the wrinkling of envelopes to have a strong influence on the friction force in some specific situations we were unable to experiment here. As those problems remain anecdotic, we will not pursue this study.

11.1.3 Conclusion on the envelope-on-envelope friction

The design and structure of envelopes therefore have no clear influence on the coefficient of friction of the envelope-on-envelope contact. Studying the friction between printing and writing papers is thus valid. We observed that the most problematic envelopes have extreme coefficients of friction (lower or higher). In the case of mix-mail stacks, this result suggests that the variability in coefficients of friction is a major factor for the feeding failures. This hypothesis will be studied in more detail in Part III.

11.2 Pads-on-paper

11.2.1 Materials and methods

Samples For clarity reasons, we studied the contact of pads on a printing and writing paper. The paper we used was the same than in previous chapters (basis weight 80 g.m^{-2}). The pads had already undergo hundreds of slidings in a franking machine feeder. Pads and paper samples were stored at 24°C / 50 % RH.

Method We used the sled presented in chapter 6.2 and the horizontal plane test method. In a first experiment, we measured the influence of 5 repeated slidings in the same/reversed directions on the pads-on-paper friction. We then studied the influence of temperature (from 24°C to 46°C), humidity (25 %, 50 %, and 67 % RH), and static electricity discharging on the coefficients of friction. The methods used to

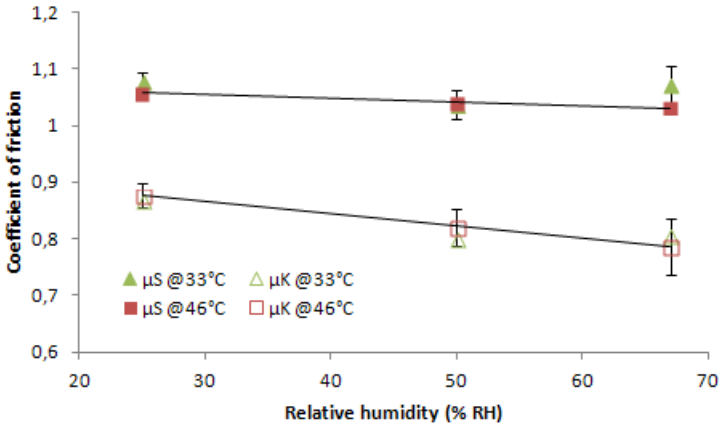

Figure 11.4: Influence of the relative humidity and temperature on the coefficients of static and kinetic friction of the pads-on-paper contact. For clarity reasons, the 24°C measurement is not represented.

modify those parameters are the same as those used in chapter 10. To finish with, we studied the influence of varying normal forces (from 8 N to 18 N) and varying sled velocities (from 0.5 mm.s^{-1} to 5 mm.s^{-1}). We made 10 measurements for each experiment.

11.2.2 Results and discussion

Coefficients of static and kinetic friction We measured the coefficients of static and kinetic friction of the pads-on-paper contact equal to 1.04 and 0.80, respectively. The standard deviation was 6 and 7 %, respectively.

Temperature and humidity The influence of temperature on the pads-on-paper friction is represented on Figure 11.4. We observe that the plate temperature had a negligible influence on the coefficients of friction of the pads-on-paper contact (approx. -1 % from 24°C to 46°C). On the other hand, an increase in relative humidity (from 25 to 67 % RH) decreased the coefficient of kinetic friction (-10 %) but did not change the coefficient of static friction, as represented on Figure 11.4. A possible mechanism for this decrease is the water condensation creating a lubricant layer that reduces friction. The behavior is however opposed to the one observed for the paper-on-paper contact. Consequently, high relative humidities are expected to create more multiple feedings in the selection process of franking machines. We suppose that surface chemistry, texture, and structure explain this difference in influence of relative humidities on friction forces.

Repeated slidings, static electricity, normal load and velocity We measured no influence on friction forces of (i) repeated slidings in the same/reversed directions, (ii) static electricity discharging, (iii) normal load (from 8 N to 18 N), and (iv) sled velocities (from 0.5 $mm.s^{-1}$ to 5 $mm.s^{-1}$). The absence of influence of repeated slidings on the friction force confirms that the decrease with repeated slidings is specific to the paper-on-paper contact [44]. For the sled velocity, we may criticize that the studied velocities are far from velocity observed in franking machines (1.2 $m.s^{-1}$). A complementary study should thus be carried out.

11.2.3 Conclusion on the pads-on-paper friction

We observed that the friction pads have coefficients of static and kinetic friction roughly equal to 1.0 and 0.8, respectively. These coefficients are higher than the envelope-on-envelope ones. This situation is particularly interesting when considering the envelopes selection in franking machines feeders. These coefficients are reduced for high humidities. On the other hand, we observed no influence on friction force of temperature, repeated slidings, static electricity, normal load, and sled velocities. Compared to the paper-on-paper contact, the pads-on-paper contact thus appears much less sensitive. To control the pads-on-paper friction, one may therefore ensure that the relative humidity is measured and/or controlled.

11.3 Rollers-on-paper

11.3.1 Literature

Sliping between rollers and paper The driving rollers of franking machine feeders move the envelopes at roughly 1.2 $m.s^{-1}$. We may suggest at first glance that the rollers stick on envelopes. However, small slippings occur between rollers and envelopes. The difference between the envelopes and rollers velocities is rouhgly 0.5 % at low speeds and 1 % when rollers rotate at 1 $m.s^{-1}$ [85]. Consequently, the low speed test method for measuring the rollers-on-paper friction (5 $mm.s^{-1}$) is adapted to measure the coefficient of friction of rollers "sticking" on envelopes at 1.2 $m.s^{-1}$. The high speed test method is adapted to the measurement of the rollers-on-paper friction when rollers clearly slide on envelopes, with a relative speed of 1.2 $m.s^{-1}$.

Normal load The rollers-on-paper contact was mainly studied in the frame of printers. The coefficient of kinetic friction of the rollers-on-paper contact is usually considered higher than the paper-on-paper one. However, it was shown that the coefficient of kinetic friction for rollers-on-paper decreases with normal load [97], as represented on Figure 11.5. A model for this decrease is given by:

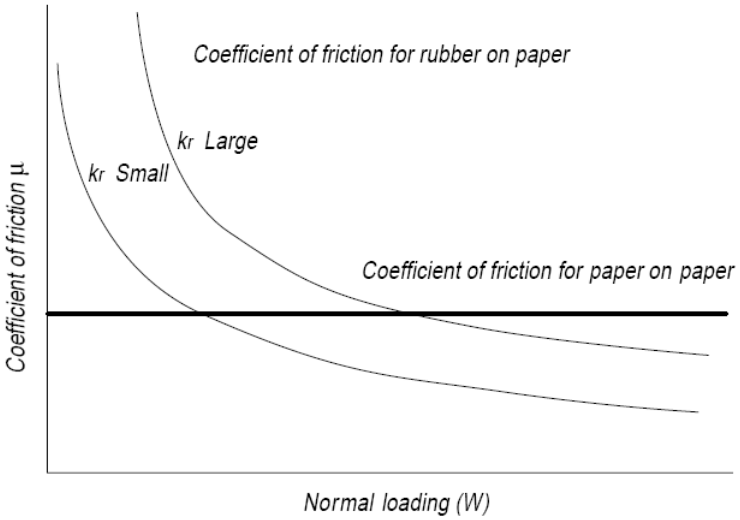

Figure 11.5: Comparison between the evolution of the paper-on-paper friction coefficient and the rubber-on-paper one. The influence of the k_R parameter on coefficient of friction is also represented. Adapted from [97]

$$\mu_R = k_R \left(\frac{W}{W_0} \right)^{-1/3} \tag{11.1}$$

With μ_R, k_R, W, and W_0 representing the coefficient of kinetic friction of the rollers-on-paper contact, a parameter of the model characterizing the rubber of the rollers, the normal load, and the reference normal load, respectively. This trend is supposed to be due to the viscoelastic nature of rubbers that makes the real contact area evolve with a non-linear trend with the normal load [97].

Temperature and speed The friction between rollers and non-paper materials has also been studied, in particular the contact between tires and roads. The most interesting observation is that the rubber friction strongly depends on temperature and speed. The influences of temperature and speed are equivalent. This equivalence is described by a transformation equation first proposed by Williams, Landel, and Ferry and called WLF [98] [99], as represented on Figure 11.6. The equivalence between temperature and speed comes from the viscoelasticity of the material. Indeed, at high temperatures, molecules are excited: their free volume and the chain movements reduce the modulus of the material. In contrast, the higher the speed is, the higher the excitation frequency is and the less the chains have time to respond to the applied load, increasing the modulus. The master curve represented on Figure 11.6 thus summarizes the temperature and speed influences on friction for a given specific contact. This curve strongly depends on the considered materials, but we did not find the curve associated to the rubber-on-paper contact.

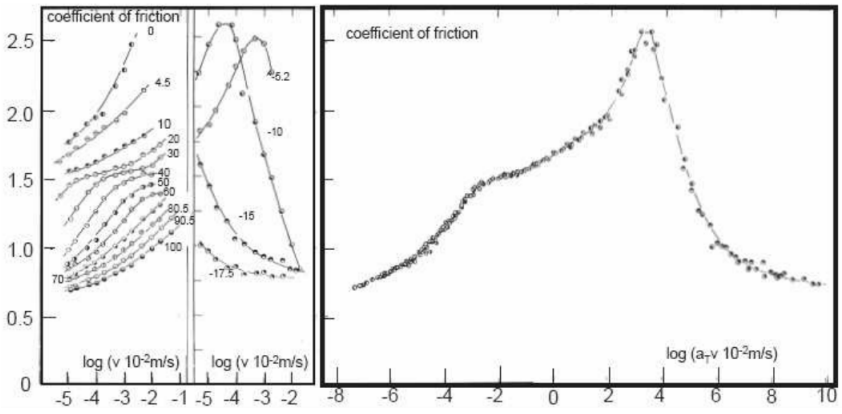

Figure 11.6: Evolution of the friction force between gum and silicon as a function of speed for different temperatures (left) and associated master curve (right) [99]. The master curve is created by translating the curves representing the coefficient of friction vs. speed for different temperatures (left). This translation is permitted by the equivalence between temperature and speed (WLF theory).

11.3.2 Materials and methods

Samples We used the same printing and writing paper (basis weight 80 g.m^{-2}) than in the previous chapters. We used rollers from Neopost Omega franking machines. The rollers also underwent hundreds of feedings. The papers and rollers were stored in a 24°C and 50 % RH room during more than 24h00.

Low-speed measurement method We used the sled presented in chapter 6.3 and the horizontal plane test method. We set the sled velocity to 5 mm.s^{-1} and made 10 measurements for each experiments. This method characterizes the friction force between rollers and envelopes in the case of reduced slippings (e.g. when driving rollers seem to "stick" on envelopes while moving at 1.2 m.s^{-1}). In a first experiment, we measured the influence of 5 successive slidings in the same/reversed directions on the rollers-on-paper friction. In a second experiment, we studied the influence of temperature (from 24°C to 46°C), humidity (25 %, 50 %, and 67 % RH), and static electricity discharging on the coefficients of friction. The methods used to modify those parameters are the same as those used in chapter 10. Finally, we studied the influence of varying normal loads (from 8 N to 18 N). We did not study the influence of low velocities on the rollers-on-paper friction force as such constraints are not met in franking machines. Indeed, either the rollers stick on the envelopes, either they slide at high speeds (up to 1.5 m.s^{-1}).

High-speed measurement method We used the high-speed measurement method presented in chapter 6.3. Indeed, this method permits the study of (i) the influence

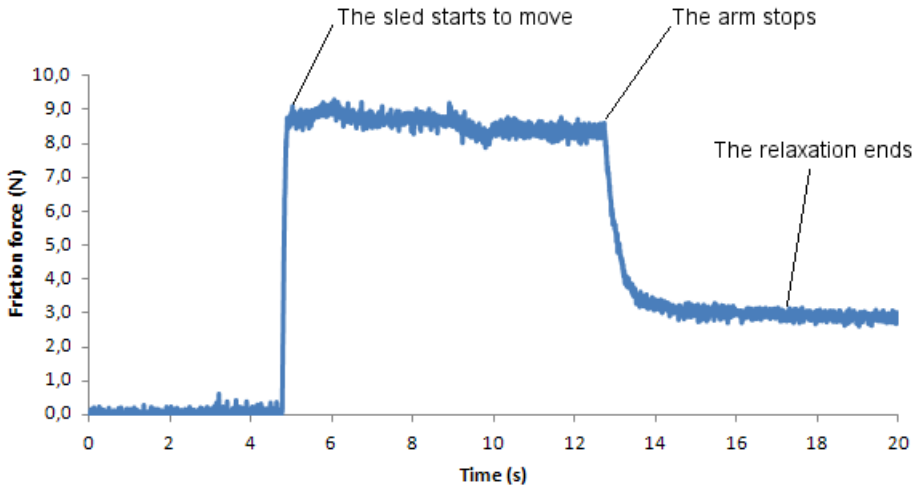

Figure 11.7: Typical measurements observed during the rollers-on-paper experiments using the horizontal plan test method

of high velocities on the rollers-on-paper friction, and (ii) lower normal loads than in methods involving weighted sleds. We thus proposed the measurement of the coefficient of kinetic friction for normal loads from 100 g to 2.5 kg and for speeds of 1.5 m.s^{-1}. We glued the printing and writing paper on the bottom of the bottommost envelope. The paper material was in contact with 6 rollers. For a given sled/stack weight, the pressure underwent by each roller is thus twice lower than in the low-speed method.

11.3.3 Results and discussion

Static and kinetic friction forces During the low-speed experiment (800 g, 24°C, 50 % RH), we observed no peak in friction force at the begining of the sliding, as represented on Figure 11.7. This result suggests that the static friction is not observed. We also observed that after the arm stopped, the sled pursued its sliding: the pulling force decreased with an exponential shape. We suppose this phenomenon to reflect the viscous nature of rollers-on-paper friction [100]. In this situation, the friction force increases with speed. The relaxation observed at the end of the sliding would thus be due to the simultaneous decrease in velocity and friction force. Similarly, the initial peak in friction force would be masked by the viscous component of the friction force after the sliding got established.
Those results suggest that the coefficient of static friction of the rollers-on-paper contact was not observed. However, the studied velocity is similar to the relative velocity of the small slippings occuring between rollers and envelopes when the envelopes move at 1.2 m.s^{-1} (when the rollers seem to "stick" on the envelopes).

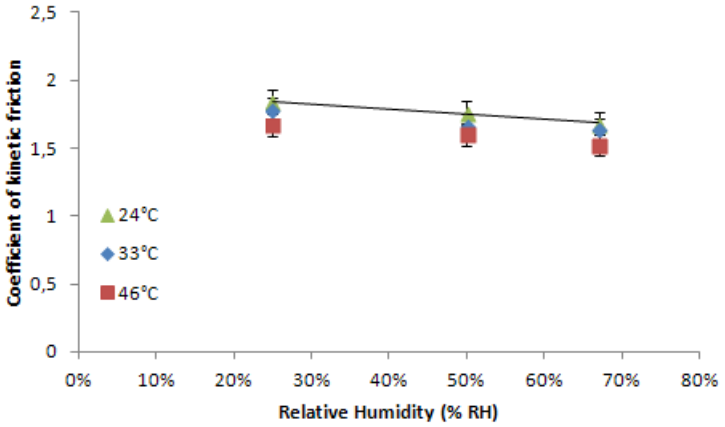

Figure 11.8: Evolution of the coefficient of kinetic friction between rollers and paper for varying relative humidities and temperatures

Thus, we can assimilate the friction force measured to the break-away force of the rollers-on-paper contact.

Temperature and humidity The evolution of the coefficient of kinetic friction for the rollers-on-paper contact and for varying relative humidities and temperatures is represented on Figure 11.8. We observe a slight decrease in friction force with relative humidity (-8 % from 25 to 67 %), similarly to the pads-on-paper contact, suggesting that humidity acts as a lubricant. Moreover, we observe that higher temperatures led to lower coefficients of kinetic friction (-8 % from 24°C to 46°C), confirming the WLF theory [98] [99]. We recommend this study to be extended to a wider range of temperatures in order to draw a more general conclusion.

Normal force We observed a decrease of the coefficient of friction with the normal force, as represented on Figure 11.9. Considering high speed measurements, the coefficient of friction is very high for low normal stresses (up to 4.0) and low for high normal stresses (1.5 for approx. 10 N). Considering low speed measurements, the normal load varied from 1.7 to 8.2 N. We observed a decrease of approximately -14 % of the coefficient of kinetic friction. This result, opposed to the Coulomb law of friction, confirms the results of the literature [97, 98, 100]. We consider this non-linear behavior of the friction force with normal stress to be due to the viscoelastic nature of rollers. The first consequence is that the material is highly deformed when the contact reaches its break-away force. The second consequence of the viscoelasticity is that the real contact area is no more proportional to the normal stress. Consequently, low normal loads still create high real contact areas, and thus increase the coefficients of friction.

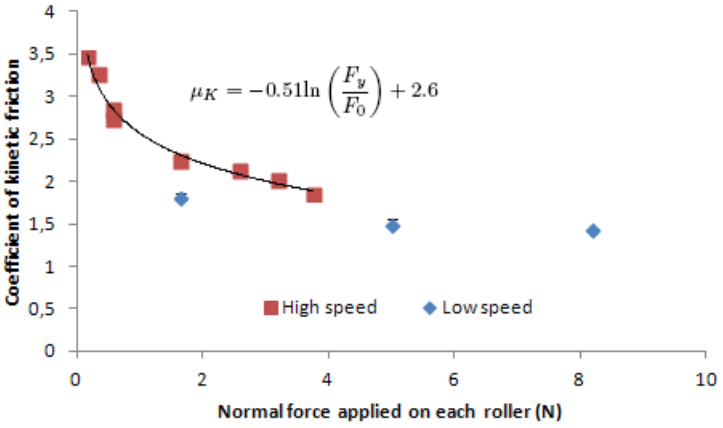

Figure 11.9: Coefficient of friction of the rollers-on-paper contact vs. normal load. The low-speed (5 mm.s^{-1}) and high-speed (1 m.s^{-1}) measurements are represented. The logarithmic fit curve is also represented along with its equation. In this equation, μ_K, F_y, and F_0 represent the coefficient of kinetic friction, the normal force applied on each roller, and normal force taken as reference, respectively.

Sliding velocity The low-speed and high-speed measurements had a good repeatability (standard deviation of 3 %). The coefficient of friction was higher for high-speed measurements than for low-speed ones (+25 %, from 2.0 to 2.5), as observed on Figure 11.9. As a reminder, we assimilated the coefficient of friction of low-speed measurements to the coefficient of static friction. The difference may be explained either by the influence of speed on rollers-on-paper friction, either by the modification of the sample surface. Indeed, the high-speed method involves slidings on few meters while the low-speed method involves slidings on few centimeters only. Consequently, the high-speed measurements lead to (i) a glossier aspect of the paper material, (ii) black marks of rubber gum, and (iii) an increase in surface temperature[2]. This method thus causes a low accuracy on the measurement of the rollers-on-paper friction force.

Repeated slidings and static electricity We observed no influence of repeated slidings in same/reversed directions on the friction force. This result confirms that the evolution of the friction force with repeated slidings is specific to the paper-on-paper contact [44]. We also observed no influence of static electricity discharging on the rollers-on-paper friction force.

[2]The increase in temperature can be easily felt when touching the paper. However, it is very complex to measure, as it is a surface property and not a mass property.

11.3.4 Conclusion on the rollers-on-paper friction

The static friction was not observed, a phenomenon possibly due to the viscoelasticity of the material. However, it is approached by the measurement at low speed and appears lower (-20 %) than the coefficient of kinetic friction at 1.2 $m.s^{-1}$. We moreover observed a high dependency of the coefficient of friction with the normal load (from approx. 4.0 to 1.3). Considering that the misfeeds usually occur for small envelope stacks (below 100 g), coefficients of static and kinetic friction of 2.0 and 2.5 for the rollers-on-paper contact can be considered. The rollers-on-paper contact has a higher coefficient of friction than the pads-on-paper contact (approx. 1.0). Finally, we observe that high temperatures and low humidities slightly increase the rollers-on-paper coefficient of friction. Further works are however required to confirm this result.

Summary and Conclusion of Chapter 11

Frictions involved in feeders In the previous chapter we studied the paper-on-paper contact. However, franking machine feeders involve envelope-on-envelope, pads-on-envelope, and rollers-on-envelope contacts. We thus studied the friction of those contacts. The main results are summarized on Table 11.2:

Contact	μ_S	μ_K	Normal load	Humidity	T°	Velocity
Envelope-on-envelope	0.6	0.5	0	+	-	0
Pads-on-paper	1.0	0.8	0	-	-	0
Rollers-on-paper	2.0	2.5	-	-	-	+

Table 11.2: Coefficients of static and kinetic friction of the main contacts involved in franking machine feeders. The influence of the increase in several factors on those coefficients is also represented. (+), (-), and (0) stand for an increase, a decrease, and no influence on coefficients of friction, respectively.

Some particular cases The friction between envelopes can be assimilated to the friction between the paper material they are made of. Extreme values of coefficients of friction between envelopes are often associated to multiple feedings and/or misfeeds in franking machine feeders. For mix-mail stacks, we thus suggest that the variability in coefficients of friction is a major factor of the feeding failures.
Due to the viscoelasticity of rollers, the rollers-on-paper coefficient of static friction was not observed. However, the coefficient of static friction can be approximated and is lower than the coefficient of kinetic friction at 1.2 $m.s^{-1}$. We observed a sharp decrease in coefficient of kinetic friction with normal load: for low load, it was measured up to 4.0.

Conclusion As expected, the coefficient of friction of the envelope-on-envelope contact is lower than the pads-on-paper one, itself lower than the rollers-on-paper one. This result was intuitively suggested as a condition for the feeding of envelopes in franking machine feeders. However, this relation may evolve with protocolar and environmental parameters, such as relative humidity, stack weight, or mix-mail diversity for example.

Perspectives This study may have several technological applications in the future, by allowing (i) the adaptation of the machine design to the protocolar and environmental factors and (ii) the control of the coefficients of friction of the contacts with paper. This study also gave some data associated to the friction forces involved in franking machine feeders. Those data permit the development of a model of the franking machine feeders. This model will allow the improvement of the reliability of the machine feeders: it is the goal of the last part of this study.

Part IV

Improving feeders

Forewords

We want to improve the selection process of franking machine feeders. The process consists in displacing the bottommost envelope of an envelope stack without displacing the other envelopes, as represented on Figures 11.10a and 11.10b. The main challenge is to avoid the selection failures that were introduced in chapter 1.5. In particular, *multiple feedings* and *misfeeds* that are represented on Figures 11.10c and 11.10d, respectively. This problem is particularly difficult, as the dynamics of an envelope in the stack is strongly linked to (i) the dynamics of all the other envelopes, and (ii) their mutual interactions. To address this problem, we model the dynamics of each envelope stack in the franking machine feeder to characterize the conditions avoiding the selection failures. This model is developed in 4 chapters:

- **Chapter 12:** we propose the formalisms associated to the model.
- **Chapter 13:** we detail the balance of forces applied on an envelope in an envelope stack and express the friction force applied between two envelopes.
- **Chapter 14:** we use the balance of forces to describe the dynamics of an envelope in a stack and compare it to the experience.
- **Chapter 15:** we conclude on the conditions avoiding the selection failures and study the case of selection mechanisms based on friction pads.

We integrate in the model the knowledge acquired in the previous parts, in particular the orders of magnitude of the coefficients of friction.

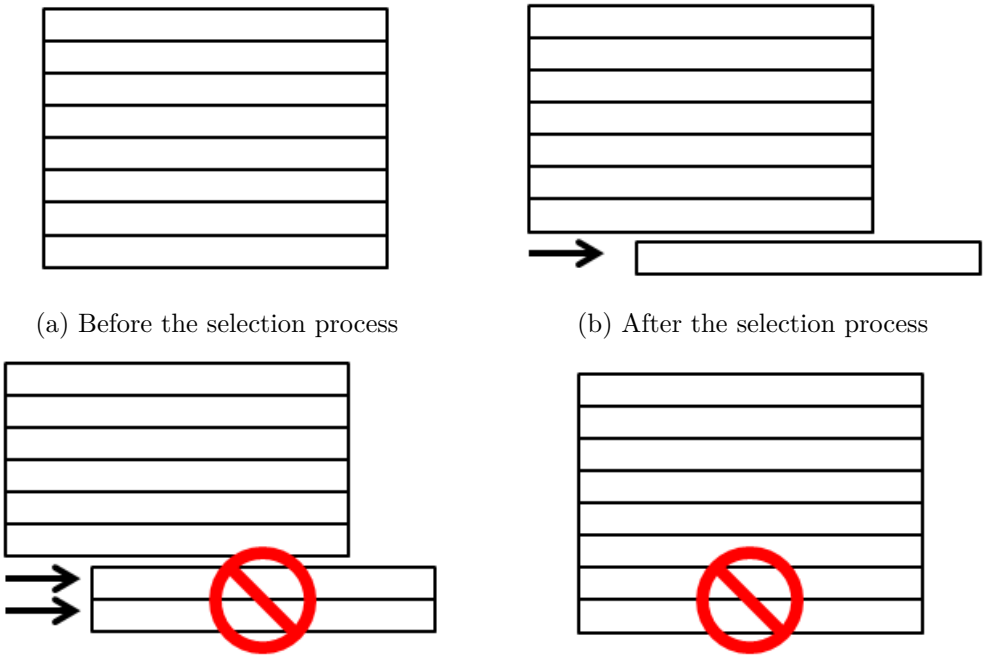

(a) Before the selection process

(b) After the selection process

(c) Failure: multiple feeding

(d) Failure: misfeed

Figure 11.10: Envelope stack before/after the selection process and in the case of a multiple feeding/misfeed (failures)

Chapter 12

Chosen formalism

The model of stack dynamics in a franking machine feeder has to be built on clear formalisms. In this chapter, we detail those formalisms and notations. In particular, we give a mathematical definition of a correct feeding, i.e. a selection process without any failure.

12.1 Referential

We use the referential represented on Figure 12.1:

- $\vec{x}$ is oriented in the driving direction of the envelope. The $x = 0$ value is defined at the nip of the extraction rollers, i.e. the exit of the feeder.
- $\vec{y}$ is oriented in the normal direction. The $y = 0$ value is defined at the top of feeder rollers.

The document stack usually lays horizontally on the feeder. However, in the following calculations, we will consider an angle α between the horizontal and the document stack as represented on Figure 12.1.

12.2 Several definitions

Envelopes We consider a stack of n envelopes noted E_i, with $i \in \{1..n\}$ numbered from bottom to top. An envelope E_i has a m_i mass, a L_i length, a $\vec{v}_i$ velocity and a resultant of forces noted $\vec{\Sigma}_i$. The tangential position of the front of the envelope E_i is noted x_i. Due to the low envelope thickness, the normal displacement of envelopes is considered as zero. The envelope velocity is thus assimilated to its tangential component: $\vec{v}_i = v_i.\vec{x}$. The envelopes are considered as rigid bodies: they do not undergo neither bending nor compressibility phenomena.

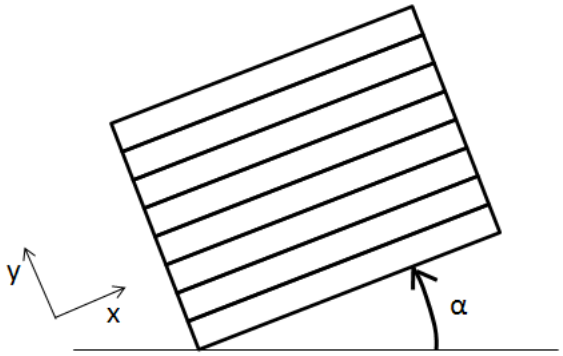

Figure 12.1: Angle, α, between the horizontal and the stack

Interfaces The *interface* between the envelopes E_i and E_{i+1} is noted I_i. We introduce Δ_i as $\Delta_i = \text{sign}(v_i - v_{i+1})$.

External systems Finally, different external systems are considered and numbered k. Such systems consist, for example, in the belts, rollers, pads or the vertical plate.

Blocks We propose to divide the stack into *blocks* defined as groups of envelopes in contact having the same speed. The acceleration of a block B is noted $\vec{a}_B$. Due to the envelope thickness, the normal acceleration of blocks is supposed to be negligible. We thus assimilate the block acceleration to its tangential component: $\vec{a}_B = a_B.\vec{x}$.

12.3 Objective of the study

The objective of this study is to find the main physical parameters permitting a *correct feeding*. We define a correct feeding as a process permitting a constant horizontal distance between the envelopes that went out of the feeder. The distance between two envelopes E_i and E_{i+1} is called *gap*. The distance between the fronts of the two envelopes, $(x_i - x_{i+1})$, is called *pitch* and equal to $(L_i + gap)$. *Gap* and *pitch* are represented on Figure 12.2. The condition for a good selection is thus formalized by equation 12.1:

$$x_{i+1} > L_{i+1} \Rightarrow x_i - x_{i+1} = L_i + gap \tag{12.1}$$

In the previous equation, the $(x_{i+1} > L_{i+1})$ condition ensures that the envelope E_{i+1} escapes from the feeder. The *pitch* is fixed by machine specifications and roughly equal to 30 cm for common envelopes. The feeder working by cycles (one envelope being ejected from the feeder during each cycle) the period of the cycles is noted

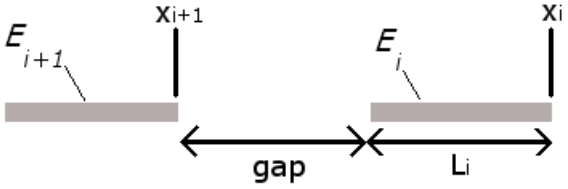

Figure 12.2: The distance, called *pitch*, between E_i and E_{i+1} is $L_i + gap$

$T(i)$ and equal to:

$$T(i) = \frac{gap + L_i}{v_m} \tag{12.2}$$

With v_m representing the velocity of the machine beyond the feeder, assumed to be constant. The envelopes having various lengths, the period is variable.

The following conditions guarantee a correct feeding:

1. **Feeding of the bottommost envelope (Condition 1) -** At the end of the cycle, the position of the bottommost envelope verifies:

   $$x_\zeta(t_f) = L_\zeta \tag{12.3}$$

   Where ζ and t_f represent the level of the bottommost envelope and the final time of the cycle ($t_f = t_0 + T(\zeta)$), respectively. This condition permits the design of the franking machine feeders' automation.

2. **Avoiding the displacement of upper blocks (Condition 2) -** During a cycle, envelopes above the first one (from 2 to n) must have a limited tangential displacement, preventing multiple feedings and stack destruction. In particular, to avoid multiple feedings, those envelopes have to remain in the feeder ($x_i < 0$). Similarly, we can introduce the maximal acceptable backward displacement, noted D_{min}. We thus obtain a condition on the possible tangential displacement of envelopes above the bottommost one:

   $$\forall i \in \{2..n\}, \forall t \in \{t_0..t_f\}, D_{min} \leq x_i(t) \leq 0 \tag{12.4}$$

   D_{min} being usually low ($0 > D_{min} > -1$ cm), equation 12.4 becomes:

   $$\forall i \in \{2..n\}, \forall t \in \{t_0..t_f\}, x_i(t) \approx x_i(t_0) \tag{12.5}$$

3. **Avoiding envelopes and rollers damages (Condition 3) -** No envelope nor roller have to be damaged during the process. In particular, we avoid (i) envelopes crushes, and (ii) surface damages. We thus have to ensure that the envelope surface never (i) exceed the critical crushing forces, and (ii) slip on rollers.

In the following chapters, we determine the parameters of the selection process that permit the fulfillment of those three conditions.

Summary and Conclusion of Chapter 12

Topology of a document stack A stack composed of envelopes can be divided into blocks. Blocks consist in groups of envelopes in contact together with the same speed. Consequently, the interfaces inside a block are characterized by static friction, while the interfaces between blocks are in kinetic friction.

Correct feeding The goal of this study is to determine the conditions permitting correct feedings. A correct feeding is defined as the feeding of a single envelope. On franking machine feeders, this envelope is the bottommost envelope of the stack. The conditions guaranteeing correct feedings are:

- **Feeding of the bottommost envelope (Condition 1) -** Guarantees that the bottommost envelope is displaced on a sufficient distance to permit its escape from the feeder.
- **Avoiding the displacement of upper blocks (Condition 2) -** Guarantees that only one envelope is fed at the same time in the feeder.
- **Avoiding envelopes and rollers damages (Condition 3) -** Guarantees that no envelope nor roller is damaged during the process. In particular, the envelopes must never undergo any crushing or slipping on rollers.

Chapter 13

Forces applied on envelopes

In the previous chapter, we gave the conditions to avoid failures in the feeder operation - a situation we called "correct feeding". The conditions 1 and 2 however suppose the calculation of the equation of the movement for each envelope. To permit this calculation, we need to formulate an expression of the balance of forces applied on every envelope in the stack. It is the purpose of this chapter.

13.1 The forces underwent by an envelope

Four different forces An envelope E_i undergoes four different forces represented on Figures 13.1a and 13.1b:

- **Weight:** The weight of the envelope, $\vec{W}_i$, defined by:

$$\vec{W}_i = -m_i g(\cos\alpha.\vec{y} + \sin\alpha.\vec{x}) \tag{13.1}$$

- **The interaction with E_{i-1}:** The envelope E_i undergoes a force $\vec{F}_{i-1}$ from the envelope E_{i-1} (if it exists):

$$\vec{F}_{i-1} = F_{i-1,x}.\vec{x} + F_{i-1,y}.\vec{y} \tag{13.2}$$

  The tangential component basically corresponds to a friction force.

- **The interaction with E_{i+1}:** E_i applies a force $\vec{F}_i$ on E_{i+1} (if it exists). E_i therefore undergoes a force $-\vec{F}_i$ defined similarly to equation 13.2:

$$-\vec{F}_i = -F_{i,x}.\vec{x} - F_{i,y}.\vec{y} \tag{13.3}$$

- **The forces applied by external systems:** Each external system (such as rollers, selection pads or vertical plates) applies a force on E_i. The external

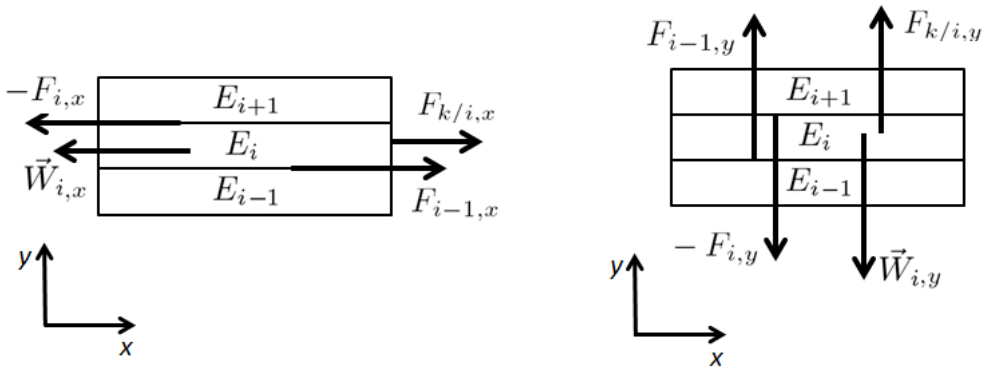

(a) Tangential components (b) Normal components

Figure 13.1: Tangential and normal components of the forces applied on the envelope at the level i, E_i. $\vec{W}_i$, $\vec{F}_{i-1}$, $\vec{F}_i$, and $\vec{F}_{k/i}$ represent the weight of E_i, the force applied by E_{i-1} on E_i, the force applied by E_i on E_{i+1}, and the force applied by the external system k on E_i, respectively.

system number k applies a force on the envelope E_i that is noted $\vec{F}_{k/i}$ and defined by:

$$\vec{F}_{k/i} = F_{k/i,x}.\vec{x} + F_{k/i,y}.\vec{y} \tag{13.4}$$

In particular, the vertical force applied by rollers on the bottommost envelope of a stack is one of the main components of those forces.

Balance of forces The balance of forces applied on E_i can thus be written:

$$\vec{\Sigma}_i = \Sigma_{i,x}.\vec{x} + \Sigma_{i,y}.\vec{y} = \sum_k \vec{F}_{k/i} + \vec{W}_i + \vec{F}_{i-1} - \vec{F}_i \tag{13.5}$$

With $\vec{\Sigma}_i$ representing the balance of forces applied on envelope E_i.

13.2 Normal components

In the previous section, we gave an expression of the balance of forces applied on the envelope E_i (see equation 13.5). In this section, we formulate complete expressions of the forces components in the normal direction. Indeed, we considered in chapter 12.2 the normal displacement and acceleration of envelopes as negligible. The fundamental principle of dynamics thus suggests that the balance of forces in the normal direction is also zero. From equation 13.5 applied in the normal direction,

we obtain:

$$\Sigma_{i,y} = \sum_k F_{k/i,y} - m_i g \cos\alpha + F_{i-1,y} - F_{i,y} = 0 \tag{13.6}$$

$$\Leftrightarrow \quad \sum_k F_{k/i+1,y} - m_{i+1} g \cos\alpha + F_{i,y} - F_{i+1,y} = 0 \tag{13.7}$$

$$\Leftrightarrow \quad F_{i,y} = F_{i+1,y} - \sum_k F_{k/i+1,y} + m_{i+1} g \cos\alpha \tag{13.8}$$

By reccurrence along the stack, equation 13.8 becomes:

$$F_{i,y} = \sum_{j=i+1}^{n} (m_j g \cos\alpha - \sum_k F_{k/j,y}) \tag{13.9}$$

The normal force applied by an envelope E_i on E_{i+1} is therefore equal to the sum above I_i of (i) the normal components of the envelopes weight, and (ii) the external normal forces applied on envelopes.

13.3 Tangential components

13.3.1 Use of the static model of friction

Applying equation 13.5 in the tangential direction gives:

$$\Sigma_{i,x} \quad = \quad \sum_k F_{k/i,x} - m_i g \sin\alpha + F_{i-1,x} - F_{i,x} \tag{13.10}$$

To formulate an expression of $F_{i-1,x}$ and $F_{i,x}$, we propose to use the static model of friction (see chapter 3.2). We choose this model because of its simplicity and its ability to characterize the paper friction. The static model of friction considers two regimes of friction between surfaces in contact: (i) the static friction, when the surfaces stick together and (ii) the kinetic friction, when they slide on each other.

13.3.2 Kinetic friction

The first drawback of the static model of friction is that it is discontinuous, leading to many expressions depending on the friction regime. In the case of a kinetic friction, an expression of the friction force applied by E_i on E_{i+1} is given by equation 13.11:

$$F_{i,x} = \mu_{K,i} F_{i,y} \Delta_i \tag{13.11}$$

With $F_{i,x}$, $\mu_{K,i}$, $F_{i,y}$, and Δ_i representing the friction force at the interface I_i, the coefficient of kinetic friction of I_1, the normal force applied by E_i on E_{i+1}, and the sign of $(v_i - v_{i+1})$, respectively. For example, if an envelope has a higher speed than the envelope just above, then the force of kinetic friction applied by the first envelope on the second one is positive. In other words, the friction force is opposed

to the sliding. In particular, the kinetic friction characterizes the friction force above and below a block $B = \{E_a..E_b\}$:

$$\begin{cases} F_{b,x} = \mu_{K,b} F_{b,y} \Delta_b \\ F_{a-1,x} = \mu_{K,a-1} F_{a-1,y} \Delta_{a-1} \end{cases} \tag{13.12}$$

For example, in the case of homogeneous mail ($\mu_{K,b} = \mu_{K,a-1}$), the friction force is higher at the bottom of the block than on its top.

13.3.3 Static friction

Problem The second major drawback of the static model of friction is that it gives no expression for the force of static friction. All we know is that the two surfaces in contact stick together. Based on the balance of forces applied on an envelope in the tangential direction, we propose the formulation of an expression of the forces of static friction the envelope undergoes.

Block under acceleration control A first category of blocks consists in blocks under acceleration control. For example, on franking machine feeders, an acceleration control is typically applied by rollers and by vertical plates (acceleration null). To characterize the force of static friction between envelopes of such blocks, we consider a block $B = \{E_a..E_b\}$. The envelopes have the same speed and thus the same acceleration: $\forall i \in \{a..b\}, \vec{a}_i = \vec{a}_B = a_B.\vec{x}$, with $\vec{a}_B$ representing the acceleration of the block B. The fundamental principle of dynamics and equation 13.10 give:

$$\Sigma_{i,x} = m_i a_B = \textstyle\sum_k F_{k/i,x} - m_i g \sin\alpha + F_{i-1,x} - F_{i,x} \tag{13.13}$$

$$\Leftrightarrow \quad F_{i,x} = F_{i-1,x} + \textstyle\sum_k F_{k/i,x} - m_i g sin\alpha - a_B m_i \tag{13.14}$$

By recurrence inside the B block, two expressions of the static friction force can be deduced from equation 13.14: by taking for reference either the lower or upper envelope of the block. We obtain respectively:

$$\forall i \in \{a..b\}, F_{i,x} = F_{a-1,x} - \sum_{j=a}^{i} \left[m_j (a_{B,x} + g sin\alpha) - \sum_k F_{k/j,x} \right] \tag{13.15}$$

$$= F_{b,x} + \sum_{j=i+1}^{b} \left[m_j (a_{B,x} + g sin\alpha) - \sum_k F_{k/j,x} \right] \tag{13.16}$$

Those expressions can be used indifferently, in particular when the blocks are under acceleration control. However, the acceleration control supposes an external force which value is unknown. Consequently, depending on the location of this external force inducing the acceleration control, one expression may be more useful than the other. For example, if the block is under acceleration control by its bottommost envelope, then the second equation may be easier to use as it depends only on the acceleration control.

Free block We call *free block* a block that is not under acceleration or position control. In franking machine feeders, the blocks that are in contact with neither the rollers nor the vertical plate are typical example of free blocks. They only undergo forces of kinetic friction on their upper and lower interfaces. To study such blocks, we consider a free block $B = \{E_a..E_b\}$. The calculation of the force of static friction requires the calculation of the block acceleration. The balance of forces applied on the block B is given by:

$$\sum_{j=a}^{b} m_j a_B = F_{a-1,x} - F_{b,x} + \sum_{j=a}^{b} \sum_{k} F_{k/j,x} - \sum_{j=a}^{b} m_j g \sin\alpha \tag{13.17}$$

The fundamental principle of dynamics finally gives:

$$a_B = \frac{1}{\sum_{j=a}^{b} m_j} \left[F_{a-1,x} - F_{b,x} + \sum_{j=a}^{b} \sum_{k} F_{k/j,x} \right] - g \sin\alpha \tag{13.18}$$

Equation 13.18 can be integrated into either equation 13.15 or 13.16. In the first case, we obtain:

$$\begin{aligned}
\forall i \in \{a..b\}, F_{i,x} &= F_{a-1,x} + \sum_{j=a}^{i} \sum_{k} F_{k/j,x} \\
&\quad - \frac{\sum_{j=a}^{i} m_j}{\sum_{j=a}^{b} m_j} \left[F_{a-1,x} - F_{b,x} + \sum_{j=a}^{b} \sum_{k} F_{k/j,x} \right] \\
&= F_{a-1,x} \frac{\sum_{j=i+1}^{b} m_j}{\sum_{j=a}^{b} m_j} + F_{b,x} \frac{\sum_{j=a}^{i} m_j}{\sum_{j=a}^{b} m_j} \\
&\quad + \frac{\sum_{j=i+1}^{b} m_j}{\sum_{j=a}^{b} m_j} \sum_{j=a}^{i} \sum_{k} F_{k/j,x} - \frac{\sum_{j=a}^{i} m_j}{\sum_{j=a}^{b} m_j} \sum_{j=i+1}^{b} \sum_{k} F_{k/j,x} \\
&= \frac{\sum_{j=i+1}^{b} m_j}{\sum_{j=a}^{b} m_j} \left[F_{a-1,x} + \sum_{j=a}^{i} \sum_{k} F_{k/j,x} \right] \\
&\quad + \frac{\sum_{j=a}^{i} m_j}{\sum_{j=a}^{b} m_j} \left[F_{b,x} - \sum_{j=i+1}^{b} \sum_{k} F_{k/j,x} \right]
\end{aligned} \tag{13.19}$$

With $F_{a-1,x}$ and $F_{b,x}$ expressed in equation 13.12. The same expression is obtained with equation 13.16. The static friction force does not depend anymore on the acceleration of block but on the kinetic friction forces on the block boundaries.

13.3.4 Switch between static and kinetic friction

From static to kinetic Sliding occurs at the interface I_i if the friction force F_i overcomes the break-away force:

$$|F_{i,x}| > \mu_{S,i} F_{i,y} \tag{13.20}$$

This condition is easily computable. For example, in the case of a block under acceleration control by its bottom, and using equation 13.16, we obtain:

$$\left| \mu_{K,b} F_{b,y} \Delta_b + \sum_{j=i+1}^{b} \left[m_j (a_{B,x} + g sin\alpha) - \sum_k F_{k/j,x} \right] \right| > \mu_{S,i} F_{i,y} \tag{13.21}$$

From kinetic to static The switch from kinetic to static friction occurs when E_i and E_{i+1} are (i) in contact, and (ii) have the same speed ($\Delta_i = 0$). Considering $v_i(t_0)$ and $v_{i+1}(t_0)$ the velocities of E_i and E_{i+1} at a time t_0, the time t_f at which the sticking appears is defined by:

$$\begin{aligned} \Delta_i(t_f) = 0 \quad &\Leftrightarrow \quad v_i(t_0) + \int_{t_0}^{t_f} a_i \, \mathrm{d}t = v_{i+1}(t_0) + \int_{t_0}^{t_f} a_{i+1} \, \mathrm{d}t \\ &\Leftrightarrow \quad \int_{t_0}^{t_f} (a_{i+1} - a_i) \, \mathrm{d}t = \Delta_i(t_0) \end{aligned} \tag{13.22}$$

In the case of constant accelerations, equation 13.22 becomes:

$$\begin{aligned} \Delta_i(t_f) = 0 \quad &\Leftrightarrow \quad (a_{i+1} - a_i)(t_f - t_0) = \Delta_i(t_0) \\ &\Leftrightarrow \quad t_f = t_0 + \frac{\Delta_i(t_0)}{a_{i+1} - a_i} \end{aligned} \tag{13.23}$$

Unless friction parameters change, the condition for sticking is therefore that $\Delta_i(t_0)$ and $(a_{i+1} - a_i)$ have an opposed sign.

Summary and Conclusion of Chapter 13

In this chapter, we characterized the forces applied on each envelope of a stack placed in a franking machine feeder. We formulated an expression of the normal force between envelopes (see equation 13.9). We also proposed different expressions for the friction force between envelopes, summarized in Table 13.1.

Interface	Frictional state	Equation
Between blocks	Kinetic	13.11
Inside a block under acceleration control	Static	13.15 or 13.16
Inside a free block	Static	13.19
Switching from static to kinetic	Transient	13.20
Switching from kinetic to static	Transient	13.22

Table 13.1: The different expressions describing the friction force between envelopes

Those expressions of the normal and tangential forces can be integrated to the balance of forces proposed in equation 13.5.

We clearly observe on Table 13.1 that the static model of friction leads to many different expressions of the friction force. This drawback is compensated by clear and simple expressions that will make the next chapters more intelligible.

Chapter 14

Stack dynamics

We want to improve the reliability of the franking machine feeders. Therefore, we aim at developing a dynamics model for an envelope stack placed in a franking machine feeder. In the previous chapter, we formulated an expression of the balance of forces applied on an envelope. Here, we will introduce the stack dynamics and show how it is linked to the blocks separations. In a second part, we will study the blocks splits in detail, based on the balance of forces on each envelope. We will explain the different mechanisms leading to blocks splits and distinguish blocks under acceleration control and free blocks. In a third and last part, we will experimentally validate this model.

14.1 Stack dynamics

Introducing the split function The selection process is strongly linked to the ways a stack splits, something we call *stack dynamics*. We thus introduce the *split function* that describes the conditions leading to the split of a given interface. The split function is defined as the difference between the break-away force and the friction force of the considered interface. An expression of the split function, S_i, of the interface I_i is:

$$S_i = \mu_{S,i} F_{i,y} - F_{i,x}.\text{sign}(F_{i,x}) \tag{14.1}$$

Considering that the force of friction is lower or equal to the break-away force, the split function is always positive or zero. The split occurs at the interface I_i when its split function is zero. This formalism simplifies the determination of the location of the first splits of a block.

A model for stack dynamics A split of the stack usually occurs due to an external sollicitation mainly due to the franking machine (e.g. rollers acceleration). The split function represents the conditions permitting the split of a given interface. However, other weaker interfaces within the block may split first, modifying the balance of forces and the split function of the considered interface, as represented

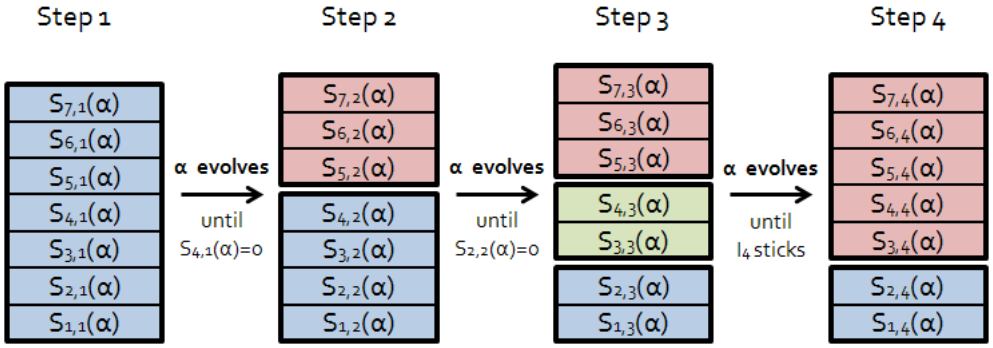

Figure 14.1: Principle of the model. On step 1, an envelope stack with 7 interfaces (8 envelopes) is placed on a franking machine feeder. The interfaces are characterized by their split function $S_{i,1}$. On step 2, a design parameter, represented by α, evolved until one of the split function became zero (here it is $S_{4,1}$). The stack thus splits at the fourth interface, and new split functions have to be calculated, noted $S_{i,2}$. On step 3, the α parameter evolved until a split function became zero (here it is $S_{2,2}$). The bottommost block thus splits and new split functions have to be calculated, noted $S_{i,3}$. On step 4, the α parameter evolved until the fourth interface sticks again. New split functions have to be calculated, noted $S_{i,4}$.

on Figure 14.1. Sliding interfaces may also stick again, merging blocks and changing the split functions. In both cases, new split functions have to be calculated each time a split occurs, because this last split potentially avoids or favors the slipping of the considered interface, as represented on Figure 14.1. The split of an interface is thus strongly linked to the split of other interfaces and determining the location of the first splits is fundamental.

Reduced model The calculation of the stack dynamics is possible using the model introduced in the previous paragraph. However, such computing are of limited interest, in particular because of their complexity. We thus propose to focus on a limited aspect of the problem.
The main problem we face during the selection process consists in multiple feedings: more than one envelope is fed into the machine at the same time. To avoid this problem, conditions 1 and 2 introduced in chapter 12.3 have to be fulfilled. Condition 1 requires the bottommost envelope to be driven into the machine. This condition is usually fulfilled by the mean of rollers or belts. Condition 2 requires the other envelopes to have a limited tangential displacement. This condition is usually fulfilled by the mean of vertical plates or friction pads for example. It is therefore technically easy to fulfill those two conditions taken individually. However, those two conditions taken together are more complex to fulfill, because they require the bottommost interface to slide. The main challenge is therefore to find the conditions

permitting the split of the bottommost interface, called I_1. In the following chapters, we thus propose to focus on the split of the bottommost block. In particular, we will focus on the split of its bottommost interface.

Different types of blocks On franking machine feeders, the bottommost block is in contact with driving rollers or driving belt. Those rollers are under position control by a proportional-integral-derivative controller (PID). We thus expect the acceleration of rollers to be constant, and it was verified experimentally for low stacks (below 1 kg). Consequently, we consider that the bottommost block is under acceleration control and we will focus our study on this particular case.
However, the displacement of heavy stacks may require higher electrical intensity than the intensity available for the motors, so that the torque applied on rollers becomes limited. Heavy stacks may therefore undergo a constant force on their bottommost envelope. In this situation, the bottommost block becomes a free block rather than a block under acceleration control. We moreover think that future feeders may involve a controlled torque applied on rollers, rather than a controlled position. Consequently, we will introduce in a second part the case of free blocks splits.

14.2 Blocks under acceleration control

14.2.1 Split function

Situation We consider that the bottommost of size b ($B = \{E_1..E_b\}$) is under acceleration control by its bottom. For example, the bottommost envelope is in contact with driving rollers. The study could however be extended to blocks elsewhere in the stack and still under acceleration control.

Initial acceleration For clarity reasons, we propose to consider here the case $F_{i,x} > 0$ and $\Delta_b > 0$, corresponding for example to the beginning of the selection process. In this situation, the force of static friction applied by envelope E_i on E_{i+1} was described by equation 13.16. The split function becomes:

$$\begin{aligned} S_i &= \mu_{S,i}F_{i,y} - \mu_{K,b}F_{b,y} - \sum_{j=i+1}^{b}\left[m_j(a_{B,x} + gsin\alpha) - \sum_k F_{k/j,x}\right] && (14.2)\\ &= \mu_{S,i}\sum_{j=i+1}^{b}(m_j g\cos\alpha - \sum_k F_{k/j,y}) + (\mu_{S,i} - \mu_{K,b})F_{b,y} \\ &\quad - \sum_{j=i+1}^{b}\left[m_j(a_{B,x} + gsin\alpha) - \sum_k F_{k/j,x}\right] && (14.3)\\ &= S_{i,1} + S_{i,2} + S_{i,3} && (14.4) \end{aligned}$$

With $S_{i,1}$, $S_{i,2}$, and $S_{i,3}$ representing the contribution of envelopes, below the I_b interface, above I_b, and of the external forces, respectively. The complete expression is given hereafter:

$$\begin{cases} S_i = S_{i,1} + S_{i,2} + S_{i,3} \\ S_{i,1} = (\mu_{S,i} g \cos\alpha - g \sin\alpha - a_{B,x}) \sum_{j=i+1}^{b} m_j \\ S_{i,2} = (\mu_{S,i} - \mu_{K,b}) \sum_{j=b+1}^{n} (m_j g \cos\alpha - \sum_k F_{k/j,y}) \\ S_{i,3} = \sum_{j=i+1}^{b} \sum_k \left(F_{k/j,x} - \mu_{S,i} F_{k/j,y} \right) \end{cases} \tag{14.5}$$

Influence of external forces We introduce β_i and $F_{ext,i}$ representing the angle to the horizontal and the norm of the external forces applied on E_i, respectively. β_i and $F_{ext,i}$ are defined as:

$$\begin{cases} F_{ext,i} \cos\beta_i = \sum_k F_{k/i,x} \\ F_{ext,i} \sin\beta_i = \sum_k F_{k/i,y} \\ F_{ext,i} = \sqrt{\left(\sum_k F_{k/i,x}\right)^2 + \left(\sum_k F_{k/i,y}\right)^2} \end{cases} \tag{14.6}$$

We also introduce the angle ρ_i defined by:

$$\begin{cases} \sqrt{\mu_{S,i}^2 + 1} \cos\rho_i = 1 \\ \sqrt{\mu_{S,i}^2 + 1} \sin\rho_i = \mu_{S,i} \end{cases} \tag{14.7}$$

On the inclined plane test method, the angle ρ_i is the angle when sliding begins. Considering $\mu_{S,i} = 0.6$ for example, we obtain $\rho_i = 31°$. In materials science, the ρ_i is also known as the angle of the *cone of friction*, as represented on Figure 14.2. The β_i, $F_{ext,i}$, and ρ concepts clarify the $S_{i,3}$ expression:

$$\begin{aligned} S_{i,3} &= \sum_{j=i+1}^{b} \sum_k \left(F_{k/j,x} - \mu_{S,i} F_{k/j,y} \right) \\ &= \sum_{j=i+1}^{b} F_{ext,j} \left(\cos\beta_j - \mu_{S,i} \sin\beta_j \right) \\ &= \sum_{j=i+1}^{b} F_{ext,j} \sqrt{\mu_{S,i}^2 + 1} (\cos\rho_i \cos\beta_j - \sin\rho_i \sin\beta_j) \\ &= \sum_{j=i+1}^{b} F_{ext,j} \sqrt{\mu_{S,i}^2 + 1} \cos(\rho_i + \beta_j) \end{aligned} \tag{14.8}$$

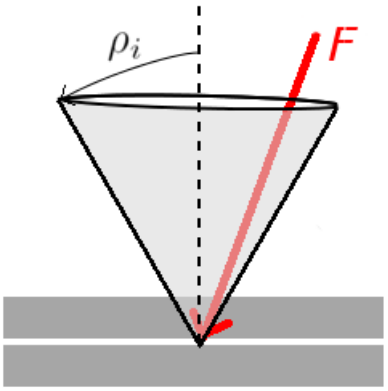

Figure 14.2: The *cone of friction*: a force F is applied on two surfaces sticking together. The surfaces remain in static friction until the force goes out of the (virtual) cone, i.e. until the angle between the normal and the external force becomes higher than ρ_i.

Based on equation 14.8, the split function is finally expressed as:

$$\begin{cases} S_i = S_{i,1} + S_{i,2} + S_{i,3} \\ S_{i,1} = (\mu_{S,i} g \cos\alpha - g \sin\alpha - a_{B,x}) \sum_{j=i+1}^{b} m_j \\ S_{i,2} = (\mu_{S,i} - \mu_{K,b}) \sum_{j=b+1}^{n} (m_j g \cos\alpha - \sum_k F_{k/j,y}) \\ S_{i,3} = \sqrt{\mu_{S,i}^2 + 1} \sum_{j=i+1}^{b} F_{ext,j} \cos(\rho_i + \beta_j) \end{cases} \tag{14.9}$$

This expression is easier to understand as the norm and orientation of the external forces applied on the envelopes are split.

Factors Determining a general solution for equation 14.9 is impossible. The equation however highlights the main parameters influencing the block division, as represented on Figure 14.3:

- **Machine design:** (i) the acceleration of the block ($a_{B,x}$), (ii) the norm and orientation of the external forces, and (iii) the stack tilt (α). Those parameters are easy to contol.
- **Properties of interfaces, envelopes, and stacks:** (i) the "strength" of the I_i interface ($\mu_{S,i}$), (ii) the "strength" of the considered block boundary ($\mu_{K,b}$), and (iii) the weight of the envelopes above I_i. Those input parameters are unknown and expected to remain constant during the selection process.
- **Stack's structure:** characterized by the sizes and distribution of blocks within the stack. This parameter is fundamental to the fulfillment of the

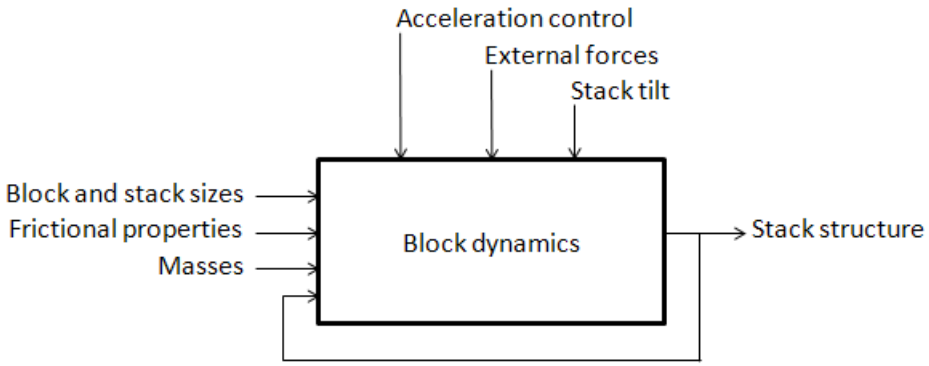

Figure 14.3: The different parameters of the selection process

conditions for a correct feeding. However, this parameter is not under direct control and evolves during the selection process. In fact, the modification of the machine design is the only way to modify this stack structure.

In the following sections, we will study the influence of machine design and envelopes/interfaces properties on the selection process. In particular, the parameters associated to the machine design being intended at varying during the selection process, we will study the influence of their evolution on the selection process. The structure of the stack evolving during the selection process, it will be studied along with the other parameters.

14.2.2 Evolving acceleration

Critical acceleration The block we consider is under acceleration control by its bottommost envelope. This acceleration evolves during the selection process. For clarity reasons, we introduce the $A(i)$ function, called *critical acceleration*, and representing the acceleration of the block required to split the I_i interface. In this situation, the split function is zero: $S_i(A(i)) = 0$. For example, if the acceleration is equal to the critical acceleration of the first interface, then the first interface splits. Using equation 14.9:

$$\begin{aligned} S_i(A(i)) = 0 \quad &\Leftrightarrow \quad \begin{cases} S_{i,1} + S_{i,2} + S_{i,3} = 0 \\ S_{i,1} = (\mu_{S,i} g \cos\alpha - g \sin\alpha - A(i)) \sum_{j=i+1}^{b} m_j \\ S_{i,2} = (\mu_{S,i} - \mu_{K,b}) \sum_{j=b+1}^{n} (m_j g \cos\alpha - \sum_k F_{k/j,y}) \\ S_{i,3} = \sqrt{\mu_{S,i}^2 + 1} \sum_{j=i+1}^{b} F_{ext,j} \cos(\rho + \beta_j) \end{cases} \\ &\Leftrightarrow \quad A(i) = \mu_{S,i} g \cos\alpha - g \sin\alpha + \frac{S_{i,2} + S_{i,3}}{\sum_{j=i+1}^{b} m_j} \end{aligned} \tag{14.10}$$

Equation 14.10 is fundamental for the design of systems using acceleration control to split envelope stacks. Indeed, the minimum in critical acceleration indicates the

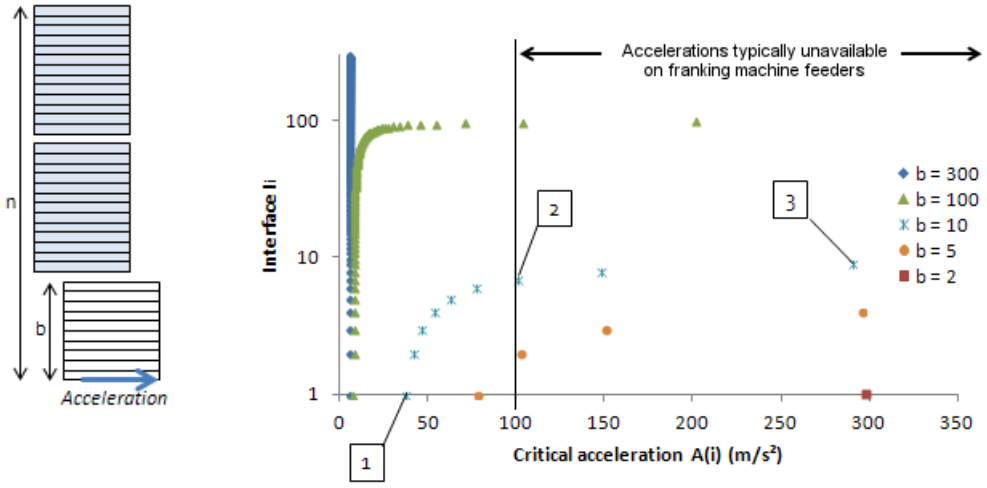

(a) Situation (b) Acceleration $A(i)$ required to split the interface I_i

Figure 14.4: An acceleration is applied on the bottommost block of a $n = 300$ envelopes stack. Different block sizes b are studied. The points (1), (2) and (3) refer to a $b = 10$ envelopes block at the bottom of the stack. (1) To split the bottommost interface, roughly 40 m.s^{-2} must be applied on the bottommost envelope. (2) To split the 7th interface, roughly 100 m.s^{-2} must be applied on the bottommost envelope. (3) To split the 9th interface, roughly 300 m.s^{-2} must be applied on the bottommost envelope. ($\mu_S = 0.6$, $\mu_K = 0.5$, $m = 0.01$ kg and $\alpha = 0$.)

location of the first split and the acceleration it requires. Equation 14.10 can be easily integrated in a computer program.

Simplified model As we are only interested in the acceleration variations, we study a simplified model. In the case of a vertical stack ($\alpha = 0$) with homogenous mass (m) and frictional properties (μ_S and μ_K) undergoing no external forces ($S_{i,3} = 0$), equation 14.10 becomes:

$$A(i) = \mu_S g + \frac{n-b}{b-i}(\mu_S - \mu_K)g \tag{14.11}$$

A numerical application is proposed on Figure 14.4. The figure is onerous but contains many interesting information, such as (i) the position of the splits within the stack, and (ii) the acceleration control required. We detail the main points of its analysis hereafter.

First split At the beginning of the selection process, the whole stack is a single block ($b = n = 300$). The critical acceleration is so that all the forces of static friction are equal to the break-away force ($a_{B,x} = \mu_S g$). The frictional properties

being the same, the critical acceleration is therefore the same for all the interfaces, as represented on Figure 14.5a. It is consequently impossible to predetermine which specific interface will split first.

Next splits After the first split, a sliding occurs at interface I_b ($b < n$). A kinetic friction thus appears on top of the bottommost block, as represented on Figure 14.5b. The force of kinetic friction that appeared on top of the bottommost block is defined by equation 13.12. Considering $\mu_S > \mu_K$, the critical acceleration now depends on the position of the considered interface. The acceleration applied on the bottommost envelope thus increases until reaching the critical acceleration of an interface of the bottommost block, as represented on Figure 14.4, and a new split then occurs. In particular, equation 14.11 shows that considering $\mu_S > \mu_K$, the critical acceleration increases with a decrease in block size, i.e. with successive splits[1]. This result shows that splits appear one by one as the acceleration increases. Equation 14.11 also shows that the critical acceleration is lower for interfaces at the bottom of the block. Consequently, the next splits should occur at the bottom of the stack, as observed on Figure 14.5b. The acceleration necessary to this split (the critical acceleration) may however exceed technical limits, as represented on Figure 14.4b.
The conditions 1 and 2 of a correct feeding suggest that the bottommost interface (I_1) of the stack should split during the selection process. Another study could thus consist in characterizing the required acceleration to split the bottommost interface as a function of the stack size (n). Equation 14.11 clearly shows that in this situation, the critical acceleration is a linear function of the stack size: the higher the envelope stack is, the higher the acceleration should be in order to split the bottommost interface. The selection process is therefore more difficult for high stacks.

Summary We studied in this section the case of an envelope stack under acceleration control by its bottommost envelope. Based on equation 14.10, we explained the mechanisms leading to a block split: as the acceleration increases, the static friction force increases until the break-away force of a block interface is reached and the interface splits. In the following sections, we will study the other parameters influencing the split of the bottommost block.

14.2.3 Evolving external force

Situation In the previous section, we considered an increasing acceleration. We now consider that the bottommost block of size b ($B = \{E_1..E_b\}$) undergoes a constant acceleration a_B on its bottom. This situation is typically observed when the rollers of a franking machine feeder reach their nominal acceleration (approx.

[1]For example, on Figure 14.1, the block size is equal to $b = 7$ during step 1, $b = 4$ during step 2 and $b = 2$ during steps 3 and 4.

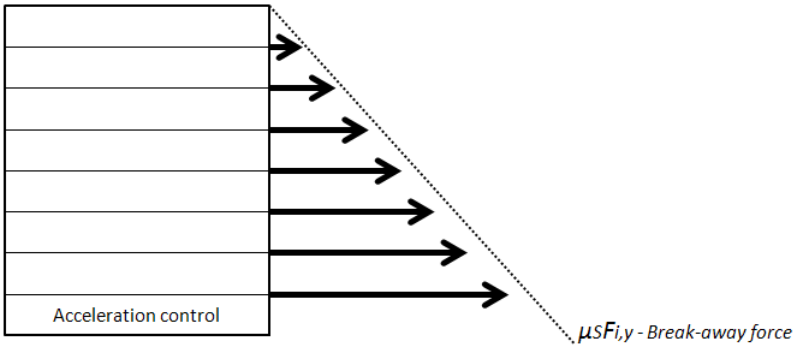

(a) The stack is a single block: all the interfaces are in static friction.

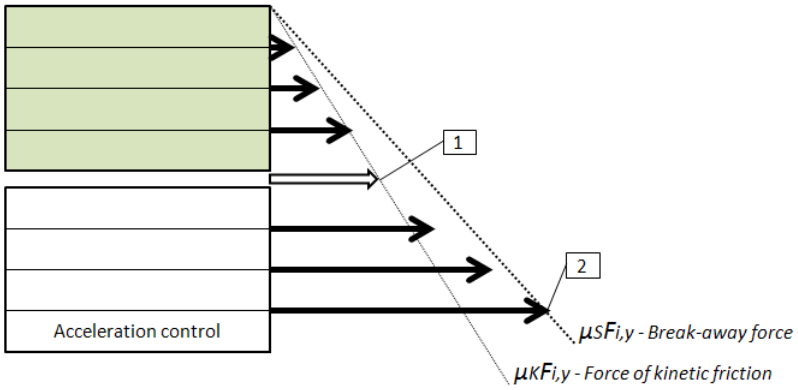

(b) (1) The stack split in two blocks, and a force of kinetic friction appeared between them. (2) The acceleration applied is so high that the force of static friction at the bottommost interface reaches its break-away force: the interface splits.

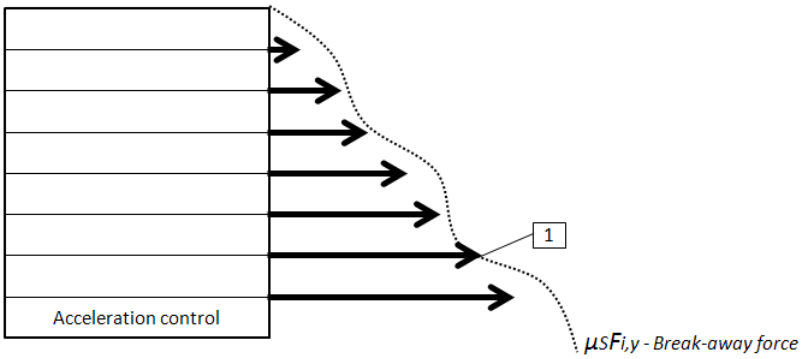

(c) The stack is a single block: all the interfaces are in static friction. (1) The frictional properties evolve along the block. The split occurs above the bottommost interface.

Figure 14.5: Static friction forces (full arrows) and kinetic friction forces (empty arrows) in a stack under acceleration control by its bottom.

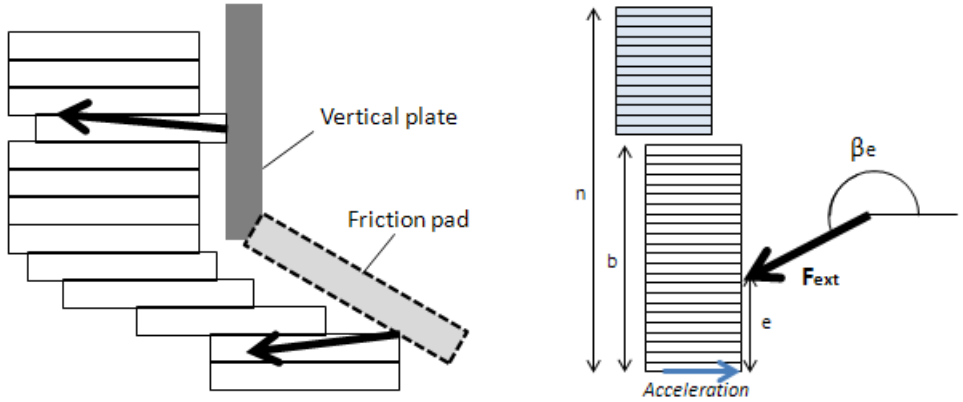

(a) Forces created by vertical plates and friction pads (b) Proposed model

Figure 14.6: External force (arrows) applied by vertical plates and friction pads on an envelope stack and proposed model. On Figure 14.6a, the arrows are slightly oriented tangentially to the surfaces, because we considered friction phenomena.

100 m.s^{-2}) or their nominal speed (approx. 1 m.s^{-1}). To permit the block split, external forces are applied on envelopes by friction pads or vertical plates for example, as represented on Figure 14.6a. We propose a simplified model consisting in an external force F_{ext} applied on the envelope E_e, as represented on Figure 14.6b. If $(e > b)$, the external force is applied above the block. If $(i < e \leq b)$, the external force is applied somewhere on the block, above the interface I_i. If $(i \geq e)$, the external force is applied below the interface I_i. The external force makes an angle β_e with the horizontal.

Critical external force The external force evolving, we search both the norm and orientation of the external force permitting the block separation at a given interface I_i. The force is called *critical external force*, noted $F_{c,e}(i)$, and verifies $S_i = 0$, with S_i representing the split function of interface I_i. The critical external force is reached when the force of static friction is equal to the break-away force of the considered interface, i.e. when the split function is zero. Equation 14.9 gives verifies:

$$\begin{cases} 0 = S_{i,1} + S_{i,2} + S_{i,3} \\ S_{i,1} = (\mu_{S,i} g \cos\alpha - g \sin\alpha - a_{B,x}) \sum_{j=i+1}^{b} m_j \\ S_{i,2} = (\mu_{S,i} - \mu_{K,b}) \sum_{j=b+1}^{n} (m_j g \cos\alpha - \sum_k F_{k/j,y}) \\ S_{i,3} = \sqrt{\mu_{S,i}^2 + 1} \sum_{j=i+1}^{b} F_{ext,j} \cos(\rho_i + \beta_j) \end{cases} \tag{14.12}$$

We deduce from this equation that an external force applied below the considered interface has no influence on the split of this interface $(i \geq e)$. We also deduce that in the case of a tangential external force applied above the block, equation 14.12

becomes:

$$F_{c,e,y} = \frac{\mu_{S,i} g \cos\alpha - g \sin\alpha - a_{B,x}}{\mu_{S,i} - \mu_{K,b}} \sum_{j=i+1}^{b} m_j + \sum_{j=b+1}^{n} (m_j g \cos\alpha) \tag{14.13}$$

To finish with, if the force is applied between the considered interface and the top of the bottommost block ($i < k \leq b$):

$$\begin{aligned} F_{c,e} \cos(\rho_i + \beta_e) = \; & \frac{1}{\sqrt{\mu_{S,i}^2+1}} (a_{B,x} + g \sin\alpha - \mu_{S,i} g \cos\alpha) \textstyle\sum_{j=i+1}^{b} m_j \\ & - \frac{1}{\sqrt{\mu_{S,i}^2+1}} (\mu_{S,i} - \mu_{K,b}) \textstyle\sum_{j=b+1}^{n} (m_j g \cos\alpha) \end{aligned} \tag{14.14}$$

Those expressions are fundamental for the design of systems using external forces to split envelope stacks. Indeed, the minimum in critical external force along the stack indicates the location of the first split and the external force required. The formula being complex, we will study a simplified model.

Simplified expression Considering a homogeneous and vertical stack, the expression is simplified:

$$\begin{cases} F_{c,e,y} = \frac{\mu_S g - a_{B,x}}{\mu_S - \mu_K} (b-i)m + (n-b)mg & \text{if } e > b \\ F_{c,e} \cos(\rho_i + \beta_e) = \frac{(a_{B,x} - \mu_S g)(b-i)m - (\mu_S - \mu_K)(n-b)mg}{\sqrt{\mu_S^2+1}} & \text{if } i < e \leq b \end{cases} \tag{14.15}$$

Equation 14.15 clearly shows that three parameters permit the control of the splits at constant acceleration and stack tilt: (i) the norm of the external forces, (ii) their orientations, and (iii) their points of application. For numerical applications, we represent the critical external forces of a 3 kg stack and for different b levels on Figure 14.7.

Mechanisms involved The influence of external forces thus depends on their point of application on the stack:

- **If the external force is applied above the bottommost block:** the tangential component of the external force is not transmitted to the bottommost block because of the sliding occurring at interface I_b. Normal component however modifies the normal forces applied on interfaces below the point of application of the force, as represented on Figure 14.8a. Normal components thus reduce the break-away forces and forces of kinetic friction of the interfaces below the point of application of the force.
- **If the external force is applied on the block and above the interface we want to split:** the normal component still modifies the break-away force. But the tangential component of the force also changes the shearing strength

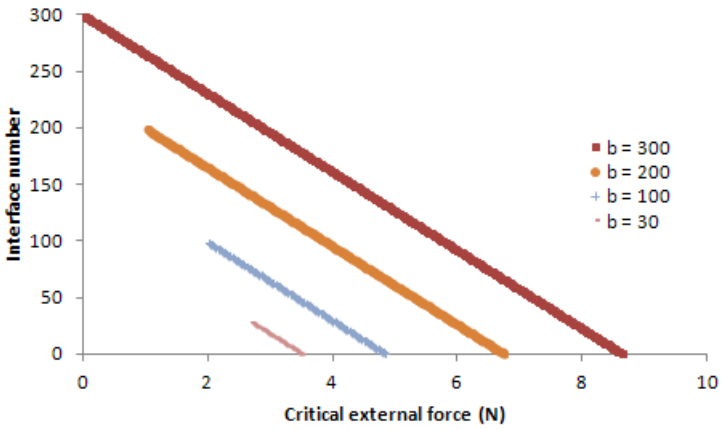

(a) a_B =3 m.s^{-2} ($a_B < \mu_S g$)

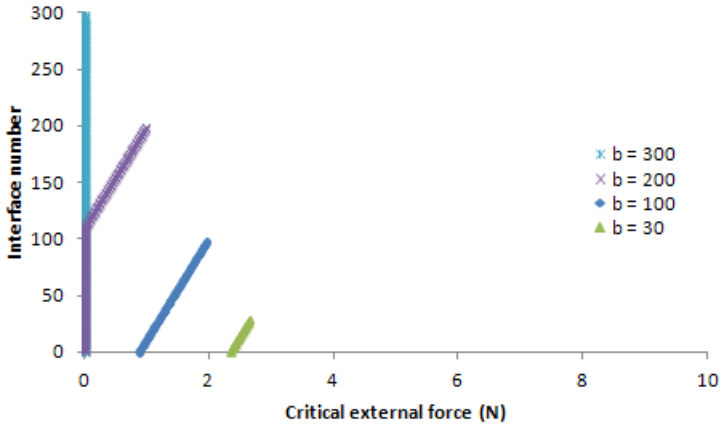

(b) a_B =7 m.s^{-2} ($a_B > \mu_S g$)

Figure 14.7: Influence of an external backward tangential force on the static friction forces. The force is applied on the topmost envelope of the bottommost block (E_b). Different block sizes (b) are represented. $\mu_S = 0.6$, $\mu_K = 0.5$. Stack of $n = 300$ envelopes of $m = 10$ g each.

of the interfaces in the block, causing or avoiding block division, as represented on Figure 14.8c. Consequently, the contribution of the external force to the split has the sign of $\cos(\rho_i + \beta_e)$, where ρ_i and β_e represent the strength of the interface I_i (see equation 14.7) and the orientation of the external force (see equation 14.6), respectively. The contribution of an external force to the split function is therefore positive for $-\frac{\pi}{2} > \rho_i + \beta_e > \frac{\pi}{2}$ and negative otherwise, as represented on Figure 14.9. More precisely, the norm of the critical external force is minimal for $\beta_e = -\rho \pm \pi$. This angle β_e can be considered as optimal, because it reduces the norm of the required external force.

- **If the external force is applied below the interface we want to split:** the external force has no influence on the split.

The mechanisms associated to the normal and tangential components of external forces are thus different, but their result on block division is quite similar.

Where does the stack split? Equation 14.15 and Figure 14.7 clearly show that the splitting ability of the external forces strongly depends on the sign of $(a_{B,x} - \mu_S g)$. The reason behind this phenomenon involves a competition between the inertia of envelopes and the break-away force of the interfaces. To explain this mechanism, we consider a group of envelopes in the bottommost block of a stack. The mass of the group is noted M. The contribution of the group inertia to the static friction force of interfaces below the group is thus given by $(Ma_{B,x})$. On the other hand, the contribution of the group weight to the break-away force of the interfaces below the group is given by $(M\mu_S g)$. Consequently:

- When the acceleration is low ($a_{B,x} < \mu_S g$), the net contribution of the group to the split function of interfaces below the group is positive: the mass of the group favors the break-away force and the sticking of interfaces. By iteration, the bottommost interfaces appear more difficult to split than the topmost ones, and high external forces are required to permit interface splits, as represented on Figure 14.7a. Upper interfaces thus have a higher split probability than the lower one, as represent on Figure 14.8b.

- When the acceleration is high ($a_{B,x} > \mu_S g$), the inertia of the group strongly contributes to the static friction force of interfaces below the group, while its contribution to break-away forces remains unchanged. Consequently, the net contribution of the group to the split function of interfaces below the group is negative, facilitating their split. By iteration, the lower interfaces appear weaker than the upper interfaces, as represented on Figure 14.7b. The lower interface thus may split first, as represented on Figure 14.8c.

Those results are of particular interest in the case of franking machine feeders, because the goal is to split only the bottommost interface. The results show that to

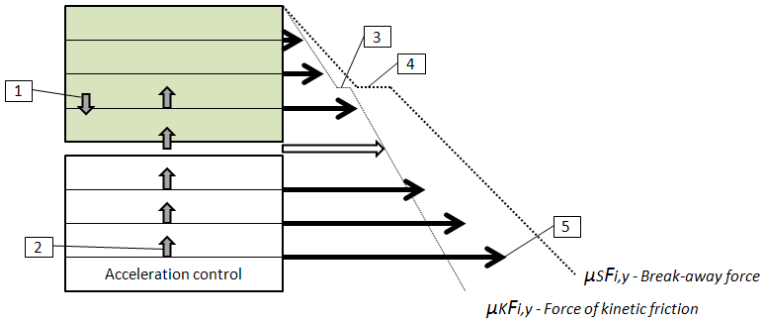

(a) (1) Normal force oriented downward. (2) The external force creates normal forces between envelopes, modifying the break-away force (3) and forces of kinetic friction (4) of the interfaces. (5) The force of static friction at the first interface thus no more reaches its break-away force (no split).

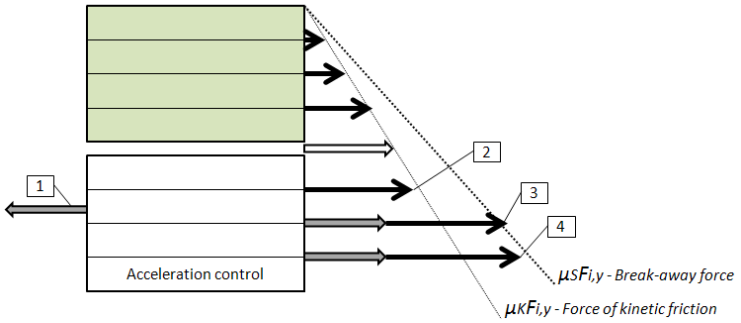

(b) (1) Backward force with low acceleration ($a_{B,x} < \mu_{S,i}g$). (2) The static frictions above this envelope are unchanged. (3) The force of static friction at the second interface reached its break-away force and the interface splits, contrary to the first interface (4).

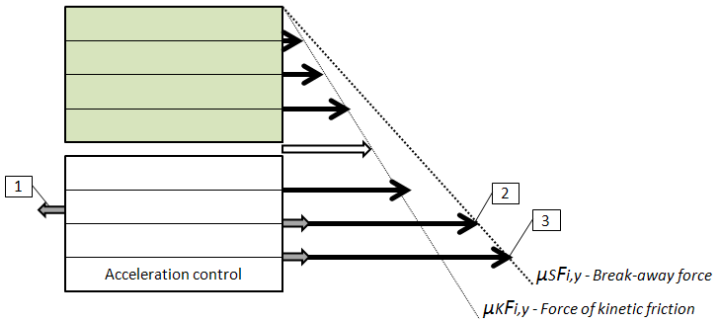

(c) (1) Backward force with high acceleration ($a_{B,x} > \mu_{S,i}g$). The situation is the same than on Figure 14.8b, but the first interface splits (3) and not the second (2).

Figure 14.8: Effect of external forces on the static friction forces of a stack under acceleration control by its bottom. Thin arrows represent the static friction forces. Thick and empty arrows represent the kinetic friction forces. Thick and full arrows represent the external forces (1) and their contribution to the static friction forces.

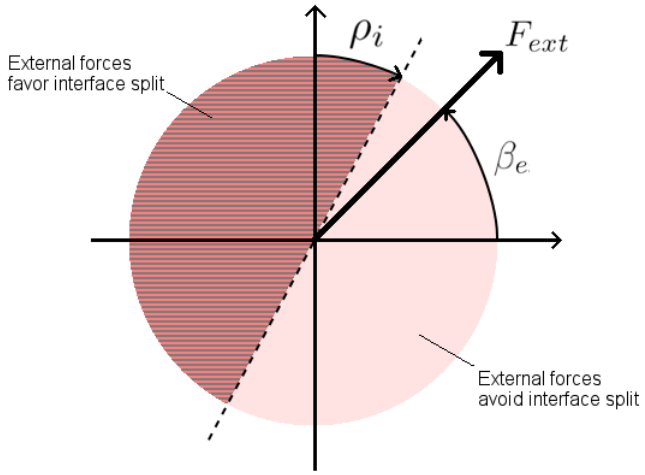

Figure 14.9: A block of b envelopes is at the bottom of a stack of n envelopes. The block is under acceleration control by its bottommost envelope. An external force is applied on the block, on an envelope E_e above the interface we want to split. The external force has an orientation β_e and a norm F_{ext}. The "strength" of the considered interface is represented by the angle ρ_i, an angle representing the coefficient of static friction.

permit such a split, using strong accelerations ($a_{B,x} > \mu_S g$) is necessary. It is also technically feasible.

14.2.4 Evolving stack tilt

Critical tilt We showed in chapter 1 that some franking machine feeders are tilted to the rear (approx. 5°): the envelope stack is not vertical, as represented on Figure 12.1 ($\alpha > 0$). This solution is intended at easing the separation of envelopes but it may also become the main mechanism permitting the selection process. To characterize this solution, we consider a stack of envelopes undergoing constant external forces, the bottommost block of size b ($B = \{E_1..E_b\}$) undergoing a constant acceleration a_B on its bottom. The block lays on an inclined plane. The tilt of the plane to the horizontal, α, increases from 0 to $\frac{\pi}{2}$. This increase in stack tilt induces a stack split. We propose to determine the exact position of this split. We thus search for the *critical tilt*, $\alpha(i)$, leading to a split of the interface I_i (i.e. verifying $S_i = 0$). This critical tilt will thus give information concerning the location of the split and the angle required to permit it.

General expression and mechanisms Based on equation 14.9, the critical tilt verifies:

$$\begin{cases} 0 = S_{i,1} + S_{i,2} + S_{i,3} \\ S_{i,1} = (\mu_{S,i} g \cos\alpha(i) - g \sin\alpha(i) - a_{B,x}) \sum_{j=i+1}^{b} m_j \\ S_{i,2} = (\mu_{S,i} - \mu_{K,b}) \sum_{j=b+1}^{n} (m_j g \cos\alpha(i) - \sum_k F_{k/j,y}) \\ S_{i,3} = \sqrt{\mu_{S,i}^2 + 1} \sum_{j=i+1}^{b} F_{ext,j} \cos(\rho + \beta_j) \end{cases} \tag{14.16}$$

We observe two mechanisms involved:

- A positive stack tilt induces a backward component of the stack weight that increases the static friction.
- A stack tilt also reduces the normal component of the stack weight and finally (i) the break-away force, and (ii) the forces of kinetic friction of the interfaces. This reduction is negligible for low stack angles (few degrees) but becomes a major factor for high angles.

Reduced expression In the case of a homogeneous stack undergoing no external force, equation 14.16 becomes:

$$\begin{aligned} & (\mu_S g \cos\alpha(i) - g \sin\alpha(i) - a_{B,x})(b-i) + (\mu_S - \mu_K)(n-b) g \cos\alpha(i) = 0 \\ \Leftrightarrow \quad & \cos\alpha(\mu_S(n-i) - \mu_K(n-b)) - \sin\alpha(b-i) = \tfrac{a_{B,x}}{g}(b-i) \\ \Leftrightarrow \quad & \cos\alpha \tfrac{\mu_S(n-i) - \mu_K(n-b)}{b-i} - \sin\alpha = \tfrac{a_{B,x}}{g} \\ \Leftrightarrow \quad & \cos(\alpha + \theta_i) = \tfrac{a_{B,x}}{L_{\theta,i} \cdot g} \end{aligned} \tag{14.17}$$

With $L_{\theta,i}$ and θ that are easily computable and defined by:

$$\begin{cases} L_{\theta,i} = \sqrt{\left(\frac{\mu_S(n-i) - \mu_K(n-b)}{b-i}\right)^2 + 1} \\ L_{\theta,i} \cos\theta_i = \frac{\mu_S(n-i) - \mu_K(n-b)}{b-i} \\ L_{\theta,i} \sin\theta_i = 1 \end{cases} \tag{14.18}$$

The critical angle is a function of (i) the block acceleration, (ii) the stack structure, and (iii) the frictional properties of the interfaces. A numerical application is represented on Figure 14.10b.

Qualitative observations The influence of stack tilt on the stack splits is similar to the influence of increasing accelerations. The stack tilt increasing, it reaches a level at which all the interfaces can split, as represented on Figure 14.10b This situation is due to the homogeneous properties of the envelopes and to the absence of external forces. In this situation, it is impossible to predict the exact location of the first

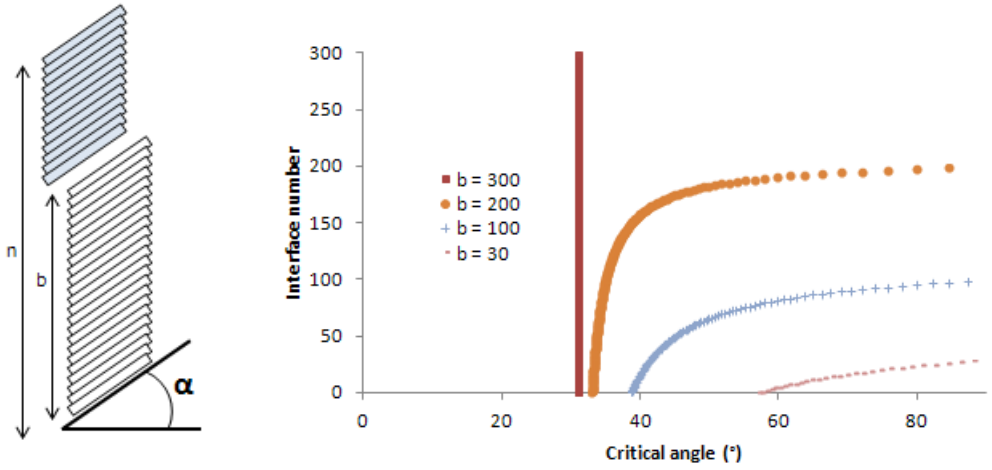

(a) Situation (b) Critical angles

Figure 14.10: A stack of $n = 300$ envelopes undergoes no acceleration control nor external forces. We consider the bottommost block of this stack, a block of b envelopes. The graphic represents the stack tilt (α, in degrees) required to split the different block interfaces and called *critical angle*. $\mu_S = 0.6$, $\mu_K = 0.5$, $m = 10$ g.

split. After the first split, a bottommost block of size b appeared. The tilt required to create new splits within the block increases with the decrease in bottommost block size (b). In other words, higher tilts are required to permit the next splits. An interesting observation is that stack tilt favors the split of the bottommost interfaces: similarly to increasing accelerations, the critical angle of bottommost interfaces is lower than the critical angle of upper ones.

Quantitative observations From a quantitative point of view, we observe that the critical tilts are high, above 30°. The tilt observed on franking machine feeders is usually lower than 5°. Consequently, the stack tilt observed on franking machines is far from permitting the split of the stack. Moreover, the required tilt increases with a decrease in bottommost block. For blocks below 100 envelopes, the required tilt to permit successive stack divisions increases beyond 40°. At the extreme, the split of the bottommost interface in the case of a double would require a tilt of 90°. As a conclusion, the stack tilt is not sufficient to permit the split of the stack at the desired interface, but contributes to the split at the bottommost interface.

Remark In this section, we studied the influence of a stack tilt on the interfaces split. In this situation, the feeder is tilted while the rest of the machine remains horizontal. Beyond 5°, the transition from an inclined feeder to an horizontal envelopes path bends and damages the envelopes, as represented on Figure 14.11a. The use

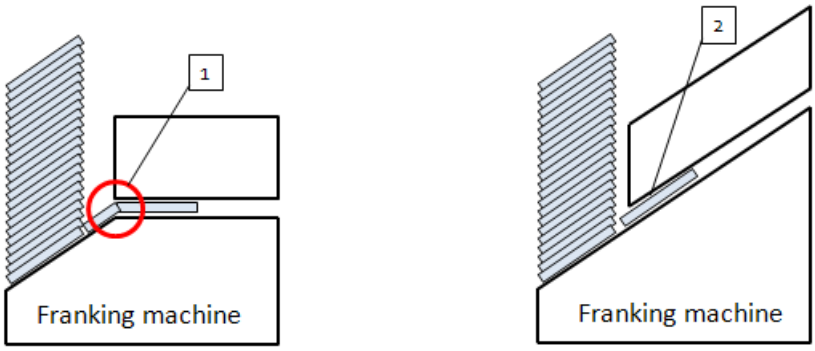

(a) Tilted feeder (b) Tilted machine

Figure 14.11: To use highly inclined stacks without bending the envelopes (1) and (2), the whole machine could be inclined (right) rather than just the feeder (left).

of an increasing stack tilt as a unique separation mechanism therefore appears to be not adapted to horizontal machines. A solution consists in inclining the whole franking machines, as represented on Figure 14.11b. Beyond an improved selection process, this solution would also reduce the size of the machine and allow the storage of large number of envelopes at the exit of the machine.

Fixed stack tilt Previous results showed that using stack tilts as the unique mechanism for block splits is technically difficult. However, a fixed stack tilt favors the selection process and may be associated to high accelerations for example. To characterize this influence, we studied the case of an inclined envelope stack under acceleration control by its bottom, as represented on Figure 14.12a. We try to split the block of two envelopes at the bottom of the stack. The critical acceleration required to split the bottommost block for different stack tilts is represented on Figure 14.12b. We observe that for stack tilts from -15° to 15°, the influence of the tilt on the critical acceleration is negligible. Tilts beyond 45° however have a clear influence on the critical accelerations: in the situation represented on Figure 14.12b, the acceleration required to split the block of 2 envelopes is 300 $m.s^{-2}$ for a vertical stack and 200 $m.s^{-2}$ for $\alpha = 45°$. This technological solution may permit low-cost improvements of the franking machine feeders in the future.

14.2.5 Dispersion in frictional properties

Situation Envelopes stacks are often constituted by envelopes of various types, called *mix-mail*. Consequently, the frictional properties of the interfaces are expected to evolve along the stack. Variations in frictional properties may modify the break-away forces, the forces of kinetic friction, and finally the split functions. In this section, we propose to study how those frictional properties influence the split

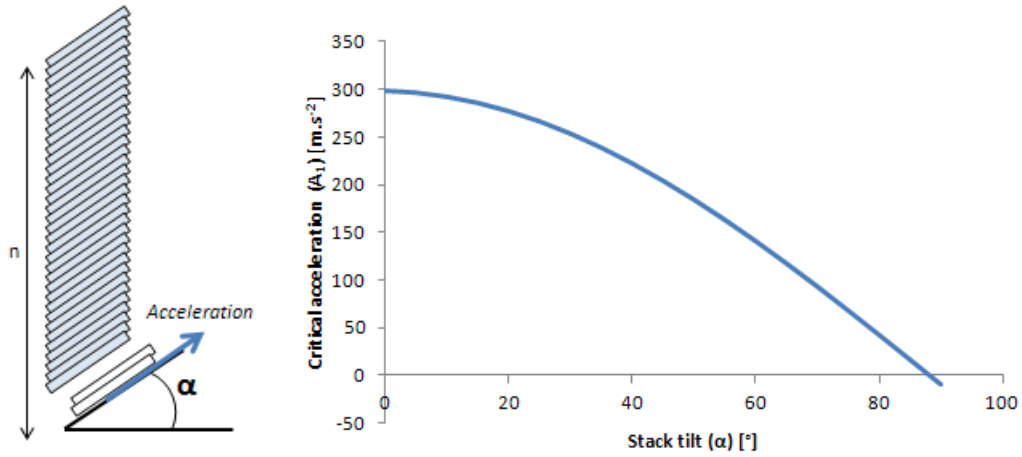

(a) Situation (b) Critical acceleration for various stack tilts

Figure 14.12: A stack of $n = 300$ envelopes is placed on the feeder. A block of two envelopes is at its bottom (also called *double*). This bottommost block is under acceleration control by its lower envelope. The figure represents the acceleration $A(i)$ required to split the block for different stack tilts. $\mu_S = 0.6$, $\mu_K = 0.5$ and $m = 0.01$ kg.

function of an interface I_i.

Coefficients of static friction First of all, we study the sensibility of the split function to the coefficients of static friction. Equation 14.5 shows that the split function is independent from the coefficient of static friction of interfaces other than that studied. We thus consider two values for the coefficient of static friction of the I_i interface, that are named $\mu_{S,i}$ and $\mu'_{S,i}$, respectively: Based on equation 14.5, we introduce:

$$\Delta S_i = S_i - S'_i = \Delta\mu_{S,i} \left[(n-i)mg\cos\alpha - \sum_{j=i+1}^{n} \sum_{k} F_{k/j,y} \right] \tag{14.19}$$

Equation 14.19 shows that the variation in split ability of an interface (ΔS_i) is equal to the variation in interfaces strength ($\Delta\mu_{S,i}$) multiplied by the normal force underwent by the interface (the sum of (i) the weight, and (ii) the normal component of external forces applied above the considered interface). In other words, the higher the strength of the interface is, the lower its split ability is, i.e. the higher its split function is, as represented on Figure 14.5c. To split the bottommost interface, the coefficients of static friction should thus increase with the height in the stack, as represented on Figure 14.13. It is however important to remind that making such an evolution is technically highly complex because the operator has no control on the frictional properties of the different interfaces.

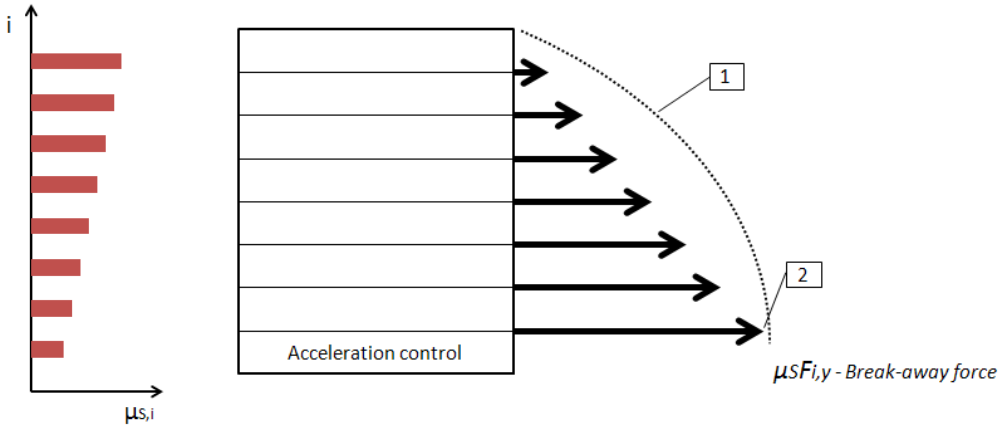

(a) Situation (b) The forces of static friction.

Figure 14.13: Effect of increasing coefficients of static friction with the height in the stack. (1) The break-away forces are modified, and (2) the bottommost interface has a higher probability of split.

Coefficients of kinetic friction We now study the sensibility of the split function S_i of the interface I_i to the coefficients of kinetic friction. Equation 14.5 shows that the split function only depends on the coefficient of kinetic friction of the upper interface. We thus consider two values for the coefficient of kinetic friction of the I_b interface, that are named $\mu_{k,b}$ and $\mu'_{K,b}$, respectively: Based on equation 14.5, we obtain:

$$\Delta S_i = -\Delta\mu_{K,b} \sum_{j=b+1}^{n} (mg\cos\alpha - \sum_{k} F_{k/j,y}) \tag{14.20}$$

The equation shows that the variation in split ability of an interface in the bottommost block (ΔS_i) is equal to the variation in strength of the upper interface of the block ($\Delta\mu_{K,b}$) multiplied by the normal force underwent by this upper interface (the sum of (i) the weight, and (ii) the normal component of external forces applied above the block). In other words, the higher the strength of the sliding interface is, the higher the split ability of the block interfaces is, i.e. the lower their split functions are. However, this influence is equal for all the interfaces in the block, similarly to the action of tangential external forces (see Figures 14.8b and 14.8c). In particular, high coefficients of kinetic friction favor the split of lower interfaces if the acceleration of the block is high ($a_{B,x} > \mu_{S,i} g\cos\alpha$), as represented on Figure 14.8c.

Conclusion The split function of a given interface I_i is influenced by (i) the coefficient of static friction of the considered interface, and (ii) the coefficient of kinetic friction of the upper interface of the block. In a first approach, and to favor the

split of the bottommost interface, we recommend the interfaces with the lower coefficients of static friction to be placed low in the stack. However, low coefficients of static friction are usually associated with low coefficients of kinetic friction and may finally reduce the split ability of the lowest interface. Even if the problem is easily computable using the split functions, a general solution to the problem can be hardly proposed. In particular, we would recommend placing the envelopes so that the coefficients of static friction increase with the position in the stack: low coefficients at the bottom and high coefficients at the top. However, this method is particularly difficult considering that an accurate measurement of all the coefficients of friction is impossible.

14.2.6 Dispersion in masses

Situation and method In non-homogeneous envelope stacks (*mix-mail*), the mass of envelopes often varies from ten to hundreds of grams, depending on their sizes and contents. To study the influence of such variations on the stack splits, we consider a stack of envelopes with constant tilt, frictional properties, external forces, and acceleration control on the bottommost envelope. The split function of the interface I_i is called S_i. We then introduce variations in the mass of an envelope E_e called *singular envelope*: its mass is then called m'_i. The split function of the interface I_i becomes S'_i. We introduce the ΔS_i parameter defined as the difference between the two split functions ($\Delta S_i = S_i - S'_i$). The ΔS_i parameter thus represents the influence of the variations in mass of the singular envelope on the split ability of the considered interface I_i.

The singular envelope is above the block In this paragraph, we consider that the singular envelope is above the bottommost block ($e > b$). Based on equation 14.5, an expression of the ΔS_i parameter becomes:

$$\Delta S_i = S_i - S'_i = (\mu_S - \mu_K) g \cos\alpha (m_i - m_e) \tag{14.21}$$

In this situation, placing an heavy envelope above the bottommost block increases the split function and thus avoids the split of the considered interface I_i. Indeed, heavy envelopes above the bottommost block increase both (i) the force of kinetic friction above the block, and finally the forces of static friction inside the block, and (ii) the break-away forces inside the block. The coefficient of static friction being usually higher than the coefficient of kinetic friction, the increase in break-away force with envelopes mass is higher than the increase in force of kinetic friction. However, the difference between the two coefficients of friction being usually low, the influence of the mass of the singular envelope is low in this situation.

The singular envelope is in the block, above the considered interface We now consider that the singular envelope is above the considered interface I_i but

remains inside the block ($b \geq e > i$). Based on equation 14.5, an expression of the ΔS_i parameter becomes:

$$\Delta S_i = S_i - S'_i = (\mu_S g \cos\alpha - g \sin\alpha - a_{B,x})(m_i - m_e) \tag{14.22}$$

In this situation, we observe that the influence of mass variations on the split ability of the interface I_i depends on the acceleration control:

- At the beginning of the selection process, the acceleration is low ($\mu_S g \cos\alpha - g \sin\alpha > a_{B,x}$). In this situation, placing heavy envelopes above the considered interface but inside the block increases the split function and finally avoids the interface split. Indeed, for low accelerations, the weight of upper envelopes mainly contributes to the break-away force.
- After the first splits, the acceleration is expected to be high ($\mu_S g \cos\alpha - g \sin\alpha < a_{B,x}$). In this situation, heavy envelopes placed above the interface I_i reduce its split function and finally ease its split. Indeed, for high accelerations, the weight of upper envelopes mainly contributes to the inertial component of the force of static friction.

The singular envelope is below the considered interface In this situation, the mass of the singular envelope has no influence on the split of the considered interface: the singular envelope is "masked" by the acceleration control of the block.

Conclusion We clearly showed that the influence of mass dispersion depends on (i) the structure of the stack, and (ii) the acceleration control. However, considering that the main problem we try to solve are the *multiple feedings* met in franking machine feeders, we can limit our study to the case of high accelerations and small blocks at the bottom of the stack. In this situation, it is possible reducing the multiple feedings by placing (i) the light envelopes at the top of the stack, and (ii) the heavy envelopes at the bottom of the stack. We only made a simple qualitative analysis of the influence of mass on the selection process. However, exact calculations can be easily carried out by integrating equation the split functions into a computer program[2].

14.2.7 Conclusion

We studied in this section the case of blocks under acceleration control, for example due to their contact with the franking machine rollers. We showed that the block stability can be studied and computed using the split function described in equation 14.9. This split function shows that different factors affect the block stability: (i) the

[2]Remark: variations in envelopes mass may be associated to variations in thickness and mechanical properties, potentially modifying the selection process reliability.

machine design (acceleration, external forces, and stack tilt), (ii) the envelopes and interface properties (mass of envelopes, coefficients of static, and kinetic friction), and (iii) the structure of the stack (sizes of the stack and of the block). We showed that all those factors have different properties.

The selection process of franking machine feeders we want to improve is mainly based on the split of the bottommost interface of the envelope stack. Different strategies may be based on smart controls of the factors influencing the split function in order to control of the block splits and, for example, favor the split of the bottommost interface.

14.3 Free blocks

14.3.1 Split function

Situation We now consider the case of *free blocks*. Free blocks are defined as blocks that are neither under acceleration nor position control. In franking machine feeders, a typical case of free blocks are blocks above the bottommost block that are not in contact with the vertical plate. Consequently, we can consider that the bottommost interface of a stack in a franking machine feeder is never in a free block. The study of free blocks may thus appear useless for improving the selection process. This assertion is false for two reasons:

- We suggested that the electrical intensity available may be limited. Consequently, the torque applied on the driving rollers may also be limited. In the case of heavy stacks, this limitation may limit the acceleration of the rollers. In this situation, the bottommost block undergoes a constant tangential force from the rollers. The bottommost block can then be considered as a free block.

- New technical systems may be based on a control of the torque applied on the rollers, rather than on their speed.

We thus propose a qualitative study of the dynamics of free blocks. For clarity reasons, we consider the block $B = \{E_a..E_b\}$ as undergoing kinetic friction forces on its bottommost and topmost interfaces. The block is not under acceleration control: in particular, it is not in contact with the rollers or vertical plate of the franking machine feeder.

Split function Combining equations 14.1 and 13.19, an expression of the split function is:

$$S_i = \mu_{S,i} F_{i,y} - \frac{1}{\sum_{j=a}^{b} m_j} \left| \sum_{j=i+1}^{b} m_j F_{a-1,x} + \sum_{j=a}^{i} m_j F_{b,x} + e(i) \right| \tag{14.23}$$

Where $e(i)$ characterizes the asymmetry in tangential external forces above and below the interface I_i. The $e(i)$ function is defined by:

$$e(i) = \sum_{j=i+1}^{b} m_j \sum_{j=a}^{i} \sum_{k} F_{k/j,x} - \sum_{j=a}^{i} m_j \sum_{j=i+1}^{b} \sum_{k} F_{k/j,x} \tag{14.24}$$

Reduced expression In the case of a homogeneous-mail stack undergoing no external forces, the split function is simplified as follows:

$$S_i = mg\cos\alpha(\mu_S - \mu_K)(n-i) \tag{14.25}$$

To permit the split of the block ($S_i = 0$), the coefficients of static and kinetic friction must be equal ($\mu_S = \mu_K$). This case being not observed for homogeneous-mail, the block should not split in the absence of external forces or sticking with other blocks. This situation is represented on Figure 14.14a. This stability of the free blocks is of particular interest for the stack dynamics: after their creation, blocks usually do not split again and the study of stack dynamics is greatly simplified. We now propose a quick analysis of the main parameters leading to block splits.

14.3.2 Evolving external forces

The contribution of external forces to the block splits is described by the $e(i)$ function of the split function. Contrary to controlled blocks, an external force applied on a free block has an influence on all the interfaces, as represented on Figure 14.14b. This influence has opposite signs above and below the point of application of the external force. Moreover, the closer the considered interface is from the external force and the higher it undergoes this influence. Applying an external force on a free block thus favors the block split around the point of application of the force.

14.3.3 Evolving stack tilt

For a mix-mail block undergoing no external forces, the split function proposed in equation 14.23 is simplified as follows:

$$\begin{aligned} S_i &= -\frac{g\cos\alpha}{\sum_{j=a}^{b} m_j} \left| \sum_{j=i+1}^{b} m_j \sum_{j=a}^{n} m_j \mu_{K,a-1}\Delta_{a-1} + \sum_{j=a}^{i} m_j \sum_{j=b+1}^{n} m_j \mu_{K,b}\Delta_b \right| \\ &\quad + g\cos\alpha\mu_{S,i} \sum_{j=i+1}^{n} m_j \end{aligned} \tag{14.26}$$

We clearly observe that the split function (S_i) is a function of the stack tilt (α). The higher the tilt is, the closer the forces of static friction and the break-away forces are and finally, the weaker the interfaces become. However, the condition for block

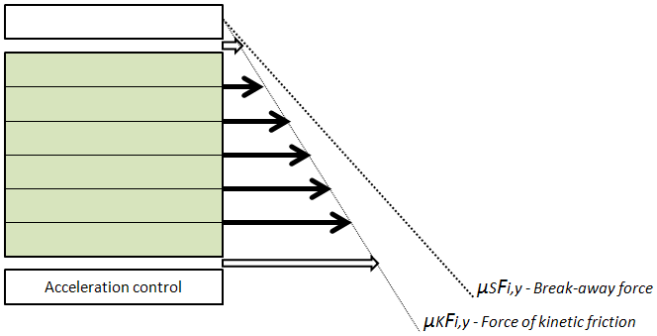

(a) The block undergoes forces of kinetic friction on its top and bottom interfaces. In the case of a homogeneous stack, the forces of static friction inside the block are thus proportional to the coefficient of kinetic friction. No force of static friction reaches the break-away force.

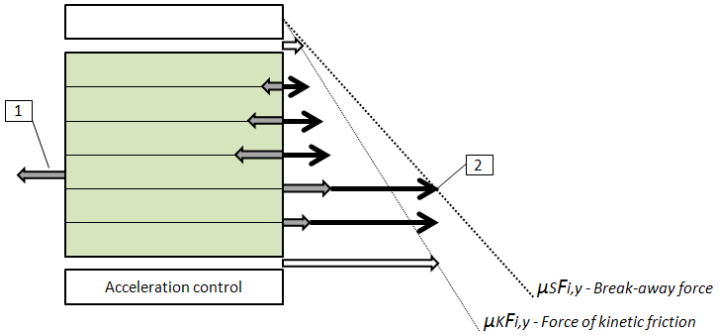

(b) (1) External backward force applied on an envelope of the block. The external force contributes to the forces of static friction and some interfaces may reach their break-away force, in particular the interface just below the external force (2). For forward forces, the situation is reversed and the split should occur just above the external force.

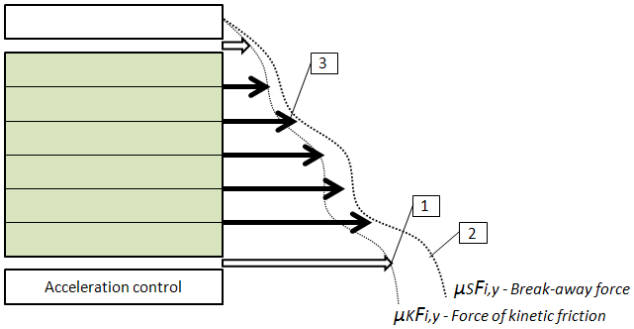

(c) In the case of a heterogeneous stack, the coefficients of kinetic and static frictions vary (1) (2). Some interfaces inside the block may thus reach their break-away force and slip (3). This situation is however unlikely, because it usually means that the considered interface is weaker than the upper and lower interfaces and may thus have split first.

Figure 14.14: Static friction forces in a free block at the middle of an envelope stack. Thin arrows represent the static friction forces. Thick and empty arrows represent the kinetic friction forces. Thick and full arrows represent the external forces and their contribution to the static friction forces.

split ($S_i = 0$) is no more a function of the stack tilt. In conclusion, tilting the stack is not sufficient to permit the block split and also does not favor a specific location of the split. Tilting the stack however weakens the block interfaces, so that external forces can more easily split the block.

14.3.4 Dispersion of frictional properties

Similarly to blocks under acceleration control, the coefficients of static friction may vary along the stack. Low coefficients of static friction then create weak points where the block splits become likely, as represented on Figure 14.14c. The split function being easily computable, the exact determination of the positions of the block splits is easy. However, in the absence of external forces, the split of the block is unlikely because the coefficient of static friction of the considered interface should be lower than the coefficients of kinetic friction of the boundary interfaces. A free block is thus expected to remain stable in the absence of external forces.

14.3.5 Dispersion in masses

Method The influence of a dispersion in masses on the free block splits could be studied using the same method and formalisms than those used for blocks under acceleration control (see chapter 14.2.6). However, this method would lead to complex expression of the ΔS_i parameter. We thus propose a simple graphical and qualitative analysis of this influence.

Situation We study the case of a vertical envelope stack with homogeneous frictional properties and without external forces. The forces of static and kinetic friction were represented on Figure 14.14a. We can easily imagine that placing an heavy envelope in the stack is like gluing some of those envelopes together. By extension, placing a light envelope in the stack is like placing a thinner envelope with the same density. In the following paragraphs, we will use the concept of *singular envelope* presented in chapter 14.2.6: a singular envelope is an envelope introduced in a homogeneous stack, the mass of the singular envelope being different from the mass of other envelopes.

Absence of external forces The force of static friction, the break-away force, and the split function of an interface are not modified by the mass of a singular envelope placed below this interface, as represented on Figures 14.15a and 14.15b. However, placing the singular envelope above the considered interface modifies the force of static friction, the break-away force and the split function of the considered interface, as represented on Figure 14.15b. Those modifications can be assimilated to the insertion or removal of envelopes in the stack. Consequently, the forces of static friction and break-away forces remain proportional to the coefficient of kinetic friction.

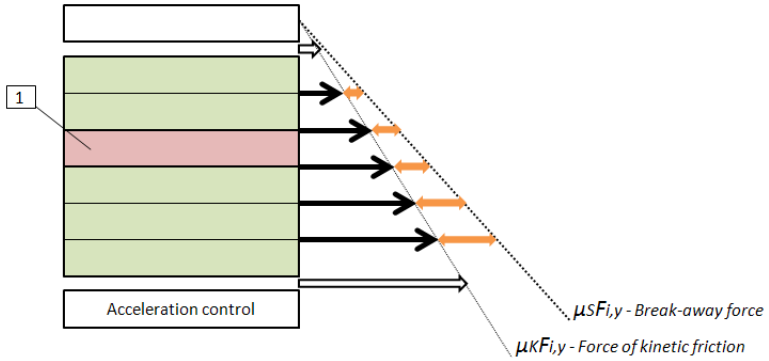

(a) (1) The singular envelope has the same mass than the other envelopes.

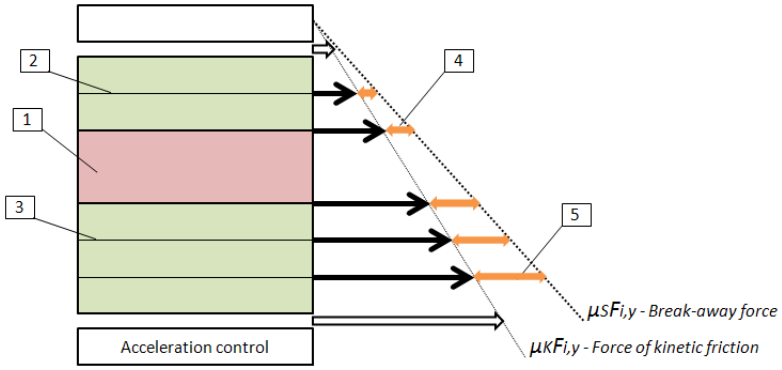

(b) (1) The singular envelope has a mass that is twice the mass of other envelopes. The force of static friction (2) and the split function (4) of the interfaces above the heavy singular envelope remain unchanged. The force of static friction (3) and the split function (5) of the interfaces below the heavy singular envelope increase linearly.

Figure 14.15: Static friction forces in a free block at the middle of an envelope stack. Thin arrows represent the static friction forces. Thick and empty arrows represent the kinetic friction forces. Thick and full double arrows represent the split functions, i.e. the force required to make the interface split.

Consequences on block splits In the case of a homogeneous stack without external forces, a modification in the mass of the singular envelope is not sufficient to permit a block split. In the case of a dispersion in frictional properties, the weak points thus remain the same with changing masses, as represented on Figure 14.14c. To finish with, the external forces required to make an interface split are proportional to the split functions of the interfaces. In the previous paragraph, we observed that the split functions of the interfaces below the singular envelope are proportional to the mass of the singular envelope. The force required to split an interface below the singular envelope is thus proportional to the mass of this envelope.

Conclusion In conclusion, the dispersion in masses has no influence on the stability of the free block, except in the case of external forces. We thus consider the masses dispersion as a minor factor of the free blocks stability.

14.3.6 Conclusion

In this section, we studied the case of free blocks, i.e. blocks that are neither in acceleration nor position control. In franking machine feeders, free blocks are typically the blocks that are in contact with neither the rollers nor the vertical plate. They therefore have a limited interest for the selection process. However, we showed that the electrical intensity being limited, the acceleration of the driving rollers may be reduced in the case of heavy stacks. The bottommost blocks of heavy stacks could then be considered as free blocks. Similarly, new mechanisms may involve rollers under torque control rather than position control. Consequently, it appeared interesting to give a quick understanding of the mechanisms involved in the split of free blocks and their differences with blocks under acceleration control. We observed that the same factors are involved in the block split, but their influence is slightly different. New strategies based on a smart control of those factors should thus be developed.

14.4 Validation of the model

14.4.1 Materials and methods

Goal We propose a qualitative experimental validation of the model. A quantitative analysis was impossible due to the number of parameters that could not be controlled. In particular, it was impossible to measure all the coefficients of friction, in particular because they are modified by the measurement itself. We thus qualitatively characterized the split of a stack under various conditions and compared those results to the ones obtained with the model.

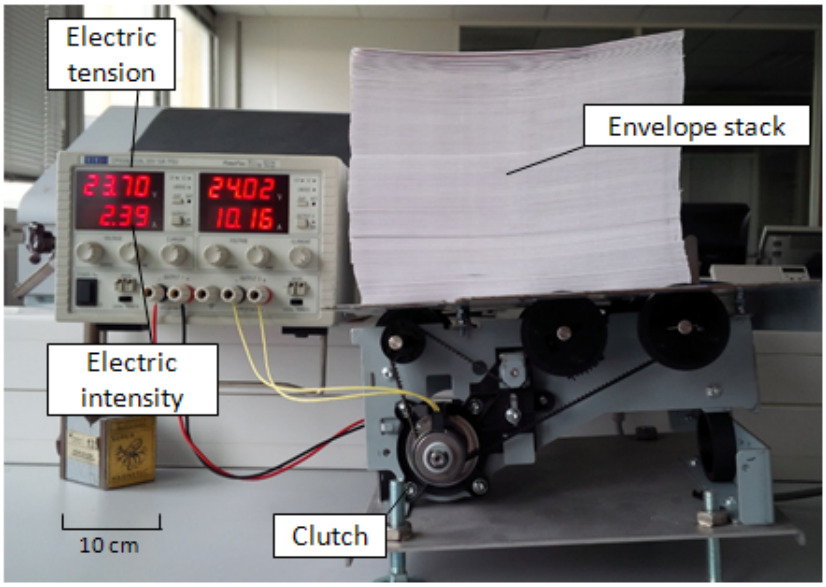

Figure 14.16: Equipment used to qualitatively verify the model. An envelope stack is placed on driving rollers. The rollers are mounted on a clutch.

Materials We studied 300 envelopes of type C4 FR 12957, filled with one sheet of paper and weighting 10 g each. The coefficients of static and kinetic friction were measured (0.54 and 0.43, standard deviation 5 %, see chapter 11.1). We ensured that the envelopes did not present apparent defects.

Method We used the mechanism of a franking machine hopper. The mechanism was powered with the nominal tension of the motor (24 V, max 3 A). The clutches were activated during approximately 0.3 s and then deactivated. We then measured the height of the interfaces that clearly slide (displacement of more than 10 mm). The experiment was carried out 10 times for each experiment. After each experiment, the envelopes that slide were removed from the stack.

Experiments The so-called standard experiment consists in placing 150 envelopes on the horizontal hopper, as represented on Figure 14.16. No external force was applied on the stack. We then carried out four different experiments intended at verifying the theoretical results obtained with the model:

- The number of envelopes is increased from 150 to 300.
- A vertical plate is placed in front of the stack, avoiding the displacement of its upper part.
- The hopper is tilted of an angle α, as represented on Figure 12.1.

- A different envelope is placed at different positions in the stack.

The results of those experiments are compared to the conclusions of the model, as described in this chapter.

14.4.2 Results and discussion

Standard experiment A typical result of the standard experiment is represented on Figure 14.17a. We observe a relative displacement between 4 apparent blocks, the two lower blocks being single envelopes. In particular, the lower interface splits quite every time. The whole stack moved from about 30 cm, while the relative displacement between blocks was roughly equal to 3 cm. This result is consistent with the theory: the topmost block undergoes an acceleration of $\mu_K g \approx 5$ m.s^{-2}. It thus reaches the nominal speed (1 m.s^{-1}) in 0.2 s. The average speed of the topmost block during this transient period was 0.5 m.s^{-1}. The transient period lasting 0.2 s, the topmost block thus had a relative displacement to the bottommost block of about 10 cm. This relative displacement between blocks is low, highlighting the role of systems reducing the blocks displacement (e.g. gates or friction pads).

As the dispersion in the positions and number of splits was high, the cumulative number of splits on 10 experiments is represented on Figure 14.17b for clarity reasons. We observe two distinct areas. The first area consists in interfaces between the tenth and the topmost one. We observe that the higher an interface is, the fewer splits occurred above this interface. The decrease is quite linear, suggesting that splits above the tenth interface occurred randomly. This result supports the conclusion of chapter 14.2.2 concerning the first split of a stack under acceleration control. The second area consists in interfaces below the tenth interface. We observe that the number of splits sharply increased, from 13 to 29. In other words, between 1 and 2 splits statistically occur between the first and tenth interfaces. This result supports the conclusion of chapter 14.2.2 concerning the splits after the first split of a stack under acceleration control. This analysis is only semi-quantitative, but it supports the main trends of our model of stack dynamics for a stack under acceleration control.

Heavy stacks When placing 300 envelopes on the hopper, we observed only one split, as represented on Figure 14.18. This critical situation was not predicted by the model. Different causes can lead to this situation. In particular, the weight of the stack increasing, the required electric power increases but remains limited by the power supply. The acceleration actually delivered by rollers could thus be significantely reduced, reducing the split of I_1.

Tangential external force By placing a vertical plate in contact to the stack, we observed that the split mainly occurs just below this plate, as predicted by the model. In particular, a vertical plate does not favor the split of the bottommost

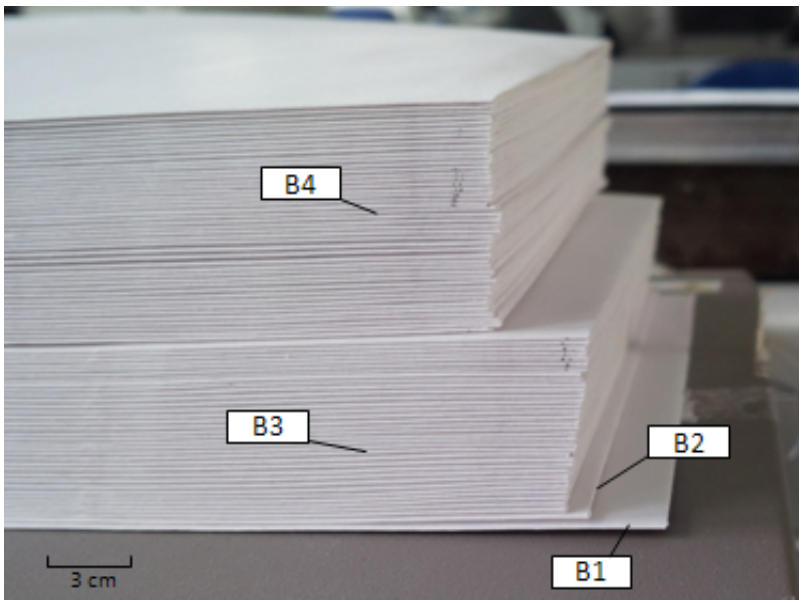

(a) Typical structure of the stack at the end of the experiment. The figure clearly shows that 4 blocks appeared in the stack (called $B1$, $B2$, $B3$ and $B4$), the two bottommost blocks being single envelopes.

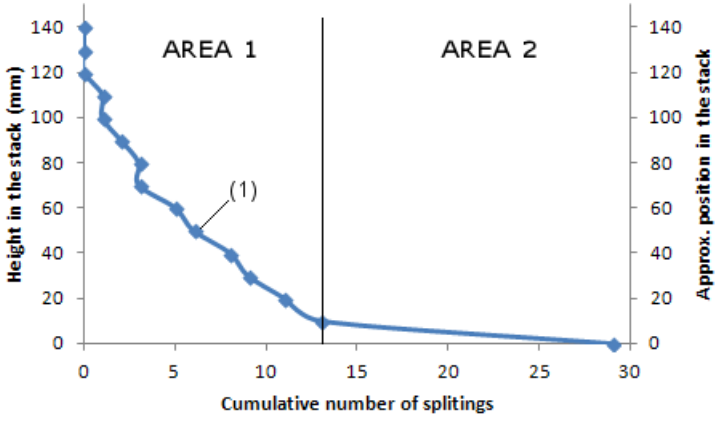

(b) Number of splits in a 150 envelopes stack from the top to a considered height in the stack. The number is cumulated on 10 experiments. For example, the value represented at the point (1) represents the number of splits observed above this height in the 10 experiments we carried out. Two different trends are observed and represented by area 1 and area 2, respectively. The number of envelopes above an interface is evaluated based on the envelopes compressibility described in annex D.

Figure 14.17: Results of the experiment with 150 envelopes.

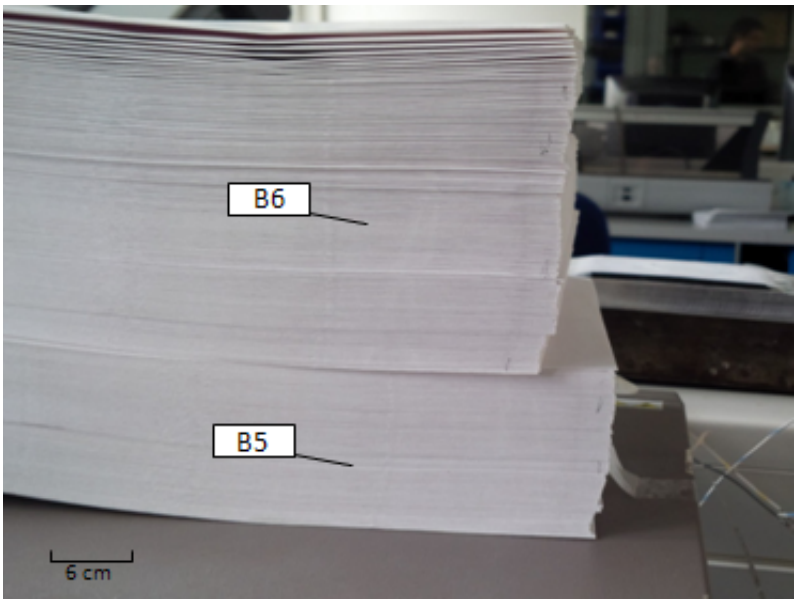

Figure 14.18: Typical structure of the stack at the end of the experiment with 300 envelopes in the hopper.

interface. However, when a gap was initially created between the plate and the stack, splits sometime occurred far below the contact point. Indeed, when creating an initial gap between the plate and the stack, the first splits are due to acceleration. As observed in the experiment, the splits may thus occur far below the contact point.

Stack tilt By making the angle between the hopper and the horizontal vary from 0° to 45°, we observed the same results than the previous experiment. Indeed, a split at the bottom of the stack is favored. For $\alpha \approx 30°$, the stack splits before the rollers are even powered. This result confirms the inclined plane test method results. This phenomenon makes the stabilization of the stack difficult: a vertical plate placed behind the stack permits its stabilization but adds an external forward force that modifies the balance of forces. The blocks above the bottommost one tend to remain at their initial position, easing the fulfillment the condition 2 of a correct feeding (see chapter 12.3).

Dispersion in frictional properties When placing an envelope of a different type in the middle of the stack, we systematically obtained a split above the considered envelope. We suppose that the coefficient of static friction at this interface was lower than at the other interfaces. The result thus confirms the model.

Final remark To finish with, we observed that when not removing the envelopes that slide, the split was eased at this interface during the next experiments. This observation is explained considering that coefficient of static friction was low due to (i) the initial "weakness" of the interface (low coefficient of static friction), and (ii) a decrease associated to repeated slides in the same direction.

14.4.3 Conclusion

The experiments show how difficult it is predicting the exact way a stack will split, so that quantitative model validations are difficult. The results of our experiments however confirm the main conclusions of the model. The acceleration of rollers appears to be a major parameter of stack splitting, as highlighted by literature in the case of top feeders [101, 102]. In particular, it can be sufficient to split the bottommost interface in the case of low or medium stacks.

A deeper analysis should however be carried out, in particular by controlling and measuring the acceleration of rollers under various conditions. It would be also very interesting to measure the tangential external force applied by the vertical plate on the stack under various conditions.

Summary and Conclusion of Chapter 14

Split function For a given interface, we defined the split function as the difference between its break-away force and force of static friction. The function is positive and becomes zero when the interface starts to slide.

Stack dynamics model The split function of an interface is strongly linked to all the other interfaces. To model the stack dynamics, we thus have to study the stack splits chronologically. This complex task can be achieved using a computer program. In addition, we studied the main principles governing the stack splits.

Blocks under acceleration control The selection process relies on the split of the bottommost block. This block is usually under acceleration control by the feeder's driving rollers. The split function (see equation 14.9) then depends on:

- **Machine design -** Those parameters are the rollers acceleration, the external forces, and the stack tilt. They are controlled by the machine. We fully characterized their influence on the selection process. In particular, for low rollers accelerations or stack tilt, external forces favor the split of interfaces around the application point of the force. For high accelerations, the first split is random and the next splits usually occur at the bottom of the stack.
- **Interface and envelopes properties -** Those parameters are the frictional properties of the interfaces and the weight of the envelopes. Those parameters are nearly impossible to control but remain roughly constant during the selection process. To favor the split of the block at its bottom, we recommend placing weak interfaces and heavy envelopes low in the stack.
- **Structure of the stack -** The size of the stack and the block size are major parameters of the block split. They are nearly impossible to control, evolve during the selection process, but are predictable.

Free blocks Blocks may be under no acceleration or position control. In this situation, they only undergo forces of kinetic friction on their boundaries. A typical example consists in the blocks above the bottommost block that are in contact with no external system. In this situation, the split function was given by equation 14.23.

Validation of the model We carried out a qualitative validation of the model that supported the conclusions of the model. We confirmed the influence of rollers acceleration, tangential external forces, stack tilt, interfaces properties, and envelopes properties on the stack dynamics. We however observed too few splits in heavy stacks. This issue may be due to a reduction in rollers acceleration.

Chapter 15

Improving envelopes feeding

We want to improve the reliability of the franking machine feeders. To do so, we first formalized the three conditions permitting a correct feeding. We then developed a model that characterizes the behavior of an envelope stack under various test conditions. The goal is now to use the model to deduce the solutions permitting the fulfillment of the correct feeding conditions. We will conclude by using this knowledge in the case of friction pads.

15.1 Feeding envelopes (Condition 1)

Description The condition 1 for a correct feeding guarantees that the bottommost envelope is fed into the machine (see chapter 12.3). In current franking machine feeders, the bottommost envelope is in contact with driving rollers or belts. Moreover, the condition 3 of a correct feeding requires that the bottommost envelope always sticks on rollers. Consequently, to guarantee that the bottommost envelope is fed into the machine, we just have to ensure that the evolution of the rollers speed is adapted to such a displacement.

Mathematical expression Rollers are controlled in velocity by a proportional-integral-derivate controller (PID): the evolution of their velocity and acceleration is defined and controlled. As the bottommost envelope is sticking on the rollers, its position $x_1(t)$ is given by:

$$\forall t, x_1(t) \quad = \quad \iint_0^t a_R \mathrm{d}t \tag{15.1}$$

With a_R representing the acceleration of rollers. To ensure that the bottommost envelope is driven out of the feeder, the total displacement of the rollers during a given period t_f thus has to be higher than the length of the bottommost envelope

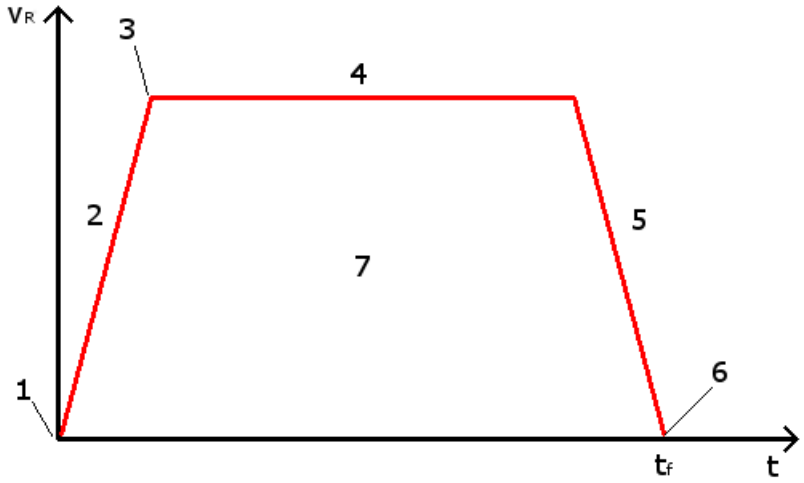

Figure 15.1: Simplified evolution of the rollers speed (v_R) during the feeding of the bottommost envelope. At the beginning of the process, the rollers start moving (1). They reach their nominal acceleration (2) (approx. 100 m.s^{-2}). The rollers decelerate (3) as they reach their nominal speed (4): the pseudo-oscillations in rollers speed due to the speed control are not represented here. At the end of the process, the rollers decelerate (5) before stopping at a time t_f (6). The macroscopic displacement of the bottommost envelope occurs during the phases 2, 4, and 5. During these phases, the displacement of envelopes makes the external forces evolve. The area under the curve (7) corresponds to the total displacement of rollers during the selection process: the condition 1 for correct feedings supposes this area to be greater than the length of the bottommost envelope.

(L_1):

$$\iint_0^{t_f} a_R \mathrm{d}t \quad > \quad L_1 \tag{15.2}$$

The period t_f represents the duration of the selection process and may evolve with the length of the bottommost envelope. This condition is summarized on figure 15.1: the area under the curve of the rollers velocity has to be higher than the length of the bottommost envelope.

Numerical application On franking machines, we observed a rollers acceleration of $a_R = 100$ m.s^{-2} and a maximal speed of $v_R \approx 1.2$ m.s^{-1}. The goal is to obtain a displacement of the rollers equal to (L_1 + gap) ≈ 0.3 m. Basic considerations show that the duration of the step is $\left[\frac{L_1}{V_R} + V_R/(2.a_R)\right] = 0.3$ s. This duration is compatible with the 3 Hz throughput of the machine usually observed.

15.2 Split of the bottommost interface

15.2.1 General approach

Problem Condition 2 for a correct feeding requires the envelopes above the bottommost one not to move into the feeder. Because the feeding condition (condition 1) supposes the forward displacement of the bottommost envelope, the split of the bottommost interface is required (i.e. the interface between the first and second envelopes). In this section, we will study the fulfillment of this prior condition to conditions 1 and 2.

Parameters involved As observed in the previous chapter, the stack split is due to an evolution of (i) the acceleration control, (ii) the external forces, or (iii) the stack tilt. In the case of franking machine feeders, those parameters evolve as follows:

1. The acceleration increases, as represented by step 1 on Figure 15.1. In current machine designs, the initial acceleration of rollers is imposed. During this step, the external forces and stack tilt applied on the stack remain constant. First splits can occur.

2. As far as the rollers velocity is positive, the movement of envelopes is macroscopic, as represented by steps 2, 4 and 5 on Figure 15.1. Envelopes' deformations and mobile mechanisms create increasing tangential external forces. These external forces can lead to new splits within the stack.

3. The acceleration decreases because the rollers reached their maximal velocity, as represented by step 3 on Figure 15.1.

4. At the end of the process, the bottommost envelope escaped from the feeder. The rollers slow down and the stack comes back to an immobile state, as represented by steps 5 and 6 on Figure 15.1, respectively.

Consequently, on current franking machine feeders, the split of the bottommost interface is first induced by an increase in rollers acceleration and then by an increase in external forces. In the following sections, we show how those different steps induce block splits.

15.2.2 Generation of the first split

Probability At the beginning of the selection process, the whole stack constitutes a single static block. With the increase in acceleration control, the stack interfaces undergo increasing shearing strengths. In particular, the first split of a homogeneous stack occurs when the rollers acceleration reaches the critical acceleration $A = \mu_S g$, with μ_S representing the coefficient of static friction between envelopes. We proposed to consider a coefficient of static friction between envelopes of 0.6. A typical

value of this acceleration is therefore 6 $m.s^{-2}$. This critical acceleration is far lower than the 100 $m.s^{-2}$ acceleration measured on franking machines. Consequently, the acceleration of the driving rollers of franking machines feeders is sufficient to permit this first split.

Position However, the position of this split is difficult to predict. In the case of a homogeneous mail, the split may occur everywhere in the stack, as shown on Figure 14.5a. Considering varying coefficients of static friction however, the split may typically occur at the interface having the lower coefficient of static friction. Considering now that an external force is applied somewhere on the stack, the situation is quite different as shown in 14.2.3. Basically, considering that we apply a backward and/or upward force on a given envelope, the split should occur below this envelope.

Role in envelopes' selection The coefficients of friction of the envelopes are not controlled. Moreover, applying the external force specifically on the second envelope is difficult because of the low and varying envelopes' thickness. It is therefore unlikely that the first split of the envelope stack appears at the bottommost interface and several splits may be required before the split of the bottommost interface becomes possible. Controlling the position of the first split can however favor a correct selection. Indeed, we deduced from the previous chapter that the size of the bottommost block is a major parameter of the split of the bottommost interface. Controlling the position of the first split (e.g. by a smart use of external forces) thus permits the control of the size of the bottommost block and can finally favor the split of the bottommost interface.

15.2.3 Methods for splitting the bottommost interface

15.2.3.1 General situation

After the first split, the stack is divided in at least two blocks. The bottomost block undergoes an acceleration control on its bottom and a kinetic friction on its top. As observed in chapter 14.2.2, in the absence of external forces and considering a homogeneous mail stack, the next split should occur at the bottom of the block. However, varying frictional properties may lead to a split of the block above the bottommost interface. Moreover, the required acceleration may overcome the technological limits (measured at 100 $m.s^{-2}$). Several other methods however permit an improved control of the bottommost interface split.

15.2.3.2 Very high rollers acceleration

From a theoretical point of view, we deduced from chapter 14.2.2 that an increasing acceleration is sufficient to permit the split of the bottommost interface. Equation

14.10 characterizes the acceleration required to make a given interface split. The most critical case for splitting the bottommost interface consists in having the two bottommost envelopes forming a single block ($b = 2$) in a vertical homogeneous stack without external forces. In this situation, the acceleration required to split the bottommost interface is expressed as:

$$A(1) = \mu_S g + (n-2)(\mu_S - \mu_K)g \tag{15.3}$$

Numerical applications are represented on Table 15.1.

Cases	A	B	C	D
Size of the stack, n	300	**98**	300	300
COSF, μ_S	0.6	0.6	**0.65**	0.6
COKF, μ_K	0.5	0.5	0.5	**0.45**
Required acceleration, $A(1)$ (m.s^{-2})	298	100	445	444

Table 15.1: Numerical applications for the maximum acceleration required to split the bottommost interface of a vertical homogeneous stack without external forces. COSF and COKF stand for coefficients of static and kinetic friction, respectively.

In the case we studied (300 envelopes, $\mu_S = 0.6$ and $\mu_K = 0.5$), the acceleration required to split a bottommost block composed of two envelopes is 300 m.s^{-2} (case A on Table 15.1). This acceleration is far higher than the rollers acceleration available on franking machine feeders (approx. 100 m.s^{-2}). The limit in stack size associated to the current franking machines is therefore 98 envelopes (case B on Table 15.1). The situation worsen when considering higher coefficients of static friction or lower coefficients of kinetic friction: an increase of +10 % increases the required acceleration by a factor of +50 %. Those values are technically far from those obtained on current franking machines but could be reached in the future. For the moment, other methods are required to ease the split of the bottommost interface.

15.2.3.3 Creation of a reduced block

Introducing the method We previously observed that the acceleration control is a useful but limited method favoring the split of the bottommost interface. An improved method consists in forcing the creation of a reduced bottommost block. The size of this reduced block is so that (i) the available acceleration becomes sufficient to split the first interface, and (ii) no interface above the bottommost one is split. The creation of such a reduced block is made possible by the use of a vertical plate for example. We now propose a determination of the size of the reduced block required.

Minimum size of the bottommost block First of all, the available acceleration being limited, a minimum size (b) of the bottommost block is required. Below

this size, the acceleration of the rollers is no more sufficient to permit the split of the bottommost interface, as represented on Figure 15.2c. This minimum size is called b_{min} and can be calculated using the concept of critical acceleration defined in chapter 14.2.2. This concept represents the acceleration control required to make a given interface split, and noted $A(i)$ with i representing the considered interface. The minimum block size permitting the split of the bottommost interface thus verifies $A(1) = a_R$, with a_R the maximal available acceleration of rollers. For example, considering a homogeneous mail without external forces, we obtain:

$$\begin{aligned} A(1) = a_R &\Leftrightarrow \mu_{S_1} g + \frac{n - b_{min}}{b_{min} - 1}(\mu_{S_1} - \mu_{K,b})g = a_R \\ &\Leftrightarrow (n - b_{min}) = (b_{min} - 1)\frac{a_R - \mu_{S_1} g}{g(\mu_{S_1} - \mu_{K,b})} \\ &\Leftrightarrow b_{min}\left(1 + \frac{a_R - \mu_{S_1} g}{g(\mu_{S_1} - \mu_{K,b})}\right) = n + \frac{a_R - \mu_{S_1} g}{g(\mu_{S_1} - \mu_{K,b})} \\ &\Leftrightarrow b_{min} = \frac{n + \frac{a_R - \mu_{S_1} g}{g(\mu_{S_1} - \mu_{K,b})}}{1 + \frac{a_R - \mu_{S_1} g}{g(\mu_{S_1} - \mu_{K,b})}} \end{aligned} \tag{15.4}$$

The nominal acceleration of rollers is very high (approx. 100 m.s^{-2}). We can thus consider that $(a_R - \mu_{S_1} g) \approx a_R$. The equation thus becomes:

$$\begin{aligned} A(1) = a_R &\Leftrightarrow b_{min} \approx \frac{ng(\mu_{S_1} - \mu_{K,b}) + a_R}{g(\mu_{S_1} - \mu_{K,b}) + a_R} \\ &\Leftrightarrow b_{min} \approx 1 + \frac{ng(\mu_{S_1} - \mu_{K,b})}{a_R} \end{aligned} \tag{15.5}$$

For example, considering a stack of n =300 envelopes with coefficients of friction of $\mu_{S,1}$ =0.6 and $\mu_{K,b}$ =0.5 under an acceleration control of a_R =100 m.s^{-2}, we obtain $b_{min} = 4$. In other words, if the bottommost block is smaller than 4 envelopes, then the acceleration control is no more sufficient to permit the split.

Maximum size of the bottommost block On the other hand, the block size (b) is limited by a maximal size (b_{max}) above which an increase in acceleration would split the block above the bottommost interface, as represented on Figure 15.2a. Using the concept of critical acceleration (i.e. the acceleration required to split a given interface), b_{max} is the higher block size so that the bottommost interface has the lower critical acceleration ($\forall i \in \{2..b_{max}\}, A(i) > A(1)$). This size is mainly function of the heterogeneity in coefficients of friction along the block. In particular, we can easily show that the most critical situation consists in having the maximal coefficient of static friction for the bottommost interface and the minimal one for

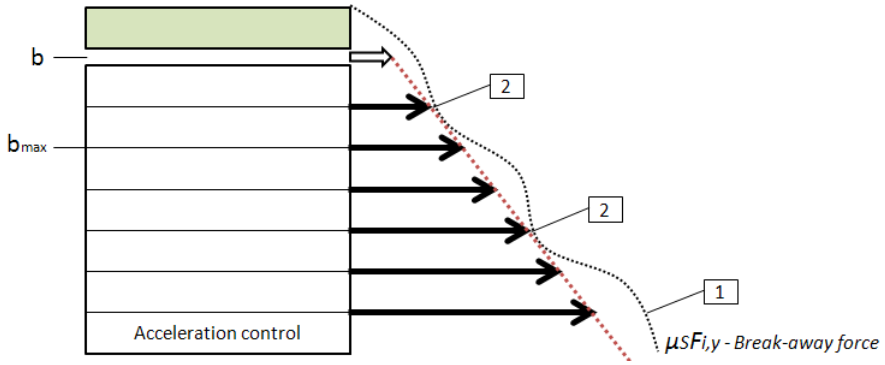

(a) The stack size is higher than the maximal acceptable block size ($b > b_{max}$). In this situation, the block splits above the bottommost interface (2) before the force of static friction of the bottommost interface reaches its break-away force (1).

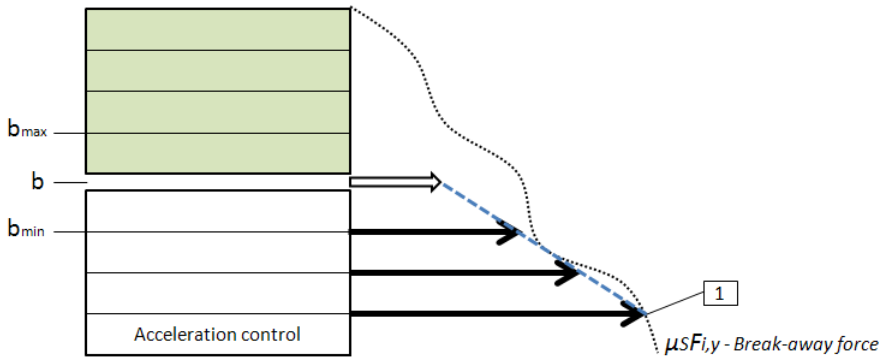

(b) The stack size is between the minimal and maximal acceptable block sizes ($b_{max} > b > b_{min}$). The bottommost interface splits first under increasing acceleration (1).

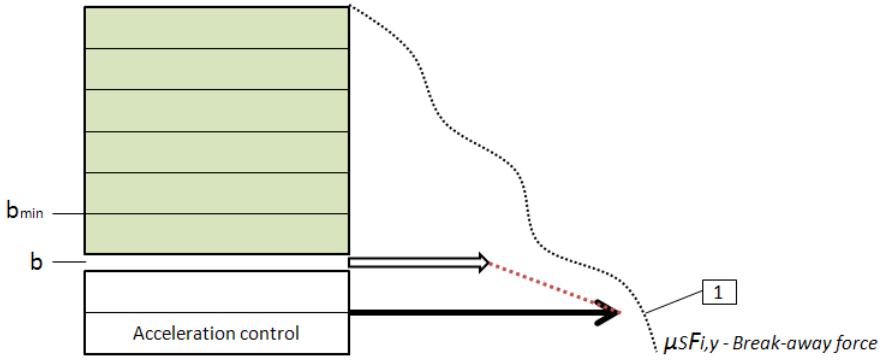

(c) The stack size is lower than the minimal acceptable size ($b < b_{min}$). In this situation, the available acceleration is too low to permit the split of the bottommost interface (1).

Figure 15.2: Influence of the bottommost block size (b) on the split of the bottommost interface (1) in the case of an heterogeneous stack. The block undergoes a force of kinetic friction on its top boundary, represented by thick arrows. The forces of static friction are represented by thin arrows.

the second bottommost interface (I_2). In this situation, we obtain:

$$\begin{aligned}
A(1) = A(2) \quad &\Leftrightarrow \quad \mu_{S,1} + \frac{n - b_{max}}{b_{max} - 1}(\mu_{S,1} - \mu_{K,b}) = \mu_{S,2} + \frac{n - b_{max}}{b_{max} - 2}(\mu_{S,2} - \mu_{K,b}) \\
&\Leftrightarrow \quad \Delta\mu_S = (n - b_{max}) \left(-\frac{\mu_{S,1} - \mu_{K,b}}{b_{max} - 1} + \frac{\mu_{S,2} - \mu_{K,b}}{b_{max} - 2} \right) \\
&\Leftrightarrow \quad \Delta\mu_S = (n - b_{max}) \frac{(b_{max} - 1)\Delta\mu_S + (\mu_{S,1} - \mu_{K,b})}{(b_{max} - 2)(b_{max} - 1)} \\
&\Leftrightarrow \quad \Delta\mu_S(n - 2) = \frac{n - b_{max}}{b_{max} - 1}(\mu_{S,1} - \mu_{K,b}) \\
&\Leftrightarrow \quad \Delta\mu_S = \frac{n - b_{max}}{(b_{max} - 1)(n - 2)}(\mu_{S,1} - \mu_{K,b}) \qquad (15.6)
\end{aligned}$$

Finally, considering that the stack is far greater than the maximal size of the bottommost block ($n >> b_{max}$), the equation becomes:

$$A(1) = A(2) \quad \Leftrightarrow \quad b_{max} \approx 1 + \frac{\mu_{S,1} - \mu_{K,b}}{\Delta\mu_S}$$

Where $\Delta\mu_S = \mu_{S,1} - \mu_{S,2}$. The approximation is valid for $n >> b_{max}$.

Limits in the size of the bottommost block We finally obtain the condition on the bottommost block size (b) permitting the split of the bottommost interface using only the rollers acceleration:

$$1 + \frac{ng}{a_R}(\mu_{S_1} - \mu_{K,b}) \leq b \leq 1 + \frac{1}{\Delta\mu_S}(\mu_{S,1} - \mu_{K,b}) \qquad (15.7)$$

Numerical applications for this condition are summarized on Table 15.2 In particular, on a common printing and writing paper, we measured $\Delta\mu_S \approx 5.10^{-3}$, $\mu_S = 0.6$, and $\mu_K = 0.5$ (see Table 4.2). In this situation, splitting the stack between the 4th and 22th envelopes guarantees that the next split due to an increasing acceleration occurs at the bottommost interface.

Limits to the method This method however depends on numerous parameters. Indeed, considering that the acceleration is reduced for heavy stacks, the domain of validity of the bottommost block size is sharply reduced, as represented by cases B and C on Table 15.2. The domain of validity is also reduced by (i) reducing the gap between coefficients of static and kinetic friction, or (ii) increasing the dispersion in coefficients of static friction, as represented by cases D and E on Table 15.2, respectively. To finish with, the optimal position of the vertical plate strongly depends on the thickness of the envelopes. In conclusion, the proposed method is not adapted to heavy or mix-mail stacks.

Cases	A	B	C	D	E
Rollers acceleration, a_R (m.s^{-2})	100	**20**	100	100	100
Size of the stack, n	300	300	**30**	300	300
COSF, $\mu_{S,1}$	0.6	0.6	0.6	**0.57**	0.6
COKF, $\mu_{K,b}$	0.5	0.5	0.5	**0.53**	0.5
Maximal dispersion in COSF, $\Delta\mu_S$	0.005	0.005	0.005	0.005	**0.05**
Minimal size of the lower block, b_{min}	4	16	2	3	4
Maximal size of the lower block, b_{max}	21	21	21	9	3

Table 15.2: Numerical applications for the conditions in bottommost block size that guarantee the split of the bottommost interface with an increasing acceleration. COSF and COKF stand for coefficients of static and kinetic friction, respectively.

Conclusion We propose to place the vertical plate at a position of approximately 5 or 6 envelopes. Due to the variations in envelopes thickness, we propose to make this position adjustable by the machine operator.

15.2.3.4 Stack tilt

In the previous chapter, we observed that a pronounced stack tilt favors the split of the bottommost interface by (i) creating a tangential component of the weight, and (ii) reducing the break-away forces of the block interfaces. In particular, the second point permits huge reductions of break-away forces in the case of heavy stacks. An expression of the stack tilt required to split a given interface was given by equation 14.16.
To characterize the interest of such a method for the selection process, we study the critical case consisting in a bottommost block composed of two envelopes. In this situation, and considering a homogeneous stack undergoing no external forces, the tilt (α) required to make a bottommost block split is described by:

$$\cos(\alpha + \theta_1) = \frac{a_{B,x}}{L_{\theta,1}.g} \tag{15.8}$$

With θ and $L_{\theta,1}$ defined by:

$$\begin{cases} L_{\theta,1} = \sqrt{\left(\mu_S(n-1) - \mu_K(n-2)\right)^2 + 1} \\ L_{\theta,1}\cos\theta_1 = \mu_S(n-1) - \mu_K(n-2) \\ L_{\theta,1}\sin\theta_1 = 1 \end{cases} \tag{15.9}$$

Some numerical applications are proposed on Table 15.3.

Cases	A	B	C	D	E
Size of the stack, n	300	300	300	300	300
Rollers acceleration, a_R (m.s^{-2})	100	**200**	**250**	**250**	**250**
COSF, μ_S	0.6	0.6	0.6	**0.65**	0.6
COKF, μ_K	0.5	0.5	0.5	0.5	**0.45**
Required stack tilt, α (°)	69	46	31	55	55

Table 15.3: Numerical applications for the stack tilt that permits the split of the bottommost interface with an increasing acceleration. COSF and COKF stand for coefficients of static and kinetic friction, respectively.

In the studied case (case A of Table 15.3), a stack tilt of 69° is required to split a bottommost block composed of two envelopes. This tilt may be too high for technological applications. Therefore, this method appears not sufficient for the selection process. The cases B and C represented on Table 15.3 however show that the stack tilt may be of particular interest for high rollers acceleration available: a tilt of 45° is technically possible and would reduce the required acceleration from about 33 %. Increasing the rollers acceleration being a complex task, an increase in stack tilt appears as a simple and interesting solution for improving the selection process. The required stack tilt however still strongly depends on the dispersion in coefficients of static and kinetic friction, as represented by cases D and E on Table 15.3, respectively.
In conclusion, a stack tilt favors the split of the bottommost interface and could be used in addition of other methods. New concepts of franking machines could thus benefit from this influence, but the whole franking machine would have to be adapted (see chapter 14.2.4).

15.2.3.5 External forces

Introduction We proposed several methods to split the bottommost interface. However, the acceleration control, the creation of a reduced block, and the stack tilt were unable to process a bottommost block composed of two envelopes. We propose now to study how external forces could contribute to the process of such a critical case.

Expression of the required external force The contribution of external forces to the split of the bottommost interface was described by equation 14.14, simplified in the case of a vertical stack with homogeneous mass to equation 14.15. Considering a bottommost block composed of two envelopes, the expression of the external force required to split the block becomes:

$$\begin{cases} F_{c,e,y} = \frac{\mu_S g - a_{B,x}}{\mu_S - \mu_K} m + (n-2)mg & \text{if } e > 2 \\ F_{c,e} \cos(\rho_1 + \beta_e) = \frac{(a_{B,x} - \mu_S g)m - (\mu_S - \mu_K)(n-2)mg}{\sqrt{\mu_S^2 + 1}} & \text{if } e = 2 \end{cases} \tag{15.10}$$

With e, $F_{c,e}$, β_e, and ρ_1 representing the position of the point of application of the force on the stack, the norm, and orientation of the external force and the strength of the bottommost interface, respectively. The influence of the external force on the bottommost block split differs depending on the point of application of the external force.

External force applied above the bottommost block Some numerical applications are proposed on Table 15.4 in the case of an external force applied above the bottommost block. In the studied situation (case A in Table 15.4), the normal external force required is equal to 20 N (approx. 2 kg), oriented upward. To apply such a force on envelopes, asperities may be added to the vertical plate. This contribution is strongly influenced by the stack size (case B), the rollers acceleration (case C), and the coefficients of static and kinetic friction (cases D and E, respectively).

Cases	A	B	C	D	E	F
Size of the stack, n	300	**200**	300	300	300	300
Rollers acceleration, a_R (m.s^{-2})	100	100	**200**	100	100	100
COSF, μ_S	0,6	0,6	0,6	**0,65**	0,6	0,6
COKF, μ_K	0,5	0,5	0,5	0,5	**0,45**	0,5
Mass of the envelopes, m (g)	10	10	10	10	10	**20**
Normal external force, $F_{c,e,y}$ (N)	20	10	10	23	23	40

Table 15.4: Numerical applications for the normal external force, $F_{c,e,y}$, that permits the split of the block. The normal external force is applied above a bottommost block of two envelopes. COSF and COKF stand for coefficients of static and kinetic friction.

External force applied on the second envelope Some numerical applications are also proposed on Table 15.5 in the case of an external force applied on the second envelope. The norms of the required external force are much reduced compared to the case of a normal external force applied above the bottommost block (about 10 times lower). However, we observe same trends with variations in stack size, rollers acceleration, frictional properties, and envelopes mass (cases B, C, D, E and F). The orientation of the external force influences the norm of the required external force (cases G et H). The norm of the force is minimal for an orientation verifying:

$$\beta_e = \pi - \rho_1 \tag{15.11}$$

In the studied case, this angle is 149° and represented by case G on Table 15.5. This angle may be reached by using (i) high pads-on-paper coefficients of friction and/or (ii) high orientation of the pad to the horizontal (very low angle γ). We also represented the case of an external force oriented upward (case H): we clearly

observe that the norm of the required force is high (3.3 N) but much lower than the norm required if the force was applied above the bottommost block.

Cases	A	B	C	D	E	F	G	H
Size of the stack, n	300	**200**	300	300	300	300	300	300
Rollers acc., a_R ($m.s^{-2}$)	100	100	**200**	100	100	100	100	100
COSF, μS	0.60	0.60	0.60	**0.65**	0.60	0.60	0.60	0.60
COKF, μK	0.50	0.50	0.50	0.50	**0.45**	0.50	0.50	0.50
Envelopes mass, m (g)	10	10	10	10	10	**20**	10	10
Orient. of the force, β_e (°)	180	180	180	180	180	180	**149**	**90**
"Strength" of I_1, ρ_1 (°)	31	31	31	33	31	31	31	31
External force, $F_{c,e}$ (N)	2.0	1.0	1.0	3.4	3.4	4.0	1.7	3.3

Table 15.5: Numerical applications for the external force that permits the split of the bottommost interface. The external force is applied on the second envelope. COSF and COKF stand for coefficients of static and kinetic friction.

Conclusion Applying the external force on the second bottommost envelope thus appears as an interesting solution for splitting the bottommost interface. However, applying the external force on this specific envelope is difficult, the thickness of envelopes varying and being low. We thus recommend applying external forces oriented backward and/or upward on the bottom of the stack. The force must be applied as low as possible in the stack, but should not prevent the displacement of the bottommost envelope.

15.2.3.6 Other methods

We proposed several other methods intended at favoring the split of the bottommost interface. In particular, the machine operator should be aware that placing heavy envelopes low in the stack favors the selection process.
Placing the lowest coefficients of friction low in the stack also favors separation. However, this method is not practicable as it would be time consuming.
The selection process would also benefit from an increase in coefficients of kinetic friction and a reduction in coefficients of static friction of the bottommost interfaces. However, the modification of frictional properties is a complex task. For example, the use of modified humidities or temperatures is an expensive solution with high latencies.
The last solution we recommend consists in reducing the dispersion in frictional properties within the stack. In particular, the machine operator has to ensure that the envelopes have the same frictional histories and were stored in the same environmental conditions. For more details on the factors influencing those frictional properties, the reader is invited to refer to the part II. An interesting (but hypo-

thetical) solution would consist in applying repeated tangential oscillations of the bottommost envelope. The stack would thus split on its weaker interfaces. Those interfaces would slide in alternate directions. Consequently, as seen in chapter 9.1.5, their coefficients of static friction would increase. The dispersion in frictional properties would be finally reduced and the selection process improved. A deeper study of this mechanism - we call a *stack shake-up* - has however to be carried out.

15.2.3.7 Conclusion

Splitting the bottommost interface is fundamental to permit the fulfillment of conditions 1 and 2. Several methods favoring this splitting were introduced, but none appeared sufficient for all the situations. We thus strongly recommend the use of several of those methods together.

15.3 Avoiding multiple feedings (Condition 2)

Situation After the splits, the blocks above the bottommost one are no more controlled in acceleration. They only undergo kinetic friction forces on their bottom and top boundaries. Consequently, condition 2 requires that those blocks are not fed into the machine in order to avoid multiple feedings. Considering that their velocity at the beginning of the process was zero, condition 2 requires the balance of forces to be also zero. In particular, guaranteeing that the second bottommost block has a zero velocity is sufficient to guarantee that all the blocks above are also not moving. Considering that the bottommost interface split, this condition 2 is usually easy to fulfill.

Mathematical expression The equation of a block not controlled in acceleration was given in equation 13.18 and we obtain:

$$\frac{1}{\sum_{j=a}^{b} m_j}\left[F_{a-1,x} - F_{b,x} + \sum_{j=a}^{b}\sum_{k} F_{k/j,x}\right] - g\sin\alpha = 0 \qquad (15.12)$$

For clarity reasons, we propose to study the case of a homogeneous mail stack undergoing no normal external forces. In this case, the previous equation becomes:

$$\begin{aligned}(b-a+1)mg\,(\sin\alpha - \mu_K\cos\alpha) &= \sum_{j=a}^{b}\sum_{k} F_{k/j,x} - \mu_K F_{k/j,y} \\ &= \sum_{j=a}^{b} F_{ext,j}(\cos\beta_j - \mu_K\sin\beta_j) \\ &= \sum_{j=a}^{b} F_{ext,j}\sqrt{\mu_K^2+1}\cos(\beta_j+\zeta) \quad (15.13)\end{aligned}$$

Similarly to the definition of the ρ parameter, we introduced ζ defined by:

$$\begin{cases} \sqrt{\mu_K^2 + 1} \sin \zeta = \mu_K \\ \sqrt{\mu_K^2 + 1} \cos \zeta = 1 \end{cases} \tag{15.14}$$

Physically, the parameter represents the angle of the inclined plane that permits a displacement of the sled at a constant velocity. For $\mu_K = 0.5$, we obtain $\zeta = 26°$. Finally, we obtain a characterization of the external forces required to avoid the displacement of blocks above the bottommost envelope:

$$\sum_{j=a}^{b} F_{ext,j} \cos(\beta_j + \zeta) \quad = \quad \frac{(b - a + 1)mg \left(\sin \alpha - \mu_K \cos \alpha\right)}{\sqrt{\mu_K^2 + 1}} \tag{15.15}$$

External force This condition 2 being easy to fulfill, we only introduce two technical solutions. The first mechanism consists in external forces. The external forces that should be applied on the considered block in order to avoid its displacement may be calculated from equation 15.15. We observe that (i) the norm of the external force varies with the block weight, (ii) the force has to be applied on the block, and (iii) its optimal orientation (the orientation that reduces the norm of the required force) is defined by:

$$\beta = \pi - \zeta \tag{15.16}$$

Two types of technological solutions exist. The first one consists in placing a vertical plate in front of the envelopes above the first one. This solution, called *gap feeder*, is however not adapted to mix-mails, as their thickness varies. The other solution consists in placing a friction material (friction pads or belt) that (i) applies a friction force on the second bottommost block, oriented backward and upward, and (ii) still permits thick and thin envelopes to be fed into the machine thanks to a mobile mechanism. The case of friction pads will be studied in details in the last section of this chapter.

Stack tilt The second mechanism consists in inclining the envelope stack. We observe that a stack tilt of $\alpha > \tan^{-1} \mu_K$ permits a zero force in equation 15.15 and some numerical applications are proposed on Table 15.6.

COKF, μ_K	0.3	0.35	0.4	0.45	0.5	0.55	0.6
Required stack tilt (°)	17	19	22	24	27	29	31

Table 15.6: Stack tilt (α) required to avoid the displacement of blocks above the bottommost envelope. We consider the case of envelopes of mass $m = 10$ g with coefficients of kinetic friction (COKF) of $\mu_K = 0.5$.

Some numerical applications of the contribution of lower tilts to the external force required to fulfill condition 2 are represented on Table 15.7. In particular, several franking machines feeders have a stack tilt of 5° that permits the reduction of the required external force from about 18 %.

α (°)	0	5	10	15	20	25	30
External force (N)	0.25	0.20	0.16	0.11	0.06	0.01	-0.03
Influence	0 %	-18 %	-36 %	-55 %	-74 %	-94 %	-113 %

Table 15.7: Influence of the stack tilt (α) on the external tangential force required to avoid the displacement of blocks above the bottommost envelope. We consider the case of envelopes of mass $m = 10$ g with coefficients of kinetic friction of $\mu_K = 0.5$.

15.4 Avoiding envelopes and rollers damages (Condition 3)

15.4.1 Envelope-on-rollers slipping

General expression The slipping between rollers and envelopes may lead to envelope damages and a low durability of rollers due to abrasion. We therefore need to avoid this situation. The balance of forces on the bottommost block (called B) was given in equation 13.14 and we obtain an expression of the force (F_R) applied by rollers on the bottommost envelope:

$$F_R = \sum_{j=1}^{b} m_j(a_R + g\sin\alpha) + F_{b,x} - \sum_{j=1}^{b}\sum_{k\neq R} F_{k/j,x} \tag{15.17}$$

With:

$$F_{b,x} = \mu_{K,b}\sum_{j=b+1}^{n}\left(m_j g\cos\alpha - \sum_{k} F_{k/j,y}\right) \tag{15.18}$$

Slipping between rollers and the bottommost envelope thus occurs if:

$$|F_R| > \mu_{S,R}\sum_{j=1}^{n}\left(m_j g\cos\alpha - \sum_{k} F_{k/j,y}\right) \tag{15.19}$$

Influence of acceleration For clarity reasons, we consider a vertical stack ($\alpha = 0$) of homogeneous mail with a forward force applied by rollers on the bottommost envelope ($F_R > 0$) in absence of external forces. The equation becomes:

$$b(a_R - \mu_K g) > ng(\mu_{S,R} - \mu_K) \tag{15.20}$$

This result shows that the acceleration required to make rollers slip on the bottommost envelope is sufficient to permit the split of bottommost interface. Indeed, the

rollers-on-paper interface is stronger than the paper-on-paper one. We thus simplify the previous equation by considering that the bottommost interface already split ($b = 1$). The equation becomes:

$$n < \frac{a_R - \mu_K g}{g(\mu_{S,R} - \mu_K)} \tag{15.21}$$

Numerical applications for this condition are proposed on Table 15.8.

Cases	A	B	C	D	E	F
Rollers acceleration, a_R	100	**19**	**20**	**200**	100	100
Rollers-on-paper COSF, $\mu_{S,R}$	2	2	2	2	**1.8**	**11**
Maximal stack size, n	<7	<1	1	<14	<8	<1

Table 15.8: Maximal stack size leading to slipping between the rollers and the bottommost envelope. The influence of rollers acceleration (cases B and C) and rollers-on-paper coefficient of static friction (cases D and E) are presented. The coefficient of kinetic friction of the paper-on-paper contact is considered equal to $\mu_K = 0.5$. COSF stands for coefficient of static friction.

In the studied case (case A), we clearly observe that below 7 envelopes the rollers may slip on the bottommost envelope, leading to misfeeds. This result is supported by direct observation of the machine behavior: misfeeds usually occur for very low envelope stacks. We also observe that to avoid the slip between rollers and the bottommost envelope, the rollers acceleration should be reduced below 20 m.s^{-2} (cases B and C). Similarly, sharply increasing the acceleration of rollers (e.g. to ease the split of the bottommost interface) increases the slip problems for small stacks (case D). We also observe that variations in coefficient of friction of the rollers-on-paper contact has a reduced influence on the problem (case E). This result is of particular interest, because it shows that the environmental factors (e.g. humidity or temperature) are not the main cause of rollers-on-envelopes slipping. To finish with, a coefficient of static friction of 11 would be required between rollers and paper to avoid the slipping problems (case F). Finding rubbers with such properties appears impossible in the current state of the art.

Influence of external forces We propose to introduce the angle ρ_R defined by:

$$\begin{cases} \sqrt{\mu_{S,R}^2 + 1}\cos\rho_R = 1 \\ \sqrt{\mu_{S,R}^2 + 1}\sin\rho_R = \mu_{S,R} \end{cases} \tag{15.22}$$

Considering the inclined plane test method, the angle ρ_R is the tilt at which rollers start to slide on a paper materials and some numerical applications are proposed on Table 15.9.

Rollers-on-paper COSF, $\mu_{S,R}$	1.6	1.7	1.8	1.9	2	2.1
ρ_R (°)	58	60	61	62	63	65

Table 15.9: Values of the angle ρ_R for different coefficients of static friction between rollers and paper materials ($\mu_{S,R}$).

We thus can give an expression of the norm of the minimal external force required to make the rollers slip on the bottommost envelope:

$$\begin{cases} F_{ext,y} = \frac{\mu_{S,R}g - a_{B,x}}{\mu_{S,R} - \mu_K} m + (n-1)mg & \text{if } k > 1 \\ F_{ext}\cos(\rho_R + \beta) = \frac{(a_{B,x} - \mu_{S,R}g)m - (\mu_{S,R} - \mu_K)(n-1)mg}{\sqrt{\mu_{S,R}^2 + 1}} & \text{if } k = 1 \end{cases} \tag{15.23}$$

Where k represents the position of the point of application of the external force on the stack. We clearly observe that the split of the rollers-on-envelope interface is favored by (i) a backward/upward external force applied on the bottommost envelope, (ii) a upward external force applied above the bottommost envelope. Consequently, the external forces have the same action on the rollers-on-paper interface than on paper-on-paper interfaces. However, the coefficients of friction of the paper-on-paper and rollers-on-paper contacts are highly different. Thus, the influence of external forces on the friction of the paper-on-paper and rollers-on-paper interfaces is different. In particular, the action of external forces is optimal for the slipping between the rollers and envelopes for:

$$\beta = \pi - \rho_R \tag{15.24}$$

This orientation is therefore critical for the rollers-on-paper sticking.

How to avoid rollers-on-paper slipping To avoid slipping between rollers and envelopes, several strategies may be involved. We propose three of them hereafter:

1. First of all, a reduction of the acceleration of the rollers for small stacks can reduce the slipping of rollers on the bottommost envelope, as characterized by equation 15.21. This method can be achieved by the mean of a proximity sensor placed at a given vertical level in the hopper. The proximity sensor would detect small stacks, allowing the control system to reduce the electric current delivered to the motors, reducing the acceleration of rollers. This would be a reliable and cheap solution.

2. Secondly, we recommend to ensure that the orientation of the external forces is close from the optimal orientation (as defined by equation 15.24).

3. To finish with, we propose to apply a normal external force oriented downward of about 1 N. This force can be created by a roller and/or tongue placed above the envelopes, before the friction pads. This force would guarantee that the bottommost envelope always undergo a sufficient normal force to stick on the

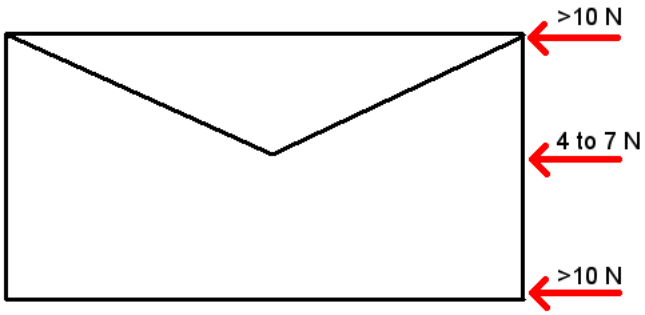

Figure 15.3: Tangential force required to crush an envelope, measured on different points of its width. Measurement carried on 10 envelopes.

rollers, avoiding misfeeds. The drawbacks of this method are (i) a cost increase, and (ii) a slight reduction of the maximal capacity of the feeder from about 10 envelopes (-3 %).

15.4.2 Envelope crush

Problem introduction Condition 3 also requires envelopes not to crush in the machine. Such a crush occurs when the tangential stress applied on envelopes is too high. The crush of paper materials was heavily studied for copiers and printers [103]. However, the crush of envelopes in machines is poorly documented. Even if this situation is rare and goes beyond the frame of this study, we propose to find the conditions avoiding such a situation.

An approximation of the condition leading to an envelope crush We measured the force required to make an envelope crush by pressing the front-end of an envelope on a force sensor. We observed that this critical force greatly evolves along the envelope width: the critical force was between 4 and 7 N on their middle and more than 10 N on their extremity, as represented on Figure 15.3. In other words, if a friction pad applies a tangential force greater than 4 N on the front end of an envelope, the envelope may crush.

Remarks This result is just mentioned to give an order of magnitude of the force leading to an envelope crush. First, there is a great dispersion in mechanical properties for different types of envelopes. Secondly, the paper sheets in the envelope may be in contact with the envelope extremity - or not. Consequently, the thickness of the envelope at an extremity varies from 2 to 5 or 8 layers, as represented on Figure 15.4 and the tangential stiffness thus greatly varies. To finish with, an envelope in a stack is pressed in the normal direction, reducing the normal deformations of the

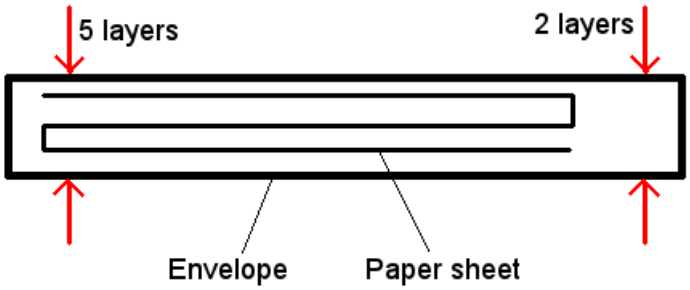

Figure 15.4: The number of paper layers varies, depending on the position of the paper sheet in the envelope. Consequently, the stiffness of the envelope evolves along its length.

envelope. Adversely, our measurements were carried on envelopes that outstrip the stack by about 1 cm, so that the envelope could easily deform. We thus consider our measurements as purely indicative.

15.5 Intermediate summary

The goal of this study is to improve the reliability of the franking machine feeders. In this chapter, we studied the different conditions and technological solutions that guarantee a correct feeding. A summary is proposed hereafter.

Feeding the bottommost envelope (Condition 1) - This condition guarantees that the bottommost envelope is displaced on a sufficient distance to escape the feeder. The condition is characterized by equation 15.2 and permits the design of the feeder's automation.

Split of the bottommost interface This condition guarantees that the bottommost interface is split. The condition is particularly critical in the case of heavy stacks with great dispersions of coefficients of static friction. To fulfill this condition, we proposed the use of (i) high rollers acceleration (from 2 to 10 times the current acceleration of rollers), (ii) a vertical plate with an adaptable position, (iii) a high stack tilt (e.g. 45°), (iv) external forces applied on the bottom of the stack with an optimized orientation (see equation 15.11), (v) placing, if possible, heavy envelopes and lowest coefficients of static friction low in the stack, (vi) a reduction of the dispersion in coefficients of friction by using the same storage and processes for all the envelopes, and (vii) a shake-up of the stack, potentially increasing the coefficient of static friction of the weaker interfaces.

Avoiding multiple feedings (Condition 2) This condition guarantees that no envelope above the bottommost one moves into the machine. The critical situation is described by equation 15.12. To fulfill this condition, we proposed the use of (i) external forces with an orientation close from the optimal orientation (as defined by equation 15.16), and (ii) a positive stack tilt ($\zeta \approx 30°$).

Rollers slipping on envelopes (Condition 3) This condition guarantees that the rollers do not slip on the bottommost envelope, avoiding the damages of the envelopes and rollers. The worst situation was described by equation 15.19 and usually consists in small stacks. To fulfill this condition, we proposed (i) a reduced acceleration of rollers for low stacks, (ii) an orientation of the external forces close from the optimal orientation (as defined by equation 15.25), and (iii) a slight downward external force (approx. 1 N) applied on the bottommost envelopes by a roller or a tongue.

Envelopes crushes (Condition 3) This condition avoids the crushing of envelopes due to the external forces they undergo. To fulfill this condition, we have to ensure that the tangential external force applied by a friction pad or friction belt on the front of envelopes is lower than roughly 4 N.

Remark on external forces The use of external forces (e.g. created by friction pads or belts) appears as an effective solution to permit correct feedings. External forces should be applied low in the stack. The norm of the external forces required was characterized by the correct feeding conditions. On the other hand, the orientation of the external forces influences the fulfillment of the correct feeding conditions, as represented on Figure 15.5. We observe the particular case of external forces verifying:

$$\frac{3\pi}{2} - \rho > \beta > \frac{3\pi}{2} - \rho_R \tag{15.25}$$

Where ρ and ρ_R are defined by equations 14.7 and 15.22, respectively, and are functions of μ_S and $\mu_{S,R}$, respectively. For example, considering $\mu_S = 0.6$ and $\mu_{S,R} = 2$, this optimal angle is defined by $207° < \beta < 239°$. In this situation, the external forces (i) favors the sticking of rollers on the bottommost envelope, (ii) favors the split of the bottommost interface, and (iii) avoids the displacement of envelopes above the bottommost envelope.

15.6 The example of friction pads

15.6.1 Problem and situation

A challenging problem We observed that neither the rollers acceleration nor the stack tilt are sufficient to permit correct feedings. Current franking machines

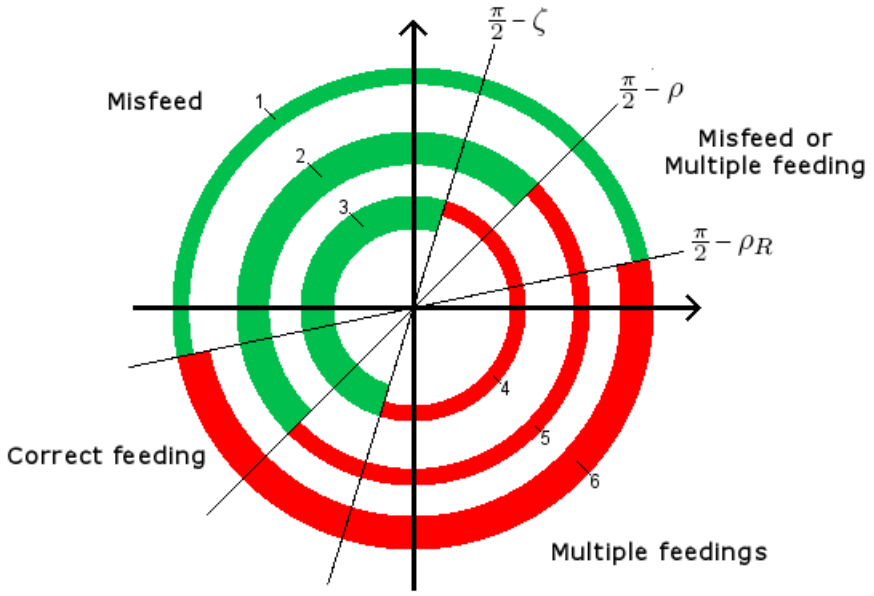

Figure 15.5: Influence of the orientation of the external forces on the fulfillment of different correct feeding conditions. The external circle represents the sticking of rollers on the bottommost envelope (condition 3). The circle at the middle represents the sliding of the bottommost interface. The smaller circle represents the conditions avoiding the displacement of envelopes above the bottommost one (condition 2). Thick circles represent the orientations that favor the fulfillment of the conditions, while thin circles represent the orientations that avoid the fulfillment of the conditions. (1) The rollers slip on the bottommost envelope. (2) The bottommost interface slips. (3) The envelopes above the bottommost one do not move. (4) The envelopes above the bottommost one move into the machine. (5) The bottommost interface sticks. (6) The rollers stick on the bottommost envelope.

thus heavily rely on external forces applied on the bottommost envelopes.

Current technonological solutions The external force may be applied by a vertical plate. In this situation, the feeder would be called a *gate feeder*. However, in the case of mix-mails, the thickness of envelopes varies. The size of the gate being constant, the use of a vertical plate becomes problematic for the selection process. That is the reason why franking machine feeders use mobile systems, such as friction pads or friction belts. Those systems adapt to the thickness of the bottommost envelope. However, the influence of those systems on the selection process is complex and poorly understood.

Goal In this chapter, we studied different conditions that guarantee correct feedings. We proposed different mathematical expressions reflecting the fulfillment of those conditions. We propose to apply this knowledge to the friction pads/belts, in order to study their contribution to the selection process. This section thus constitutes an example of application of the acquired knowledge.

Situation The coefficients of static and kinetic friction of the pad-on-paper contact were measured in chapter 11.2. The obtained values were approximately 1. The Neopost franking machine feeders have two stages of 3 friction pads each, placed above the envelope path, as represented on Figure 15.6a. On the pre-selection stage, the three pads rotate. We measured that they globally apply a normal force of approximately 9.5 N at their bottom (approx. 3 N per pad). On the selection stage, the pads have a vertical displacement axis. We measured that they globally apply a 5.3 N normal force (approx. 2 N per pad). However, the selection stage is often removed or does not exist. For clarity reasons, we will therefore focus our study on the pre-selection stage. As observed on Figures 15.6a, 15.6b, and 15.6c, the angle of friction pads to the horizontal evolves from about -16° to about 0°, depending on the position and thickness of envelopes. In particular, an angle of 0° is reached when the envelope is below the friction pad, the pad sliding on the front face of the envelope.

Forces applied by friction pads on envelopes Envelopes can be considered as compressible materials (see in particular annex D). In a first approach, we can consider that the norm and orientation of the force applied by envelopes on the pad depend on the compression of envelopes on the pad. This compression is however nearly impossible to predict, because of the variations in content, position or properties of the considered envelopes. In reaction to this force, the pad applies two types of forces on envelopes:

- A force normal to the pad, called F_p, as represented on Figure 15.7. The force is created by springs situated behind the friction pad and therefore easily

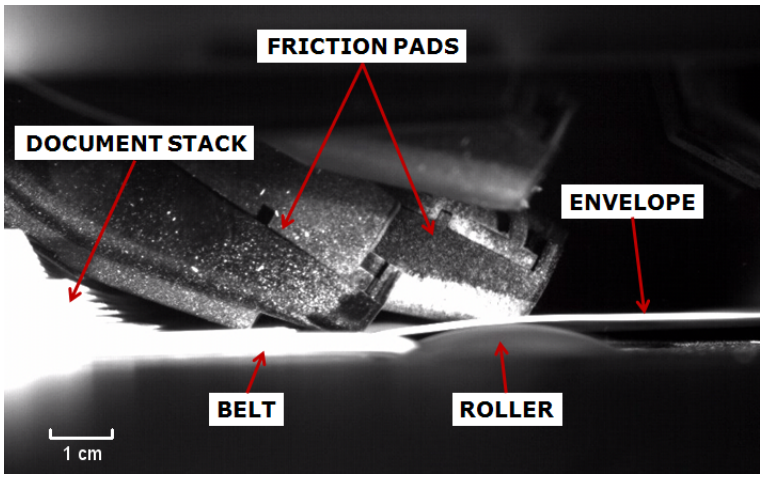

(a) Friction pads, rollers, belts and envelopes in a franking machine feeder (Omega). The bottommost envelope is escaping successfully the feeder.

(b) Friction pads of the selection stages of a franking machine feeder (Omega)

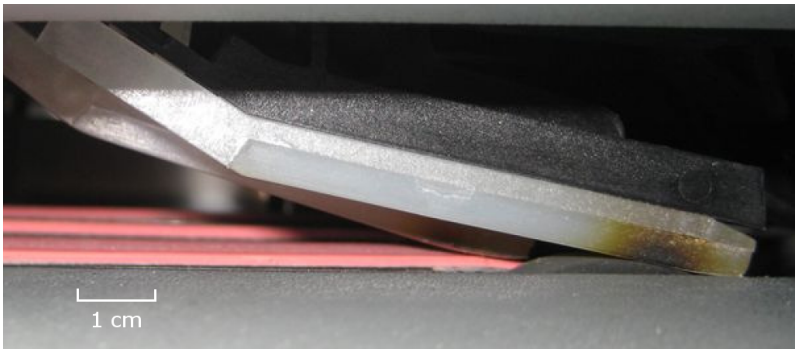

(c) Friction pads of the pre-selection stages of a franking machine feeder (Delta)

Figure 15.6: Friction pads in franking machine feeders

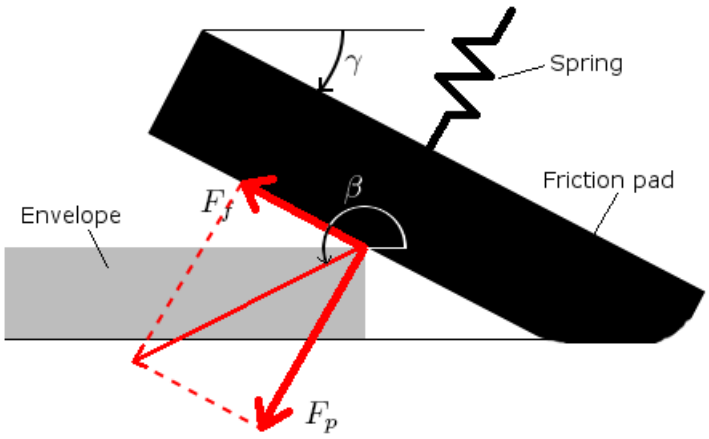

Figure 15.7: A friction pad applies (i) a force F_p normal to the pad, and (ii) a friction force F_f on an envelope. The pad makes an angle γ with the horizontal. The force applied by the pad on the envelope has an angle β with the horizontal.

adjustable and measurable.

- A friction force, F_f, tangential to the pad, as represented on Figure 15.7. The coefficients of static and kinetic friction being equal to 1, the force ranges from 0 to F_p.

As the applied force (norm and orientation) by each envelope on the pad is unknown, the reaction force of the pad on each envelope is also unknown.

Simplified model For clarity reasons, we simplify the problem as follows:

- The β angle of the force applied by the pads on envelopes is constant along the block, as represented on Figure 15.7.
- The compression of envelopes in the tangential direction is constant.
- The stack is considered vertical.

The angle of the force applied by pads on envelope thus ranges from $\frac{5\pi}{4}+\gamma$ (when the friction force is equal to the normal force) to $\frac{3\pi}{2}+\gamma$ (when the friction force is zero). Considering that $0 > \gamma > -\frac{\pi}{6}$ in current franking machines, we have $\pi < \beta < \frac{3\pi}{2}$. In other words, the reaction force of the friction pad on the envelopes is always oriented backward and downward.

Friction belts system In Pitney Bowes machines, the friction pads are replaced by friction belts moving in a direction opposed to the mail-flow. The material used for those belts may be different from the polyurethane used for friction pads. The

coefficients of friction on paper may therefore be different. The friction belts sliding on envelopes, they are in kinetic friction with envelopes. This regime does not produce a higher friction force (as it may be suggested at first glance). However, the force of kinetic friction applied by the belt on each envelope remains equal to the normal force applied by the belt on the envelope ($F_f = F_p$). The orientation of the force applied by the belt on the envelopes, β, thus remains constant, as we suppose in the proposed simplified model. The technological solution is not more efficient and is much more expensive, but the friction is more stable. The model we propose here thus fits with the mechanisms based on friction belts, but the coefficients of friction on paper should be adapted.

15.6.2 Correct feeding conditions

Method We consider the simplified model proposed in the previous paragraphs. In a first step, we list the different correct feeding conditions the friction pads have to fulfill. In a second step, we will make the model parameters vary in order to study their influence on the correct feeding conditions.

Feeding envelopes (Condition 1) The first condition guarantees the feeding of envelopes (Condition 1). This condition guarantees that the bottommost envelope is moved on a distance equivalent to its length, permitting the envelope to escape the feeder. On franking machine feeders, this condition is usually fulfilled by the use of sensors placed at the exit of the feeder. The sensors determine when the bottommost envelope escapes the feeder and then stop the rollers. This automation thus permits the fulfilling of the first condition whatever are the envelopes' lengths.

Split of the bottommost interface We showed that to guarantee correct feedings, the bottommost interface must split. The shearing strength at the bottommost interface thus has to overcome the break-away force of the interface. To fulfill this condition, the required force applied by pads on envelopes was characterized by equation 14.15. Considering the critical case consisting in a bottommost block composed of two envelopes, an equation of the required force is:

$$F_p > \frac{(a_{B,x} - \mu_S g)m - (\mu_S - \mu_K)(n-2)mg}{\sqrt{\mu_S^2 + 1}\cos(\beta + \rho)} \tag{15.26}$$

To split the bottommost interface, the external force applied by pads on envelopes should verify this equation.

Avoiding multiple feedings (Condition 2) At the same time the friction pads apply an increasing shearing strength on the bottommost interface. They contribute to the non-displacement of envelopes above the bottommost one. This non-displacement is required to avoid multiple feedings. In the absence of other external

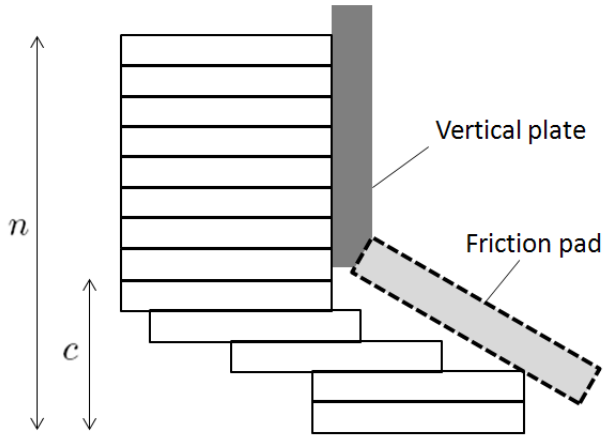

Figure 15.8: Structure of the stack in front of a friction pad mechanism. The n and c parameters represent the size of the stack and the number of envelopes in front of the friction pad, respectively.

forces, the force required to avoid the displacement of a block was given by equation 15.15. Considering a vertical homogeneous stack, the force applied by friction pads on a block $B = \{E_a..E_b\}$ should thus verify:

$$\sum_{j=a}^{b} F_{p/j}\sqrt{\mu_K^2+1}\cos(\beta+\zeta) = \mu_K(a-b-1)mg \tag{15.27}$$

However, all the envelopes in the stack are not in contact with pads. We can consider that above a level c, envelopes are no more in contact with the friction pad but with the vertical plate, as represented on Figure 15.8. Consequently, the contribution of the friction pad to the stabilization of the blocks above the bottommost envelope can be characterized by:

$$\sum_{j=2}^{c} F_{p/j} > \frac{\mu_K(1-c)mg}{\sqrt{\mu_K^2+1}\cos(\beta+\zeta)} \tag{15.28}$$

This force should be ideally applied mainly on the second bottommost envelope.

Avoiding rollers-on-envelope slipping (Condition 3) Another condition to guarantee correct feedings is to ensure that the rollers never slip on the bottommost envelope (Condition 3). Equation 15.23 gives the condition of a slip between the rollers and the bottommost envelope in the case of a vertical homogeneous stack. This critical force is minimal when the external force is applied only on the bottommost envelope itself, and the equation becomes:

$$F_p > \frac{(a_{B,x}-\mu_{S,R}g)m - (\mu_{S,R}-\mu_K)(n-1)mg}{\sqrt{\mu_{S,R}^2+1}\cos(\rho_R+\beta)} \tag{15.29}$$

Avoiding envelopes crushes (Condition 3) The last condition of a correct feeding is to ensure that the envelopes never crush. In chapter 15.4.2 we considered that the crush of an envelope becomes possible if the tangential component of the force applied by a pad is higher than 4 N. Considering that three pads are in contact with the envelope, we obtain:

$$F_p < \frac{12}{-\cos\beta} \tag{15.30}$$

With F_p expressed in Newtons. It is however important to remind that the value of this critical tangential force may greatly vary with envelopes or contents.

Summary of the correct feeding conditions The conditions guaranteeing a correct feedings are summarized as follows:

$$\begin{cases} F_p > \frac{(a_{B,x}-\mu_S g)m-(\mu_S-\mu_K)(n-2)mg}{\sqrt{\mu_S^2+1}\cos(\beta+\rho)} \\ F_p > \frac{\mu_K(1-c)mg}{\sqrt{\mu_K^2+1}\cos(\beta+\zeta)} \\ F_p > \frac{(a_{B,x}-\mu_{S,R} g)m-(\mu_{S,R}-\mu_K)(n-1)mg}{\sqrt{\mu_{S,R}^2+1}\cos(\beta+\rho_R)} \\ F_p < \frac{12}{-\cos\beta} \end{cases} \tag{15.31}$$

If the friction pad applies on the stack an external force that verifies those conditions, then we may guarantee correct feedings.

15.6.3 Optimizing the friction pad mechanism

15.6.3.1 Reference case

Definition As a starting point, we consider a typical case called *reference case*, which consists in a typical use of the franking machine feeders. This case is characterized by the parameters presented on Table 15.10.

Symbol	Signification	Value
n	Max. number of envelopes in the stack	300
m	Mass of the envelopes	10 g
$\mu_{S,R}$	Coeff. of static friction between rollers and envelopes	2
$\mu_{S,p}$	Coeff. of static friction between pads and envelopes	1
μ_S	Coeff. of static friction between envelopes	0.6
μ_K	Coeff. of kinetic friction between envelopes	0.5
a_R	Acceleration of rollers	100 m.s^{-2}
c	Number of envelopes below the vertical plate	20
γ	Orientation of the friction pad	-16° to 0°

Table 15.10: Numerical values of the parameters characterizing the reference case

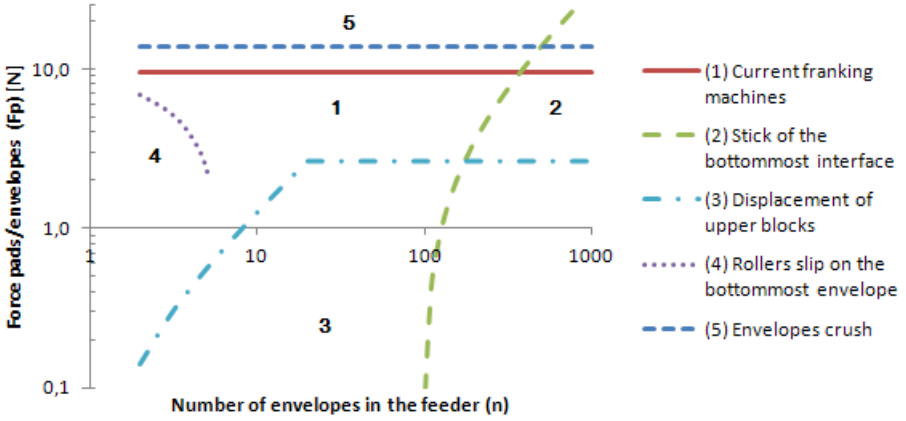

Figure 15.9: Characteristic curves of the reference case. They represent the different regimes associated to varying stack sizes and force applied by friction pads on envelopes. The values used correspond to the reference case (see Table 15.10). The different regimes are (1) correct feedings, (2) the sticking of the bottommost interface (misfeed/multiple feeding), (3) the displacement of blocks above the bottommost envelope (multiple feeding), (4) the slipping of rollers on the bottommost envelope (misfeed), and (5) an envelope crush, respectively. We also represented the current design of the machine (full line numbered 1).

Characteristic curves We integrate the parameters of the reference case (see Table 15.10) in the correct feeding conditions detailed in equation 15.31. The orientation of the friction pad evolves from -16° to 0° along the stack. Thus, for each correct feeding condition, we consider the worst orientation of the pad. We finally obtain the conditions on the norm of the force applied by pads on envelopes (F_p) to permit correct feedings in the reference case. The conditions are represented for a number of envelopes varying from 1 to 1000 on Figure 15.9. We call those curves the *characteristic curves* of the machine. The characteristic curves thus represent the required force applied by pads on envelopes to avoid any problem during the selection process (i) for evolving stack sizes, and (ii) considering all the possible orientations of the pads. We also represented the force applied by the pads on the envelopes in the current franking machines.

Discussion We first observe that the force applied by pads on envelopes on the current franking machines globally fits with the correct feeding conditions. In particular, a constant force for varying stack weights appears adapted to fit the correct feeding conditions. For example, a higher force applied by pads on envelopes would lead to an envelope crush (5), whereas a lower force would create misfeeds (4) or multiple feedings (2).
We observe that the franking machine feeder processes stacks up to 380 envelopes.

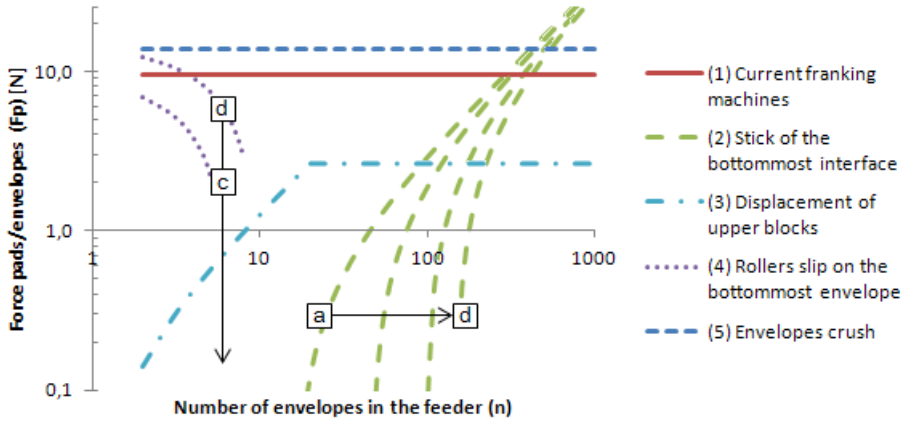

Figure 15.10: Characteristic curves for an acceleration of rollers ($a_{B,x}$) equal to (a) 20 m.s^{-2}, (b) 50 m.s^{-2}, (c) 100 m.s^{-2}, and (d) 150 m.s^{-2}. The condition leading to rollers-on-envelope sliping is not represented in the cases a and b, because the critical pad-on-envelope force, F_p, is lower than 0.1 N.

This maximum capacity is slightly higher than the maximum capacity usually observed on franking machines (approx. 300 envelopes). This slight difference will be explained later, but the order of magnitude is respected.
To finish with, we observe that the feeding problems in franking machine feeders strongly depend on the size of the stack. For low stacks, we observe that slight variations in pads-on-envelope force are sufficient to create misfeeds (4) or envelope crushes (5). Consequently, this explains why these two failures are the typical failures observed on low stacks. Similarly, for big stacks, the main failures are multiple feedings and/or envelope crushes. Those results confirm the experimental observations made on franking machine feeders.
In the following paragraphs, we will study how different parameters influence the selection process.

15.6.3.2 Influence of machine parameters

Rollers acceleration We represented the characteristic curves for rollers accelerations ranging from 20 to 150 m.s^{-2} on Figure 15.10. We observe that the capacity of the machine is increased (reduction of multiple feedings) but no-feeds are more likely to appear. We calculated the maximal range of rollers accelerations that guarantee correct feedings, as indicated on Table 15.11.

Symbol	Ref.	Min (Capacity)	Max (Capacity)
Mass of envelopes, m (g)	10	0 (Inf.)	14 (300)
Paper-on-rollers COSF, $\mu_{S,R}$	2	1.95 (380)	Inf. (380)
Pads-on-paper COSF, $\mu_{S,p}$	1	0.62 (120)	1.02 (390)
Paper-on-paper COSF, μ_S	0.6	0.5 (Inf.)	0.99 (23)
Paper-on-paper COKF, μ_K	0.5	0 (64)	0.59 (Inf.)
Rollers acceleration, a_R (m.s^{-2})	100	0 (270)	120 (400)
Env. below the vertical plate, c	20	1 (380)	70 (380)
Orientation of the pad, γ	-16°	-16.6° (680)	0° (380)

Table 15.11: Reference, minimum, and maximum values for the different machine and stack parameters. The feeder capacity (max number of envelopes) is also represented between brackets. "Inf." stands for "infinite". For clarity reasons, the orientation γ of the pads is supposed here to be constant. In this situation, the feeders have a maximal capacity of 670 envelopes. In practice, the orientation of the pads evolves and the capacity is 300 envelopes max.

We also calculated the feeder's maximal capacity that is associated to the range of rollers accelerations. The results confirm that for a slight increase in rollers acceleration (from 100 to 120 m.s^{-2}), the misfeeds become very likely. The result explains why the rollers acceleration was not increased beyond its actual level. We proposed several technological solutions to avoid such rollers-on-paper slipings, in particular:

- A level sensor that reduces the acceleration of rollers for low stacks
- Tongues or rollers above the bottommost envelopes that slightly increase the normal load applied on bottommost envelopes.

Using those solutions would avoid the misfeeds. Consequently, the rollers acceleration could be sharply increased. Finally the capacity of the feeder would be increased. We thus strongly recommend the implementation of those technological solutions in franking machine feeders.

Pads orientation The pads orientation evolves depending on the envelopes thicknesses and positions. In this paragraph only, and for clarity reasons, we consider that the orientation of the pad remains constant. We represented the characteristic curves for different constant pads orientations on Figure 15.11. We observe that making the pad more horizontal (i) decreases the probability of misfeeds, and (ii) increases the probability of multiple feedings. Above an angle of -16.6° misfeeds occur for low stacks, as indicated on Table 15.11. On franking machines, the pads have an orientation, γ, equal to -16°. In other words, the current pads orientation is only slightly lower than the critical angle we calculated. Our model thus supports and justifies the choice of this pads orientation.

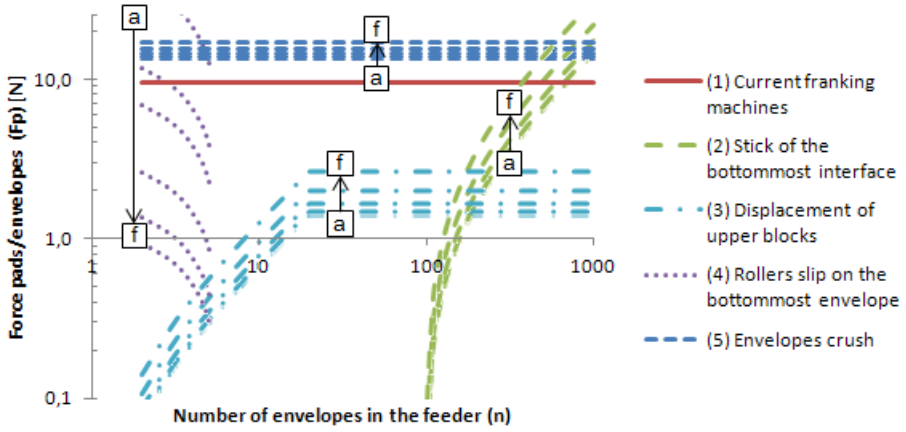

Figure 15.11: Characteristic curves for an orientation of the pad (γ) constant and equal to (a) -18°, (b) -17°, (c) -16°, (d) -12°, (e) -6°, and (f) 0°.

Vertical plate position We represented the characteristic curves for a vertical plate at different positions on Figure 15.12. We observe that the vertical plate has a limited influence on the selection process. The highest acceptable position is much higher than the current position (70th envelope), as indicated on Table 15.11. However, placing a vertical plate so high in the stack would induce many technological problems, among which an increase in friction pads' size. On franking machines, the vertical plate is approximately at the level of the 20th envelope. The current position of the vertical plate thus appears adapted to the selection process.

15.6.3.3 Influence of materials

Friction pads We represented the characteristic curves for different coefficients of friction between pads and envelopes on Figure 15.13. We observe that increasing the coefficient of static friction of the pads-on-envelope contact (i) increases the misfeeds and envelopes crushes, and (ii) decreases the multiple feedings. In particular, increasing this coefficient of static friction permits an increase in feeder's capacity, as indicated in Table 15.11. However, the increase in coefficient of static friction of the pads-on-envelope contact is limited to the value 1.02. On current franking machines, we measured a coefficient of static friction between the pads and envelopes of approximately 1. In other words, the material currently used for friction pads is already optimal. Again, the model supports the experimental results obtained when designing the machine.

Driving rollers We represented the characteristic curves for different coefficients of friction between rollers and envelopes on Figure 15.14. We observe that an increase in rollers-on-envelopes coefficient of static friction obviously reduces the slipping of

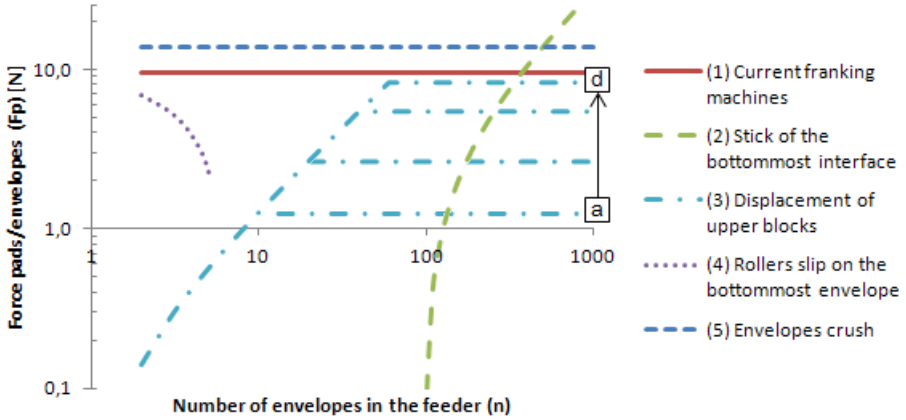

Figure 15.12: Characteristic curves for a vertical plate placed at a level (c) equal to (a) 10, (b) 20, (c) 40, and (d) 60.

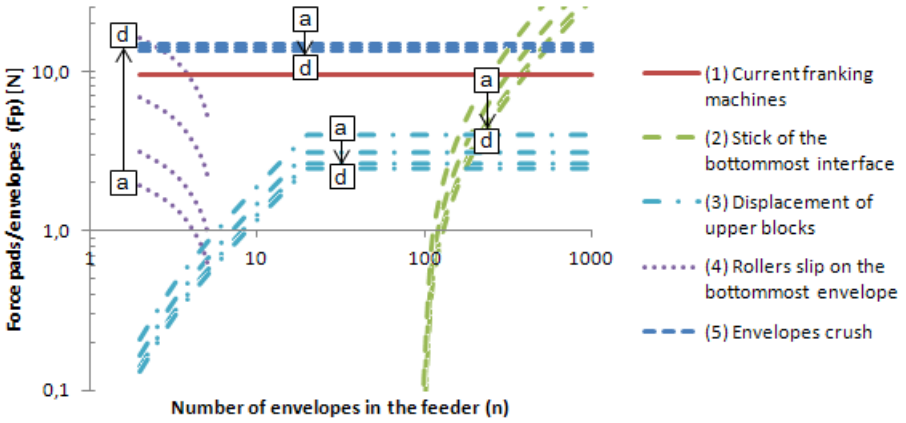

Figure 15.13: Characteristic curves for a coefficient of static friction of the pads-on-envelope contact equal to (a) 0.8, (b) 0.9, (c) 1.0, and (d) 1.05.

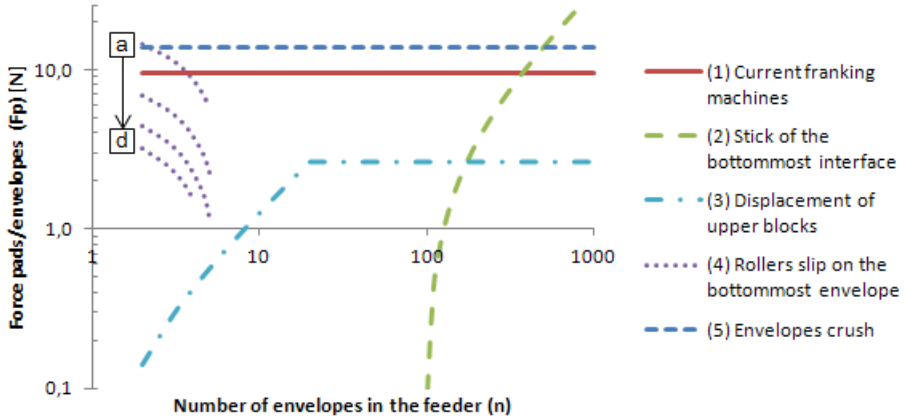

Figure 15.14: Characteristic curves for a coefficient of static friction of the rollers-on-envelope contact equal to (a) 1.9, (b) 2.0, (c) 2.1, and (d) 2.2.

rollers on envelopes (misfeeds). However, the value of the critical coefficient of static friction is not trivial. We calculated that for a coefficient of rollers-on-envelope static friction below 1.95, the misfeeds become very likely, as indicated on Table 15.11. On current franking machines, we measured a coefficient of friction between the rollers and envelopes of approximately 2. In other words, the material currently used for rollers has a friction with envelopes that is nearly critical. The model suggests no particular benefit for this material choice. However, higher coefficients of static friction are usually permitted by softer materials that have a lower durability. We thus validate the choice of the selected materials for franking machines. The choice also appears optimal.

15.6.3.4 Influence of envelopes

Frictional properties We represented the characteristic curves for varying coefficients of static and kinetic frictions for the envelope-on-envelope contact on Figure 15.15 and 15.16, respectively. We observe that the selection process is favored by (i) an increase in coefficients of kinetic friction, and (ii) a decrease in coefficient of static friction. In other words, reducing the gap between the coefficients of static and kinetic friction favors the correct feedings.
Obviously, the possible variations in coefficients of friction are limited, as represented on Table 15.11. In particular, the coefficient of static friction of the envelope-on-envelope contact has to remain lower than the coefficient of static friction of the pads-on-envelope contact. Even if the variations in coefficients of static friction are limited, their influence on the feeder's capacity is huge. In particular, similar values of coefficients of static and kinetic friction would lead to an unlimited feeder's capacity.
The problem is that modifying the frictional properties of materials is a complex

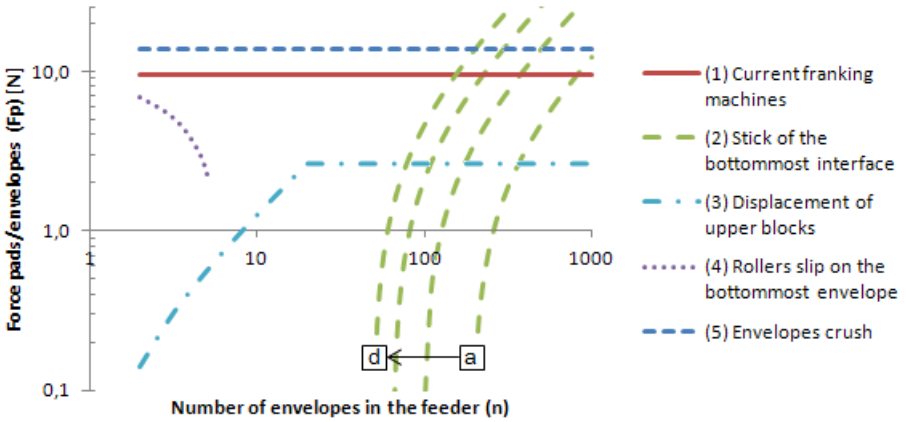

Figure 15.15: Characteristic curves for a coefficient of static friction of the envelope-on-envelope contact equal to (a) 0.55, (b) 0.6, (c) 0.65, and (d) 0.7.

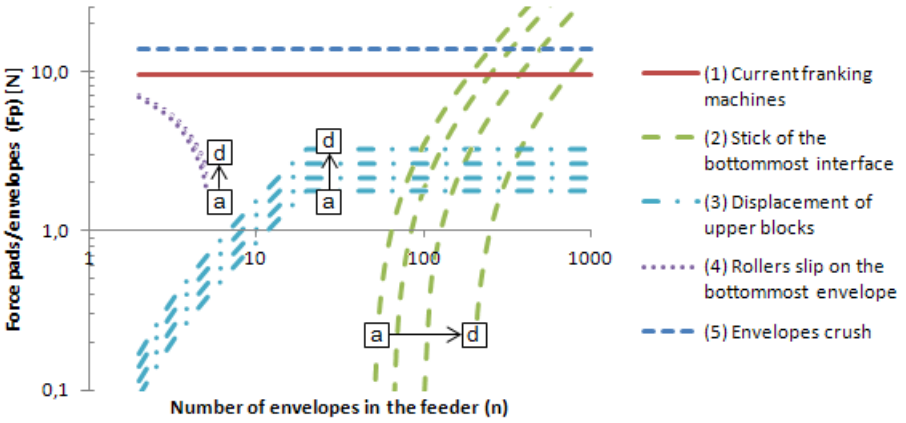

Figure 15.16: Characteristic curves for a coefficient of kinetic friction of the envelope-on-envelope contact equal to (a) 0.4, (b) 0.45, (c) 0.5, and (d) 0.55.

subject. We however showed in the previous part that heating the envelopes (approx. 40°C) sharply reduces the gap between the coefficients of static and kinetic frictions. Heating the stack may thus permit the processing of heavy stacks.
The influence of frictional properties of envelopes on the selection process is of particular interest when considering varying envelope types. We previously measured the frictional properties of different envelope types, as summarized in Table 11.1. We thus calculated the maximal capacity of the feeder for each of those envelopes. We summarized the results in Table 15.12.

Name	$\mu_{S,1}$	$\mu_{K,1}$	$\mu_{S,1} - \mu_{K,1}$	n_{max}
Curtis 1000 524-11	0.63	0.50	0.13	280
Columbia #10	0.69	0.58	0.11	290
Printmaster 450973	0.68	0.57	0.11	290
C4 US 30394	0.66	0.55	0.11	310
Printmaster 03975	0.59	0.47	0.12	320
Printmaster 3957	0.64	0.53	0.11	320
Printmaster 27561	0.58	0.47	0.11	360
C4 FR 12957	0.54	0.43	0.11	380
CO375	0.56	0.47	0.09	450

Table 15.12: Maximum capacity of the feeder (n_{max}) for different types of envelopes. The coefficients of static and kinetic friction were taken from Table 11.1. The other parameters of the model are described by the reference case (see Table 15.10).

We observe strong variations in feeder's capacity (from 280 to 450). We propose to highlight those variations in machine's specifications. We also observe that the capacity of the feeder is approximately 300 envelopes in most cases. This capacity is similar to the capacity usually admitted for current franking machine feeders. Again, the model supports the experimental results obtained when designing the machine.

Mass We considered 10 g envelopes. However, heavier envelopes sometime have to be processed. We represented the characteristic curves for different envelope masses on Figure 15.17. We clearly observe that heavy envelopes tend to increase the risks of misfeeds and multiple feedings. Heavy envelopes thus reduce the capacity of the feeder.
We calculated on Table 15.11 the maximal acceptable mass of envelopes. We found a maximal mass of 14 g with a feeder capacity of 300 envelopes. Above 14 g, the rollers slip on the bottommost envelope. This result confirms the observations made on franking machines: small stacks of heavy envelopes tend to slip on rollers as rollers start rotating. This defect is usually considered as minor, as it does not stop the feeding process. Furthermore, the defect could be easily avoided by reducing the

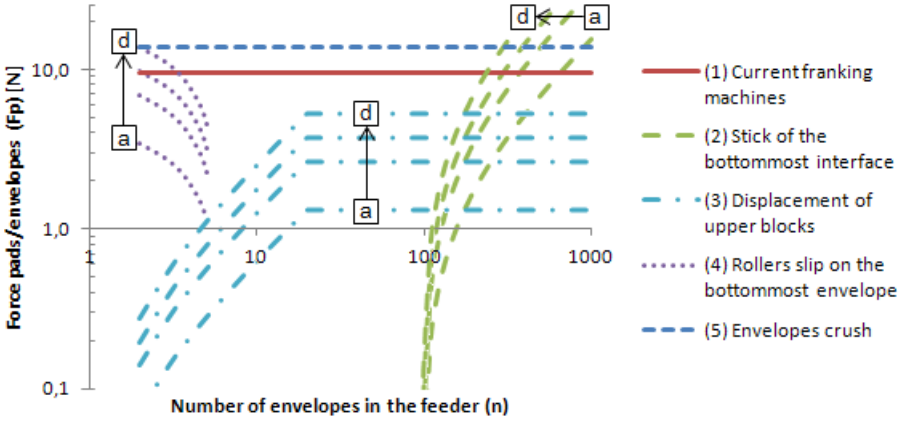

Figure 15.17: Characteristic curves for a mass of envelopes equal to (a) 5 g, (b) 10 g, (c) 14 g, and (d) 20 g.

rollers acceleration for low stacks, as proposed previously.
For heavier envelopes, the capacity of the machine is reduced. This result is intuitive and confirms the observations made on the machines. As the maximal weight of the stack remains roughly constant, heavy envelopes are associated to a lower number of envelopes.

15.6.4 Conclusion

Most of the observations made on the machine were supported and justified by the proposed model. The reference case appears to be a good optimization of the studied feeder mechanism. We showed that the conclusions are similar for the friction belt.
To improve the selection process, new mechanisms are therefore required. We proposed two of them:

- For reducing misfeeds, the use of a level sensor to decrease the rollers acceleration for low stacks. Alternatively, we recommend the use of tongues or rollers for slightly increasing the normal load on bottommost envelopes.
- For reducing multiple feedings, the use of (i) higher rollers accelerations, (ii) pads that are more vertical, and (iii) a higher coefficient of static friction for the pads-on-envelope contact. However, a compromise should be found to avoid misfeeds.

We recommend future works to study the heating of the envelopes and the bottom shake-up of the stack. We also recommend a deeper investigation on the crushing of envelopes. Indeed, a reduction in envelopes crushes would allow the use of much higher forces applied by pads on envelopes, thus improving the selection process.

Summary and Conclusion of Chapter 15

Goal The goal of this study was to improve the reliability of the franking machine feeders. In this chapter, we studied the different conditions and technological solutions that guarantee a correct feeding.

Correct feeding conditions We detailed the conditions that have to be fulfilled in order to guarantee the correct feedings:

- **Feeding the bottommost envelope** (Condition 1). Guarantees that the bottommost envelope is displaced on a sufficient distance to escape the feeder.
- **Split of the bottommost interface**. Prior condition to conditions 1+2.
- **Avoiding multiple feedings** (Condition 2). Guarantees that no envelope above the bottommost one moves into the machine.
- **Rollers slipping on envelopes** (Condition 3). Guarantees that the rollers do not slip on the bottommost envelope to avoid damages of envelopes and rollers.
- **Envelopes crushes** (Condition 3). Avoids the crushing of envelopes.

Example of friction pads We studied the case of friction pads, but the method can be applied to any selection mechanism. Three main defects appear:

- A slipping of rollers on the bottommost envelope of light stacks.
- A sticking of the bottommost interface for heavy stacks (multiple feedings).
- A crush of envelopes for high forces applied by the pads on envelopes.

Those issues are influenced by the machine parameters and the envelope properties. Our study gave explanations and supported the design choices.

Increasing the feeders' capacity According to our study, the machine design is already mostly optimized. Increasing the feeders' capacity thus requires the implementation of new technological solutions.

For short term improvements, we proposed (i) a reduction of the rollers acceleration for low stacks, (ii) an increase in rollers acceleration for heavy stacks, (iii) the use of tongues or rollers applying a slight downward force above the bottommost envelopes, (iv) similar storage and processes for all the envelopes of the stack, (v) the sorting of envelopes by placing heavy envelopes and lowest coefficients of static friction low in the stack, and (vi) a higher stack tilt.

For long term improvements, we also proposed a deepen investigation on (i) the envelopes crushes, (ii) a shake-up of the stack by its bottom before the selection process, and (iii) the heating of the stack.

Part V

Summary, Conclusion, and Perspectives

Chapter 16

General Summary

Situation Franking machines are used to print imprints on envelopes. The bottommost envelope of envelopes stacks are fed one by one by a feeder. This feeding process is permitted by (i) driving rollers with high accelerations, (ii) friction pads/belts to reduce the displacement of the bottommost envelopes, (iii) vertical plates to prevent the displacement of the stack, and (iv) a stack inclination to the rear.
However, multiple feedings often occur and consist in the feeding of more than one envelope at the same time. Conversely, misfeeds occur when the driving rollers cannot displace the bottommost envelope. Finally, envelopes damages occur when envelopes crash or are altered during the feeding process.
The goal of this study is to optimize the process to avoid those failures and increase the capacity of the feeder. To do so, we need a better understanding on the friction forces involved and a model of the selection process.

Measuring the friction force The different test methods we studied are compared on Table 16.1. In particular, we observe that the inclined plane test method does not characterize the force of kinetic friction. On the other hand, the horizontal plane test method has a low accuracy due to stick-slip phenomena and high accelerations of the sled.
We improved the horizontal plane test method by placing a spring between the moving arm and the sled. The elongation of the spring is measured by a position sensor. We thus measure the pulling force and the acceleration of the sled, allowing more accurate measurements (about 3 times). The amplitude of the stick-slip oscillations is reduced, controlled, and measured. Finally, the method allows the measurement of the friction force at different velocities and accelerations.
The ring-on-plane test method measures the friction force between paper samples at high speeds (1 $m.s^{-1}$). The method also characterizes the abrasion of the samples.

	Inclined plane	Horizontal plane	Strip-on-drum	Oscillating sled	Ring-on-plane
Coeff. of variation μ_S	1.8 %	3.4 %	-	1.1 %	Not measured
Coeff. of variation μ_K	Not measured	3.7 %	-	0.9 %	1.1 %
Presliding displacements	No	No	No	Yes	No
Long runs and abrasion	No	No	Yes	No	Yes
Repeated slidings	No	Yes	Yes	Yes	Yes
Constant speed	Yes	Yes	Yes	No	Yes
Speeds	0	0.5 to 5 $mm.s^{-1}$	0 to 1.2 $m.s^{-1}$	5 to 70 $mm.s^{-1}$	0 to 1.2 $m.s^{-1}$
Acceleration	No	No	No	0 to 0.6 $m.s^{-2}$	No
Stick-slip	No	Unmastered	Unmastered	Mastered	Unmastered
Samples bending	No	No	Yes	No	No
Samples deformation	No	No	Yes	No	No
Sliding movement	Linear	Linear	Linear	Linear	Rotation
Asymmetry in frict. hist.	No	Yes	Yes	Yes	No
Constant normal load	No	Yes	No	Yes	No
Limit in normal load	No	No	300 g	No	No
Cost	Low	High	High	High	High

Table 16.1: Comparison between of the different methods for measuring the friction force between paper materials.

Factors	Paper-on-paper	Pads-on-paper	Rollers-on-paper
Typical coeff. of frict. (static/kinetic)	0.6/0.5	1.0/0.8 (1)	2.0/2.5 (2)
Resin acids	+50 %/+50 % (3)	-/-	-/-
Fatty acids, oleophilic materials	-50 %/-50 % (3)	-/-	-/-
Sharp-edge particles	+90 %/+90 % (3)	-/-	-/-
Lamellar particles	-90 %/+90 % (3)	-/-	-/-
CD/CD, anisotropy, smoothness	+10 %/+15 % (3)	-/-	-/-
MD/MD, isotropy, roughness	-10 %/-15 % (3)	-/-	-/-
Repeated slidings in the same direction (5x)	-50 %/-50 %	0 %/0 %	-/0 %
Repeated slidings in reversed directions (5x)	+60 %/+60 %	0 %/0 %	-/0 %
Velocity (0-1 $m.s^{-1}$)	-/+25 %	-/-	-/+25 % (4)
Normal load (1.6-8.2 N)	0 %/0 %	0 %/0 %	-/-15 %
Abrasion (sliding distances > 150 m)	-/-65 %	-/-	-/-
Humidity (25-67 % RH)	+25 %/+7 % (5)	0 %/-10 %	-/-8 %
Temperature (24-46°C)	-20 %/-7 %	0 %/0 %	-/-8 %
Electrostatic discharging	0 %/0 %	0 %/0 %	-/0 %

Table 16.2: Main factors and their influence on the coefficients of friction between paper materials (static/kinetic). The values are orders of magnitudes given for information and may not be considered as exact results. In particular, variations below 3 % (7 % for pads-on-paper and rollers-on-paper) are assimilated to 0 %. -/- stands for non-measured parameters. (1) The 800 g load is distributed on 3 pads. (2) Estimation for a 100 g load. (3) Results from the literature. (4) Different methods are used and the result may be not representative. (5) For the kinetic friction, the evolution is only observed at the first sliding. Several other factors are not represented because we observed no influence on the friction force (e.g. time at rest, ramp time, acceleration, backing).

Friction of paper materials A summary of the main factors influencing the friction of paper materials is represented on Table 16.2. We observe that the chemistry, frictional history, and environmental factors are the main parameters of the paper-on-paper friction. In particular, we showed that a potential of friction stored in samples may be associated to the influence of frictional histories on friction. This potential of friction would possibly be created by the disorder in fibers surface elements. We also suggested that the water condensation creating water bonds is the main mechanism linking the friction force to environmental factors. The pads-on-paper and rollers-on-paper contacts appear less sensitive than the paper-on-paper contact. But the force of kinetic friction of the rollers-on-paper contact decreases with normal load.

Improving envelopes feeding We showed that a stack splits when the force of static friction between two envelopes exceeds their break-away force, a condition described by the *split function*. This function is complex due to the number of machine and stack parameters and their interactions. We therefore explained the different mechanisms of stack split and proposed different strategies for separating the bottommost envelope from the stack. Considering the current machine feeders, the main optimizations are listed on Table 16.3.

Parameter	Reference	Min value	Max value
Mass of envelopes	10 g	0 g (Inf.)	14 g (300)
COSF rollers-on-paper	2.0	1.95 (380)	Inf. (380)
COSF pads-on-paper	1.0	0.62 (120)	1.02 (390)
COSF paper-on-paper	0.6	0.5 (Inf.)	0.99 (23)
COKF paper-on-paper	0.5	0 (64 env.)	0.59 (Inf.)
Acceleration of rollers	100 $m.s^{-2}$	0 $m.s^{-2}$ (270)	120 $m.s^{-2}$ (400)
Vertical plate's position	20	1.0 (380)	70 (380)
Orientation of the pad	-16°	-16.6° (680)	0° (380)

Table 16.3: Reference, minimum, and maximum tolerable values for the different machine and stack parameters. Between brackets, the feeder's capacity (max number of envelopes). Inf., COKF, and COSF stand for Infinite, coefficient of kinetic friction, and coefficient of static friction, respectively.

We also proposed (i) a reduction of the rollers accelerations for low stacks, (ii) an increase in rollers accelerations for heavy stacks, (iii) the use of tongues or rollers applying a slight downward force above the bottommost envelopes, and (iv) similar storage and histories for all the envelopes of the stack. Further works should investigate (i) the envelopes crushes, (ii) the stack shake-up before the selection process, and (iii) the heating of the stack.

General Conclusion

The current design of franking machine feeders heavily relies on decades of empirical improvements. Our study explains the mechanisms involved and supports the design choices. Our study however shows that physical limits of the feeding process are reached. The improvement of the process therefore requires the development of new technological solutions. For example, we proposed the adaptation of the rollers acceleration to the stack size. Beyond those technological solutions, we highlighted the interest of the understanding and control of the paper frictional properties. In particular, the storage conditions and the history of the paper materials are critical for the feeding process. In the future, the understanding and control of paper frictional properties may also allow more reliable feeding processes. For example, the frictional properties may be controlled by modifying the frictional histories of the paper materials and/or their environment. A deep understanding of those mechanisms may go far beyond the franking machines. For example, we can glimpse the development of surfaces with adaptive frictional properties along with a better understanding of friction itself.

Appendix A

Other techniques for feeding paper materials

In chapter 1.4, we did a state of the art the envelopes feeding in franking machines. We now propose to extend this state of the art to other techniques aiming at feeding paper materials, such as paper sheets and boards. This state of the art exceeds the frame of this study but may inspire new technological solutions for feeding envelopes in franking machines.

Manual solutions This solution requires very simple mechanisms permitting small and cheap machines, as represented on Figure 1.1a. However, an operator is required and the throughput is highly reduced.

An intermediate solution between the manual and automated feeding consists in easing the selection. For example, fanning the documents before placing them in a feeder introduces a blanket of air between them. It is a very common technique when feeding a copier with paper sheets, but not possible for envelopes because of their stiffness. Another solution consists in lifting up the back end of envelopes in a franking machine feeder. This solution is intended at easing the envelope feeding.

Vacuum Vacuum attracts the topmost or bottommost document of a stack, permitting or easing its separation and transportation. Vacuum solutions are typically used for heavy-duty machines (thousands of pages per hour). They are also used to manipulate delicate products for which friction and sideways movements are not suitable [104], as for example folded and stitched brochures or embossed documents. The solution is however expensive and requires heavy installations such as vacuum pumps.

A typical solution involving vacuum consists in sucker bars. Sucker bars are moving bars on which are placed several vacuum-powered suction cups, called *suckers* (see Figure A.1). The bar picks up the topmost sheet of a document stack, lifting it

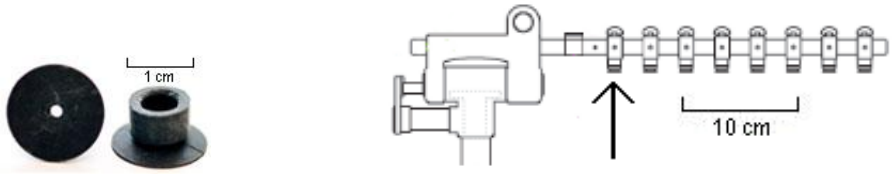

(a) Suckers [105] (b) Sucker bar, indicated by an arrow [106]

Figure A.1: An example of suction system used to process paper materials. The system is used on the Horizon Collator machine, which feeder's speed reaches 27,000 sheets per hour [105]

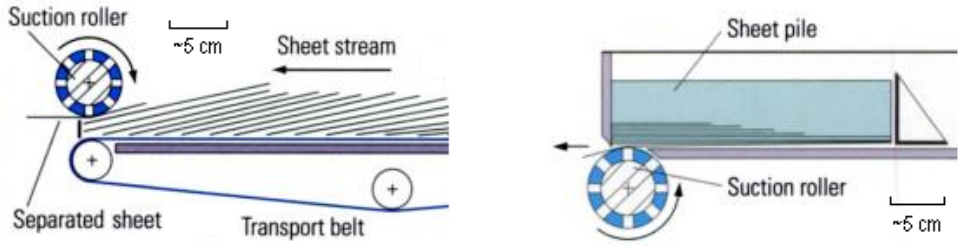

(a) In a stream feeder (b) In a box feeder

Figure A.2: Suction rollers used as top and bottom feeders [104]

for transfer to a feedboard. This solution is widely used in printing processes such as offset machines.

To permit bottom feeding, the vacuum-powered suction cups can be placed behind a transportation belt. This system, called *suction belts*, eases the gripping of documents carried by the belt, facilitating the document transportation and separation.

To finish with, another solution consists in *suction rollers*, also called *drum vacuum feeders*. These are vacuum-powered rollers used as top-feeder or bottom-feeder and represented on Figures A.2a and A.2b, respectively.

Air blowing At the contrary of vacuum solutions, air blowing permits the introduction of an air blanket between the documents to ease their separation. Printing presses often use air blasts from various ways to separate documents. For example, Figure A.3 (left) represents an air blast at the front end of the paper stack. This air blast floats the top sheet, whereas the feeder suckers catch it and lift it to the edge of the feedboard. Another system, represented on Figure A.3 (right), consists in lifting the corner of a document, and then blowing air between the document and the stack. The whole document is then separated from the stack [107].

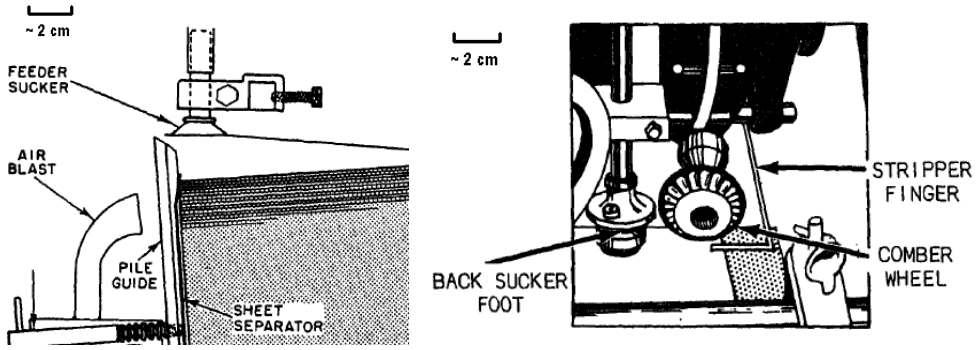

Figure A.3: Examples of air blasts uses for paper separation [107]

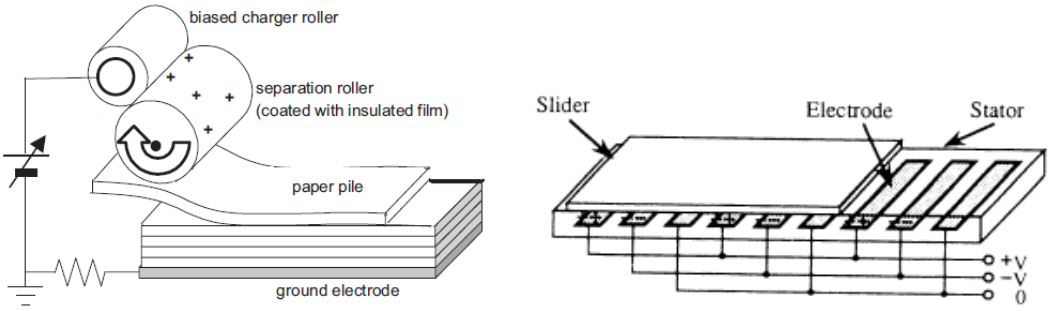

(a) Top feeder [108] (b) Bottom feeder [109]

Figure A.4: Experimental electrostatic sheet feeders

Electrostatics Electrostatic solutions are studied within the frame of small paper sheet feeders, such as copier feeders. Those solutions are similar to those involving vacuum, but the attraction is created by the Coulomb law of electrostatics. An example of is represented on Figure A.4a. In this example, a separation roller placed above the top of the paper stack is covered by an insulated film coating. The roller is charged, so that the topmost envelope is lifted.

Other solutions are developed to permit bottom feeding. For example, a tangential displacement of documents is possible by creating a tangential difference of potential between the electrodes and a sled, as represented on Figure A.4b. The main drawback of those solutions consists in the weakness of the Coulomb force involved. Those solutions permit only the displacement of light documents and remain mainly experimental.

It is also common using systems to reduce the electrostatic potential between paper materials. In particular, (i) the use of brushes in contact with the document, and (ii) the blowing of ionized air or specific gas on the document stack.

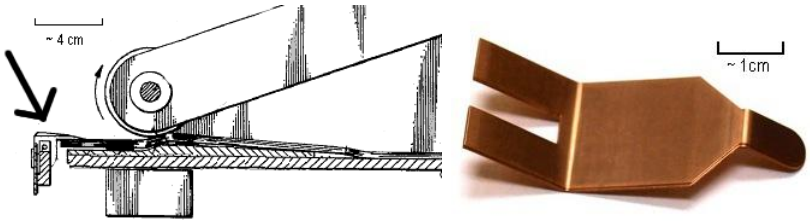

Figure A.5: Snubbers used in a sheet feeding apparatus [110] [111]

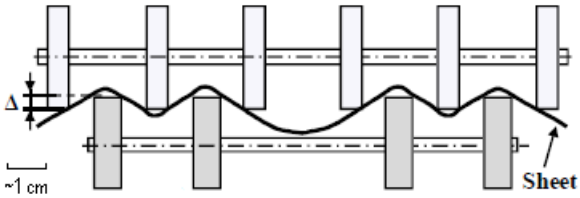

Figure A.6: W-Separation system [113]

Documents bending For thin documents that can be slightly bent (paper sheets for example), the deformation of a document permits its separation from the rest of the stack.

Snubber tabs and *separator fingers* are small pieces usually placed at the top, front edge of the topmost sheet of a paper stack, as represented on Figure A.5. They ensure that the selection system lifts only one sheet at a time [107] [110] [112], whatever is the selection system. For example, on Figure A.5, we represented a system that bends the topmost document to permit its separation from the stack. The advantage of the solution is that it is very cheap and can be found in copiers, for example.

Another solution consists in the *W-separation*, also called *waved deformation* or *buckle separation*. This solution consists in shifting belts, rollers or friction pads between the top and bottom of the paper path, as represented on Figure A.6. The W-separation permits to avoid having a friction nip point during the frictional documents separation. It also creates an air blanket between documents. Both are supposed to contribute to easing the separation of documents.

Friction In chapter 1.4, we listed several frictional materials used in franking machines. A last example of frictional materials consists in *brushes*, as represented on Figure A.7. The friction they produce is low and difficult to master. Brushes may also be damaged with use. However, it is frequent observing such systems in addition to conventional top sheet feeders. For example, in sheet fed press feeders,

(a) Separator brushes

(b) Brush wheels

Figure A.7: Brushes used to ease the documents separation [114]

separator brushes ensure that the pickup suckers lift only one sheet at a time. To our knowledge, this system is however not used in franking machines.

Appendix B

A comparative study of several franking machines

In chapter 1, we made a state of the art of technological solutions permitting the feeding of paper materials. In this section, we will present the solutions actually used in franking machines feeders.

The studied franking machines 7 machines are studied and described on Table B.1.

Name	Company	Description
Omega	Neopost	The heavy-duty Neopost franking machine
MMF IJ	Neopost	The Omega ancestor
Delta	Neopost	The Neopost average-size franking machine
AFS IJ (abbr. IJ)	Neopost	The Delta ancestor
DM400	Pitney Bowes	Pitney Bowes equivalent to Neopost Delta
DM1000	Pitney Bowes	Pitney Bowes equivalent to Neopost Omega
Ultimail	Francotyp	A third equivalent to Neopost Delta

Table B.1: The seven studied franking machines

The study is divided into 5 parts corresponding to the different sections of typical franking machine feeders and represented on Figure B.1. After the extraction rollers, the feeder sometime also (i) measures the thickness of envelopes, and (ii) seals them with glue. Those functions are however out of the scope of this study.

The hopper The hopper usually consists in rollers on which the envelope stack is placed. To ease the document separation, the hopper often presents (i) an angle to the horizontal (tilted hopper), and (ii) eccentric rollers. In addition, some techniques permit the stacking of envelopes at the back of the machine: (i) back inclination

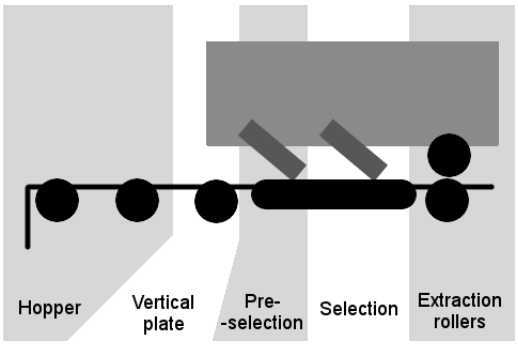

Figure B.1: The five sections of a franking machine feeder

(the operator side is raised), (ii) lateral holds, and (iii) rollers orientation. Finally, some machines have a metal hopper floor connected to the electric mass, permitting the discharge of envelopes. A comparison between the hoppers of the seven studied franking machines is proposed on Table B.2.

Functionality	Ω	MMF	IJ	Δ	IJ	DM400	DM1000	Ultimail
Tilted hopper	0	0	0	-	0	5°	0
Back inclination	Yes	No	Yes	-	Yes	Yes	No
Lateral holds	1	2	1	-	1	0	1
Rollers orientation	No	No	Yes	-	Yes	Yes	No
Rollers	12	12	9	-	8	7	0
Eccentric rollers	0	0	0	-	3	5	0
Belts	0	0	0	-	0	0	1

Table B.2: Comparison between the hoppers of the seven studied franking machines

Vertical plate The vertical plate and the corresponding part of the hopper base permit the separation of a first block of envelopes (about 2cm). The used techniques are the curvature of the plate and sometime some friction materials. In addition, eccentric rollers are supposed to ease the selection. A comparison between the vertical plates of the seven studied franking machines is proposed on Table B.3.

Functionality	Ω	MMF IJ	Δ	IJ	DM400	DM1000	Ultimail
Plate	Yes	Yes	Yes	Yes	Yes	Yes	Yes
Curvature	Yes	No	Yes	Yes	Yes	Yes	Yes
Friction materials	3	0	0	0	0	0	0
Rollers	3	3	3	7	0	0	0
Eccentric rollers	3	0	0	0	0	0	0
Belts	3	3	0	0	3	3	1

Table B.3: Comparison between the vertical plates of the seven studied franking machines

The pre-selection The first stage of the selection line is optional and called pre-selection. The pre-selection usually consists in friction pads, belt and/or flexible tongue. To permit the feeding of envelopes of different thickness, the friction pads and/or belts rotate (y-axis) or have a vertical displacement (z-axis). In addition, the machines sometime have mobile blades that are used as selection plates. A comparison between the pre-selection stages of the seven studied franking machines is proposed on Table B.4.

Functionality	Ω	MMF IJ	Δ	IJ	DM400	DM1000	Ultimail
Axis	y	y	z	z	-	y	z
Friction plates	3	3	2	3	-	1	4
Blade	No	No	Yes	Yes	-	No	Yes
Tongue	Yes	No	No	No	-	No	No
Selection belt	0	0	0	0	-	2	0
Rollers	0	0	3	4	-	0	3
Eccentric rollers	0	0	0	0	-	0	0
Belts	3	3	0	0	-	3	0

Table B.4: Comparison between the pre-selection stages of the seven studied franking machines

The selection The second stage, the selection itself consists in friction pads, separation rollers or belts. The system can be retracted or softened in order to ease the document transportation. Finally, the selection can be mechanically couple with the pre-selection in the vertical direction. In this situation, the pre-selection lifts-up when the selection does so. A comparison between the selection stages of the seven studied franking machines is proposed on Table B.5.

Functionality	Ω	MMF IJ	Δ	IJ	DM400	DM1000	Ultimail
Axis	z	z	z	z	y	y	-
Friction plates	3	3	2	0	0	0	-
Separation rollers	0	0	0	0	2	2	-
Separation belt	0	0	0	0	2	2	-
Retractable	Yes	No	Yes	Yes	No	No	-
Softenable	No	No	No	No	Yes	Yes	-
Coupled with presel.	No	No	Yes	Yes	No	No	-
W-selection	Yes	No	No	Yes	No	No	-
Rollers	3	3	2	3	0	0	-
Eccentric rollers	0	0	0	0	0	0	-
Belts	0	0	0	0	3	3	-

Table B.5: Comparison between the selection stages of the seven studied franking machines

The extraction rollers After the selection line, the bottommost envelope is supposed to be well separated from the other envelopes. As soon as an envelope appears between the extraction rollers, placed after the selection line, the motors in uphill from the extraction rollers are disconnected, so that the only envelope to be driven is the bottommost one. In particular, the extraction rollers are driven to permit the feeding of the bottommost envelope at the desired moment.

Appendix C

Stick-slip model

We introduced the stick-slip phenomenon as a sequential build-up and release of stored energy in elastic components. The stick-slip thus results in cyclical relative acceleration and deceleration of the surfaces in contact. We propose in this annex a simplified model of stick-slip. This model is intended at giving a mathematical description of the movement observed on the oscillation sled test method, and also sometimes on the horizontal plane test method.

C.1 Situation

As a model, we consider the mass-spring system. A sled is in contact with a plane. A spring is fixed on the one end to the sled, and on the other end to a moving arm, as represented on Figure C.1. The arm gets displaced at a constant speed V.

C.2 Equation of the movement

First sticking When the sled sticks on the plane, the sled is immobile and its position is x_A. For clarity reason, we take this position as a reference ($x_A = 0$). On the other hand, the arm moves at a constant speed and an expression of its position, x_B, is:

$$x_B = l_0 + Vt \tag{C.1}$$

Where l_0 and t represent the initial length of the spring and the time, respectively. The length of the spring, l, can therefore be expressed as:

$$l = x_B - x_A = l_0 + Vt \tag{C.2}$$

From this expression, we deduce the expression of the pulling force, F_p, applied by the spring on the sled:

$$F_p = k(x_B - x_A - l_0) = k(l - l_0) = kVt \tag{C.3}$$

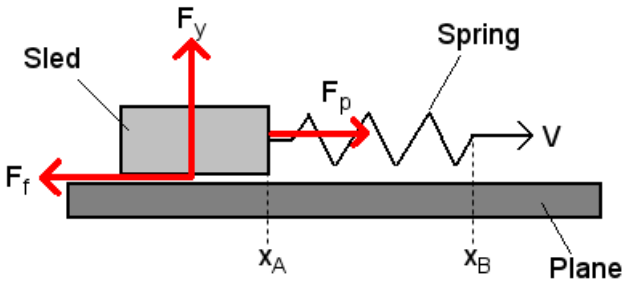

Figure C.1: A simplified model for the stick-slip phenomenon. F_y, F_f, and F_p are the forces applied on the sled and represent the reaction of the plane to the sled's weight, the force of friction between the plane and the sled, and the pulling force applied by the spring, respectively.

The pulling force increases until reaching the break-away force, F_S, defined by:

$$F_S = \mu_S F_y = \mu_S mg \tag{C.4}$$

Where μ_S, F_y, m, and g represent the coefficient of static friction, the reaction of the plane to the weight of the sled, the mass of the sled, and the standard gravity ($g = 9.81$ m.s^{-2}), respectively. The sled therefore starts sliding at a time t_0 defined by:

$$kVt_0 = \mu_S mg \Rightarrow t_0 = \frac{\mu_S mg}{kV} \tag{C.5}$$

As the sliding starts, the velocity of the sled is zero.

Slipping After t_0, the sled undergoes a pulling force ($F_p = k(Vt - x_A)$) and the force of kinetic friction ($F_f = \mu_K mg$). The fundamental principle of dynamics gives:

$$\begin{aligned} & F_p - F_f = k(Vt - x_A) - \mu_K mg = m\tfrac{\mathrm{d}^2 x_A}{\mathrm{d}t^2} \\ \Rightarrow \quad & \tfrac{\mathrm{d}^2 x_A}{\mathrm{d}t^2} + \tfrac{k}{m} x_A = \tfrac{k}{m} Vt - \mu_K g \\ \Rightarrow \quad & \tfrac{\mathrm{d}^2 x_A}{\mathrm{d}t^2} + \tfrac{k}{m} x_A = \tfrac{k}{m} V(t - t_0) + (\mu_S - \mu_K) g \\ \Rightarrow \quad & \tfrac{\mathrm{d}^2 x_A}{\mathrm{d}t^2} + \omega^2 x_A = \omega^2 V(t - t_0) + (\mu_S - \mu_K) g \end{aligned} \tag{C.6}$$

Where μ_K and ω represent the coefficient of kinetic friction and the pulsation ($\omega = \sqrt{\frac{k}{m}}$), respectively. A general form of the solution is:

$$x_A = C_1 \sin(\omega(t - t_0)) + C_2 \cos(\omega(t - t_0)) + V(t - t_0) + \frac{(\mu_S - \mu_K) g}{\omega^2} \tag{C.7}$$

Where C_1 and C_2 are parameters of the solution. The initial conditions of this equation were described in the previous section: $x_A(t_0) = 0$ and $\frac{\mathrm{d}x_A}{\mathrm{d}t} = 0$. From

equation C.7, we thus deduce an expression of the movement of the sled during the sliding phase:

$$x_A = -\frac{V}{\omega}\sin(\omega(t-t_0)) + \frac{\mu_S - \mu_K}{\omega^2} g\left[1 - \cos(\omega(t-t_0))\right] + V(t-t_0) \tag{C.8}$$

The movement ends at a time t_1 when the sled velocity is zero ($\frac{\mathrm{d}x_A}{\mathrm{d}t} = 0$). This t_1 time is therefore described by:

$$\frac{\mathrm{d}x_A}{\mathrm{d}t}(t_1) = -V\cos(\omega(t_1-t_0)) + \frac{\mu_S - \mu_K}{\omega} g\sin(\omega(t_1-t_0)) + V = 0 \tag{C.9}$$

Finally, we obtain the expression of the time t_1:

$$t_1 = t_0 + \frac{2}{\omega}\left[\pi - \arctan\left(\frac{(\mu_K - \mu_S)g}{\omega V}\right)\right] \tag{C.10}$$

The position of the sled when it stops is therefore determined by equations C.8 and C.10, and we finally obtain:

$$x_A = V(t_1 - t_0) + 2\frac{(\mu_S - \mu_D)mg}{k} \tag{C.11}$$

$$F_{p,min} = (2\mu_K - \mu_S)mg \tag{C.12}$$

Where $F_{p,min}$ represents the minimum pulling force, reached as the slipping ends.

Sticking The sled remains immobile on the plane until t_2. During this time, the pulling force linearly increases with time:

$$F_p = kV(t - t_1) + F_{p,min} \tag{C.13}$$

For $t = t_2$, the pulling force reaches its break-away force:

$$\mu_S mg = kV(t_2 - t_1) + (2\mu_K - \mu_S)mg \Leftrightarrow t_2 - t_1 = \frac{2g(\mu_S - \mu_K)}{\omega^2 V} \tag{C.14}$$

After that period, the slipping occurs and the process repeats until the arm stops.

C.3 Conclusion

We observed that the difference in friction forces between the static and kinetic frictions creates oscillations of the sled, as represented on Figure C.2. The period of the oscillations is given by $(t_2 - t_1)$, described in equation C.14. The amplitude of the oscillations is given by:

$$\delta x = x_1 - x_0 = V(t_1 - t_0) + 2(\mu_S - \mu_K)g\frac{m}{k} \tag{C.15}$$

The slipping phase being usually shorter than the stick phase, this amplitude can be simplified as:

$$\delta x \approx 2(\mu_S - \mu_K)g\frac{m}{k} \tag{C.16}$$

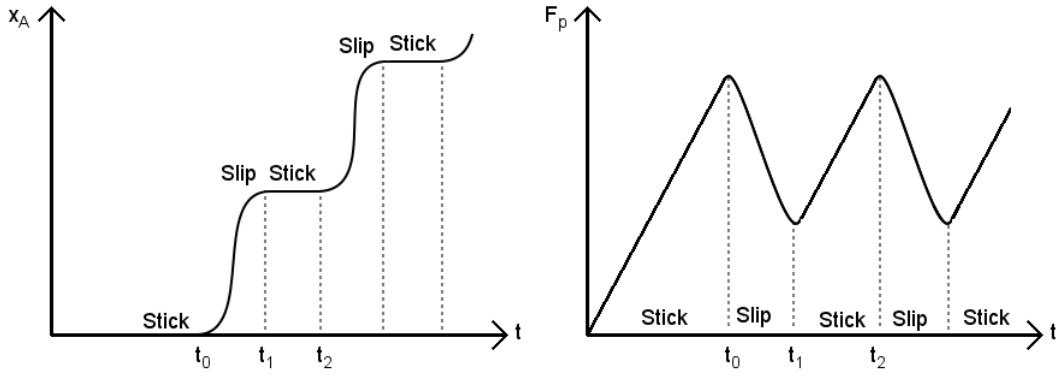

(a) Evolution of the sled position.

(b) Evolution of the pulling force.

Figure C.2: The model of stick-slip oscillations. The position of the sled and the pulling force are represented.

Appendix D

Envelopes compressibility

Envelopes are made of paper, a compressible fibrous material. For envelopes under low loads, the volume of an envelope is mainly occupied by void, as represented on Figure 11.2. The thickness of an envelope is thus expected to have a sharply non-linear evolution with increasing normal load. In this chapter, we propose to characterize the compressibility of envelopes in the range of loads usually involved on franking machine feeders.

D.1 Materials and methods

We used common envelopes of type 12957. The envelopes were filled with one sheet of printing and writing paper.
In a first experiment, we characterized the evolution of the envelope thickness under low loads. To do this, we measured the height of an envelope stack ranging from 1 to 16 envelopes. In a second experiment, we characterized the evolution of an envelope thickness under high loads. To do this, we measured the height of an envelope stack of 100 envelopes for loads ranging from 70 g to 5 kg.

D.2 Results and discussion

Envelopes under low load The thickness of an envelope increased non-linearly with normal load, as represented on Figure D.1a: we observed a sharp decrease in envelope thickness for loads increasing from 0 to 0.3 N (-51 %). We suppose this decrease to be due to the disappearence of air in the envelope. From 0.3 to 1.5 N, the decrease is negligible.

Envelopes under high load For loads above 0.7 N, we suppose the influence of air in the envelopes to be negligible. However, we observed a decrease in stack height up to to 50 N (-20 %, from 10.3 to 8.4 cm). Under a 50 N load, the thickness

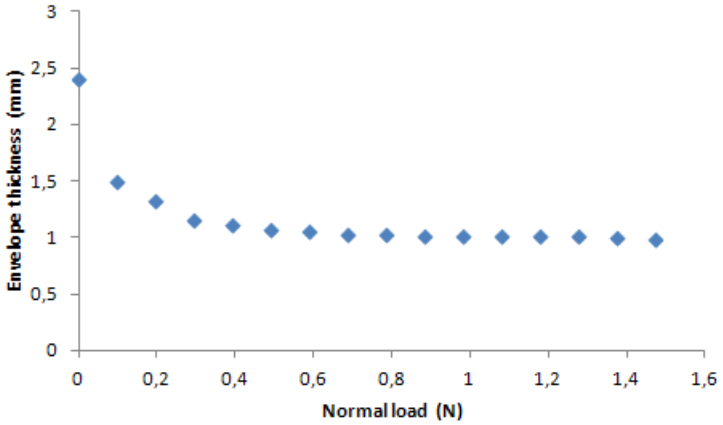

(a) Influence of normal load on envelopes thickness

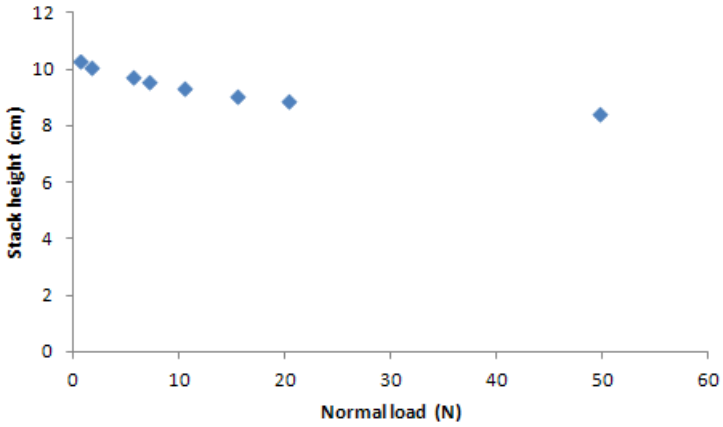

(b) Influence of normal load on the height of a 100 envelopes stack

Figure D.1: Compressibility of envelopes under various normal loads

of envelopes is about -64 % the thickness under no load. We suppose this decrease to be due to deformation of the fibrous structure.

D.3 Conclusion

The thickness of an envelope under a load of 0.3 N is about half the thickness of the envelope under no load, a decrease that is mainly due to the disparition of the air in the envelope. For normal loads above 0.3 N, the decrease is more reduced (about -20 % from 0.7 to 50 N) and is supposed to be mainly due to the deformation of the fibrous structure. The design of franking machines should thus consider that topmost envelopes are much thicker than the other envelopes.

Bibliography

[1] Universal Postal Union. The evolution of the postal sector - implications for the stakeholders (2006-2012). pages 1–137, 2007.

[2] Arcep. Observatoire statistique des activités postales. *Public document*, pages 4–5, 2005.

[3] J. Kruse and A. Liebe. Netzzugang und wettbewerb bei briefdiensten. *Hamburgisches Welt-Wirtschafts-Archiv (HWWA)*, 257, 2005.

[4] R.W. Holbrook. Front end feeder for mail handling machine. *United States Patent and Trademark Office*, US 4.973.037, 1988.

[5] Multigraf AG. Operating manual suction feeder 235.201 / pss. http://www.infoseal.com/support/pdf/ps600tech.pdf. [Online; accessed 21-September-2011].

[6] S. Yanabe and T. Maeda. Skew of paper transferred by rubber rollers in printers. *ASME Information Storage and Processing Systems Conference*, pages 1–3, June 21-23, 2006.

[7] R.C. Benson and E.M. Mockensturm. *Modern Tribology Handbook - Chapter 40: Mechanics and Tribology of Flexible Media in Information Processing Systems*. CRC Press LLC, 2001.

[8] D. Gunderson. Concerning coefficient of friction. *TAPPI Journal*, 83:39–41, 2000.

[9] D. Dowson. *History of Tribology, Second Edition*. Profesionnal Engineering Publishing, 1998.

[10] N. Garoff. *The Friction between Paper Surfaces*. Royal Institute of Technology, Stockholm, Sweden, 2002.

[11] S. Serafin. *The Sound of Friction: Real-Time Models, Playability and Musical Applications*. Stanford University, Cambridge, USA, 2004.

[12] D.P. Markov. Development of ideas on friction mecahnisms. *Journal of Friction and Wear*, 34:70, 2012.

[13] F. Altpeter. *Friction Modeling, Identification and Compensation.* Ecole Polytechnique Fédérale de Lausanne, Lausanne, Switzerland, 1999.

[14] Centre Technique du Papier. Résistance au glissement des papiers. *(internal document)*, (1861):1–11, 1984.

[15] B. Armstrong-Hélouvry, P. Dupont, and C. Canudas de Wit. A survey of models, analysis tools and compensation methods for the control of machines with friction. *Automatica*, 30:1083–1138, 1994.

[16] F. P. Bowden and D. Tabor. The friction and lubrication of solids. *Oxford University Press, London*, 1950.

[17] N. Kawashima, J. Sato, and T. Yamauchi. Paper friction - effect of real contact area. *Sen'i gakkaishi*, 64:329–335, 2008.

[18] F. Altpeter, D. Necsulescu, and R. Longchap. Friction modeling and identification issues for electric drives. *Electromotion '97*, pages 149–154, 8-9 May 1997.

[19] T. Yamamoto. Mechanism of friction and real contact area. *JTEKT Engineering Journal English Edition*, 2007.

[20] M. Ingram, H. Spikes, J. Noles, and R. Watts. Contact properties of a wet clutch friction material. *Tribology International*, 43:815–821, 2010.

[21] M. Eguchi and T. Yamamoto. Shear characteristics of a boundary film for a paper-based wet friction material: friction and real contact area measurement. *Tribology International*, 38:327–335, 2005.

[22] T. Baumberger, F. Heslot, and B. Perrin. Crossover from creep to inertial motion in friction dynamics. *Nature*, 367:544–546, 1994.

[23] F. Heslot, T. Baumberger, B. Perrin, B. Caroli, and C. Caroli. Creep, stick-slip, and dry-friction dynamics: Experiments and a heuristic model. *Physical Review E*, 49, 1994.

[24] Technical Association of the Pulp and Paper Industry. Coefficient of static friction (slide angle) of packaging and packaging materials (including shipping sack papers, corrugated and solid fiberboard) (inclined plane method). *TAPPI standards*, T 815 om-01, 2001.

[25] Association Française de Normalisation. Paper and board - paper, board, corrugated board and their components - determiantion of the coefficient of static friction (inclined plan method). *AFNOR standards*, NF Q 03-083, 1984.

[26] Technical Association of the Pulp and Paper Industry. Coefficient of static friction of uncoated writing and printing paper by use of the inclined plane method. *TAPPI standards*, T 548 om-90, 1990.

[27] Technical Association of the Pulp and Paper Industry. Coefficient of friction (angle of slide) of packaging papers (inclined plane method). *TAPPI standards*, T 542 om-88, 1990.

[28] F. P. Bowden and J. E. Young. Friction of diamond, graphite, and carbon and the influence of surface films. *Proceedings of the Royal Society of London*, 208:444–455, 1951.

[29] H.G. Howell and J. Mazur. Amonton's law and fibre friction. *Journal of the Textile Institute*, 44:T59–T69, 1953.

[30] E.L. Deladi, M.B. de Rooij, and D.J. Schipper. Modeling of static friction in rubber-metal contact. *Tribology International*, 40:588–594, 2007.

[31] E. L. Back. Paper-to-paper and paper-to-metal friction. *TAPPI Proceedings - International Paper Physics Conference*, pages 49–65, 1991.

[32] Internation Standard Organization. Paper and board - determination of the static and kinetic coefficients of friction - horizontal plane method. *ISO standards*, 15359, 1999.

[33] Technical Association of the Pulp and Paper Industry. Coefficients of static and kinetic friction of uncoated writing and printing paper by use of the horizontal plane method. *TAPPI standards*, T 549 pm-90, 1990.

[34] Technical Association of the Pulp and Paper Industry. Coefficient of static friction of corrugated and solid fiberboard (horizontal plane method). *TAPPI standards*, T 816 om-92, 1992.

[35] Association Française de Normalisation. Paper and board - paper, board, corrugated board and their components - determination of the coefficient of static friction and estimation of the coefficient of dynamic friction (dynamometer method). *AFNOR standards*, NF Q 03-082, 1984.

[36] W. Nuninger, W. Perruquetti, and J.-P. Richard. Bilan et enjeux des modèles de frottements : tribologie et contrôle au service de la sécurité des transports. *KEF'06, 5th European Conference on Braking*, 2006.

[37] P.A. Lischinsky. *Compensation de frottement et commande en position d'un robot hydraulique industriel*. Laboratoire d'Automatique de Grenoble, Grenoble, France, 2007.

[38] A. Johansson, C. Fellers, D. Gunderson, and U. Haugen. Paper friction - influence of measurement conditions. *TAPPI Journal*, 81(5):175, 1998.

[39] C. Fellers, M. Backstrom, M. Thun, and G. Lindholm. Paper-to-paper friction - paper structure and moisture. *Nordic Pulp and Paper Research Journal*, 13:225–232, 1998.

[40] J. Sato, G. de Silveira, and I.M. Hutchings. Measurement of the friction of paper by the strip-on-drum method. *Tribology Internation*, 30:633–640, 1997.

[41] G. de Silveira and I.M. Hutchings. *The fundamental of paper Materials - Determination of the friction of paper and board.* C.F. Baker, ed. Pira International, Surrey, UK, 1997.

[42] M.C. Singleton and R.J. Allan. Factors influencing paper friction and its reproductibility: is third test best? *Appita*, 50:481–485, 1997.

[43] H. Olsson, K.J. Aström, C. Canudas de Wit, M. Gäfvert, and P. Lischinsky. Friction models and friction compensation. *European Journal of Control*, 4:176–195, 1998.

[44] N. Garoff, C. Fellers, and N.-O. Nilvebrant. Friction hysteresis of paper. *Wear*, 256:190–196, 2003.

[45] A. Emmanuel and N.J. Collins. Paper mill frictionizing trials using chemical additives to increase layer to layer coefficient of friction. *Appita*, 48:129–133, 1999.

[46] Dunkermotoren. Product datasheets. http://www.dunkermotoren.com/default.asp?id=69, 2014. [Online; accessed 13-February-2014].

[47] E. Orsenna. *Sur la route du papier.* Editions Stock, 2012.

[48] H. Goyal. Grades of paper. http://www.paperonweb.com/grade.htm. [Online; accessed 11-March-2014].

[49] S. Dias. Des tests de diagnostic sur support papier. http://www.bulletins-electroniques.com/actualites/070/70798.htm, 2012. [Online; accessed 11-March-2014].

[50] J.S. Cybulski, J. Clements, and M. Prakash. Foldscope: Origami based paper-microscope. *Available online at [arXiv:1403.1211]*, 2013.

[51] INSEE. Taux de recyclage des déchets en france. http://www.insee.fr/fr/publications-et-services/default.asp?page=dossiers_web/dev_durable/recyclage_dechets.htm, 2012. [Online; accessed 11-March-2014].

[52] N. Fulleringer and B. Ponsard. Utilisation des plantes annuelles en papeterie. http://cerig.efpg.inpg.fr/memoire/2009/plante-annuelle.htm, 2009. [Online; accessed 11-January-2014].

[53] M. Alava and K. Niskanen. The physics of paper. *Reports on Progress in Physics*, pages 669–723, 2006.

[54] wikipedia.fr. Fourdrinier machine. http://en.wikipedia.org/wiki/Paper_machine. [Online; accessed 01-March-2014].

[55] Fraunhofer-Chalmers Centre. Innovative simulation of paper. http://www.fcc.chalmers.se/comp/projects/innovative-simulation-of-paper. [Online; accessed 01-March-2014].

[56] G. Broughton and J. L. Gregg. Some observations on the kinetic coefficient of friction of paper. *TAPPI*, 35:489–493, 1952.

[57] P. Vernhes, J.-F. Bloch, C. Mercier, A. Blayo, and B. Pineaux. Statistical analysis of paper surface microstructure: A multi-scale approach. *Applied Surface Science*, 254:7431–7437, 2008.

[58] M. Inoue, N. Gurnagul, and P. Aroca. Static friction properties of linerboard. *Tappi Journal*, 73:81–85, 1990.

[59] N. Garoff, N.-O. Nilvebrant, and C. Fellers. Friction of linerboard based on recycled fiber. *Journal of Applied Polymer Science*, 85:1511–1520, 2002.

[60] P. Delacroix. *Bull. Assoc. Tech. Ind. Papetière*, 1:12, 1947.

[61] G. Chinga-Carrasco. Cellulose fibres, nanofibrils and microfibrils: The morphological sequence of mfc components from a plant physiology and fibre technology point of view. *Nanoscale Research Letters*, 417, 2011.

[62] J. Laamanen. Using the scanning electron microscope. http://www.fao.org/docrep/p6645e/p6645e05.htm, 2014. [Online; accessed 14-August-2014].

[63] T. Enomae. Overview on tribology of paper. *Journal of Japan Society of Tribology*, 46:741–746, 2001.

[64] M. Bäckström, C. Fellers, and M. Htun. The influence of kappa number and surface energy on paper-to-paper friction. *Nordic Pulp and Paper Research Journal*, 14:204–208, 1999.

[65] P. Rättö, C. Barbier, and M. Rigdahl. An investigation of the friction properties of coated paper. *Nordic Pulp and Paper Research Journal*, pages 351–356, 2000.

[66] N. Gurnagul, M.D. Ouchi, N. Dunlop-Jones, D.G. Sparkes, and J.T. Wearing. Factors affecting the coefficient of friction of paper. *Journal of Applied Polymer Science*, 46:805–814, 1992.

[67] N. Garoff and S. Zauscher. The influence of fatty acids and humidity on friction and adhesion of hydrophilic polymer surfaces. *Langmuir*, 18:6921–6927, 2002.

[68] C.C. Payne. Coating paper with colloidal silicas helps stop slippage of containers. *Journal of Pulp and Paper*, 8:91, 1989.

[69] M.C. Withiam. The effect of fillers on paper friction properties. *Tappi Journal*, 74:249–256, 1991.

[70] T. Enomae, N. Yamaguchi, and F. Onabe. Influence of coating properties on paper-to-paper friction of coated paper. *Japan Wood Science*, 52:509–513, 2006.

[71] N. Jones and J.D. Peel. Frictional properties of paper and their importance in supercalandering. *Paper Technology*, 8:43–50, 1967.

[72] A. Johansson, C. Fellers, D. Gunderson, and U. Haugen. Paper friction - influence of measurement conditions. *International Paper Physics Conference*, pages 5–15, 1995.

[73] C.W. Wolgemuth. Plant biomechanics: Using shape to steal motion. *Current Biology*, 19:R409–R410, 2009.

[74] A. Filippov and S.N. Gorb. Frictional-anisotropy-based systems in biology: structural diversity and numerical model. *Scientific Reports*, pages 1–6, 2013.

[75] S. Gorb and M. Scherge. Biological microtribology: anisotropy in frictional forces of orthopteran attachment pads reflects the ultrastructure of a highly deformable material. *Proceedings of the Royal Society of London B*, 267:1239–1244, 2000.

[76] K. Autumn, C. Majidi, R.E. Groff, A. Dittmore, and R. Fearing. Effective elastic modulus of isolated gecko setal arrays. *The Journal of Experimental Biology*, 209:3558–3568, 2006.

[77] H.E. Jeong, J.-K. Lee, H.N. Kim, S.H. Moon, and K.Y. Suh. A nontransferring dry adhesive with hierarchical polymer nanohairs. *Proceedings of the National Academy of Sciences*, 106:5639–5644, 2009.

[78] A. Zmitrowicz. Models of kinematics dependent anisotropic and heterogeneous friction. *International Journal of Solids and Structures*, 43:4407–4451, 2006.

[79] J.-M. Praene, M.-A. Bueno, and A.-M. Pense. Etude phénoménologique du frottement des matériaux fibreux souples. *18ème Congrès Français de Mécanique*, 27-31 août 2007.

[80] M. Tourlonias and M.-A. Bueno. Etude phénoménologique du comportement au frottement de surfaces textiles. *19ème Congrès Français de Mécanique*, 24-28 août 2009.

[81] M. Minn and S.K. Sinha. Molecular orientation, crystallinity, and topographical changes in sliding and their frictional effects for uhmwpe film. *Tribology Letters*, 34:133–140, 2009.

[82] W. Shi, H. Dong, and T. Bell. Tribological behaviour and microscopic wear mechanisms of uhmwpe sliding against thermal oxidation-treated ti6al4v. *Materials Science and Engineering*, pages 27–36, 2000.

[83] P. Vernhes, J.-F. Bloch, A. Blayo, and B. Pineaux. Effect of calendering on paper surface micro-structure: A multi-scale analysis. *Journal of Materials Processing Technology*, 209:5204–5210, 2009.

[84] B.N.J. Persson, O. Albohr, F. Mancosuc, V. Peveric, V.N. Samoilov, and I.M. Sivebaek. On the nature of the static friction, kinetic friction and creep. *Wear*, pages 835–851, 2003.

[85] H. Umano and H. Yamaura. Velocity dependencies of paper feeding characteristics. *The Japan Society of Mechanical Engineers*, pages 2476–2485, 2011.

[86] L.S. McCarty and G.M. Whitesides. Electrostatic charging due to separation of ions at interfaces: Contact electrification of ionic electrets. *Angewandte Chemie*, 47:2188–2207, 2008.

[87] T.A.L. Burgo, C.A. Silva, L.B.S. Balestrin, and F. Galembeck. Friction coefficient dependence on electrostatic tribocharging. *Scientific reports*, 3:1–8, 2013.

[88] Sappi. Cause and effects of static electricity in paper. *Tech tips (internal document)*.

[89] M. Murtomaa, T. Hokkanen, T. Huhtala, A.-L. Tammi, J. Kärkkäinen, and V.-P. Lehto. Triboelectrification of paper in the offset printing process. *Journal of Electrostatics*, 65:593–597, 2007.

[90] E.J. Murphy. The dependence of the conductivity of cellulose, silk and wool on their water content. *Journal of Pysics and Chemistry of Solids*, 16:115–122, 1960.

[91] J.K. Lancaster. A review of the influence of environmental humidity and water on friction, lubrification and wear. *Tribology International*, 23:371–390, 1990.

[92] S. Soh, S.W. Kwok, H. Liu, and G.M. Whitesides. Contact de-electrification of electrostatically charged polymers. *ACS Publications*, 134:20151–20159, 2012.

[93] T.G.M. van de Ven. Capillary forces in wet paper. *Industrial and Engineering Research Journal*, 47:7250–7256, 2008.

[94] H.J. Butt. Capillary forces: Influence of roughness and heterogeneity. *Langmuir*, 24:4715–4721, 2008.

[95] G. Spinnler. *Conception des machines: principes et applications. Dimensionnement.* Presses Polytechniques et Universitaires Romandes, Lausanne, Switzerland, 2001.

[96] Jens Borch, M. Bruce Lyne, Richard E. Mark, and Charles C. Jr. Habeger. *Handbook of Physical Testing of Paper Volume 2.* Marcel Dekker, Inc., 270 Madison Avenue, New York, NY 10016, 2002.

[97] M. Suzuki, M. Isoda, K. Fukchi, M. Nakahashi, and Y. Tsuda. High performance rubber rollers and pads for auto sheet feeders. *Hitachi Cable Review*, pages 1–8, 1998.

[98] K.A. Grosch. *The Pneumatic Tire - Chapter 11: Rubber Friction and Tire Traction.* US Departement of Transportation - National Highway Traffic Safety Administration, 2006.

[99] K.A. Grosch. *Sliding Friction and Abrasion of Rubbers, PhD Thesis.* University of London, 1963.

[100] Manufacture Française des Pneumatiques Michelin. *Le pneu - L'adhérence.* Société de Technologie Michelin, Clermon-Ferrand, France, 2001.

[101] K.D. Stack. *A Study of Friction Feed Paper Separation.* University of Rochester, Rochester, New York, 1991.

[102] B. Wang and Wang Z.-W. Numerical simulation for friction separation of paper feed in copier. *Journal of Chongqing University of Technology (Natural Science)*, 24:95–99, 2010.

[103] S. Yanabe, M. Endo, and M. Nakanishi. Wrinkle occuring process of a paper fed to a fixing roller unit in printers and copiers. *Journal of Environment and Engineering*, 6:28–40, 2011.

[104] H. Kipphan. *Handbook of Print Media: Technologies and Manufacturing Processes.* Springer, 2001.

[105] NA Graphics. Suckers / grippers / presse parts. http://order.nagraph.com/suckers-grippers-press-parts.html. [Online; accessed 21-September-2011].

[106] Heidelberg. Sheet separation and feed. http://courtneyheffernan.com/assets/portfolio_images/490/windmill_backfull.pdf, 2010. [Online; accessed 21-September-2011].

[107] Department of the navy. *Litographer - Navedtra 10451.* Naval Education and Training Program Management Support Activity, 1987.

[108] H. Kawamoto and S. Umezu. Development of electrostatic paper separation and feed mechanism. *Journal of Electrostatics*, 65(7):438–444, 2007.

[109] T. Niino, S. Egawa, and T. Higuchi. An electrostatic paper feeder. *Journal of the Japan Society for Precision Engineering*, 60:1761–1765, 1994.

[110] N.V. Kishore. Sheet feeding apparatus. *United States Patent and Trademark Office*, US 3.687.448, 1970.

[111] National Offset Warehouse. Sheet separator for ryobi, pkg (12). http://store03.prostores.com/servlet/nationaloffsetwarehouse/the-328/Sheet-Separator-for-Ryobi%2C/Detail. [Online; accessed 21-September-2011].

[112] W. Goff. Paper guide means for reverse feed sheet paper separation device. *United States Patent and Trademark Office*, US 4.136.861, 1977.

[113] H. Cheng, H. Ikeda, and K. Yoshida. Numerical analysis on paper sheet separation using the overlap separation mechanism. *Journal of Advanced Mechanical Design, Systems and Manufacturing*, 4(1):249–256, 2010.

[114] printerparts.com. Paper separator brush - heidelberg gto / 'k' series. http://store.printersparts.com/store/index.php?main_page=product_info&cPath=140_138&products_id=1333. [Online; accessed 22-September-2011].

Summary The improvement of numerous technological processes requires a deep understanding of the paper friction phenomena. Thus, we tried to obtain a better understanding of those phenomena to improve the envelopes separation in franking machines.
The standad methods for measuring the paper-on-paper friction force appeared to be limited in terms of repeatability and experimental conditions. Thus, we developed two experimental methods, at low and high speeds, respectively. We also adapted the friction measurement methods to the different contacts found in franking machines.
We then used those methods to study the mechanisms responsible for the friction with the paper materials. In particular, we studied (i) the dependency of the paper-on-paper friction to the direction and length of the displacement, (ii) the influence of temperature and humidity on the paper-on-paper friction, and (iii) the main frictional properties of the envelope-on-envelope, rollers-on-paper, and pads-on-paper contacts, respectively.
To finish with, we developed a model of the envelopes separation inside a franking machine. This process aims at displacing - with no damage - the bottommost envelope of a stack - and only this envelope. The model allowed us to identify, to characterize, and to propose an optimization of the main process parameters.

Résumé L'optimisation de nombreux procédés technologiques requiert une compréhension approfondie des phénomènes de frottement des papiers. Nous avons donc cherché à mieux comprendre ces phénomènes pour tenter d'améliorer la séparation des enveloppes dans les machines à affranchir.
Les méthodes normalisées de mesure du frottement papier-papier se sont tout d'abord avérées limitées en termes de répétabilité et de conditions expérimentales. Nous avons donc développé deux méthodes de mesure, l'une à faible et l'autre à haute vitesses. Nous avons aussi adapté la mesure du frottement aux différents contacts papier rencontrés dans les machines à affranchir.
Dans un second temps, nous avons utilisé ces méthodes pour étudier les mécanismes responsables du frottement avec le matériau papier. Nous avons notamment étudié (i) la dépendance du frottement papier-papier à la direction et longueur du déplacement, (ii) l'influence de la température et de l'humidité sur le frottement papier-papier et (iii) les principales caractéristiques frictionnelles des contacts enveloppe-enveloppe, papier-rouleau et papier-patin.
Dans un troisième temps, nous avons développé un modèle complet de la séparation des enveloppes dans une machine à affranchir. Cette séparation vise à déplacer, sans l'abimer, l'enveloppe inférieure d'une pile - et uniquement cette enveloppe. Le modèle a permis d'identifier, de caractériser et de proposer une optimisation des principaux paramètres de ce procédé.